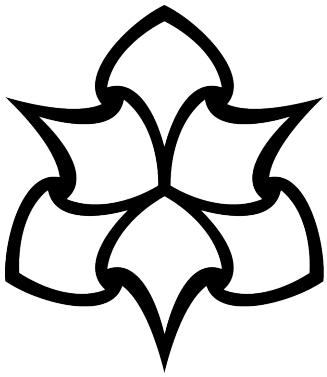

DESIGN AND DEVELOPMENT OF NEW LIGAMENT IMPLANTS

ELISA ROLDAN CIUDAD

A thesis submitted in partial fulfilment of the requirements of the Manchester Metropolitan University for the degree of Doctor of Philosophy

School of Engineering

The Manchester Metropolitan University

2018

ABSTRACT

The anterior cruciate ligament (ACL) is one of the most frequently injured ligaments of the knee. It provides joint stability by constraining anterior tibial translations or internal rotations. This ligament suffers from one of the highest injury rates and, due to the fact that it has very poor healing properties, in many cases requires surgery to be reconstructed. Nowadays the "gold standard" for surgical intervention is to reconstruct the ACL from autografts, but this procedure generates problems such as muscle weakness related to the donor site, or graft site morbidity, therefore other grafts solutions should be investigated. The aim of this thesis was to design, manufacture and test tissue engineered prototypes that could be used for surgical reconstruction of the ACL with comparable mechanical behaviour and nano and micro morphology to the native ACL. The *in vivo* mechanical behaviour of the ACL was investigated during a range of daily activities to understand its failure mechanisms and obtain the mechanical specifications to design and assess the new ACL prototypes. Currently, solely mechanical properties such as Young's modulus or ultimate tensile strength are used to determine the suitability of an ACL implant, however, the work for this thesis has shown that other aspects including dynamic loading and shear loading are crucial for accurately replicating the *in vivo* mechanical behaviour of the ACL. Electrospinning was shown to offer great potential for manufacturing ACL implants with scaffolds of fibre diameter and orientation mimicking the collagen fibres in the extracellular matrix (ECM) of the native ACL. These biomimetic scaffolds can promote cell growth and would enhance mechanical properties. The suitability of two different polymers (a natural polymer: gelatin and a synthetic polymer: polyvinyl alcohol, PVA) were tested as potential ACL scaffolds: morphologically, topographically, mechanically and chemically through degradation assays. The optimisation of solution and process parameters was essential with the aim of creating scaffolds with mechanical properties and morphologies comparable to the native ACL, all crucial aspects that were missing from the current literature in this field. To date most of the experiments with electrospinning were manufactured 2D scaffolds, which does not represent the real three dimensional structure of the ACL. Only four researchers have worked on creating 3D structures from 2D electrospun scaffolds. However, none of them managed to produce morphology nor mechanical behaviour mimicking the natural ACL. Moreover, no comparison of 2D and multiple different 3D structures was performed before the work in this thesis. This PhD establishes the fundamentals for designing and manufacturing biomimetic ACL prototypes, which could be used as a baseline for cell testing, animal models and at the final stage clinical trials.

DECLARATION

No portion of the work referred in this thesis has been submitted in support of an application for another degree or qualification at this, or any other university, or institute of learning.

Date:

Signed:

ACKNOWLEDGEMENT

Finally… happened! What I sometimes thought that would never happen it is happening right now, and here I am writing the last bit of my thesis. This has been possible without any doubt for the great support that I have received during these 3 and a half years journey.

To you Kirstie, huge huge thanks, you have been more than a "simple" supervisor for me. Apart from all very good guidance, advice, comments to improve my research, etc. You have always believed on me, motived me and listened to me when I most needed it. I am looking forward to keep working with you.

Thank you so much for your encouragement and support Glen, definitely without it I would have never finished this thesis or at least not as I wanted, I will always be very grateful for that.

Neil, your guidance, advice, support and motivation made a difference in my way to see and do research. I am very pleased and grateful to have had the opportunity to work with you. Thank you very much Neil.

My sincere thanks and gratitude to all the participants that were involved in my gait study and to the great technical staff of the MMU. Thank you very much Greg, Mike and Hayley for teaching me all I needed to perform my research.

Big thanks to my uni friends: Elisabetta, Aron, Andres, Canras, Maria, Aris, Amani and Mike, without you this journey would have not been so enjoyable. Especially to you guys, my Sis (Elisabetta) and Bro (Aron), you always have been there in the good and bad days as a real family, THANK YOU!

I cannot forget "The Greek Gang" (all of them!) who have always stayed with me and support me, making my life easier, happier and definitely more "musical",

Thank you very much all. Katerinica, Antonis what can I say that you do not know… your friendship and support have been fundamental to not go crazy in these last two years, thank you very much to both!

Venioulaaaaa honey, this goes for you. You are more than a friend more than a flatmate; you have become a really important person in my life in just 1 year. I'm gonna miss you so much!!! Thank you very much for taking care of me and cheer me up to keep going!

Como siempre he dicho, que suerte haber encontrado La Suerte! En este ultimo año he conocido a gente maravillosa alli. Gracias a todos por todos los buenos momentos que hemos pasado juntos.

A mi piñita "colada" las dos personas que pase lo que pase siempre me sacan una carcajada, sois las mejoras amigas que una pueda tener. Paula, Pau, Pauli, Pauloski, Pauloskaya, Esther, Esthercica, Struchis muchas gracias por todos vuestros consejos y animos. Os quiero mucho chicas! Y ahora a planear el viaje a Tailandia!!!

Papa, mama solo me quedais vosotros. Gracias por ser mi motor para seguir adelante, por creer en mi, por apoyarme y ayudarme en todos los sentidos. Os quiero como dirian aqui to the moon and back!

THANK YOU TO EVERYONE!

TABLE OF CONTENTS

INDEX OF FIGURES

INDEX OF TABLES

LIST OF ABREVIATIONS

ACL Anterior cruciate ligament

ECM Extracellular matrix

PVA Polyvinyl alcohol

NHS National Health System

AM Anteromedial bundle

PL Posterolateral bundle

SEM Scanning electron microscopy

GTA Glutaraldehyde

LADs Ligament augmentation devices

LARS Ligament advanced reinforcement system

CT Computed tomography

PGA Polyglycolic acid

PLLA poly-L-lactic acid

PLGA polylactic-co-glycolic acid

PCL Polycaprolactone

PUU Polyurethane urea

PU Polyurethane

Coll Collagen

PDS Polydioxanone

DOF Degree of freedom

FP Force plate

BW Body weight

HAc Acetic acid

DMSO Dimethyl sulfoxide

dH_2O Distilled water

PBS Phosphate-buffered saline

Std Error Standard error of the mean

ANOVA Analysis of variance

PUBLICATIONS BASED ON THIS WORK

Peer reviewed journal articles:

1. E. Roldán, N. D. Reeves, G. Cooper, and K. Andrews, "*In vivo* mechanical behaviour of the anterior cruciate ligament: A study of six daily and high impact activities," Gait Posture, vol. 58, pp. 201–207, 2017.

2. E. Roldán, N. D. Reeves, G. Cooper, and K. Andrews, "Design Consideration for ACL Implants based on Mechanical Loading," Procedia CIRP, vol. 49, pp. 133–138, 2016.

Peer reviewed conference publications:

1. E. Roldán, N. D. Reeves, G. Cooper, and K. Andrews, "Mechanical and morphological evaluation of 2D and 3D electrospun structures for the manufacture of tissue engineered ligaments". 29th European Conference on Biomaterials, Maastricht, Netherlands, 9th – 13th September 2018.

2. E. Roldán, N. D. Reeves, G. Cooper, and K. Andrews, "Assessment of 2D and 3D electrospun structures for use as tissue engineered ligaments: A

mechanical and morphological perspective" eCM Meet. Abstr., collection 4, p. 53, 2018.

3. E. Roldán, N. D. Reeves, G. Cooper, and K. Andrews, "Suitability of optimised PVA electrospun scaffolds for ACL replacement," eCM Meet. Abstr., collection 4, p. 118, 2018.

4. E. Roldán, N. D. Reeves, G. Cooper, and K. Andrews, "Mechanical specifications for the design of ACL implants through the investigation of the *in vivo* mechanical behaviour in daily and high impact activities", 28th European Conference on Biomaterials, Athens, Greece, 4th – 8th September 2017.

5. E. Roldán, N. D. Reeves, G. Cooper, and K. Andrews, "Suitability of gelatin electrospun scaffolds for use in the development of ligament implants: a morphological, topographical and mechanical perspective", 28th European Conference on Biomaterials, Athens, Greece, 4th – 8th September 2017.

6. E. Roldán, N. D. Reeves, G. Cooper, and K. Andrews, "Influence of solvent concentration on morphology, topography and mechanical properties of gelatin electrospun nanofibres: Analysis of induced cell behaviour," eCM Meet. Abstr., no. 5, p. 62, 2016.

7. E. Roldán, N. D. Reeves, G. Cooper, and K. Andrews, "Effects of solvent concentration on the morphology, topography and mechanical behaviour of

gelatin electrospun nanofibres for use in tissue engineering implants", MMU Science & Engineering Research Symposium, Manchester, UK, September 2016.

8. E. Roldán, N. D. Reeves, G. Cooper, and K. Andrews, "Study of the morphology, topography and mechanical properties of gelatin electrospun nanofibres based on solvent concentration", ManBioMat. Biomaterials and tissue engineering conference, Manchester, UK, 15th of June 2016.

9. E. Roldán, N. D. Reeves, G. Cooper, and K. Andrews, "Study of *in vivo* mechanical behaviour of ACL to design improved tissue engineered implants", The 8th MMU Postgraduate Research Conference 'Innovation', Manchester, UK, Thursday 5th November 2015.

1. Introduction

The anterior cruciate ligament (ACL) has the highest injury rates [1] in comparison to the rest of the knee ligaments, offering 49% of these injuries [2]. Ligament injuries are among the most common health problem affecting in the majority of the cases both recreational and professional athletes [2]. However, victims of accidents such as motor vehicle accidents may also injure their ACL [2]. It is estimated that athletes are 7 times more likely to sustain ACL injuries in competition than in practice [3], and 78% of the ACL ruptures occur during non-contact mechanisms such as landing, jumping, side and crossover cutting or pivoting [3], [4]. Athletic ACL injuries are increasing in both adult and youth athletes [5]–[7]. Among those of high school-aged, 60% of high school sport-related surgeries are associated with knee injuries and 50% of these knee injuries are related to ACL ruptures [3]. High rates of knee injuries are reported in female athletes [3], [8]–[16], being between 4 to 6 times more likely to sustain ACL injuries than male athletes [4], [17]; this fact is attributed to anatomical, environmental, hormonal, neuromuscular and biomechanical differences between gender [3], [8], [9], [12], [18].

According to a study performed in 100 United States high schools which reported ACL injuries during 9 different sports and within the 2007/08 – 2011/12 academic years, 77% of all ACL injuries required surgery [3]. In the United Kingdom, the NHS (National Health System) performs approximately 11,000 ACL reconstructions every year, with failure rates up to 25%, which can lead to further

surgery and long-term issues [2], [19], [20]. ACL injuries are among the most economically costly sport injuries, frequently requiring expensive surgery and rehabilitation [3]. The cost of an ACL reconstruction in the UK varies from private hospitals being an average £6,000 per surgery [21], to NHS hospitals being between £3,000 and £3,500 per surgery [19]. In the United States more than 200,000 patients are diagnosed with ACL ruptures every year, of which 175,000 cases require surgery, with the cost of surgery estimated at $1 billion annually [22]. ACL reconstructions performed in the United States between 1990 and 2007 have been analysed in two main studies [23], [24]. Both studies concluded that the rate of ACL reconstructions increased dramatically by 37% across this time period between 1994 and 2006 [24]. This increase was seen across all age groups, but specifically in those aged between 15 and 34 years old and the proportion of females undergoing ACL reconstruction increased by up to 47% [24]. Moreover, subsequent knee surgery was necessary in 6.5% of the cases within 1 year after the ACL replacement [23] and 20% of the patients suffered re-injury within 2 years after the surgery [5].

The use of autografts (grafts from the patient's own body) are currently considered the "gold standard" in ACL surgery. However, this technique is associated with muscle weakness at the donor site, graft site morbidity, knee pain, infection, loss of sensitivity due to nerve damage and long operation and rehabilitation time [22], [25]. Allografts (grafts from a cadaver) and xenografts (tissue taken from an animal) have issues related with the possibility of transmitting diseases, risk of immunological response and the sterilization process [26], [27]. Synthetic ligaments have been also considered for ACL reconstruction but their main disadvantage is their poor long-term behaviour, due to fatigue of the material, laxity

and subsequent mechanical failure [28]. The use of tissue-engineered ACL implants is well received among British Orthopaedic Surgeons, where 86% of surgeons surveyed said they would consider the implantation of a tissue-engineered ACL implant if it showed biological and mechanical success, providing it significantly improved the patient satisfaction or shortened surgical time [29]. Moreover, 76% of surgeons felt that using tissue-engineered ACL implants would be more appropriate than autografts, due to less scarring at the donor site and a reduction in operative time [29].

All these statistics lead to the conclusion:

Key Points:

1. ACL injuries are increasing dramatically at all ages and especially among females.
2. Current treatments for ACL injuries exhibit high failure rate, which causes issues in the quality of life of the patient and unnecessary extra costs.
3. Other alternatives to the current treatments offering potential benefits should be studied.

This chapter provides the background necessary to analyse the current problem and determine the characteristics that an ACL implant has to possess to improve its performance and behave like the natural ACL. To this end, the anatomy of the knee and ACL, the mechanical function of the ACL and ACL loading, ACL

injury mechanics, current ACL implants, manufacturing process and potential materials used to create ACL implants were studied. The important and relevant key points of all of these aspects cited above are explained. Moreover, the research questions of this thesis are included at the end of the present chapter.

Literature review

1.1. Anatomy of the Knee and the ACL

Importance:

1. The study of the anatomy of the knee aids understanding of where the ACL is located, its insertion sites, its environment and gives information about its function in the knee.

2. Knowing the environment of the ACL is crucial in understanding its healing problem, designing mechanical tests with similar environments and so designing ligament implants that can bear loads comparable to the ones that the natural ACL has to bear.

3. The study of the anatomy of the ACL is important in order to know the dimensions of the ligament, the materials that constitute the ACL and its structure. Hence allowing the mimicking of the dimension, the structure and to enable use of materials with similar mechanical properties as the ACL in new ligament implants.

The knee joint is one of the largest and most important joints in the human body. It consists of four bones (femur, tibia, patella and fibula); four major ligaments (anterior cruciate ligament, posterior cruciate ligament, medial collateral ligament and lateral collateral ligament); tendons; muscles around the joint; cartilaginous tissue in the medial and lateral meniscus and in the articular cartilage; and a joint capsule with synovial liquid in it. Figure 1.1 shows the components of the knee joint and their location.

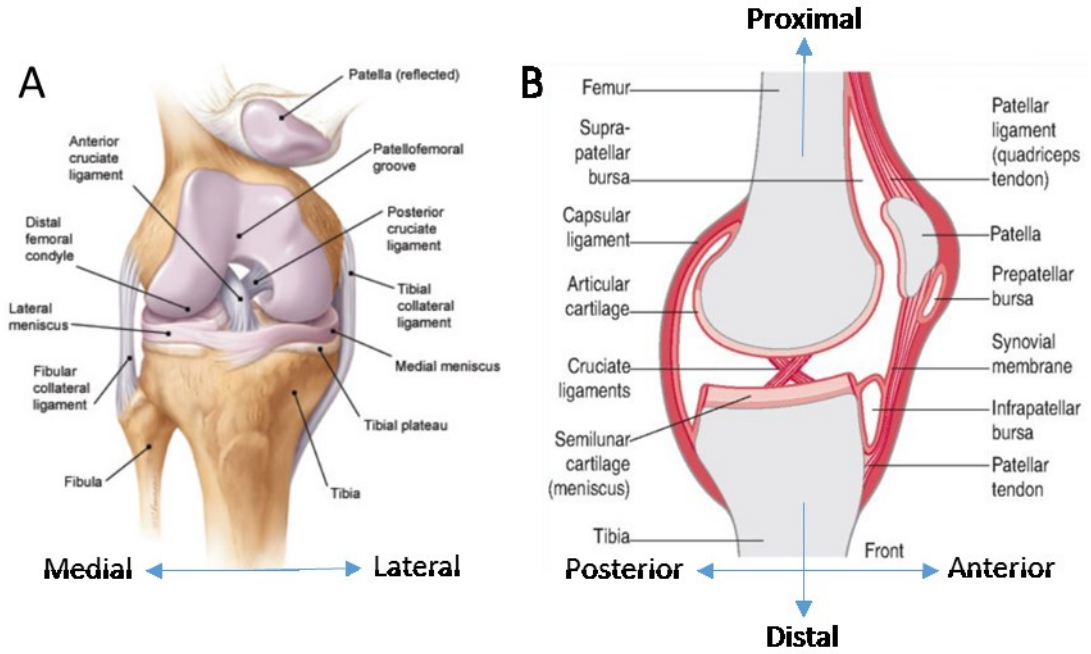

Figure 1.1Diagram of the knee joint A) Coronal plane B) Sagittal plane. Adapted from **[30]**

The anterior cruciate ligament (ACL) plays a key role in the articular mechanics of the knee connecting the tibia (anterior part of the intercondylar region) with the femur (slightly posterior to the medial surface of the lateral condyle) [31], [32]. It also plays a vital role in the stability of the knee and its biomechanics [33], restraining the anterior tibial translation and limiting the internal tibial rotation.

The ACL is an intra-articular and extrasynovial structure, located in the intercondylar notch of the knee (Figure 1.1 B) and enveloped by the synovial membrane [34]. The ligaments can be classified as extra-articular and intra-articular depending on their location. A membrane known as epiligament surrounds the extra-articular ligaments. This membrane contains cells, vascular irrigation and neural innervation; therefore, it can be considered to heal after an injury. The intra-articular ligaments are surrounded by synovial liquid; these type of ligaments have a low cell content, and poor vascularity and innervation, severely limiting their healing after an injury. [35] Figure 1.2 shows the difference between both ligaments.

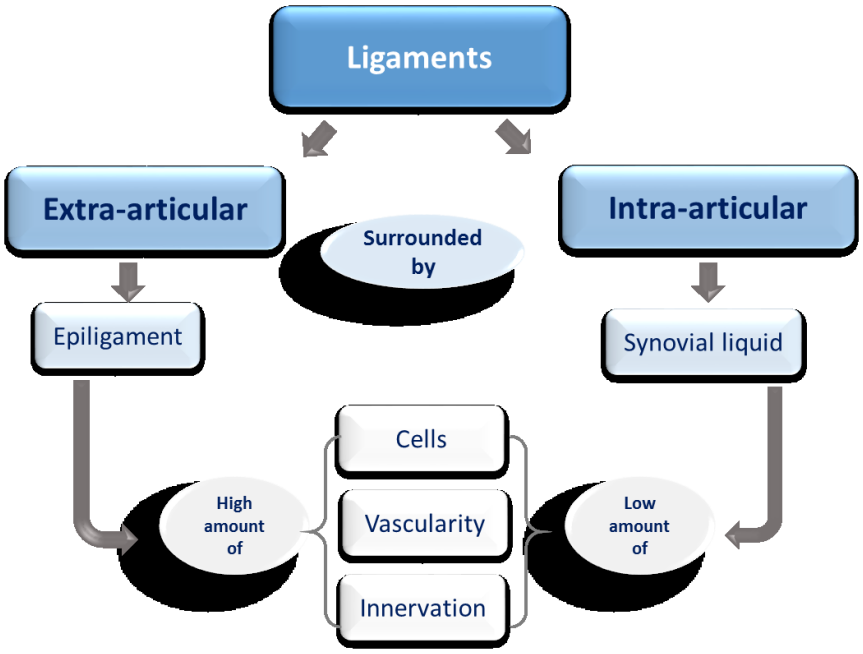

Figure 1.2 Ligament classification depending on location

The ACL is an intra-articular ligament with an abundance of collagen bundles but low vascularity and cellular activity [36], [37]. Therefore, the capacity of the ACL to regenerate itself is low and after a serious injury where the tissue is

damaged, surgery involving the use of an appropriate graft is often required to replace the ligament [22].

According to most authors who have studied the anatomy of the ACL, the ACL consists of two bundles of fibres (Figure 1.3): anteromedial (thinner) and posterolateral (main portion). These bundles, in turn, are made up multiple groups of fibres where each has a single origin and insertion point; they are not parallel, do not have the same length and therefore they are not under the same tension [16]. The hierarchical structure of ligaments and the components are explained in section 1.1.1.

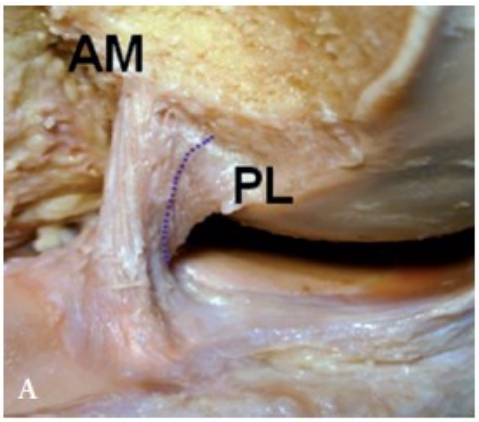

Figure 1.3 Anteromedial (AM) and posterolateral (PL) bundles of the ACL. Reproduced from **[33]**

Following on with the macrostructure of the ACL, the anteromedial bundle (AM) is formed by the fibres inserted into the proximal part of the femur and into the anterior and medial part of the tibia (Figure 1.4). Fibres that go from the most distal portion of the femoral insertion and are inserted into the posterolateral portion of the tibial anchoring constitute the posterolateral bundle (PL) [38]. The AM bundle restrains the anterior–posterior translation of the knee, while the PL bundle restrains the rotation of the knee [38]. This behaviour can be observed in Figure 1.4.

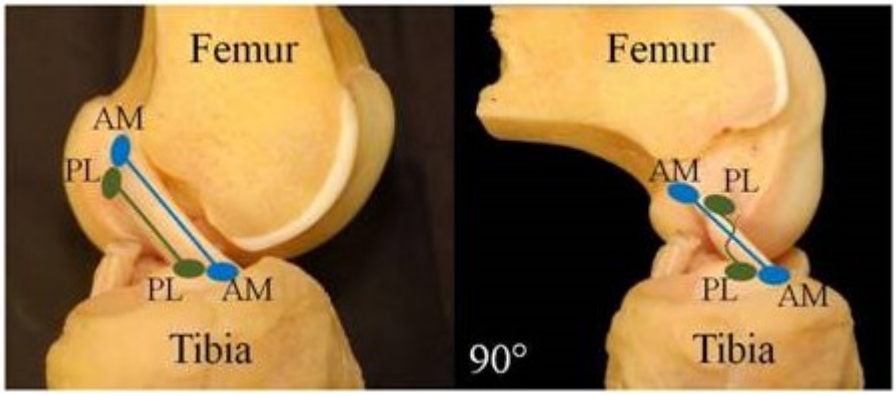

Figure 1.4 AM and PL bundle behaviour at 0º and 90º of flexion. Reproduced from **[39]**.

A key point in the design of new ACL implants is to obtain the average dimensions of the natural ACL in order to replicate those dimensions in future implants. Therefore, before explaining the micro and nano structure of the ACL, it is important to present the mean anatomical dimensions of the human ACL. These values are shown in Table 1.1.

Table 1.1 Mean anatomical dimensions of the human ACL

ACL length men (mm)	29	[40]
ACL length women (mm)	26.8	
Mean diameter of the ACL at mid-portion (mm)	6.1	[41]
ACL cross-sectional area (mm^2)	29.2	
Tibial insertion site length/width (mm)	13.4/11.1	
Femoral insertion site length/width (mm)	13.1/9.1	
Tibial footprint area (mm^2)	117.9	
Femoral footprint area (mm^2)	96.8	

The next section (section 1.1.1.) explains the general structure and components of the ligaments, and presents some morphological values of the human ACL relevant to the design of ACL implants.

1.1.1. STRUCTURE AND COMPONENTS

As an overview, ligaments are composed of dense bundles of collagen and elastin fibres that follow a specific hierarchy. This defines their mechanical behaviour and biological properties, since it offers elasticity, stiffness and an optimum environment for cell growth, proliferation, migration and differentiation [25], [42]. This hierarchical structure is shown in the figure below (Figure 1.5) and is explained through this section (section 1.1.1.).

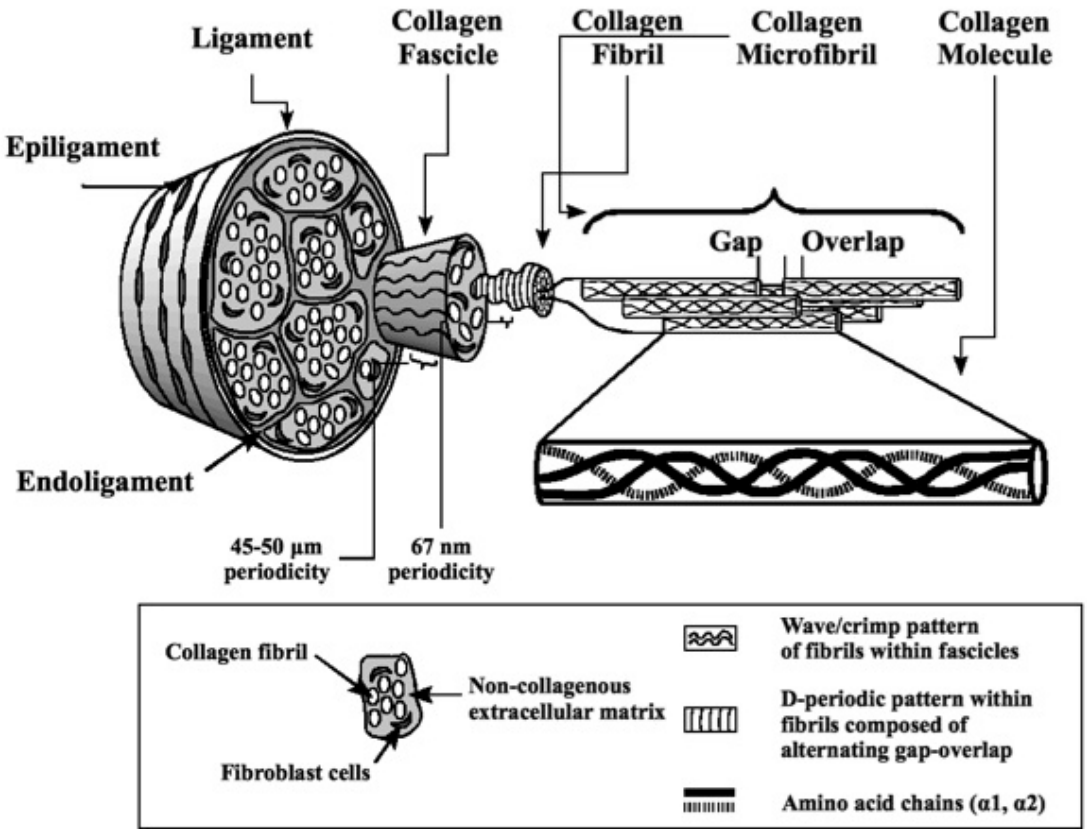

Figure 1.5 Hierarchical structure of the ligament. Reproduced from **[38], [39]**

Ligaments are mainly comprised of fibroblasts and extracellular matrix, which is composed of collagen, elastin and ground substance [25] as shown in Figure 1.6.

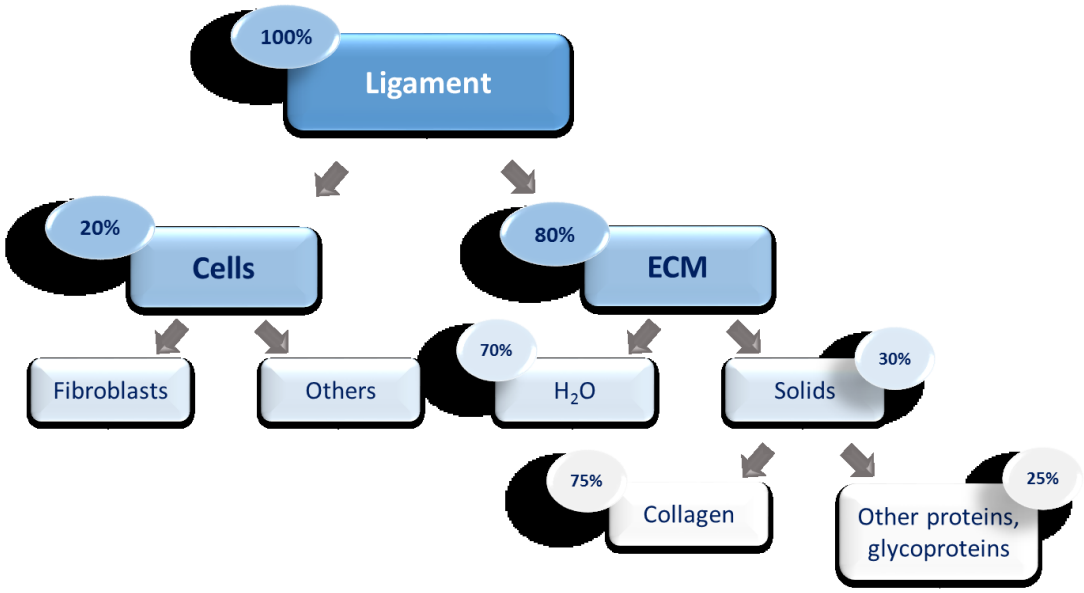

Figure 1.6 Composition of the ligament

Fibroblasts are few in number in ligaments, with approximately only 20% of these biological structures being composed of cells [43]. However, they are extremely important because they are involved in renewing both the ground substance and collagen fibres [25].

The **extracellular matrix** constitutes the major part of ligament volume and provides tensile strength and elasticity. Water is the principal component in ligaments forming 65-75% of the total volume. Considering the dry weight of the ligament, collagen is present in approximately 75% with a ratio of 9:1 between collagen type I and collagen type III. Fibrous elastin is found in values of between 10

and 15% and acid mucopolysaccharides (such as hyaluronic acid or chondroitin sulphate) are present in approximately 1% of the ligaments dry weight [25], [43].

- Collagen is a fibrous protein responsible for tensile strength and rigidity of the tissue. This protein has the property of self-assembly, and is presented organized at all levels, from microscopic to macroscopic. The collagen structural unit is tropocollagen, which comes from procollagen composed of three α polypeptide chains. Five tropocollagen molecules are joined to form the smallest ligament structural unit, the microfibril [25], [43]. The structure of the collagen is shown in Figures 1.5 and 1.7.

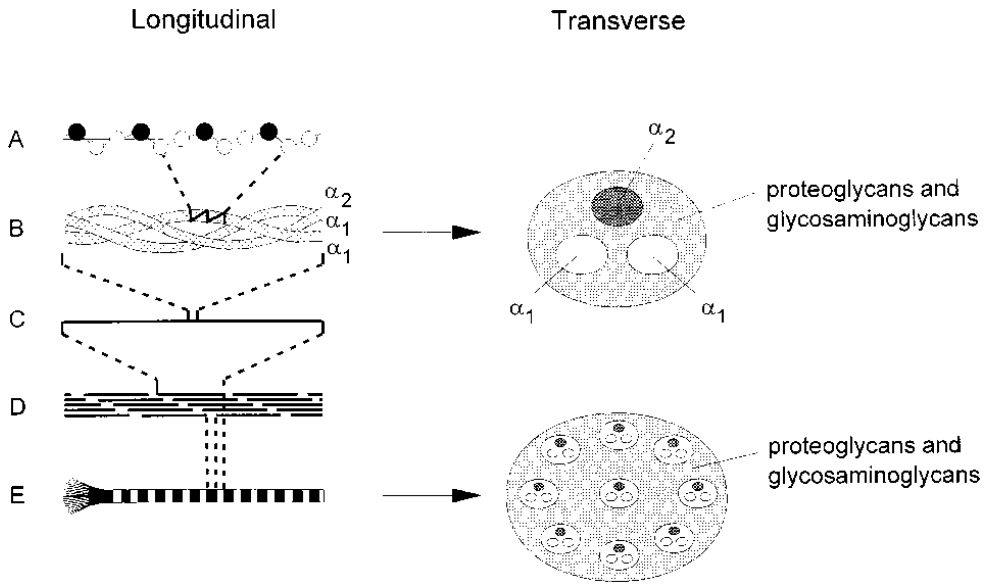

Figure 1.7 Collagen composition. Reproduced from **[42]**

Microfibrils are joined to form collagen fibrils. Fibrils are joined in bundles to create fibres adopting a crimped planar structure; when these fibres are subjected to a tensile loading they lose their crimped pattern to be oriented in the direction of the load. These fibres are joined in bundles to establish collagen fascicles, and the

bundles of fascicles constitute the ligament (Figure 1.5.). The connective tissue, which surrounds the fascicles, is called the endoligament. This tissue carries blood vessels, lymph vessels and nerves to the ligament and through it. The outer surface of the ligament is covered by a highly cellular fibrous layer called the epiligament [25], [43].

The diameter of collagen fibrils is 40-150 nm, the diameter of the fibres is between 1 and 20 μm and the fascicles have a diameter of 360 - 1500 μm in the natural human ACL [33], [44]–[47]. A SEM image of the fibres of collagen in the ACL is shown in Figure 1.8.

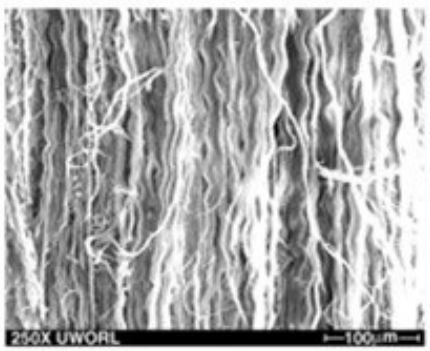

Figure 1.8 Collagen fibres of a natural human ACL reproduced from **[48]**

- Elastin is a stable and insoluble protein responsible for ligament elasticity. Although it is present in small quantities in ligaments, between 10% and 15% of the ligament dry weight, it is crucial to add elastic mechanical behaviour to the ligament's properties [25], [43] i.e. allowing the ligament to recover its original shape after being deformed.

- Ground substance is an amorphous matrix that surrounds the cells and fibres. It is mainly constituted of glycosaminoglycan chains (hyaluronic acid,

chondroitin sulphate 4 and 6) covalently bounded to different kinds of proteoglycans. Proteoglycans are present in small quantities, varying according to ligament location and load conditions. They are large negatively charged hydrophilic molecules that can store 50 times their weight of water and provide the collagen fibrils with a high capacity to resist large compressive and tensile forces. The proteoglycans also enable rapid diffusion of water soluble molecules and migration of cells [42] and give the viscoelastic behaviour of this tissue. Other important proteins that contribute to ligament and enthesis (connective tissue between ligament and bone) formation are tenascin-C and sox-9 which play a role in collagen fibre alignment and orientation [49].

Several growth factors (such as IGF-1, TGF-β, bFGF or GDF-5, -6 and -7) are involved in the activation, regulation of cellular response (such as cell proliferation, extracellular matrix elaboration or neovascularization) and in the expression of specific genes (Col I, Col III, Tenascin-C or Sox-9) that serve as markers for the detection of new ligamentous tissue generation [50]. The development and healing of ligaments can be checked through analysing the presence of these genes with a polymerase chain reaction (PCR) technique.

Key points:

1. The ACL is an intra-articular ligament with poor healing properties; therefore, once it is injured it is necessary to perform an ACL replacement to recover the stability of the knee, demonstrating the necessity of use of ACL implants.

2. The ACL is located inside the synovial capsule and surround by synovial liquid; therefore, in order to test new ACL implants in a similar environment to the natural ACL, mechanical tests should be done in wet conditions. These experiments will be shown in Chapter 6.

3. The ACL has an average length of 29 mm in males and 26.8 mm in females. These values will be used to validate the length of the ACL calculated in Chapter 3 and create scaffolds with similar dimensions in Chapters 4, 5 and 6.

4. The ACL consists of collagen fibrils of 40-150 nm in diameter, fibres of 1 and 20 μm in diameter and fascicles of 360-1500 μm in diameter. The structure of the ACL and dimensions will be replicated in the new ligament implants created in Chapter 6.

5. The main material that constitutes the ACL is collagen. Chapter 4 will focus on manufacturing scaffolds to be used as ACL implants with gelatin, a cheap polymer derivate from collagen and with similar mechanical and biological properties.

1.2. MECHANICAL BEHAVIOUR

Importance:

1. A ligament implant should ideally mimic the mechanical behaviour of the natural ligament, therefore its understanding and knowledge of its mechanical properties is crucial.

2. Different techniques are used to analyse the mechanical behaviour of the ACL. Knowing their limitations helps to determine the optimum approach to evaluate *in vivo* ACL forces and strain during daily and high impact activities.

Ligaments consist of a range of different proteins, which give them a heterogeneous character. Due to the orientation and the crimped pattern of collagen fibres they exhibit anisotropic and non-linear behaviour.

Specific aspects of mechanical behaviour and properties, such as elasticity, residual stress, creep, relaxation and hysteresis in ligaments will be explained in the next section 1.2.1.

1.2.1. General Mechanical Behaviour of Ligaments

1.2.1.1. Elastic properties

Ligaments act like "a spring" storing the motion energy, and efficiently transferring the force to the bone with minimal loss of energy [25]. However, they also have viscoelastic behaviour and their stress-strain curve shows three different areas, as it can be observed in Figure 1.9.

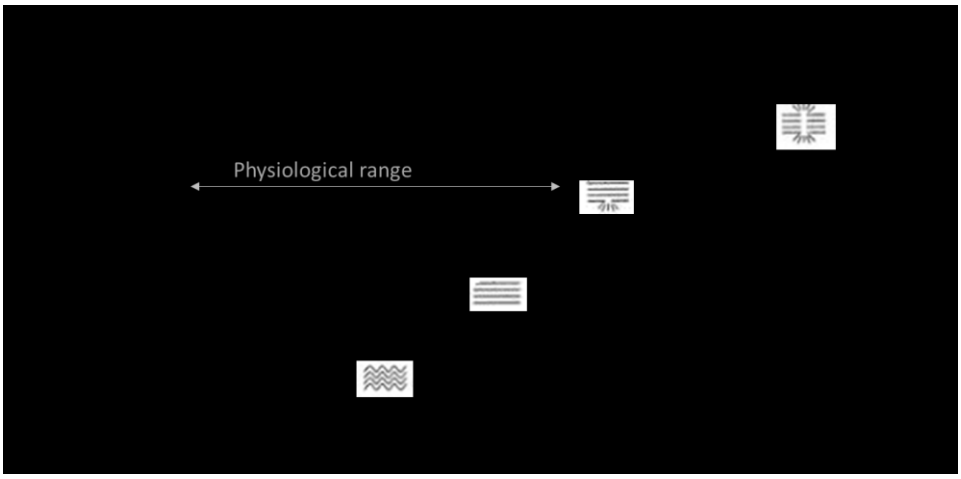

Figure 1.9 Stress-strain curve for ligaments. Reproduced from **[51]**

- Toe region corresponds to the physiological range where ligaments normally operate and where the elastic behaviour allows a deformation of 4% [25], [52]. This behaviour is due to the crimped nature of collagen fibres (Figure 1.9), since the crimp pattern of the fibres in this region are straightened in the direction of the applied load and recover their structure once the load has been removed.

- Linear region is the part of the curve where fibres lose their crimped pattern and if the stresses exceed the physiological range, the fibres begin to suffer micro-breakages. The Young's modulus of the ligament is calculated by taking the gradient from this linear region at certain strain values [25], [52].

- Breaking region is the part of the curve where the relationship between stress and strain is no longer linear, causing disruption of the fibres in the fascicles and finally tissue disruption [25], [52].

1.2.1.2. Residual stress

Ligaments are not free of stress at their unloaded configuration (when they are not subjected to any load), they present residual stress; this phenomenon can be observed when their insertion sites are dissected, since size and geometry of the ligament change to reach an equilibrium state free of tension (shortening and widening the fibres of the damaged ligament) [52].

The origins of these stresses are growth, remodelling or damage of the ligament generated throughout life.

1.2.1.3. Time dependent properties

Ligaments exhibit viscoelastic behaviour where the relationship between stress and strain is not constant but varies with the time, displacement and load [53]. Moreover, ligaments undergo phenomena of strain rate, creep, force relaxation and hysteresis due to the interaction between the viscous proteoglycan matrix and the collagen fibres [53].

Some studies have demonstrated that if strain rate increases the Young's modulus and maximum stress also increase and above the linear load point a maximum load, strain and energy to failure are observed [54], [55].

Creep is another phenomenon shown in ligaments. This can be observed when a constant force is applied to a ligament, since this force causes a progressive lengthening of the tissue over the time (Figure 1.10); in other words, the deformation of the ligament increases under constant load [53], [55].

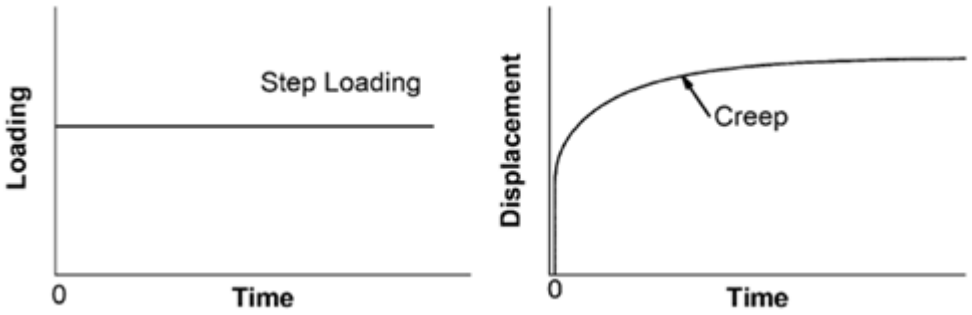

Figure 1.10 Creep behaviour. Reproduced from **[56]**.

If the length of the ligament is fixed at the peak strain, the force applied decreases over time. The more rapid the strain rate is, the larger peak force and greater the relaxation is; in other words, the stress is reduced under a constant deformation. This phenomenon is called force relaxation and is characteristic of ligaments (Figure 1.11) [53], [55].

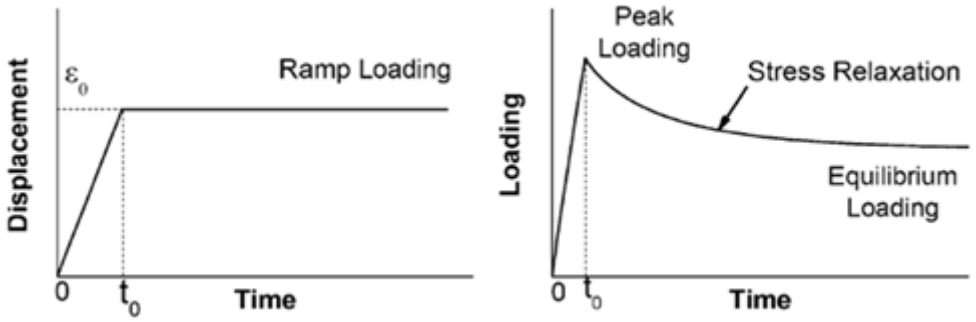

Figure 1.11 Force relaxation. Reproduced from **[56]**.

Hysteresis is another time-dependent property of ligaments. This property can be observed when loading and unloading cycles are performed at a constant strain rate. The area between both cycles is the dissipated or lost energy during the test and indicates the viscoelasticity of the tissue (Figure 1.12) [53].

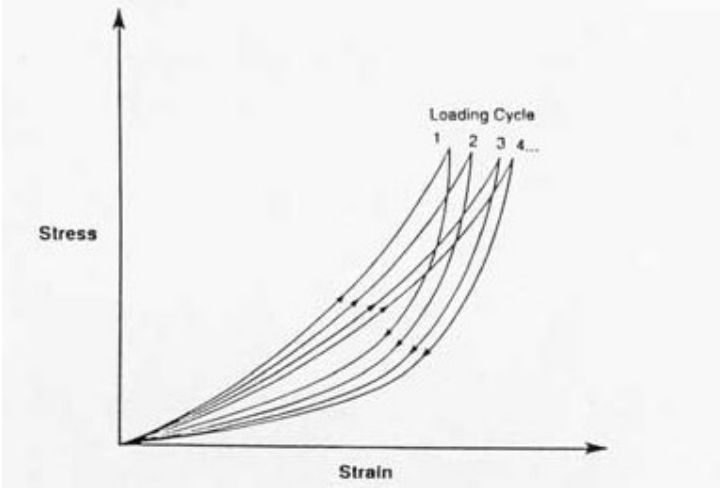

Figure 1.12 Hysteresis. Reproduced from **[57]**.

1.2.2. ACL MECHANICAL PROPERTIES

Few investigations have been performed in order to determine the ACL mechanical properties through tensile testing of isolated ACL specimens [58]–[61]. This point was underlined in a recent paper by Mclean *et al.* in 2015, where the paucity of ACL tensile data was reported in a literature review paper about ACL mechanical properties [62].

Parameters such as strain at failure, ultimate tensile stress or Young's modulus have been found in four studies [58]–[61]. Noyes *et al.,* studied the mechanical behaviour of ACLs from humans and rhesus monkeys [59]. This study proved that the ACL mechanical properties vary between species; for example, the

ultimate tensile strength in young adult monkeys was 66.1 MPa and in young adult humans (age: 16-26 years) was 37.8 MPa. The ACL Young's modulus in monkeys was reported as 186 MPa, but was reported as being lower in humans, at 111 MPa.

Chandrashekar *et al.,* studied the differences in the mechanical properties of the ACL between genders in 2005 [60]. 8 male ACLs (age: 26-50 years) and 9 female ACLs (age: 17-50 years) were mechanically evaluated. The ultimate tensile strength of 26 ± 10 MPa was reported for male ACL and 23 ± 9 MPa reported for female ACL. Regarding male ACL Young's modulus, this was reported as 128 ± 35 MPa and for female 99 ± 50 MPa. Therefore, this study concluded that gender is an important factor for the study of these properties.

A more recent study evaluated the ACL mechanical properties in a porcine model [61]. This study analysed 15 porcine ACLs and determined a modulus of elasticity of 148 ± 62 MPa and an ultimate tensile strength of 32 ± 16 MPa. However, as highlighted by Noyes *et al.* [59] the species influence on the mechanical properties of the ACL should be considered in the design of ACL implants for humans.

Currently, values for the mechanical properties of the ACL reported in Noyes *et at.* and Woo *et al.* [58], [59] in the 70's and 90's are still used as landmark papers to evaluate ACL implants [63]–[69]. Specifically, a Young's modulus of 111 MPa and ultimate tensile strength of 38 MPa are well recognised and used in many publications in the field [63]–[69], these values will therefore be used throughout this thesis to evaluate the the ACL scaffolds developed in this project.

Table 1.2 summarizes the mechanical properties of the ACL found in the studies previously cited [58]–[61].

Table 1.2 ACL mechanical properties

Characteristics of the specimens	Elongation at failure (mm)	Strain at failure	Load at failure (N)	Stress at failure (MPa)	Stiffness (N/mm)	Modulus of elasticity (MPa)	References
Human n=6, age: 16-26 years	11.91	0.44±0.08	1730±66	38±9	182±56	111±25	[59]
Human n=9, age: 22-35 years	9.99		2160		242		[58]
Human n=17, age: 17-50 years	8.17±2.41	0.28±0.07	1526±658	24±9	250±102	113±45	[60]
Porcine n=15	8.67±1.70	0.32±0.08	853±252	32±16	147±30	148±62	[61]

1.2.3. ACL MECHANICAL BEHAVIOUR

A substantial number of research studies have been performed to quantify the ACL mechanical forces and strain [40], [70]–[73], [73]–[105], when the ligament is subjected to specific knee angles, elongations, loads or different activities are performed.

Hashemi *et al.* [40] developed multi-linear regression models to predict ACL stiffness, energy, load and elongation at failure from anthropometrical parameters (ACL size, height, weight and body mass index), age and gender. This study used cadaveric knees to obtain information about the ACL size (length, minimal area and volume) and to test the ligament to failure in order to build the regression models. The conclusion of this study was that gender, age, weight, BMI, and height contributed ($p<0.05$) to all predicted structural properties. The smallest cross-

sectional area of the ACL along its length was a contributor to elongation at failure, energy at failure and linear stiffness ($p<0.05$), but not to load at failure. ACL volume was also a contributor to elongation and energy at failure ($p<0.05$), but not to linear stiffness and load at failure models. However, ACL length was not a significant contributor to any structural property [40].

Other techniques have used robotic technology to examine knee kinematics and estimate ACL tensile forces and strain by testing the specimen under certain conditions to mimic physiological knee positions [88], [89], [105]. This technique reproduced positions of physiological knee motion and calculated the change in forces experienced by the ligament [90]–[93]. Woo *et al.* (2000) [105] reported a maximum force in the ACL of 111 N when an anterior tibial load of 100 N is applied, and this ACL force decreased as the flexion angle increased. 10 Nm internal tibial torque and a combined 10 Nm valgus and 10 Nm internal tibial torque were applied to intact and the ACL-deficient knees for different flexion knee angles in Kanamori *et al.* [89]. This study concluded that the ACL plays an important role in restraining anterior tibial translation and internal tibial torque, especially when the knee is almost full extended [89]. Although robotic technology is very useful to estimate *in vitro* ACL forces and strain, limitations were exhibited in reproducing the *in vivo* mechanical behaviour of the ACL. The main issue with this technology was that these studies estimated the ACL forces by applying anterior tibial loads or rotational moments to the knee joint. However, the ACL is likely to bear higher forces during *in vivo* activities than the forces measured *in vitro* due to the muscle forces not being taken into account when determining the loading in the knee [94]. Other limitations of these studies include the difficulty in obtaining knee specimens

from healthy younger donors and consequently the difficulty in comparison between the *in vivo* ACL mechanical behaviour in younger and older donor [94].

Recently, the interest in establishing the *in vivo* ACL mechanical behaviour, joint kinematics and ACL injury mechanisms has increased, and other methods using video, motion capture techniques, strain gauges, fluoroscopy and computational models have been developed in order to create new prevention programs or estimate *in vivo* forces and ACL elongation [70]–[79], [95]–[99].

Joint kinematics and ACL injury mechanisms have been studied by video and motion capture techniques [70], [71], [95]–[97]. A systematic review of video analysis of ACL injuries was performed in Carlson *et al.* [96] where it was identified that a combination of decreased ankle plantar flexion, decreased knee flexion, and increased hip flexion provoked high-risk of ACL injuries during landing. Video analysis leads to enhanced understanding of non-contact ACL injury; however, this technique was solely used to estimate kinematics and dynamics for the knee joint and they were not used to estimate *in vivo* ACL length, strain or tensile force.

To evaluate the *in vitro* ACL strain [72] and *in vivo* ACL strain in cycling [73], stair climbing [106] and squatting [74], strain gauges were also employed. Fleming *et al.* (1998 and 1999) [73], [106] evaluated the ACL strain during cycling and climbing stairs for different machine powers and cadences. These studies concluded that strain values increased as the knee was moved from a flexed to an extended position [106] and no significant differences were found in peak strain values as a result of changes in power level or cadence [73]. This technique has the

limitation of being invasive, since it requires surgery for gauges to be implanted on the ACL, and the gauge is attached to only a small location of the ACL, not recording the strain across the whole ligament.

Experiments with motion capture and biplanar fluoroscopy [75], [76] have been used to calculate the ACL length and knee kinematics during walking and jumping. Taylor *et al.* (2013) [75] concluded that the strain in the ACL peaked at 13 ± 2% during mid-stance walking when the knee was near full extension. The peak ACL strain was found at 12 ± 7% when knee flexion angles were lowest during jumping [76]. However, these models developed to estimate the ACL strain only had a 1 degree of freedom (DOF), therefore the results can be subjected to inaccuracies due to failure to take account of movement of the knee in other planes. One of the main concerns of the fluoroscopy technique, though, is the high radiation doses that the participants would be subjected to. Moreover, the activities that can be studied using this technique are limited, as its configuration only allows movements performed within a confined space to be analysed.

Studies with motion capture and musculoskeletal simulations studied the kinematics and dynamics of different joints [98], [99] and determined ACL length and strain during walking and jumping with both legs [77]–[79]. Kar *et al.* [77] found averaged peak strains of 12 ± 4% in the right and 12 ± 3% in the left ACL during jumping. Xu *et al.* developed a 3 DOF knee OpenSim model to simulate the mechanical behaviour of the knee ligaments differentiating between the anterior and posterior bundles of the ACL and PCL (posterior cruciate ligament) [78]. These studies moved the research in the field forward developing models with more than 1

DOF for the knee; however, they do not evaluate the ACL length and force for activities associated with high injury rates such as jumping with one leg or crossover cutting. Chapter 3 used these techniques to estimate *in vivo* ACL length, strain and forces for those activities, filling the gap existing in the literature.

Table 1.3 summarizes the different existing methods u estimate the mechanical behaviour of the ACL with some of their limitations.

Table 1.3 Techniques to evaluate the ACL mechanical behaviour with their limitations.

Techniques			Limitations
Cadaveric knees+Robot			1. No *in-vivo* mechanical behaviour evaluated. 2. It is not possible to estimate ACL forces, just changes of ACL forces are estimated 3. Little availability of knee specimens from healthy younger donors
In-vivo mechanical behavior	Strain gauges		1. Invasive and requires surgery. 2. Gauge only measures the strain in a small location of the ACL.
	Motion capture +	Video	1. Do not study *in-vivo* ACL length, strain or tensile force.
		Biplanar fluoroscopy	1. Fluoroscopy is an invasive technique that involves high radiation doses. 2. Only movements performed within a confined space are studied. Therefore, these studies are limited to static trials or activities with short horizontal displacements.
		Musculoskeletal simulations	1. No studies performed during cutting or jumping with one leg.

Some studies reported peak values of percentage of ACL strain of 2.8 % during climbing stairs [106], 2% during cycling [73], up to 4% for squatting [74], and up to 2% during a forward lunge [84]. Regarding peak values of ACL tensile force, Shelburne *et al.* (2005) reported 303 N during walking on level-ground [79] and 20 N for dynamic squats [86]; these values were calculated through a 2D dynamical model simulating muscle and ligament loading. Other investigations reported between 0 N [81] to 95 N [100] for dynamic squats, 253 N was recorded for

double foot drop landing [101] and 1294 N for single-leg landing from running to stop [87].

Some studies reported peak ACL forces of 0.2 N/BW [102], however other investigations showed values higher than 1 N/BW [103], [104] during walking. Therefore, disparity of results was observed for the same activity. If different researchers reported varying values of ACL forces and strain, this introduces problems in comparing those values between different activities. This is due to the wide range of techniques used to determine *in vivo* ACL strain and force and the limitations associated with each technique.

Therefore, it is necessary to develop and implement a reliable and easy methodology to investigate different activities in one study to allow valid comparison and so write new rehabilitation protocols, new prevention programs to avoid ACL injuries or design new ACL implants that can bear the *in vivo* ACL forces and strain estimated. Observing the limitations of each technique to estimate the *in vivo* ACL mechanical behaviour, a motion capture in combination with a musculoskeletal model was used for the development of this thesis and it was explained in Chapter 3. This technique allows calculation of the *in vivo* forces and strain for multiple activities, including high impact activities such as crossover cutting, sidestep cutting or jumping with one leg, activities for which *in vivo* ACL forces and strain have not been studied to date. The next following sections (1.2.3.1 and 1.2.3.2) explain the basic concept of this technology.

1.2.3.1. Motion capture

The movement of objects or people can be recorded through a motion capture technique, which is based on the use of retroreflective markers whose movements are tracked by infrared cameras such as the one shown in Figure 1.13.

Figure 1.13 Vicon infrared camera.

Before experimentation, a calibration process has to be performed. This process allows the software to calculate the location and orientation of each camera. There are two steps for the calibration, a first static calibration where the origin or centre of the capture volume and orientation is determined and second dynamic calibration where the relative positions and orientations of the cameras are calculated through the movement of a calibration wand throughout the whole volume of study [107].

Reflective markers are attached to the participants to record the movements of the different segments of their body (head, chest, arms, pelvis, legs, knees and feet). Each marker should be visible to at least two cameras to accurately calculate its position. The displacement can be recorded with one marker, the use of two markers allows the calculation of velocity and acceleration and the system can calculate joint

angles with three markers [108]. The location of the markers is given by protocols, the most commonly used being the Helen Hayes market set and the Cleveland Clinic marker set. In Chapter 3 a modification of the Cleveland Clinic marker was used following the recommendations of OpenSim (Sim TK, Stanford, CA) web page [109]. The model with the marker set used is shown in Figure 1.14

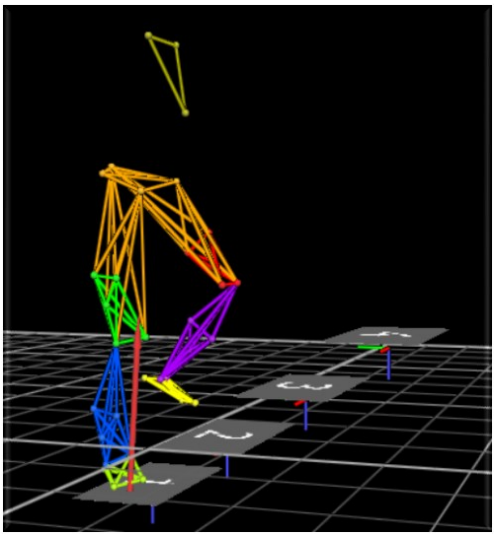

Figure 1.14 Vicon/Nexus model for stair negotiation.

Once the position of each marker is tracked, the coordinates of each marker were used to calculate the kinematics and dynamics with a musculoskeletal model implemented in OpenSim 3.3 (Sim TK, Stanford, CA).

1.2.3.2. Musculoskeletal model

OpenSim is a software capable of creating musculoskeletal models to analyse the *in vivo* behaviour of muscles, tendons and ligaments (Figure 1.15 shows the model during a static trial, stair negotiation and crossover cutting trials).

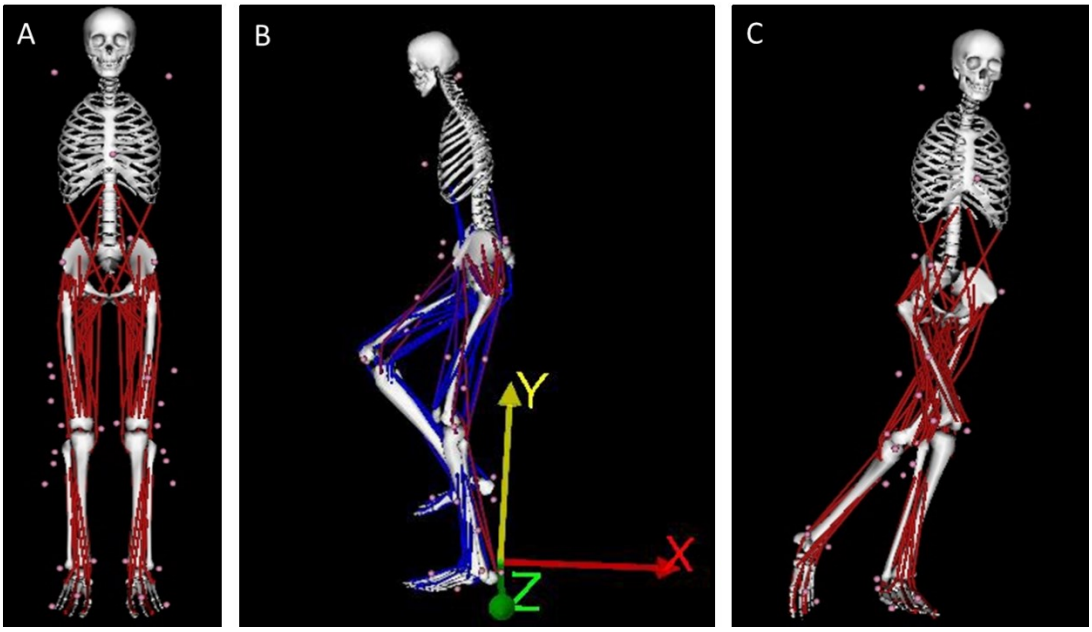

Figure 1.15 OpenSim models during A) Static trial, B) Stair negotiation and C) Crossover cutting.

OpenSim contains different tools to enable calculation of kinematics and dynamics. An understanding of the theory behind these tools is fundamental in the development of Chapter 3 of this thesis; therefore, the function of each tool is explained below. It should be noted that this section 1.2.3.2 does not constitute a methodology of the studies performed in Chapter 3, but rather a background for the use and development of OpenSim models more generally.

1.2.3.2.1. Scaling

A model is scaled thanks to a combination of two methods, the "measured-based scaling" where the distances between experimental and virtual marker positions are measured, and "manual scaling" where scale factors obtained from anthropometric measurements are used. Experimental markers are placed on specific landmarks of participants' body and their x-y-z positions are obtained from static calibration with a motion capture system. For the "measured-based scaling" a non-

scaled model with a set of virtual markers is required. These virtual markers are located at the same anatomical positions as the experimental markers, and the dimensions of each segment, muscles and ligaments are scaled matching the distances between virtual and experimental markers. Another alternative included in the scale tool implemented in OpenSim is to scale each segment of the model from anthropometric measurements; as it was indicated above; this technique is called "manual scaling" [110].

1.2.3.2.2. Inverse kinematics

With a motion capture system it is possible to track the experimental marker locations while the participants are performing an activity. The inverse kinematics (IK) tool is able to calculate joint displacements and angles from collected experimental data. For each time frame this tool computes the coordinates and positions the model in a pose that "best matches" experimental marker positions with the coordinate data, minimizing the sum of weighted squared errors of markers and coordinates [111] and obtaining the kinematics of the model.

1.2.3.2.3. Inverse dynamics

The inverse dynamics (ID) tool is necessary to validate the muscle function in the computational model. This tool is able to calculate joint forces and moments from the inverse kinematics file previously generated and a ground reaction forces (GRF) file obtained from force platform data, generated while the participants were performing the activities [112].

1.2.3.2.4. Static optimisation

Once the joint forces and moments were calculated from inverse dynamics tool, these parameters feed into the model to determine muscle forces and activations at each instant in time through static optimisation [113].

The activation of certain muscles obtained from the model can be qualitatively compared with the activation of these muscles recorded with electromyography sensors in order to validate the muscle function in the model.

1.2.3.2.5. Analysis tool

In order to calculate the ACL length at each instant in time and so to be able to calculate the ACL strain and force, an analysis tool implemented in OpenSim is used. This tool enables the users to perform muscle analysis to calculate parameters such as total muscle, fibre or tendon length; muscle, fibre or tendon force; velocities; pennation angles; moments or moment arms [114].

With this tool it is possible to track the insertion points of the ACL obtained from kinematics data and estimate the *in vivo* ACL length modelling the ligament as a nonlinear elastic passive soft tissue based on Thelen2003 [115] muscle model.

Key points:

1. The ACL exhibits a stress/strain curve with three very clearly defined regions: a toe region, a linear region and a breaking region. Different polymers will be used in Chapters 4 and 6 in order to replicate this behaviour.

2. The Young's modulus of the ACL is 111 MPa and the ultimate tensile stress is 38 MPa. These values will be used in Chapters 4, 5 and 6 to assess the manufactured scaffolds.

3. Hysteresis is a time-dependent property of the ligaments. This property will be tested in Chapter 6.

4. Different techniques have been used to understand the ACL *in vivo* mechanical behaviour and calculate the elongation and forces acting over it while different activities are performed. However, there is not any reliable and easy methodology to investigate different activities in one study to allow valid comparison, and to produce mechanical specifications in order to design ACL ligaments according to the *in vivo* mechanical behaviour of the ACL. This gap in the literature will be covered in Chapter 3 following the motion capture in combination with a musculoskeletal model technique explained in this section.

1.3. ACL INJURY MECHANICS

Importance:

1. The understanding of ACL injury and failure mechanics will help to design new ligament implants, new rehabilitation protocols and prevention programs to reduce the risk of injury.

The ACL has a fundamental role in the stabilization of the knee restraining the anterior tibial translation and internal rotation in the non-weight-bering knee [74], [116]. It has an estimated failure load of 2000 N, Young's modulus 111 MPa and ultimate tensile stress of 38 MPa [59] as shown in section 1.2.4.

ACL injuries usually happen under dynamic loading, with 78% of the injuries occuring during non-contact activities such as crossover cutting, side step cutting or landing from a jump [4]. The highest rate of ACL rupture is registered during sports such as football, basketball and skiing. It is known that this type of injury occurs during sudden accelerations, changing directions, and when decelerating from running with change in direction or landing [4]. The typical ACL injury occurs when the knee is at 30° flexion in a valgus position and the participant internally rotates the knee with the planted foot, when suddenly changing direction [117], [118]. However, the ACL injury mechanisms are complex (since the accident that provokes injury is fast, dynamic and multiple factors are involved, and the knee is a complex joint that

allows compression, translation and rotation in different axes [119]) and further investigations have to be done.

Although nowadays the specific ACL injury mechanics remain unclear, ACL injury risk factors have been detected and studied [120]–[128]. The ACL injury risk factors are classified as intrinsic and extrinsic [120], [121] and the intrinsic in turn modifiable and non-modifiable. A scheme with all of the known risk factors is presented in Figure 1.16. The knowledge and identification of risk factors is important for the development of injury prevention programs, which could reduce the risk of ACL injuries. Certain studies considered as ACL risk factors the increment in knee valgus moment, quadriceps muscle activation or the anterior tibial shear force [123]–[125]. Specifically, Hewett *et al.* [121] reported that the knee valgus moment is a predictor of risk of ACL injury. However, it was demonstrated that knee the valgus moment on its own cannot injure the ACL when the medial collateral ligament is not damaged [129].

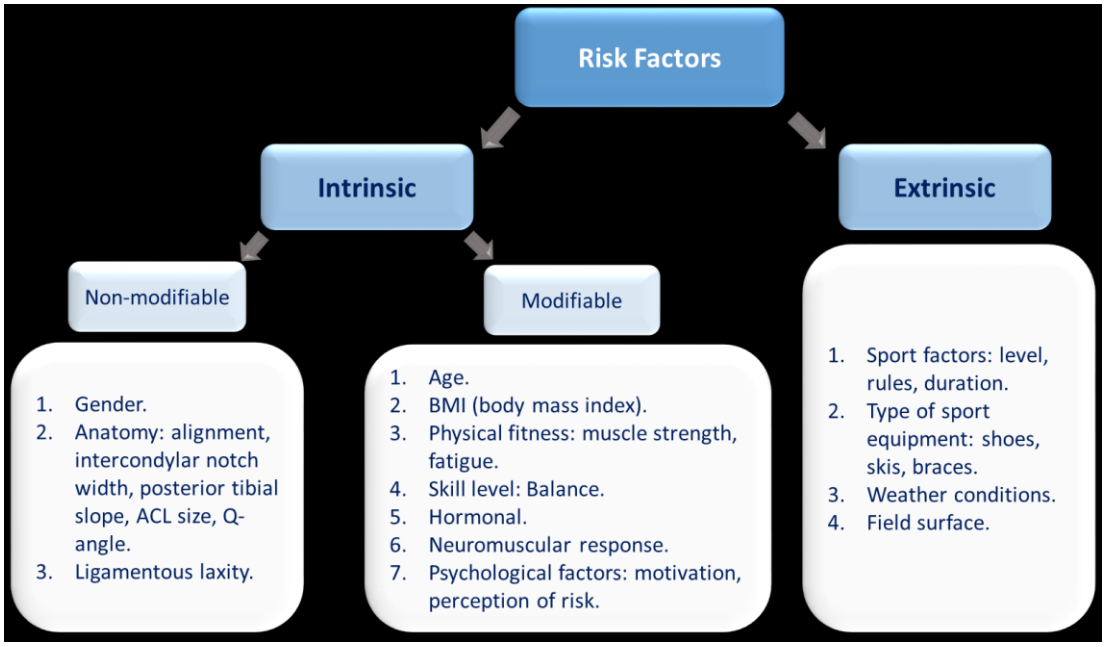

Figure 1.16 ACL risk factors.

The ACL injury is commonly called a sprain and can be classified as a grade I, II and III, depending on the clinical symptoms. Grade I sprain exhibits a minimum loss of function, minimum pain and inflammation, the fibres are stretched but no tears are observed, the knee is still stable and there is no haemorrhage. Grade II sprain occurs when the fibres are partially torn, there is a moderate swelling with some loss of function; an increase in an anterior translation of the tibia and an unstable knee. Grade III sprain presents a complete rupture of the ACL, significant loss of articular function generating instability of the knee, severe inflammation and pain [53], [130], [131].

The tearing of the ACL from its bony insertion points is called avulsion. Avulsion is more common in children rather than adults, because it occurs between unmineralized and mineralized fibrocartilage layers shown in children. Midsubstance ACL ruptures commonly happens in adults [53].

ACL injuries are diagnosed through physical assessment (with Lachman's test, anterior drawer test or pivot shift) to detect an abnormal anterior translation of the tibia; through radiographs, to check the presence of bone bruising, osteochondral fracture or to determine the notch width index (a person with ACL injury has smaller notch width index than normal) [132]; and through magnetic resonance imaging (MRI) to observe the damaged ACL.

Not all ACL injuries are surgically treated. The choice of undergoing surgery highly depends on the severity of the rupture of the ACL, the patient's symptoms, sport level and type of sport that the patient wants to keep doing [133]. Non-operative treatment or conservative treatment is recommended in grade I and grade II injuries where the knee partially maintains its stability and the injured part of the ACL remains functional. This treatment is based on physiotherapy and many patients can have asymptomatic knees following rehabilitation programs [133].

Key points:

1. The ACL is one of the most important stabilizers of the knee joint, restraining the anterior tibial translation and internal rotation of the knee. This fact was also verified with a computational model developed in Chapter 3.
2. 78% of the ACL injuries occur during non-contact activities when sudden accelerations, changes in direction, decelerations when running with changes in direction or landing are present. Chapter 3 studied the ACL biomechanics during daily (walking, climbing stairs) and high impact activities (crossover and side step

cutting, running, jumping or landing) to be able to understand more about ACL injury mechanics.

1.4. STATE OF THE ART FOR ACL IMPLANTS

Importance:

1. It is known that the failure rate of current treatments for ACL replacement is still high; therefore, further study is needed to determine the causes of failure and create new ligaments that can address and solve these issues.
2. Understanding the advantages and disadvantages of current treatments will help to design the new ligaments maintaining the advantages and reducing the disadvantages of current grafts.

The "gold standard" to treat ACL injury is to reconstruct the ACL from autografts (grafts from the patient's own body) [134]. More than 90% of the reconstructions are carried out with bone-patellar tendon-bone or hamstring tendon grafts but quadriceps tendon and iliotibial bands have been also used to replace the ACL [22]. Although the use of autologous grafts is the most common practice, this exhibits an important number of drawbacks among which are notable muscle weakness at the donor site, graft site morbidity, knee pain, infection, loss of sensibility due to nerve damage and long operation and rehabilitation time [22], [25].

Allografts (tissue taken from a cadaver) and xenografts (tissue removed from an animal) are also used for ACL reconstructions as an alternative to autografts when these are not available due to damage or from being used in a previous reconstruction. Due to the lack of young healthy cadaver donors, the Achilles tendon and the anterior tibialis and posterior tibialis tendons are also used to performed ACL replacements. Although some disadvantages of the autograft are solved through allografts such as the donor site morbidity and the necessity of a previous operation to harvest the tissue, other drawbacks are associated with the use of these specific grafts. Some of these limitations include: the possibility of transmitting diseases, risk of bacterial infection and an immunological response, limitations in the availability of donor tissue and difficulties with the sterilization of the graft, factors/conditions that could damage the graft and reduce its mechanical properties [135]. However, the major risk and disadvantage in allografts and xenografts is the transmission of infectious agents from donor to host [135], [136], therefore the sterilization technique plays a crucial role in the success of the ACL replacement. Techniques such as gamma irradiation, ethylene oxide gas, thermal treatment, beta-propiolactone, chemical processing, antibiotic soaks and Biocleanse have been used to sterilize allografts [136]. Ethylene oxide sterilization, however, is associated with high graft failure rates and persistent synovitis, therefore is not a suitable method for sterilization of allografts [135], [137]. Irradiation is the most frequently used sterilization technique; however, the use of this technique results in the loss of mechanical properties because it damages collagen fibres and causes changes in crosslinks of collagen [138]–[142]. An alternative to irradiation is the BioCleanse technique (Regeneration Technologies Inc., Alachua, FL), which involves chemical

sterilization of tissues. Conrad *et al.* reported that tendon allografts, treated them this way, exhibited higher ultimate stress and higher ultimate failure load than irradiated allografts [135]; however, Indelicato *et al.* [143] studied this technique for bone-patellar tendon-bone ACL allografts and concluded that non-significant differences were observed between allografts treated with BioCleanse and non-irradiated allografts.

Xenografts show the same advantages and disadvantages as allografts, but the risk of disease transfer is higher when the tissue is transferred from one species to another [144]. However, the main challenge for the use of xenografts is to deal with the immunological rejection [26], [27]. This immunological rejection is associated with the presence of α-galactose (α-Gal) found in the cellular and extracellular matrix of almost all mammals with the exception of humans and old world primates, who produce anti-α-Gal antibodies triggering the rejection of the graft [26], [27]. In order to reduce this risk of rejection and make them viable to be implanted in the body the tissue has to be cleaned, the α-Gal epitopes (part of the antigen recognized by the immune system) removed enzymatically, stabilized with 0.1% glutaraldehyde (GTA) and sterilized by electron beam radiation at 17.8 kGy [26], [27]. This increases the cost of the graft and incorporates toxic chemicals with possible residual components leaching into surrounding tissue. In 2014 Aperion Biologics Inc (San Antonio, Texas, USA) was granted the CE mark approval for Z-Lig®, the first porcine xenograft created for ACL replacement [27], [145]. The Z-Lig® xenograft was tested in skeletally mature monkeys with serological analysis to identify the immune response, by mechanical testing to assess performance, and through histopathological analysis to assess biological response and remodelling [27]. The

results from the preclinical performance and safety profile were promising after a twelve-month observation. The porcine xenograft was functional, the vascularization and synovial sheath were re-established, there were no signs of degenerative articular changes or adverse synovial reaction, bone consolidation was found inside the bone tunnels, the ultimate failure load increased over time at a similar rate to the allograft and no adverse findings emerged from standard clinical chemistry, serological, and haematological panels [27]. A first clinical trial was performed with humans and showed similar results.

Synthetic ligaments were designed to overcome the disadvantages found in the biological grafts, eliminating issues such as donor site morbidity, transfer diseases and long operation times. However, this type of implants have shown a lack of biocompatibility and although they retained mechanical properties similar to the natural ACL at short-term, they failed long-term mainly due to fatigue of the graft, but also laxity, stiffness, infection, synovitis and tissue degeneration, mechanical failure and re-rupture of the graft [25], [28].

Synthetic ligaments can be classified into three main groups: non-biodegradable implants, which are not designed to have any soft tissue ingrowth; ligament augmentation devices (LADs), designed to protect the implanted autograft and enhance its revascularization and maturation; and tissue engineered scaffolds, designed to encourage/promote the ingrowth of native tissue.

The first ACL reconstruction with synthetic grafts was performed in 1903 with an implant based on braided silk attached to the semitendinosus [146]. A silver

filament was used for ACL replacement in 1914 [147]. Advances in the chemical industry and in biomaterials allowed the development of permanent ACL implants made with more suitable materials such as carbon fibre, polyester, polytetrafluoroethylene and polypropylene in the 1970s and 1990s [28], [146], [147]. These grafts exhibited superior mechanical characteristics in comparison with biological scaffolds, but their poor biocompatibility and long-term mechanical complications (implant degeneration due to fatigue and consequently implant failure) meant they were not feasible for ACL replacements [28]. Moreover, ligaments based on carbon fibre were abandoned in early clinical stages due to the fact that carbon fragments were found in lymph nodes and the carbon fibres abraded the knee bones [148], [149].

Between 1986 and 1987 the Food and Drug Administration (FDA) approved the Gore-Tex ligament implant (W.L. Gore, Flagstaff, Arizona), the Kennedy LAD (3M, St. Paul, Minnesota) and the Stryker-Meadox Dacron ligament (Meadox Medical, Oakland, New Yersey; Stryker Corp., Kalamazoo, MI, USA) [28], [148], [150]. Although these implants showed satisfactory short-term results, longer-term monitoring revealed many complications such as implant degeneration and failure, synovitis and inflammation. Analysing these implants in more detail, Guidoin *et al.* [151] reviewed 117 cases of failed ACL reconstructions and found three key elements that contributed to the artificial ligament failure: inadequate fibre abrasion resistance against osseous surfaces, flexural and rotational fatigue of the fibres and loss of integrity of the textile structure due to unpredictable tissue infiltration during healing. An retrospective study of 123 patients with Gore-Tex implants showed that

26 of the implants resulted in re-rupture, 50% were loosened and the 63% of the patients had osteoarthritis after a follow-up of 5-11 years [152].

The Leeds-Keio ligament (Xiros Ltd, Neoligaments ™, Leeds, UK) and the Ligament Advanced Reinforcement System (LARS) (Surgical Implants and Devices / Corin, Arc-sur-Tille, France) were commercialized in Europe and Asia [28], [148], [150]. Murray *et al.* [153] studied 18 ACL Leeds-Keio replacements after 10-16 years of the reconstruction and concluded that knee joint laxity was increased in 51% of the grafts and re-rupture of the implant was found in 28% of the cases. However, a more recent retrospective study with 50 of the same type of grafts showed that just 12% of the replacements ended in re-rupture after 10-20 years of the operation [154]. LARS ligaments were designed in two parts, the intraosseous part and the intra-articular part. In the intraosseous part longitudinal fibres were knitted together, while the fibres in the intra-articular part were pre-twisted at 90° [155]. This configuration provided more resistance to torsional fatigue and wearing and appears to be the most efficient synthetic scaffold to date [28]. Recently grafts such as ACLip® (Amplitude surgical, Valence, France) granted with the CE mark approval in 2017 or Jewel ACL™ and Hybrid System™ (both from Xiros Ltd, Leeds, UK) have been commercialized [156] but no long-term results have been reported in the literature.

The following Table (1.4) summarises the materials, describes the grafts, and includes disadvantages of each commercial implant following different study cases [154], [157]–[163], the mechanical properties and companies for the commercial synthetic ACL implants (permanent implants and augmentation devices) found in the literature review.

Table 1.4 Commercial synthetic ACL implants **[148], [150], [157], [164]–[179]**.

Implant	Polymer	Description	Observations	Ultimate tensile strength (N)	Stiffness (N/mm)	Manufacturer
ABC Prosthetic ligament	Carbon fibre and polyester	24 braided narrow ribbons wrapped at ends	Fragments of carbon fibres observed in lymph nodes. Rupture. High rates of creep	1400	*	Surgicraft Ltd, Redditch, UK
Stryker-Meadox Dacron graft	Polyethylene terephthalate	4-6 woven tapes in tubular shell	Instability of the knee. Elongation due to creep. Ruptures at the insertions and middle part of the graft	3631	420	Meadox Medical, Oakland, New Yersey; Stryker Corp., Kalamazoo, MI, USA
Gore-Tex graft	Expanded polytetrafluorethylene	24 braids of 3 yams wrapped at the end	Fragments observed. Synovitis. Rupture after cycling loading. Infection. Loss of tension of the graft. Poor long-term results	5300	322	W.L. Gore, Flagstaff, AR, USA
Leeds-Keio artificial ligament	Polyethylene terephthalate	Woven structures	No fatigue resistance. Tissue ingrowth not aligned to restore ligament function. High rates of rupture	2000	270	Xiros Ltd, Neoligaments ™, Leeds, UK
Kennedy LAD	Polypropylene	Braided narrow ribbons	Synovitis. General inflammation of the knee	1500	280	3M, St. Paul, Minnesota
Ligament Advance Reinforcement System (LARS)®	Polyethylene terephthalate	Longitudinal fibres in two bundles orientated clockwise or anti-clockwise for right and left knees	Infection. Synovitis	From 1,500N for 30 fibres to 4,700N for 100 fibres	*	Corin/Surgical Implants and Devices, Arc-sur-Tille, France
Proplast ligaments	Teflon and carbon fibre	*	Extremely poor clinical performance at long-term. Carbon fibres abraded the bone in the knee. Carbon fragments were found out of the knee (liver). Imflamation. Poor torsion resistance	*	*	Vitex Inc, Houston, TX, USA
Polyflex	Polypropylene	Intraosseous: 6.35 mm diameter and 20 mm length each ending. Intraarticular: 4.76 mm diameter and 35-40 mm length. Woven tubular structure	Rupture of the ligament due to ligament erosion and residual rotational stress	*	511	Richard, Memphis, TN, USA
Intergraft	Carbon fibre	*	Extremely poor clinical performance at long-term. Carbon fibres abraded the bone in the knee. Carbon fragments were found out of the knee (liver). Inflammation. Poor torsion resistance	660	230×10^9	Osteonics Biomaterials, Livermore, CA, USA
Proflex	Polyester	15 concentric tubular braids of 32 yarn	Infection. Swelling. Rupture. Synovial reactions	4500	*	Protek Ltd, Bern, Switzerland
Trevira-hochfest	Polyester	8 mm wide x 300 mm long flat woven structure	Free PET particles and multinuclear giant foreign body cells were observed in the knee	1866	68.3	Telos, SARL, Marburg, Germany
Lygeron	Polyethylene terephthalate	6 ribbons in a woven tube	Low extensivity, axial splitting. Abrasive wear due to tight weaving	4500	*	Orthomed, Marsannay La Cote, France
Ligastic®	Polyethylene terephthalate	Tubular knit with polyurethane shell	Rupture. Instability. Pain. Good flexibility	4200	*	Orthomed, Marsannay La Cote, France
Ligaid	Polyacrylic acid	Twisted cord braids wrapped at ends	*	*	*	Porth-Aid, France
Raschel	Ultra-high-molecular-weight polyethylene	Knitted structure rolled into tubular shape	Flexibility due to its knitted structure	*	*	Cendis Medical, France
Braided PHP	Ultra-high-molecular-weight polyethylene	Double concentric tubular braids	*	4900	*	Cendis Medical, France
SEM graft	Polyester	Braid structure	*	2500	*	Scince et Medecine, Montrouge, France
Apex ligaments	Polyester	*	*	*	*	DePuy International, Leeds, UK
Jewel ACL™	Polyester	One tubular woven structure	*	1250	310	Xiros Ltd, Neoligaments ™, Leeds, UK
Hybrid System ™	Polyester	Widths of 3-50 mm and 500-800 mm long tubular and single structures	*	300-2250 depending on size	*	Xiros Ltd, Neoligaments ™, Leeds, UK
ACLip®	Polyester	*	*	*	*	Amplitude surgical, Valence, France

In conclusion, all of these commercial implants exhibited aceptable short-term behaviour but they have complications at long-term due to creep, fatigue and implant abrasion in the bone tunnels which provoke debris deposits causing synovitis and pain [25], [28]. These disadvantages may imply a second surgery and they are the reason why commercial implants are not as popular as autografts [25], [28].

Nowadays interest in manufacturing ACL implants through Tissue Engineering has increased due to the great appeal of producing a fully regenerated ligament with appropriate long-term mechanical properties. Manufacture of a tissue engineering ACL implant is based on producing a scaffold where fibroblasts or mesenchymal stem cells are seeded to allow neoligamentous (creation of new ligamentous tissue) growth. The main challenge of tissue engineering implants is to create a scaffold able to degrade progressively at the same rate as ligamentous tissue growth, maintaining the mechanical properties of the structure as a whole over time. An ideal scaffold must accomplish the following requirements:

- Biocompatibility: It is the ability of a material to perform with an appropriate host response in a specific aaplocation. The term biocompatibility is related to different properties of materials, such as non-toxicity, tissues compatibility, blood compatibility (hemocompatibility), and biofunctionality properties [180].
- Biofunctionality: It is the capacity of the ligament implant to perform the functions for which it has been designed, at the required period of time, effectively and with an appropriate host response [180].

- Tunable biodegradability degradation rate, while simultaneously being replaced by host tissue [181].
- Maintain appropriate mechanical properties comparable to the natural ligament before, during and after its degradation [63].
- Appropriate porosity to allow the transport of nutrients, gases, waste, regulation factors and cells from the surface to the interior of the scaffold [182].
- It should cause minimum inflammation or toxicity *in vivo* [182].
- Surgeon-friendly characteristics with easy shapes and sizes for implantation into the body [64].

Further research regarding the development of tissue engineered ACL is shown in section 1.6.2. of the present chapter.

A summary table showing the general advantages and disadvantages of these treatments is presented below (Table 1.5). This table was produced after analysing different case studies and demostrates the high potential of tissue engineered grafts and why they are nowadays increasingly popular.

Table 1.5 Advantages and disadvantages of current ACL implants **[22], [25]–[28], [183], [184]**.

ACL grafts	Advantages	Disadvantages
Autografts	1. "Gold standard" to ACL replacement. 2. Biocompatibility. 3. No transmission of diseasses.	1. Muscle weakness at the donor site. 2. Graft site morbidity. 3. Knee pain. 4. Infection. 5. Loss of sensibility due to nerve damage. 6. Long operation and rehabilitation time. 7. Risk of infection during the surgery.
Allografts	1.No availability problem. 2. Biocompatibility. 3. Reduced operation and rehabilitation time. 4. No donor site morbidity.	1.Lack of young healthy cadaver donors. 2. Risk of transmission of diseases. 3. Infection. 4. Difficulties with the sterilization of the graft, inducing an alteration of the mechanical properties of the graft or bacterial infections. 5. Risk of infection during the surgery.
Xenografts	1. No availability problem. 2. Biocompatibility. 3. Reduced operation and rehabilitation time. 4. No donor site morbidity.	1. Risk of transmission of diseases and risk of immunogenical response. 2. Infection. 3. Difficulties with the sterilization of the graft, inducing an alteration of the mechanical properties of the graft or bacterial infections. 4. Risk of infection during the surgery.
Synthetic grafts (marketed)	1. No availability problem. 2. Good short term mechanical properties. 3. Reduced operation and rehabilitation time. 4. No donor site morbidity. 5. No transmission of diseasses.	1. Lack of biocompatibility. 2. Poor long term mechanical properties. 3. Laxity. 4. Increment of stiffness of the knee joint. 5. Infection, swelling and synovitis. 6. Tissue degradation. 7. Particles of implant observed in lymphatic nodes. 8. Rupture. 9. High rates of creep. 10. Instability of the knee. 11. No fatigue resistance 12. Risk of infection during the surgery.
Tissue engineered grafts	1. No availability problem. 2. Biocompatible 3. Good short and long term mechanical properties 4. Neoligamentous growth. 5. Tunable biodegradability. 6. Appropriate porosity. 7. Reduced operation and rehabilitation time. 8. No donor site morbidity. 9. No transmission of diseasses.	1. In process. No tissue engineered ACL implants are currently commecialized. 2. Risk of infection during the surgery.

Key points:

1. Autografts are currently the "gold standard" for ACL replacement. However, they exhibit disadvantages that could be reduced with other type of grafts.

2. Tissue engineered ACL implants have huge potential and they become increasingly popular among the scientific community. However, further work has to

be done to achieve the ideal graft. Chapters 4, 5 and 6 are focussed on the development of new tissue engineered implants for ACL replacements.

1.5. MANUFACTURING PROCESS

Importance:

1. The study of all possible manufacturing processes to create scaffolds with their respective advantages and disadvantages helps to choose the best fabrication method to create tissue engineered ligaments.
2. Understanding the electrospinning process and its parameters is necessary to optimise the process and to manufacture scaffolds with mechanical properties, morphology and topography comparable to the natural ACL.

Nowadays there are numerous techniques to manufacture scaffolds for tissue engineering applications. Commonly they are classified as non-designed and designed techniques [185]. The first category includes techniques such as electrospinning, melt moulding, gas foaming, freeze drying or emulsion freezing, solvent casting or particulate leaching and phase separation [185]–[187]. The precise outcome cannot be completely pre-determined with these techniques; however their topography, morphology and with that their percentage of porosity can be controlled through different strategies depending on the manufacturing method [185]–[187]. For instance, the electrospinning technique is able to mimic the nano and micro

structure of the tissue being able to realistically represent the nanofibres of extracellular matrix, and this structure can be customized through varying solution, process or environmental parameters as will be explained in the next section (1.5.1).

The second category of manufacturing techniques is called designed technique or rapid prototyping and includes techniques such as 3D printing, laser sintering and stereolithography. Rapid prototyping is characterized as being able to create a 3D structure that mimics the natural tissue through a computational model created from medical images such as computed tomography (CT) scans or magnetic resonance imaging (MRI).

As explained in section 1.4 where tissue engineered implants were briefly presented, scaffolds should be biocompatible (coexisting with living tissues without causing harm), biofunctional, biodegradable, have appropriate mechanical properties (comparable to the natural ACL as shown in section 1.2) and an adequate porous structure to allow cells to proliferate, migrate and in the case of stem cells differentiate into fibroblasts. Therefore, the manufacturing process is crucial to create scaffolds with the appropriate morphology and mechanical properties. A brief explanation of the existing manufacturing methods is shown in section 1.5.1.

1.5.1. Different Techniques to Fabricate Scaffolds

1.5.1.1. Solvent Casting and Particulate Leaching

This technique consists of the dissolution of a polymer in a solvent. Then a porogenic agent (e.g. salt, sugar, gelatin or paraffin) soluble in water is added to the polymer solution to create a porous structure. The solution is poured into a mould with the desired shape and the solvent removed by evaporation or lyophilisation, then the porogenic agent is leached into the polymer. Finally, the mould is immersed in water to dissolve the porogenic particules immersed in the polymer, and a porous structure is created. The pore size and porosity can be controlled by modifying the size and quantity of the porogenic agent. The main concern about this method is the difficulty of control over the internal structure of the polymer matrix; as the pores could be not interconnected or uniformly distributed [185]–[187] this would make the cell migration inside the scaffold difficult.

1.5.1.2. Thermally Induced Phase Separation

This technique consists of the dissolution of a polymer in a solvent with a high boiling point. The solution is heated to a high temperature and poured into a mould. Then the solidification of the solution is induced cooling it down, introducing the solution into a refrigerator set to the gelation temperature of the polymer, generating a phase separation with a polymer-rich phase and a polymer-poor phase. The final step is to remove the solvent by extraction, evaporation or sublimation. The space originally occupied by the solvent in the polymer-poor phase becomes pores of the polymer foam. This technique allows the creation of macro and microporous

structures with high porosity and it is commonly used for bone tissue engineering [185]–[187].

1.5.1.3. Gas Foaming

In this technique a polymer is saturated with high-pressure (800 psi) N_2 or CO_2, creating intermolecular interactions between the gas and the polymer molecules. A fast depressurization of the polymer provokes thermodynamic instability creating pores in the polymer. The main disadvantage is the creation of a nonporous layer and closed pore matrix; however, this disadvantage can be improved through the addition of salt particles to the solution prior to the depressurization step. The salt particles have the characteristic of being leached away when the polymer is immersed in water, increasing the porosity of the structure [185]–[187]. The pore size and porosity can be controlled by modifying the size of the porogen particles and the salt/polymer composite ratio.

1.5.1.4. Emulsion Freeze-Drying

In this method, water is added to the polymer solution and the mixture homogenized to get an emulsion. The solution is frozen (−70°C to −80°C) and placed into a vacuum desiccator to remove the solvent and water. The porosity obtained with this method is above 90% and the scaffolds produced show interconnected pores with sizes ranging from few microns to 300 μm [185]. The porosity plays a critical role in biological tissue formation and the mechanical properties of the scaffold. The pore size has to be large enough for the cells to proliferate and migrate inside the scaffold and to enhance the interchange of nutrients and waste products. However, an increase in the pore size provokes a decrease in mechanical properties, therefore a

balance must be reached between tissue formation and mechanical properties [188] depending on the tissue to be grown. Some studies considered a minimum pore size requirement as ~100 μm for enhancing new bone formation [188]. Andrews *et al.* [189] investigated how the morphology and topography of electrospun scaffolds effect fibroblast behaviour. However, no specific optimum pore size to grow fibroblasts over scaffolds has been found; therefore, further research has to be done.

1.5.1.5. Rapid Prototyping (3D printing)

This method uses a computer-aided design software to produce a 3D structure, by adding layers over layers of material. It allows customization of the model, creating the scaffolds with desired shapes faster than with other manufacturing techniques [190]. In addition, the pore size and distribution can be controlled modifying the model. However, it has the limitations of being a process that requires expensive technology and the use of high temperature, therefore only certain polymers are appropriate to this technique [185]–[187].

1.5.1.6. Electrospinning

The electrospinning technique allows the creation of electrospun (non-woven) scaffolds with high porosity and surface area, manufacturing a net of nanofibres and microfibres, which mimics the natural extracellular matrix (ECM) of biological tissue. The morphology of the scaffolds (including diameter of the fibres, inter-fibre separation, porosity, roughness) can be controlled by modifying the environmental, polymer and machine parameters.

Fibrous scaffolds are nowadays preferred against other structures for tissue engineering applications, as they provide an environment for the cells similar to the natural extracellular matrix. This fibrous structure favours the interactions between cells and between cells and matrix, which allows creating biological tissue with the same characteristics as the tissue that they replace. Moreover, the possibility of using biodegradable and biocompatible polymers makes for an attractive technique increasing its use day-by-day to create scaffolds for tissue regeneration [191].

It is essential to undertake a study into the advantages and disadvantages of the different fabrication methods, to be able to decide which manufacturing method would be the most appropriate for creating tissue engineered ACL implants. Table 1.6 summarises all the advantages and disadvantages found in the literature.

Table 1.6 Advantages and disadvantages of different manufacturing methods to create tissue engineered scaffolds **[192]–[194]**.

ACL grafts	Advantages	Disadvantages
Solvent Casting and Particulate Leaching	1. Easy method. 2. Small amount of material required.	1. Difficulty in controlling the internal structure (pore size and shape) of the polymer matrix. 2. Use of organic solvents. 3. Time-consuming washing step. 4. Low thickness. 5. Limited pore interconnection.
Thermally Induced Phase Separation	1. Tunable mechanical properties. 2. Control over 3D shape. 3. Control over pore size and shape. 4. Simple and fast technique.	1. Long continuos fibres can not be produced. 2. Difficult to control fibre dimension and orientation. 3. Only polymers with gelation capability can be used to produce nanofibrous structures. Limited to few polymers. 4. Low yield. 5. Use of organic solvents.
Gas Foaming	1. Ease to create 3D structures. 2. No use of organic solvents. 3. No high temperatures.	1. Low pore interconnetion. 2. Formation of a nonporous skin layer on scaffold surface.
Emulsion Freeze-Drying	1. No high temperatures required. 2. No washing steps. 3. Easy technique.	1. Small pore size. 2. Long fabrication times.
Rapid Prototyping	1. Control over 3D shape. 2. Fast manufacturing process.	1. Limited to few polymers due to the high temparatures required in the process. 2. Expensive technology. 3. High level of expertise required. 4. No features at the nanoscale.
Electrospinning	1. Well established and easy technique. 2. Easy functionalization 3. Creation of long continuous fibres with diameters from micro-scale to nano-scale. 4. Control over fibre diameter and orientation. 5. Tunable mechanical properties. 6. Possibility to work with a high range of polymers. 7. No high temperatures if melt electrospinning is not used.	1. Difficult to fabricate 3D structures. 2. Difficult to control pore shape. 3. Use of organic solvents for most of the polymers.

Electrospinning was the manufacturing technique selected for being used in this thesis due to its ease of use, tunable morphology, topography and mechanical properties of the scaffolds, the possibility to work with a high range of polymers and the ability to create a nanostructure comparable to the ECM. For this reason, the next section (1.5.2.) will focus on electrospinning, explaining briefly its physical principle and the way to optimise the different parameters that take part in the process.

1.5.2. MANUFACTURING PROCESS SELECTED: ELECTROSPINNING TECHNIQUE

The main principle of electrospinning is the application of high voltage difference between a positively charged metallic needle and a grounded collector to project a polymeric solution or melt polymer creating fibres. The three major components are a high voltage power supply, a syringe connected to a flow control pump, and a metal collector (Figure 1.17) [195].

When the electrostatic force overcomes the cohesive force of the solution, an electrically charged jet emerges from the capillary creating the Taylor cone. Once the surface charge overcomes the surface tension of the polymer droplet, a polymer jet is initiated [43]. The fluid jet is accelerated and stretched by the external electric field and thins dramatically while travelling towards the collector, leading to the formation of continuous solid fibres as the solvent evaporates. Electrospinning products appear as highly porous nonwoven scaffolds made of nano/micro diameter fibres with large surface area to volume ratio. Fibre diameter, inter-fibre separation, roughness and fibre orientation can be controlled by changing the spinning parameters [195]–[197].

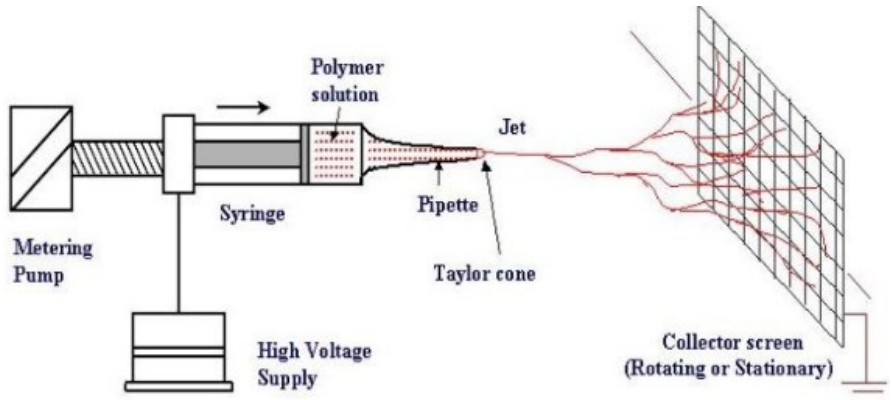

Figure 1.17 Schematic diagram showing the electrospinning set up. Reproduced from **[198]**

1.5.2.1. Optimisation of process parameters

There are three different types of parameters in the electrospinning process: solution parameters (such as viscosity, concentration, molecular weight, surface tension or conductivity), process parameters (such as voltage, flow rate or distance between the needle and the collector) and environmental parameters (such as relative humidity or temperature). All of these parameters significantly affect the formation and morphology of the created fibres. Therefore, only with the control of all these parameters can a stable Taylor cone be obtained and nanofibres produced with the desired morphology [199].

The qualitative effect of all of these parameters has been thoroughly studied [200]–[202] and certain parameters showed correlative relationships between them; however the exact values that allow obtaining the required scaffold, depend on the equipment, polymer and solvent used. Therefore, before starting with any experiment it is essential to find out a range of the parameters to obtain a stable Taylor cone that results in correct evaporation of the solvent and creation of non-beading fibres. Once a range of the parameters that creates good quality fibres is known, it is necessary to optimise those values to obtain the desired mechanical properties and morphology for the scaffolds.

One of the biggest challenges with electrospinning is to find the optimal combination between viscosity of the polymer solution and flow rate, voltage and needle-collector distance [203]. Otherwise, the electrospinning will create beads or bead-strings (instead of fibres) if the combination of these parameters is not

optimised [199]. The creation of beads or beaded fibres reduce the quality of the fibres and consequently the quality of the electrospun mesh, decreasing its material properties (Young's modulus and maximum tensile strengh) [204] and the pore size ending to issues in cell migration.

The following Table (1.7) summarises the relationship between the manufacturing parameters and their effects on fibre morphology.

Table 1.7 Electrospinning parameters/Fibre morphology **[200]–[202]**

Fabrication parameters		Effect on fibre morphology
Solution concentration/Viscosity	↑	Larger fibers and less defects
	↓	Bead formation
Solution concentration	↑	Difficulty in solution flow
	↓	Fiber breakage before reaching the collector
Conductivity/Solution charge density	↑	Uniform bead-free fibers, smaller fibers
	↑↑	Smaller fibers in general
Conductivity of solution	↑	Increased transport of charges, higher stretch and thinner fibers
	↓	Decrease transport of charges, lower stretch and thicker fibers
Surface tension		No inclusive link
Polymer molecular weight/Viscosity	↑	Reduction in the number of beads and droplets
Dipole moment and dielectric constant	↑	Successful spinning
Flow rate	↑	Thicker fibers that were not dry upon reaching the collector, beads formation
	↓	Fibers with smaller diameters
Field strength/Voltage	↑↑	Jet distortion, beading was observed and thicker fibers
	↓	Larger fibers
	↓↓	The solution has a low impulse to reach the collector
Distance between needle tip and collector	↑	Fibers may be broken, high stretch, longer and thinner fibers
	↑↑	Beads formation
	↓↓	
	↓	Short and wet fibers, no evaporation of the solvent
Needle tip design and diameter		Using a coaxial, 2-capillary spinneret, hollow fibers were produced
		Multiple needle tips were employed to increase throughput
Collector geometry		Smoother fibers resulted from metal collectors; more porous fiber structure was obtained using porous collectors
		Aligned fibers were obtained using a conductive frame, rotating drum, or a wheel-like bobbin collector
		Yarns and braided fibers were also obtained
Ambient parameters	↑	Temperature caused a decrease in solution viscosity, smaller fibers
	↑	Humidity caused appearance of circular pores on the fibers

Key points:

1. Fibrous scaffolds are preferred to other structures, since they provide an environment for the cells comparable to the natural extracellular matrix.

2. Electrospinning is a manufacturing technique that presents many advantages in comparison to other fabrication methods. The most relevant advantage is the possibility of creating scaffolds with a nanostructure comparable to the ECM. Moreover, the natural ACL morphology, topography and mechanical properties can be mimicked by optimising the electrospinning parameters. Chapters 4 and 5 will optimise the process to be able to fabricate scaffolds comparable to the natural ACL.

3. The ease of use of electrospinning, minimum cost and possibility to work with high range of polymers make this technique attractive and with high potential to be used in the development of new ACL implants. Chapters 4, 5 and 6 will use the electrospinning technique to create scaffolds for potential use as ACL implants.

1.6. POLYMERS USED IN THE MANUFACTURING OF SCAFFOLDS

Importance:

1. The study of the different natural and synthetic polymers commonly used in electrospinning (with their advantages and disadvantages) helps to determine the most promising candidates to be used to manufacture ACL implants.

2. A literature review of the materials used for electrospun ACL scaffolds is needed to find the gaps in the current literature and to direct further investigations into promising materials and post-fabrication treatments.

Polymers are the most suitable materials to develop scaffolds for tissue engineered applications, due to their mechanical properties (flexibility, strength) being comparable to biological tissue and their capacity for cell growth in biocompatible polymers. Depending on the origin of the polymer used to fabricate the scaffold, synthetic or natural scaffolds can be produced/used. Examples of natural polymers used in tissue engineering are collagen, silk, gelatin, hyaluronic acid, chitosan or alginate. The most studied synthetic polymers for tissue engineered applications are: polyglycolic acid (PGA), poly-L-lactic acid (PLLA), polylactic-co-glycolic acid (PLGA), polycaprolactone (PCL), polyurethane urea (PUU) or polyvinyl alcohol (PVA) [22], [185], [205], [206].

It was demonstrated that materials such as collagen, hyaluronic acid, chitosan, alginate, polydioxanone (PDS) or polyglutamic acid used in tissue engineering exhibit lack or loss of mechanical strength compared to silk which exhibits good tensile strengh. Silk and chitosan present limited cell adhesion. PGA, PLLA, PCL and PLGA are biologically inert, therefore there are difficulties to growing cells on and in them [22], [185], [205], [206].

Tissue engineering uses biodegradable polymers to create new biological tissue while the polymer is degrading. Biocompatibility is one of the most wanted

characteristics in a polymer, since the rejection of the scaffold cannot happen as the material degrades in time. To customize mechanical properties, degradation rate or cell response, it is essential not only to choose the right polymer but also the right scaffold fabrication technique.

1.6.1. MOST COMMON POLYMERS USED IN ELECTROSPINNING

`

The ideal electrospun scaffold should replicate the structure of the ECM, in order to provide not only appropriate mechanical properties to guarantee the integrity of the new tissue but also to favour cell adhesion and growth, differentiation and migration.

The ECM consists of a 3D structure of polysaccharides and natural polymers such as collagen, elastin, proteoglycans and fibrinogen. Each polymer has a specific function in the ECM. For instance, collagen provides tensile strength and plays a key role in cell-matrix and matrix-matrix interactions [207], [208]. Elastin provides elasticity to the tissue and proteoglycans are crucial for cell proliferation, migration and cell-matrix and matrix-matrix interactions [207].

In order to replicate the ECM there are natural and synthetic polymers able to be used with the electrospinning technique. The most used natural polymers are collagen, gelatin, elastin and silk fibroin [209]. The most used synthetic polymers to manufacture electrospun tissue-engineering scaffolds are PCL, PLLA, PGA, poly PLGA, PVA and poly urethane (PU) [210], [211]. In general, it is known that natural polymers have the capacity to be biocompatible but they lack mechanical

strength. For instance the Young's modulus for gelatin is reported as 1 MPa [212] and for collagen 14 MPa [213]. On the contrary, synthetic polymers are biologically inert but normally exhibit higher mechanical properties than the natural polymers [22], [205], for example the Young's modulus for PCL is reported to be 158 MPa [214].

The advantages and disadvantages of these most commonly used polymers are shown in Table (1.8). This table aided the decision of which polymers should be used for the experiments performed in this thesis, based principally on their biocompatibility, biodegradability, comparable stress/strain behaviour to the natural ACL, low cost and the need to avoid using harmful solvents.

Table 1.8 Advantages and disadvantages of natural and synthetic polymers **[22], [185], [205], [206]**

Polymer	Advantages	Disadvantages
Collagen	1. Biocompatible. 2. 90% of native ACL. 3. Biodegradable.	1. Expensive. 2. Lack of mechanical strength. 3. Immunogenicity. 4. Necessity of crosslinking the scaffold.
Gelatin	1. Inexpensive. 2. Higher tensile modulus than collagen. 3. Bioactive. 4. Biodegradable. 5. Biocompatible. 6. Collagen derivative. 7. Harmful solvents are not required.	1. Easy gelification in water. 2. Necessity of crosslinking the scaffold.
Elastin	1. Biocompatible. 2. Component of the natural ACL.	1. Lack of mechanical strength
Silk	1.Good tensile strength. 2. Viscolastic properties that prevents of damage due to fatigue and creep.	1. Limited cell adhesion. 2. Necessity to remove the sericin to be biocompatible. 3. Use of harmful solvents to produce the solution.
PCL	1. FDA-approved for sutures. 2. Easily manufactured	1. Use of harmful solvents to produce the solution. 2.Very slow degradation rate. 3. Biologically inert.
PLLA	1. Slow degradation rate. 2. Better cell adhesion than PGA or PLGA. 3. Easily manufactured	1.Use of harmful solvents to produce the solution. 2. Hydrophobicity. 3. Acidic degradation by product. 4. Biologically inert.
PGA	1. FDA-approved for sutures. 2. Easily manufactured. 3. Technologically mature.	1.Rapid degradation and loss of mechanical strength. 2. Hydrophobicity. 3. Use of harmful solvents to produce the solution. 4. Acidic degradation product. 5. Biologically inert.
PLGA	1. Controllable degradation rate by modifying the PLA:PGA rate. 2. Easily manufactured.	1. Use of harmful solvents to produce the solution. 2. Acidic degradation by product. 3. Biologically inert.
PVA	1. Inexpensive. 2. Water soluble. 3. Biodegradable. 4. Nontoxic. 5. Biocompatible. 6. Ease of use. 7. Normally used as baseline polymer from which the results can be extrapolated to other polymers	1. Necessity of crosslinking the scaffold
PU	1. Biocompatible. 2. Flexibility.	1. Use of harmful solvents to produce the solution. 2. Low mechanical properties of electrospun scaffolds comparing to natural ACL.

Following the tabulated information, it was determined that the two polymers with the desired characteristics for further investigation regarding ACL implant production were gelatin and PVA. Gelatin, is a natural polymer derivated from collagen (the most abundant polymer of the ECM), with similar properties to collagen and therefore hypothetically the cells would behave similarly on a gelatin scaffold compared to a collagen matrix. Gelatin is considerably cheaper than collagen, moreover gelatin exhibits higher tensile modulus than collagen fibres, biodegradability and similar bioactivity and biocompatibility to the collagen [215]. PVA is an inexpensive polymer with excellent physical, chemical and mechanical properties, during this thesis it was shown that 3 twisted/braided PVA scaffolds exhibited a maximum tensile stress of 38 MPa identical to the native ACL and displayed a Young's modulus of 129 MPa, comparable to 111 MPa reported for the natural ACL [59]. PVA is a highly hydrophilic, water soluble, biodegradable, nontoxic and biocompatible polymer [216]–[219]. In addition, due to the ease of electrospinning high quality nanofibres, it is normally used as a baseline for experiments with other materials.

1.6.2. MATERIALS USED FOR ELECTROSPUN ACL SCAFFOLDS

Since 2005 a number of investigations have been performed to produce tissue-engineered ACL through the electrospinning technique [22], [44], [214], [220]–[233]. The words "ACL" and "electrospinning" have been searched and a total of 14 results have been shown in the research database Scopus. In addition to the

previous search performed, 3 additional articles of interest related to the manufacturing of electrospun tissue-engineered ligaments have been found and incorporated in the previous search. These last articles are taken into consideration due to their mechanical results (comparable to the mechanical properties to the natural ACL). Table 1.9 shows all these articles (17 articles) with the dissolution used, the mechanical properties and results achieved. Some conclusions obtained through the analysis of these articles will be shown at the end of section 1.6.2.

Table 1.9 Tissue engineered ACL produced with electrospinning techinque **[22], [44], [214], [220]–[233]**

Paper	Date	Polymers	Dissolution	Mechanical properties	Results
Synthesis and characterization of polycaprolactone for anterior cruciate ligament regeneration	2017	Poly(ε-caprolactone) (PCL)	A solution of PCL was prepared by dissolving 0.66 g of PCL in 1.6 mL of organic solvent mixture composed of DCM and DMF at a ratio of 1:1.	Ultimate stress=0.38MPa; Max load=0.89N; Elastic modulus=0.012MPa; Ultimate strain=62.57%	Fibrous scaffolds generated with electrospinning showed weaker mechanical properties visa vis native ACL tissue in terms of ultimate stress, and elastic modulus. Also, the synthesized PCL can accommodate cell attachment when tested with hBMSCs. Put together, these observations reveal that the PCL synthesized in this study could be a good candidate as a biomaterial for ligament repair or regeneration
Microfibre-reinforced nanofibrous scaffolds with structural and material gradients to mimic ligament-to-bone interface	2017	Poly(lactic-co-glycolic acid (PLGA) (15 wt%) , poly-lactide acid (PLA) fibres with diameter of about 300 mm used to o reinforce the electrospun nanofibres and 50 nm nHA particles	PLGA (15 wt%) disolved in N,N-dimethylformamide and acetone 1 : 1	Yield force=247.37±15.63 N; breaking force=500.11±54.17 N	Microfibre-reinforced nanofibrous scaffolds were manufactured with fibre orientation and nHA/BMP-2 gradients. The composite gradients were found to regulate cellular morphology as well as direct the zonal bone-specific differentiation *in vitro* . The mechanical property of the 3D nanofibrous scaffolds was improved by the incorporation of microfibres
Mechanical properties and cellular response of novel electrospun nanofibres for ligament tissue engineering: Effects of orientation and geometry	2016	Poly(ε-caprolactone) (PCL)	10% PCL electrospinning solution was a homogenous mixture with a 3:1 chloroform to methanol	Young Modulus=158±32 Mpa; yield stress=57±23 Mpa; yield strain=0.38±0.08	Nanofibre orientation and geometry of electrospun PCL were modified to mimic the fascicles of native tendon and ligament. Aligned nanofibre bundles had the highest yield stresses and strains, while still maintaining a relatively high elastic modulus.
Use of Ultra-High Molecular Weight Polycaprolactone Scaffolds for ACL Reconstruction	2015	Ultra-high molecular weight polycaprolactone (UHMWPCL)	UHMWPCL is dissolved 10% w/w in 1,1,1,3,3,3-hexafluoro-2-propanol	Peak load=24.6±4.7 N; stiffness=8.6±2.0 N/mm	This *in vivo* study establishes the superiority of the higher molecular weight version of polycaprolactone over PCL as a scaffold material for ACL reconstruction.
In Vitro and *In Vivo* Evaluation of Heparin Mediated Growth Factor Release from Tissue-Engineered Constructs for Anterior Cruciate Ligament Reconstruction	2015	Poly(ε-caprolactone) (PCL)	PCL 10% w/w in 1,1,1,3,3, 3-hexafluoro-2-propanol	Graft with Heparin+ bFGF after 16 weeks. Peak load= 15.32±8.5 N; stiffness=10.9±5.2 N/mm	Fibroblasts cultured on these scaffolds *in vitro* demonstrated increased proliferation in the presence of bFGF immobilized using heparin. However, these results did not translate in a rodent model of ACL reconstruction, in which no differences in matrix deposition or mechanical properties were observed between grafts with and without bFGF.
In vivo evaluation of electrospun polycaprolactone graft for anterior cruciate ligament engineering	2015	Poly(ε-caprolactone) (PCL)	PCL 10% w/w in 1,1,1,3,3, 3-hexafluoro-2-propanol	Failure load=13.27±4.20N; stiffness=15.98±5.03 N/mm at 12 weeks postimplantation	PCL elicits a minimal inflammatory response in the rodent model, due to the biocompatibility and successful deposition of an aligned collagen matrix.
Electrospun Poly(L‐lactide-co-acryloyl carbonate) fibre Scaffolds With a Mechanically Stable Crimp Structure For Ligament Tissue Engineering	2014	Poly(L-lactide-co-acryloyl carbonate) (P(LLA-AC))	P(LLA-AC) in 3:1 solution of dichloromethane/dimethylformamide (DCM/DMF)	Young's modulus of the dry uncross-linked fibre scaffolds was 86 ± 5 MPa and that of the dry cross-linked scaffolds was 222 ± 28 MPa. The average modulus of the hydrated scaffolds was 26 ± 1.4 MPa.	Copolymerizing an acryloyl carbonate monomer with L-lactide yielded a copolymer with an acryloyl pendant group along its backbone that was effectively utilized to cross-link electrospun microfibres possessing an appropriate crimp structure. The cross-linked and crimped fibre scaffolds had a Young's modulus approximating that of the modulus of human anterior cruciate ligaments. Fibroblasts seeded onto these fibres effectively attached and proliferated.

The Influence of Braiding Angle Variation in Braided-Twisted fibre Scaffold Based Poly L-Lactic Acid for Anterior Cruciate Ligament Reconstruction Application	2014	Poly L-lactid acid (PLLA)	PLLA 7% wt chloroform and toluene 3:1	Tensile strength=1.318 MPa for braided-twisted fibre scaffold 40°, 60° 0.22 MPa and 80° 0.024 MPa	Bigger braiding angle of braided twisted fibre scaffold has high degradation rate, bigger pore size, and lower mechanical strength.The braided-twisted fibre scaffold exhibited a porcentage of living cell of more than 60%.
Current tissue engineering strategies in anterior cruciate ligament reconstruction (Review)	2014	Review			There is a true clinical need f or a tissue-engineered ACL graft. Tissue-engineered alternative to autografts and allografts may help to circumvent some of the complications associated with these traditional therapies. There is a lack of understanding of in vivo ACL development. To date, there is no tissue-engineered ACL construct that has been successfully implanted in humans.
Updates in biological therapies for knee injuries: Anterior cruciate ligament	2014	Review			Biological therapies are being developed and analyzed to optimize ACL injury treatment. Under the concept of biological therapy, remnant preserving ACLR seems to be the most simple, easily available, and economically viable strategy to improve ACL treatment.
Effect of fibre orientation of collagen-based electrospun meshes on human fibroblasts for ligament tissue engineering applications	2014	Poly(lactic-co-glycolic acid (PLGA), collagen I (ColI),and polyurethane (PU)	15 w/v %PLGA(85:15), 10 w/v % ColI, and 5 w/v % PU and 15 w/v% PLGA(50:50), 10 w/v % ColI, and 5 w/v % PU	Aligned fibres and PLGA (50:50): Young's modulus=348.38±12.5MPa; Max strain=98.61±12.28; Tensile Stress at Yield=8.98±0.68 Aligned fibres and PLGA (85:15): Young's modulus=63.12±18.22MPa; Max strain=91.36±17.31; Tensile Stress at Yield=7.09±1.9	The experiments were carried out with coaxial electrospinning with a core of PU and a shell of collagen and PLGA with two different ratios of PLGA (50:50 and 85:15). The Young's modulus, tensile stress at yield, and ultimate tensile strain of aligned fibre PLGA(50:50)-ColI-PU scaffolds demonstrated similar tensile properties to that of ligaments found in the knee such as anterior cruciate ligament (ACL), posterior cruciate ligament (PCL) and medial cruciate ligament (MCL). Moreover, it was demonstrated that human fibroblasts were attached and proliferated with no need for additional surface modifications a promising base material for tissue-engineered ligament in that they are a biomimetic structure, and provide the mechanical environment ligament fibroblasts encounter *in vivo* .
Cellularized Cylindrical fibre/Hydrogel Composites for Ligament Tissue Engineering	2014	Poly(lactic-co-glycolic acid (PLGA)/polyethylene glycol diacrylate (PEGDA) and poly(ester urethane) urea elastomer (PEUUR)/ PEGDA	95/5% (w/w) PLGA/PEGDA or 95/5% (w/w) PEUUR/ PEGDA polymer mixture was dissolved in HFIP to a final polymer/solvent concentration of 11/89% (w/w)	Young's modulus of the PLGA/PEGD composites=11.6 MPa and PEUUR/ PEGDA composites= 1.05 Mpa	They obtained cellularized elastomeric composites for ligament tissue engineering that could support cyclic mechanical loading and cell viability. However, they did not have enough mechanical properties for ligament replacement and the cells are not able to proliferate, due to the limited ability for the cells to adhere to and migrate through the PEG hydrogels. Moreover, a 40% decrease in the Young's modulus was observed when PLGA meshes were combined with a PEG hydrogel, the reason could be related to poor mesh/hydrogel bonding. In conclusion, the use of hydrogels for ligament tissue engineering could be very useful to get cellularized 3D scaffolds but must be studied deeper.

In vivo study of ligament-bone healing after anterior cruciate ligament reconstruction using autologous tendons with mesenchymal stem cells affinity peptide conjugated electrospun nanofibrous scaffold	2013	Poly L-lactid acid (PLLA)	1.0 g of PLLA powders in 10mL tetrafluoroethylene	Failure load (N)=82.59 ± 3.33	After implantation of grafts for 3 months, the regenerated ligament-bone insertion exhibited abundant ECM (collagen I, II, and III) and fibrocartilage growth. The tensile strength of the implant was shown to be better than the control. The findings of this study imply that nanofibrous scaffold with specific MSCs affinity peptide has great potentials in accelerating ligament-bone healing process after ACL reconstruction.
Biomimetic poly(lactide) based fibrous scaffolds for ligament tissue engineering	2012	Poly(L-lactide-co-D,L-lactide) (PLDLA), poly(D,L-lactide) (PDLLA) and poly(L-lactide) (PLLA)	PLDLA, PDLLA and PLLA are dissolved in 3:1 (volume ratio) of dichloromethane:dimethylformamide	Yield strain (cm/cm) from 0.21 ± 0.03 until 0.15 ± 0.01; Ultimate load (N) from 1.5 ± 0.2 until 0.23 ± 0.02; Modulus (MPa) from 19 ± 4 until 3 ± 0.3 depending on the polymer used.	Of the poly(lactide) based polymer fibres investigated in this study, the 250 kDa PLDLA fibre mats possessed the highest modulus, and were the most resistant to degradation. The 250 kDa PLDLA fibres were successfully treated in a heated aqueous environment to possess a crimp-like pattern. However, the crimp-like pattern was not completely recoverable upon repetitive loading. Cells and the presence of collagen accumulation were observed at the surface and interior regions of the construct, demonstrating the potential of crimp-like 250 kDa PLDLA fibres as a biomimetic scaffold for ligament tissue engineering.
Preliminary investigation of airgap electrospun silk-fibroin-based structures for ligament analogue engineering	2011	Silk fibroin (SF), polydioxanone (PDO), polycaprolactone (PCL), SF+PDO (50:50) and SF+PCL (50:50)	SF, PDO and PCL were dissolved in 1,1,1,3,3,3 hexafluoro-2-propanol at concentrations of 100 mg/ml. Solutions were both electrospun individually and in 50:50 blends by volume of SF/PDO (SPDO) and SF/PCL (SPCL).	Wound SPCL structures: Young's modulus of 113±45 MPa, peak stress of 24.36±9.38 MPa and strain at break of 0.28 ± 0.07 mm/mm	Structures made of high rotating speed are more compact, with more aligned fibres and less porous than structures made with low rotating speed or created through airgap electrospinning. The airgap electrospun scaffolds present the most porosity and thereby they are more conducive to cellular infiltration. In addition, although they not possess the same degree of fibre alignment or mechanical properties as highly aligned structures, its alignment is enough to induce a preferential direction of alignment in the fibroblasts seeded. Wound structures reach values of Young modulus and peak stress very similar to native anterior cruciate ligament, so they present good mechanical properties but poor level of porosity therefore inadequate cellular penetration. The authors of this paper suggest creating structures with a wound center core of aligned fibres to get the mechanical properties desired and a high porosity outer layer to enhance cellular infiltration.
Electrospun degradable segmented polyurethane elastomers for ligament tissue engineering (abstract conference)	2005	Plyurethane (PU)	Not shown		They present preliminary results demonstrating that they can control the diameter and degree of orientation of electrospun polyurethane fibres, and that electrospun substrates alter cell spreading, orientation, and the expression of extracellular matrix proteins.
Nanofibre alignment and direction of mechanical strain affect the ECM production of human ACL fibroblast.	2005	Plyurethane (PU)	PU 20 wt% N,N-dimethyl formamide (DMF)	Aligned fibres: Young's modulus=2500±63KPa; Max strain=1.08±0.17; Ultimate strength=3520±30KPa	HLFs cultured on aligned nanofibres had a similar morphology to ligament fibroblasts *in vivo* , and the aligned structure led to increase ECM production. Aligned nanofibres can constitute a promising base material for tissue-engineered ligament in that they are a biomimetic structure, and provide the mechanical environment ligament fibroblasts encounter *in vivo* .

Approximately 35% of the articles found developed their ACL implants with PCL [214], [220], [222], [223], 41% of the articles worked with derivates of PLA and PGA [224], [225], [227], [230]–[233] and approximately 24% of the articles produced their ligament implants with derivates of PU [228]–[230].

It was observed that mechanical properties highly depend on the manufacturing process of the scaffold and its morphology, and not only on the specific material, as it was proved that modifying the structure of scaffolds made from the same polymer provides completely different mechanical properties [214], [220], [222], [223]. For instance, a solution of PCL dissolved in 1:1 DCM and DMF created a randomly distributed nanofibre scaffold with an elastic modulus of 0.012 MPa [220]; however, a solution of 10% PCL dissolved in 3:1 chloroform and methanol produced aligned nanofibre bundles exhibiting an elastic modulus of 158 MPa [214] much closer to the natural ACL (approx. 111 MPa [59]). Full *et al.* (2014) [230] also demonstrated that aligned fibre scaffolds present higher tensile properties than scaffolds with random fibre orientation; the tensile yield stress of aligned PLGA (50:50) fibres was reported to be 8.98 MPa, however the tensile stress at yield of randomly distributed PLGA (50:50) fibres was reported 0.86 MPa.

From Table 1.9, it was shown that three articles reported mechanical values similar to the ACL [214], [224], [230], two of them achieving those values through aligned fibres [214], [230] and the other using a crosslinker agent [224]. Just one article studied 3D structures based on twisted/braided electrospun scaffolds, although its mechanical properties were not comparative to the native ACL [225]. From those

articles, it was concluded that to produce electrospun scaffolds with mechanical properties similar to the ACL, it is important to understand three issues:

- The differences in terms of mechanical properties between randomly distributed and aligned fibres of the polymer.
- How a crosslinker agent can affect the mechanical properties of electrospun scaffolds.
- Evaluation of different 3D configurations such as twisted/braided or just twisted structures in order to understand how those configurations affect the mechanical properties of the scaffold.

Following these last conclusions, the studies in Chapters 4 and 5 addressed the evaluation of the distribution of the fibres and the crosslinking process for gelatin and PVA respectively, and Chapter 6 studied different 3D configurations to determine the optimum for producing 3D tissue engineering ligaments.

Key points:

1. Gelatin, is a natural polymer derivated from collagen, with similar properties but considerably cheaper, is biodegradable and has similar bioactivity and biocompatibility to collagen. Gelatin was used in Chapter 4 to develop new ACL implants.

2. PVA is an inexpensive polymer, with better mechanical properties than other polymers used for tissue engineered applications, highly hydrophilic, water soluble,

biodegradable, nontoxic and biocompatible. This polymer was used in Chapter 5 and 6 to create 2D and 3D scaffolds for ACL replacement.

3. Mechanical properties highly depend on the manufacturing process of the scaffold and its post-fabrication process. Therefore, aspects such as fibre distribution, crosslinking process and 3D electrospun structures have to be investigated.

4. The mechanical evaluation of random and aligned distributed fibres of gelatin and PVA was respectively addressed in Chapters 4 and 5.

5. The mechanical properties of crosslinked gelatin and PVA scaffolds were investigated in Chapters 4 and 5.

6. The study of different 2D and 3D electrospun structures was performed in Chapter 6 to determine the optimum structure to produce 3D tissue engineering ligaments.

1.7. RESEARCH QUESTIONS

Once the background study and literature review of the field had been performed, it was necessary to define the current gaps and determine the research questions that this thesis needed to answer. The research questions are presented below:

- How can one develop a reliable and easy methodology to investigate the *in vivo* ACL mechanical behaviour for a large number of activities (in one study to allow comparison) and define mechanical specifications to design new biomimetic ACL grafts? (Chapter 3).

- Seeing that 25% of the ACL reconstructions lead to a further surgery and/or long-term issues, is this due to the current standardized procedure to design ACL implants not accounting for all of the loading that the natural ACL has to bear? (Chapter 3).
- Are gelatin and PVA suitable polymers to be used for the production of ACL electrospun grafts? In other words, could 2D electrospun gelatin and PVA scaffolds mimic the nano/micro morphology and the mechanical behaviour of the natural ACL once the solution and process parameters are optimised? (Chapters 4 and 5).
- Which 2D/3D electrospun structure is optimum to replicate the morphology and the mechanical properties of the natural ACL? (Chapter 6).

2. Aims and thesis structure

2.1. Aim and Objectives

The aim of this PhD was to design and manufacture biomimetic electrospun prototypes with comparable mechanical properties and morphology to natural ACL. These prototypes produced proof of concept for the design and manufacture and will be used as the baseline for cell testing, animal models and at the final stage clinical trials.

In order to achieve this aim several objectives were worked through different studies.

Objective 1 - Understanding current treatment technologies

Identification of the research questions and current gaps in the field had to be defined through the study of the ACL background and literature review.

Objective 2 - Quantify ACL Biomechanics

This study was focussed on the understanding of *in vivo* ACL biomechanics to obtain the mechanical specifications to design and assess ligament implants; to that end a novel methodology was developed.

Objective 3 - Material Evaluation

Determination of the suitability of two different polymers (gelatin and PVA) to be used in the manufacturing of ACL prototypes and optimisation of the

process in order to obtain mechanical properties and morphology comparable to the natural ACL.

Objective 4 - Implant Structure for Optimal Mechanical Performance

The last study identified the optimum prototype able to reproduce the mechanical behaviour (under cyclic tensile and shear loading and dry and wet conditions) and the nano and micro morphology of the natural ligament.

A scheme of the thesis with the aims and novelties of each study are presented in Figure 2.1.4

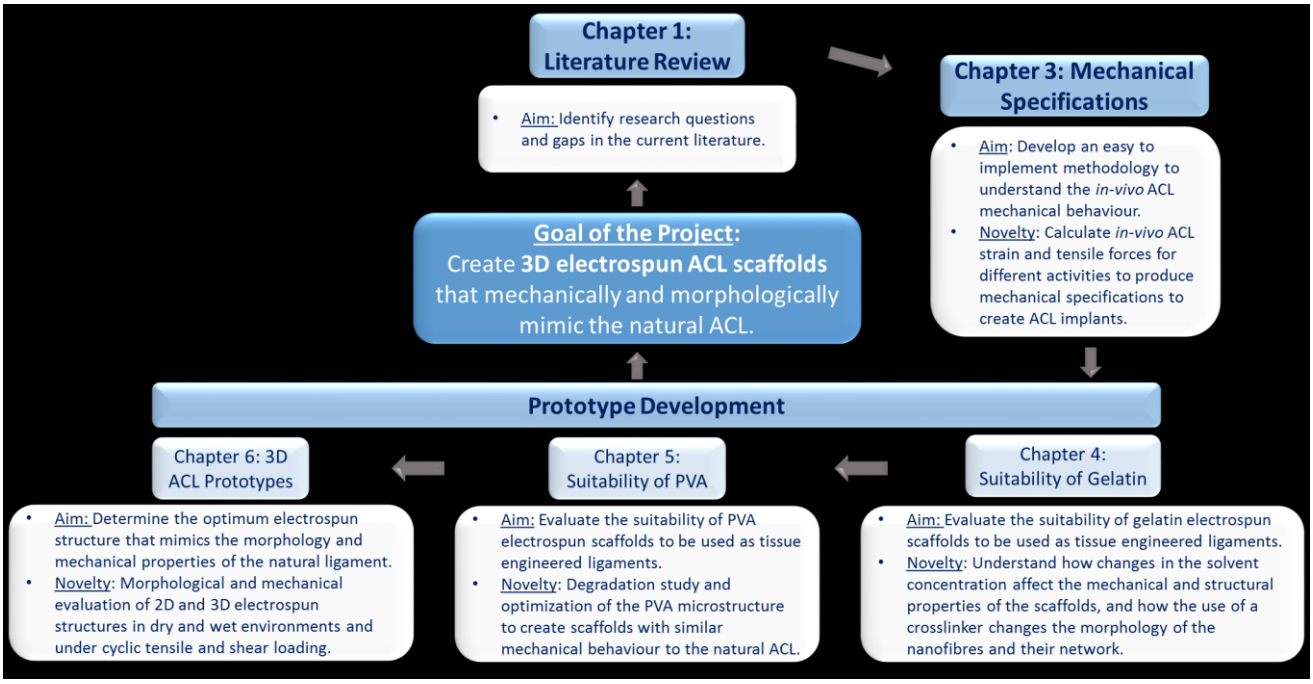

Figure 2.1 Aims and novelties of each study performed in this thesis.

2.2. THESIS STRUCTURE

This thesis consists of ten chapters. The first Chapter describes the background and literature review regarding the ACL including topics such as anatomy of the knee and the ACL, mechanical behaviour, ACL injury mechanics, state for the art of ACL implants, the manufacturing process and the polymer used in the manufacturing of scaffolds. Research questions are included at the end of Chapter 1.

Chapter 2 presents the aim and objectives of this PhD thesis and briefly explains the thesis structure.

Chapter 3 focusses on the *in vivo* mechanical behaviour of the ACL for consideration as mechanical specifications in the prototype designs. This chapter presents two different studies, the first (Biomechanics Study 1) developed a novel methodology to understand the *in vivo* mechanical behaviour of the ACL; and the second study (Biomechanics Study 2) calculated the *in vivo* strain and tensile forces on the ligament for different activities to be used in the design specifications and for assessing the prototypes.

Chapter 4 evaluates the suitability of gelatin to manufacture ACL implants. In this Chapter two studies are performed, the first study (Gelatin Study 1) focusses on the understanding of how changes in the solvent concentration affect the mechanical and structural properties of the scaffold; and the second study (Gelatin Study 2) examines the use of a crosslinker agent and any corresponding changes to the

morphology of the nanofibres and their network. The optimisation of the solution and process was also determined at the beginning of this chapter.

Chapter 5 studies the suitability of PVA for use as ACL implants. This chapter consistes of three studies. PVA Study 1 optimised the solution and process parameters achieving 2D electrospun scaffolds with morphology comparable to the natural ACL morphology. PVA Study 2 was focussed on the mechanical characterization of different scaffolds to identify the optimum i.e. with mechanical and morphological properties comparable to the native ACL. PVA Study 3 determined the degradation of the optimum scaffold.

Chapter 6 studies morphologically and mechanically different 2D and 3D PVA structures under cycles of tensile and shear loads in dry and wet conditions. The optimum prototype to move forward to cell testing and animal models was determined.

Chapter 7 presents a discussion of all the studies done with their limitations and future work.

Chapter 8 explains the conclusions obtained during this thesis.

Chapter 9 conteins the references for the thesis as a whole.

And finally, Chapter 10 presents the appendix.

3. Biomechanical specifications for designing ACL implants

3.1. ABSTRACT

The anterior cruciate ligament (ACL) plays a key role in the stability of the knee joint restricting the rotation and anterior tibial translation. However, there is a lack of knowledge of the *in vivo* ACL mechanical behaviour during high impact manoeuvres. This study aimed to understand and calculate the tensile forces while the anterior cruciate ligament (ACL) is subjected to loading during different activities. The motion of participants with healthy knees while they performed the following activities was investigated: walking, running, negotiating stairs, cross-over cutting, sidestep cutting, jumping and jumping with one leg. The *in vivo* ACL length and strain were calculated using experimental kinematic data and a three degree of freedom (DOF) knee model implemented in OpenSim. The *in vivo* ACL tensile forces were determined with a well-established force/strain relationship obtained through ACL tensile tests. Statistical regression models of ACL lengths with respect to angles for each activity have been performed in order to better understand the ACL failure mechanisms. The results determined that the forces experienced by the ACL of women during stair negotiation were highly significant compared to ACL forces in men and the ACL forces in aged people were significantly higher than in younger people. For the remaining activities, the maximum ACL tensile force was observed during jumping vertically at maximum effort and landing with both legs (1.076±0.113 N/BW). Surprisingly, the peak tensile ACL force for all participants during crossover cutting (0.715±0.2647 N/BW) was lower than during walking

(0.774±0.064 N/BW). Regression coefficients for crossover cutting indicated that excessive knee rotation and abduction angles contribute more significantly to the ACL elongation than in activities such as walking or running. These findings indicated that the ACL is subjected to multidirectional loading; further studies will be performed to investigate torsion and shear force on the ligament.

3.2. INTRODUCTION

The ACL is a key component in the stabilization of the knee joint, restricting the rotation and the anterior tibial motion and has the higher rates of injury of the human knee ligaments [1]. It is estimated that 78% of ACL injuries occur during noncontact activities, where sudden decelerations, landing from a jump, cross-over cutting or pivoting are present [4]. The majority of these injuries were recorded in young athletes [234]. Anatomical (femoral notch distance or laxity), hormonal and biomechanical factors have been researched to understand the important factors contributing to these higher rates of injury [118], [235]; however the key factors contributing to ACL mechanical behaviour during high-risk activities and ACL rupture remain unclear.

Experiments using cadaveric knees [40] determining anthropometrical parameters (ACL insertion points locations or femoral notch distance), or understanding the behaviour under mechanical loading, exhibited limitations in reproducing the *in vivo* mechanical behaviour of the ACL. Video and motion capture

techniques [70], [71] were also used to understand ACL injury mechanisms through the study of joint kinematics but disregarded the ACL length, strain or force. Strain gauges have also been employed to assess the *in vitro* ACL strain [72] and *in vivo* ACL strain in cycling and squatting [73], [74], but in the last case is invasive, requires surgery and the gauge is attached to only a small location of the ACL, not recording the strain across the whole ligament. Experiments with motion capture and biplanar fluoroscopy [75], [76] and studies with motion capture and musculoskeletal simulations [77]–[79] determined ACL length and strain during walking and jumping with both legs but activities with a high injury rates such as jumping with one leg or cutting have not been evaluated.

Due to the wide range of techniques used to determine *in vivo* ACL strain and force and the limitations associated with each technique, there are differences in the results obtained, and comparison between activities is complicated. During walking for example, there is a large disparity with some studies reporting peak ACL forces of 0.2 N/BW [102] and others of more than 1 N/BW [103], [104]. Therefore, it is necessary to develop and implement a reliable and easy methodology to investigate different activities in one study to allow valid comparison, and to have mechanical specifications to design ACL ligaments according to the *in vivo* mechanical behaviour of the ACL. In this chapter two different biomechanical studies were performed (biomechanics study 1 and biomechanics study 2). For the first study a musculoskeletal model with 23 DOFs (1 DOF at the knee joint) [236] was developed and in the second study the model was improved incorporating a total of 27 DOFs (3 DOF at the knee joint) [237]–[239]. Motion capture was used to determine the ACL length, strain and tensile force at all ranges of motion for eight

different activities: ascending stairs, descending stairs, walking, running, sidestep cutting, crossover cutting, jumping with one leg and drop landing and jumping with maximum effort with two legs. Stair negotiation was evaluated in the first study and the rest of the activities in the second study.

Nowadays, many researchers are developing new tissue engineered ligament and tendon implants. However, regarding mechanical characterization, only material properties such as Young's modulus, ultimate tensile strain or tensile stress at yield are considered to determine if the scaffold has the appropriate characteristics to be implanted. Currently, no link has been created between mechanical behaviour at all ranges of motion and the design and development of tissue engineering based ligaments.

The novelty of this Chapter 3 was in trying to understand how this ligament behaves while different activities are performed to study the failure mechanisms of the ACL and so be able to design improved implants relating to the forces experienced on these natural fibrous connective tissues.

Different aims are associated with the two different studies developed in this chapter. The first study aimed to create a novel methodology easy to implement in a large range of activities to calculate *in vivo* ACL strain and tensile force; moreover, pilot studies for gender and different ages to analyse the *in vivo* ACL mechanical behaviour were performed. The second study aimed to develop an improved musculoskeletal model with which to compare the ACL behaviour between activities

and to use to design ligaments relating to the *in vivo* ACL strain and forces experienced by the natural ACL.

3.3. METHODS

As was mentioned in the introduction (section 3.2.), this chapter aimed to understand and calculate *in vivo* forces while the ACL was subjected to loading. To achieve this goal three steps were followed:

a) Recruitment of participants with healthy knees in order to capture their motion (though a VICON system) while they were performing different activities.

b) Development of an OpenSim model to calculate the *in vivo* ACL length from kinematic data and with it be able to calculate the *in vivo* ACL strain at each moment of time.

c) Implementation of a Matlab code to calculate *in vivo* ACL tensile forces using a force/displacement relationship given by Blankevoort. *et al.* [240], to be used as mechanical specifications for the design of the ACL implants.

The *in vivo* ACL mechanical behaviour was analysed by capturing the motion of participants while different activities were performed and then creating a musculoskeletal model in order to estimate the *in vivo* ACL length, strain and tensile forces in each moment of time. The results of this chapter helped in the determination of safety thresholds for the scaffold design.

This chapter shows two different studies. Although both methods were similar, the computational models and tasks for each study were different; therefore, in order to clarify the content of each study, the method followed in each one was presented separately in sections 3.3.1 and 3.3.2.

3.3.1. BIOMECHANICS STUDY 1

The following Figure (3.1) represents the performed steps as needed in the methodology of this first study. An explanation of each task performed with OpemSim (Sim TK, Stanford, CA) was presented in Chapter 1 section 1.3.3.2.

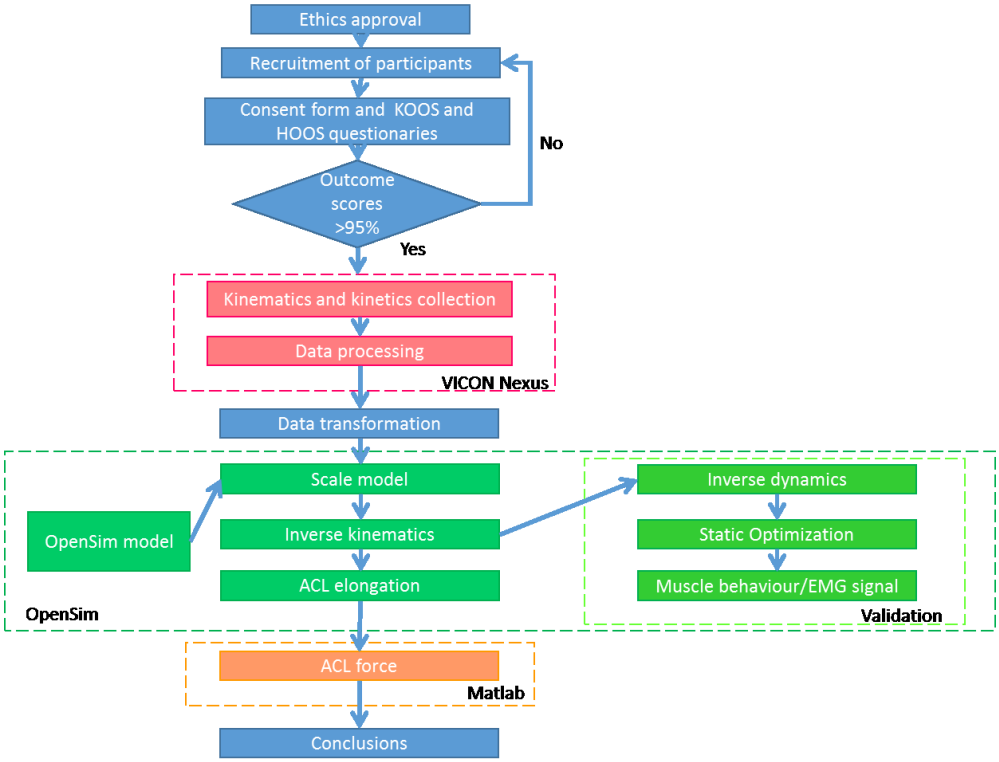

Figure 3.1 Flow chart with the performed tasks in the first study

3.3.1.1. Recruitment of healthy participants

Nine participants (6 men and 3 women; mean±SD age: 41.4±13years, height: 1.7±0.09 m and mass: 69.3±13.7 kg) were recruited for the first study, the number of participants was determined following previous studies [241]–[244]. Each participant was asked to read an information sheet, sign a consent form and to complete two questionnaires prior to beginning any activity. The questionnaires were the Knee Injury and Osteoarthritis Outcome Score (KOOS) and the Hip Injury and Osteoarthritis Outcome Score (HOOS), and they allow the assessment of knee and hip pain/symptoms and to only include in the study the participants with no history of knee injury, surgery or pain. Ethical approval was provided for the project by Science and Engineering Faculty Ethics of the Manchester Metropolitan University (ethics code: SE141530).

3.3.1.2. Motion capture

A 10-camera motion capture system (Vicon 612 system, Oxford Metrics, UK) was used to collect kinematic data sampled at 100 Hz for both studies. A modification of the Cleveland Clinic marker set [109], consisting of 33 reflective markers placed on specific anatomical landmarks of the lower and upper body of the participants, was utilized to collect the kinematic measurements. The locations of the markers can be seen in Figure 3.2.

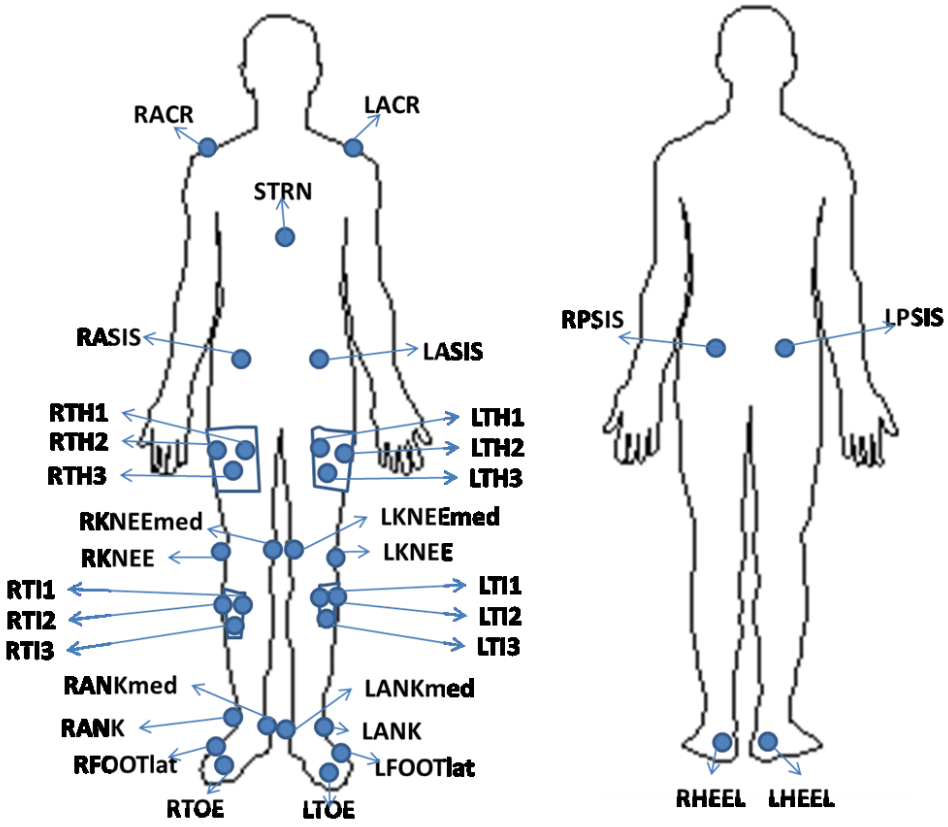

Figure 3.2 Reflective markers locations.

In addition, in the first study a set of 16 wireless surface electromyography (EMG) sensors (Delsys Inc. Boston, MA, USA) were placed on each participant,

recording the activation of the muscles *quadriceps vastus medialis*, *quadriceps rectus femoris*, *quadriceps vastus lateralis*, *tibialis anterior*, *peroneus longus*, *gluteus medius*, *medial hamstrings* and *gastrocnemius medialis* of both legs. The locations of these EMG sensors are shown in Figure 3.3. The purpose of EMG recordings was to validate the behaviour of the muscles in the first musculoskeletal model.

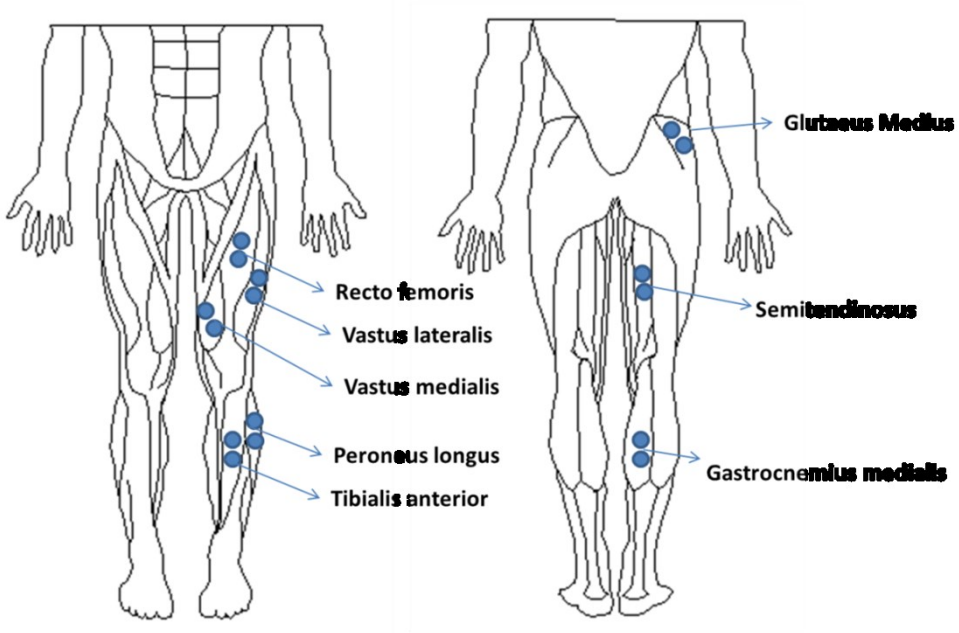

Figure 3.3 EMG sensors locations.

Before starting the experiment, the 10-camera motion capture system (Vicon 612 system, Oxford Metrics, UK) was calibrated in order to calculate the location and orientation of all the cameras, and the correct operation of the EMG electrodes was checked on each participant.

As mentioned in the introduction (section 3.2.), the first study was performed over an 8-step experimental staircase. The majority of experimental stairs used in biomechanical studies have only 1 or 2 steps [245]–[248], however this is one of the

first studies investigating ACL loading over a realistic staircase with an appropriate number of steps to simulate a real-life scenario. Therefore, a staircase with an optimum number of steps considering the resources (space, laboratory height and the number of Vicon cameras available) and the repeatability of the motion was used. This staircase had standard dimensions and contained four force platforms (Kistler, Switzerland) embedded into the middle steps. This staircase can be seen in Figure 3.4.

Figure 3.4 8-step experimental staircase.

The force plates, in the first study, were used to help inform the static optimisation solver implemented in OpenSim for the calculation of the muscle activation. An initial static trial for participant calibration (scale body segments and align joints) was performed with each participant. This first trial was considered successful when all markers were visualized. Then, the participants were asked to perform the tasks up to a total of three successful trials following previous studies

[247], [248], while kinematic data were captured and EMG signal and reaction forces were recorded.

For the first study, the participants were asked to ascend and descend the staircase at a normal self-selected speed in a step-over-step manner.

Once the data were collected, they were processed in Vicon Nexus 1.8.5. (Vicon Motion Systems Ltd, UK) software and exported to OpenSim 3.3 (Sim TK, Stanford, CA) for the kinematics analysis.

3.3.1.3. Determination of ACL elongation

The *in vivo* ACL length at each timepoint was determined by tracking the coordinates of the ACL insertion points from the processed kinematic data derived from motion capture and a musculoskeletal model scaled for each participant according to their anatomy.

A musculoskeletal model was developed based on the Gait 2392 model [249] implemented in OpenSim software, a lower extremity with back and torso model created by the developers of OpenSim. For the first study a model with 23 DOFs (1 DOF at the knee joint), with 12 elements representing the bones and 92 musculotendon actuators was developed.

The anterior cruciate ligaments were modelled as an elastic passive soft tissue that follows a straight-line path between the insertion points in the femur and tibia. A Thelen2003 muscle [115] model implemented in OpenSim and based on Hill's

model [250] was used to simulate the ACL. In order to mimic its passive character, the fibre length was set to zero and the contractile element activation was annulled.

The attachment sites were studied and incorporated in this model using the average values reported in Xu *et al.* [78] and the placement was verified through Lee *et al.* [31] and Jordan *et al.* [251]. The coordinates for femur and tibia insertion points are shown in Table 3.1.

Table 3.1 ACL insertion points.

	Insertion at femur (m)			Insertion at tibia (m)		
	X	Y	Z	X	Y	Z
Right leg	-0.0111	-0.4051	0.00705	0.00955	-0.0313	-0.00035
Left leg	-0.0111	-0.4052	-0.00705	0.00955	-0.0313	0.00035

The two ACL fibre bundles (anteromedial and posterolateral) were not considered in this model, since it was demonstrated [252] that the behaviour of both bundles is similar. Both bundles are stretched when the knee is extended and shortened when the knee is flexed. In addition, most surgeons prefer to perform a single bundle surgery to minimize loss of bone, risk of infection, time, and favour healing.

The ACL length was calculated from kinematics due to the fact that the OpenSim model allows tracking of the coordinates of the attachment sites and calculation of the elongation at each moment of time with an analysis solver.

The strain at each instant was calculated from the ligament length change at each timepoint and the unloaded length. The *in vivo* unloaded length of the ACL for each participant was determined from a reference length (ACL length at knee full extension calculated, with the coordinates of the attachment sites, for each participant) and reference strain (taken from literature [240]) following previous studies [240].

3.3.1.4. ACL Force Estimation

It is well known that ligaments have a viscoelastic character and follow a non-linear force/displacement curve due to the crimping pattern of their fibres. This chapter used the force/displacement curve defined by Blankevoort and Huiskes *et al.* [240] where a ligament was simulated by a non-linear spring, and its viscoelastic behaviour was mimicked with a damping element in parallel to the spring (Figure 3.5).

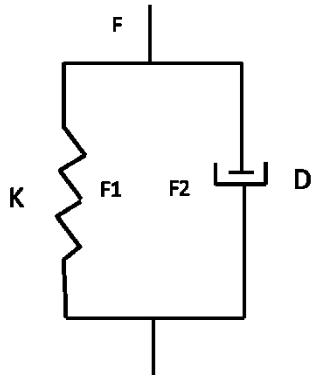

Figure 3.5 Sketch of the viscoelastic behaviour of the ACL.

The estimation of the tensile force exerted by the spring (F_1) was performed following the equations presented in [240]:

$F_1 = ¼\ k\ \varepsilon^2 / \varepsilon_l \qquad 0 \leq \varepsilon \leq 2\ \varepsilon_l$

$F_1 = k\ (\varepsilon - \varepsilon_l) \qquad \varepsilon > 2\ \varepsilon_l$

$F_1 = 0 \qquad \varepsilon < 0$

Where:

ε Strain of the ligament

ε_l Linear range threshold

k Stiffness of the spring

The strain is calculated from the ligament length (L) at each position and the zero-load length (L_0).

$$\varepsilon = (L - L_0) / L_0$$

The unloaded ligament length is difficult to obtain; therefore, it was calculated by the length (L_r) and strain (ε_r) of the ligament at full extension, the reference position in the experimental trials.

$$L_0 = L_r / (\varepsilon_r + 1)$$

The force exerted by the damper (F_2) was calculated using the equation:

$$F_2 = D\ v$$

Where:

D Damping coefficient

v Ligament velocity calculated by the central difference method.

The parameters to model the ligaments are shown in Table 3.2.

Table 3.2 Stiffness, threshold strain, reference strain and damping coefficient.

k (N)	ε_l	ε_r	D (N s/m)
5000 [240]	0.03 [240]	0.08 [240]	500 [253], [254]

Subsequently the calculated forces were normalized for Body Weight (BW) allowing comparison between participants.

It is worth noticing that although the behaviour of both ACLs were collected, for the sake of simplicity only right-handed participants were considerated and only the results for the right knees are presented in the second experiment.

Similar approaches to determine the ACL elongation and tensile force were used in Debski, Darcy and Woo *et al.* [255] when testing cadaveric knees.

3.3.1.5. Muscle validation

In order to validate the correct muscle function of the first model, the activation of certain muscles around the knee were recorded with EMG sensors and this activation was qualitatively compared with the forces of that muscles estimated from the OpenSim model. Figure 3.6 shows how the peaks of recorded activation for vastus lateralis are in the same instant of time as the peaks of force for the same muscle.

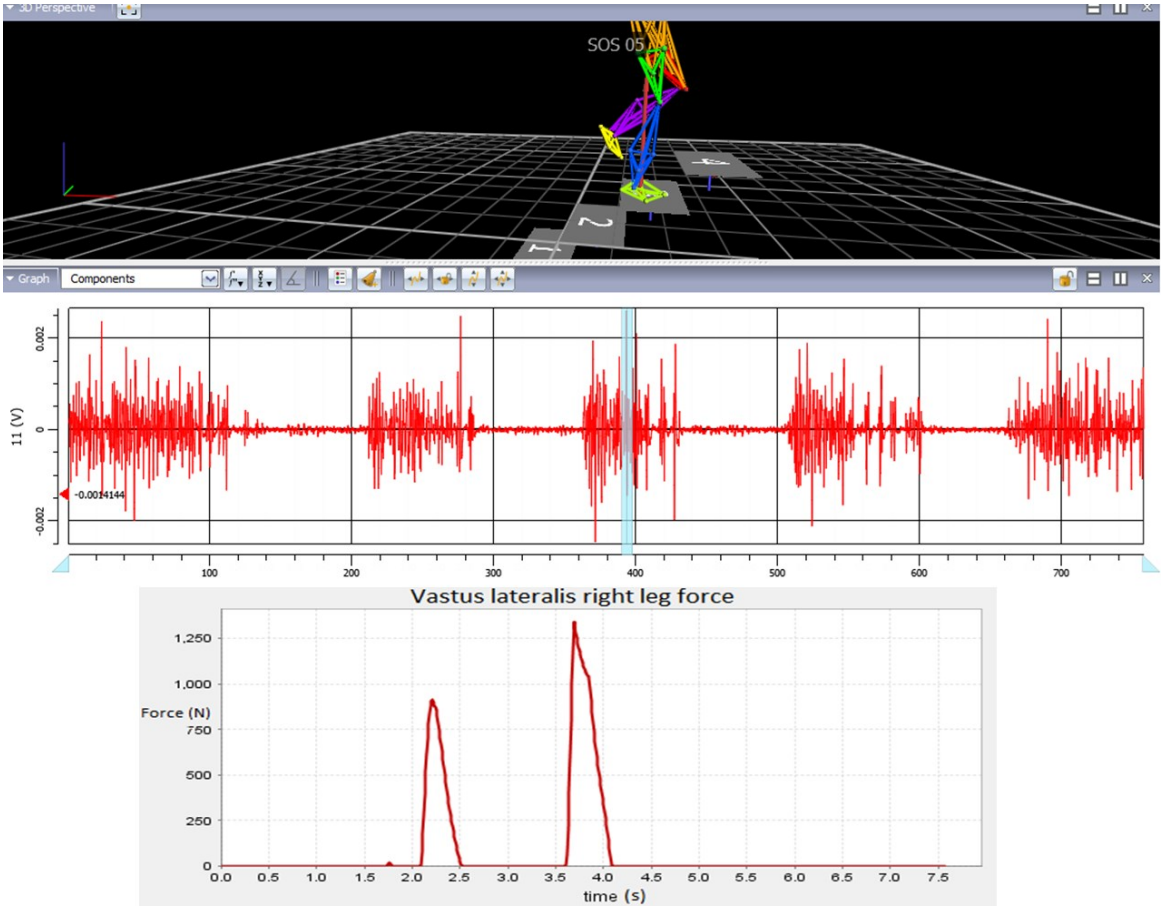

Figure 3.6 Vastus lateralis activation given by EMG and forces calculated by OpenSim model.

3.3.1.6. Statistical analysis

For the first study, no outliers in the data were observed from visual inspection. Moreover, differences between estimated ACL forces on both knees for sex, age and activities groups were compared using a one-way and two-way analysis of variance (ANOVA) with a 95% confidence interval, for the first experiment.

All statistical analyses were conducted using SPSS (IBM Inc., Chicago, Illinois).

3.3.2. BIOMECHANICS STUDY 2

The following Figure (3.7) represents all the performed steps needed in the methodology of this second study.

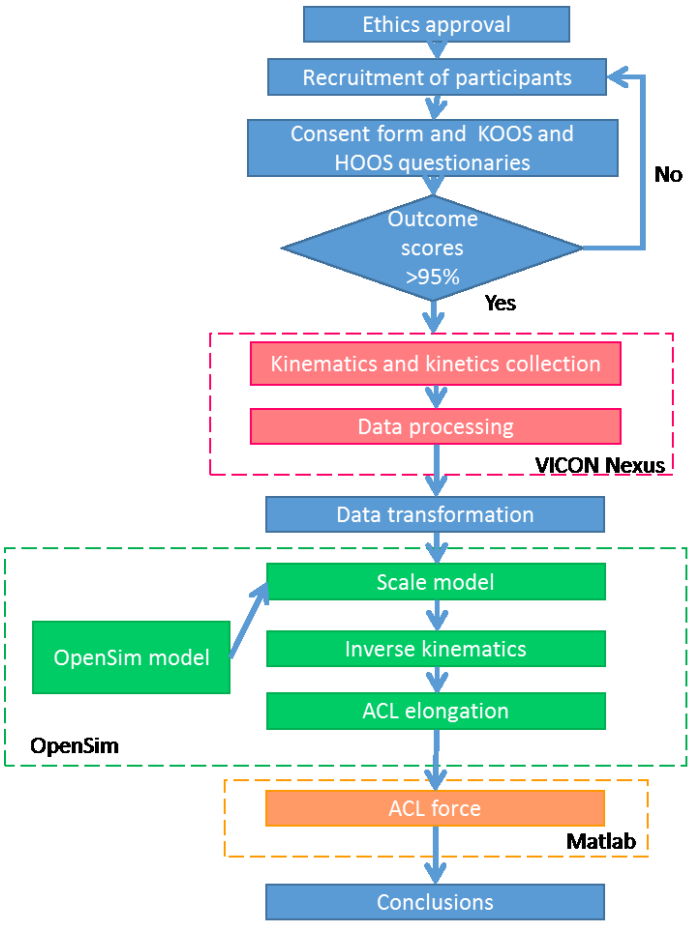

Figure 3.7 Flow chart with the performed tasks in the second study

3.3.2.1. Recruitment of healthy participants

Twelve young adults with no previous ACL injuries (7 men and 5 women; mean ± SD age: 27.3 ± 3.3 years, height: 1.7 ± 0.1 m and mass: 71.6 ± 15.5 kg) were recruited for the second study following the number of participants in Morisson *et al.*

[102]. Test participants gave informed consent and the study was approved by the University's Faculty Ethics committee as was explained for the first study in section 3.2.1.1.

3.3.2.2. Protocol

As in the first study, a 10-camera motion capture system (Vicon 612 system, Oxford Metrics, UK) was used to collect kinematic data sampled at 100 Hz. A modification of the Cleveland Clinic marker set [109], consisting of 33 reflective markers placed on specific anatomical landmarks of the lower and upper body of the participants, was utilized to collect the kinematic measurements.

All activities involved in the second study were performed over level ground and the participants were asked to perform them at their self-selected speed in order to eliminate interference with the correct execution of the task. Activities were: walking, running in a straight line, crossover cutting turning suddenly, sidestep cutting running straight then stepping at the right side with the right leg and keeping running straight, dropping from a 30 cm height jumping box and performing a vertical maximum effort jump with both legs, and jumping horizontally three times with one leg. The setup of this experiment can be seen in Figure 3.8.

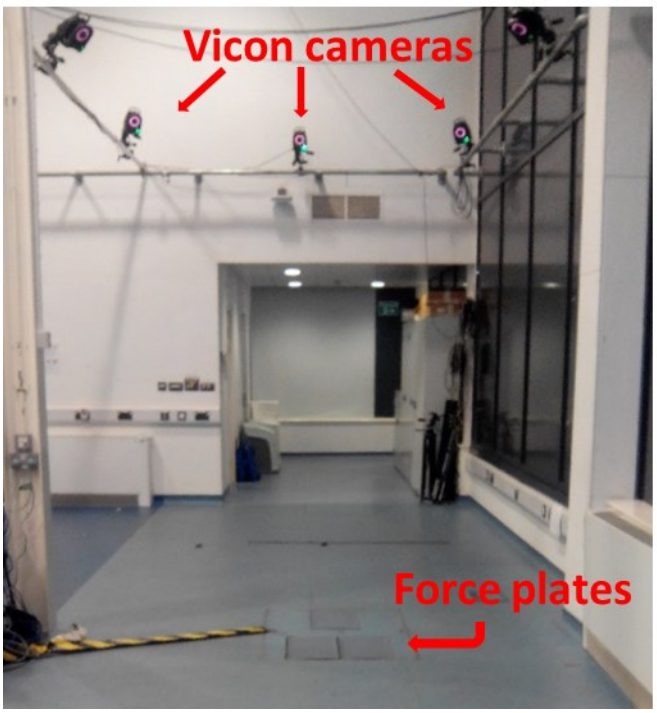

Figure 3.8 Setup of Vicon cameras and force plates for the experiment over level ground

Tape was placed on the floor for the purpose of all participants undertaking the activity in the same manner; moreover three force plates were used, in the second study, just for reference points to perform the tasks. The tape was used to indicate the starting and ending point of all the activities and the trajectories of the cutting tasks. Once the participants were familiarised with the activities (performing them until their execution were correct) the kinematic data was collected for each participant over three successful repeated trials.

For this second study, they were asked to walk straight as normally as possible and step over the second force plate (FP2), as shown in Figure 3.9.

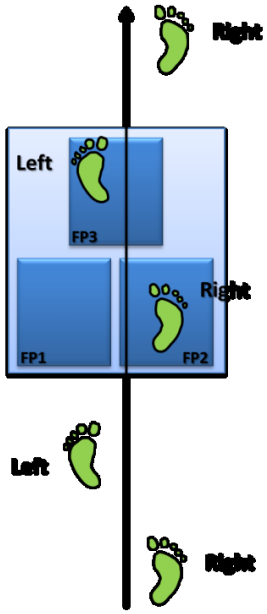

Figure 3.9 Walking trial.

Afterwards, the participants run straight as normally as possible, stepping over one force plate (FP2) (Figure 3.10).

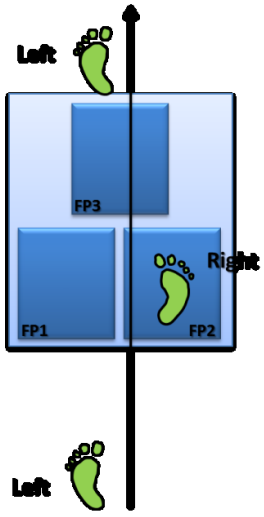

Figure 3.10 Running trial.

For the next task, they were asked to run at a certain angle and step over the FP2 force plate with the right leg and then turn and step over the FP3 with the left leg to perform a crossover cutting maneuver (Figure 3.11).

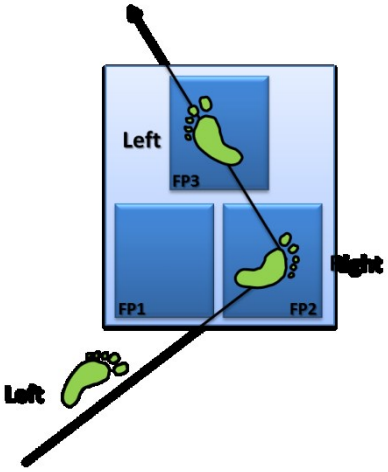

Figure 3.11 Crossover cutting trial.

Immediately after, they performed a sidestep cutting maneuver, running straight, stepping over the FP2 force plate with the right leg and keeping running straight (Figure 3.12).

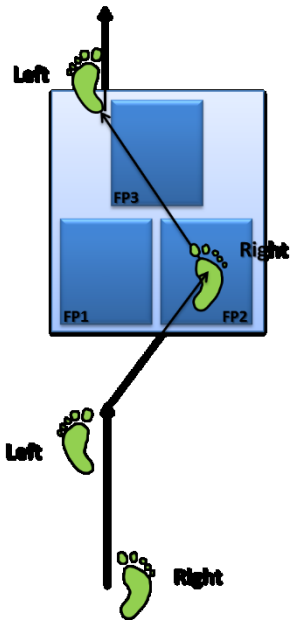

Figure 3.12 Sidestep cutting trial.

In the next activity, the participants were asked to drop from a 30cm height jumping box to the force plates (FP1 and FP2) and then jump as high as possible (Figure 3.13).

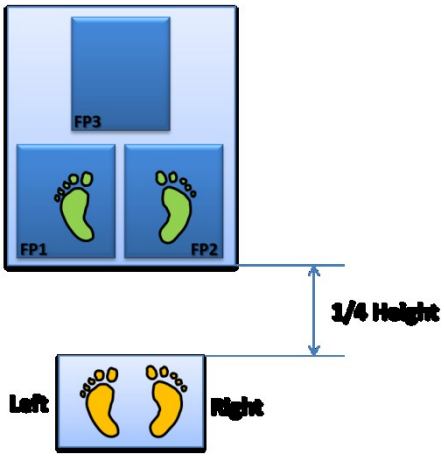

Figure 3.13 Jumping trial.

The last activity for this second study was to jump with one leg. For this activity they were asked to jump with one leg to the FP2 then to the FP3 and finally to the floor (Figure 3.14).

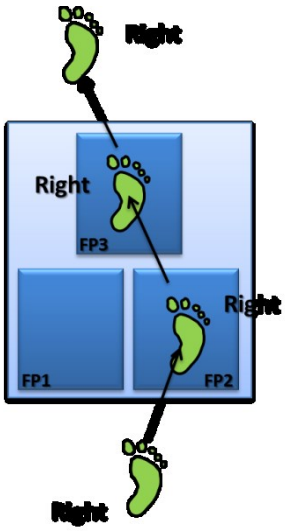

Figure 3.14 Jumping with one leg trial.

The data were processed in Vicon Nexus 1.8.5. software (Vicon Motion Systems Ltd., UK) and exported to OpenSim 3.3 (Sim TK, Stanford, CA) for the kinematics analysis.

3.3.2.3. ACL elongations and force calculation

The *in vivo* ACL length at each timepoint was determined by tracking the coordinates of the ACL insertion points from the processed kinematic data derived from motion capture and a musculoskeletal model scaled for each participant according to their anatomy. The initial model developed for the first study was improved incorporating a total of 27 DOF of which 6 corresponded to the knee joints (3 DOF for each knee), 12 segments represented the bones and 92 the musculotendon actuators. The anterior cruciate ligaments were modelled as an elastic passive soft tissue as previously described in Roldán *et al.* [236] and in section 3.3.1.3 of the present thesis.

The strain at each instant was calculated from the ligament length change at each timepoint and the unloaded length. The *in vivo* unloaded length of the ACL for each participant was determined from a reference length (ACL length at knee full extension calculated for each participant) and reference strain (taken from literature [240]) following previous studies [236], [240]. The equations used to calculate the ACL length and strain can be found in Section 3.3.1.4.

ACL tensile forces were calculated from a force/strain relationship reported in Blankevoort and Huiskes [240] where the ligament was simulated by a non-linear

spring, and its viscoelastic behaviour was mimicked with a damping element in parallel to the spring following the method implemented in previous studies [236] and section 3.3.1.4 of this chapter. Subsequently these calculated forces were normalized for Body Weight (BW) allowing comparison between participants.

Notice that although the behaviour of both ACLs were collected, for the sake of simplicity only the results for the right knees are presented. Similar approaches to determine the ACL elongation and tensile force were used in Debski *et al.* [255] when testing cadaveric knees.

3.3.2.4. Statistical analysis

For the second study, multiple linear regressions were performed to calculate the relationship between the right ACL length and the right knee angles for each activity (considering positive sign to knee flexion, external rotation and abduction angles). The coefficient of determination (R^2) decreases considerably when the sample size increases. In this case, the sample size for each activity was very large, reaching 3410 degrees of freedom for the two-legged jumping activity. Therefore, in order to verify the goodness of fit it was necessary not only to consider the R^2 value, but also to have low standard error of the calculation, a highly significant F test with a value of F above unity, highly significant regression coefficients (P value < 0.001) with short confidence intervals, non-colinearity between independent variables with a condition index below 15, and the normal distribution of the residuals. The Pearson coefficient signs indicated the behaviour of the ACL length when one of the knee angles varied. The sign of regression coefficients and Pearson coefficients could be different, since Pearson coefficients measure how an independent variable is related

to the dependent variable and the regression coefficients indicate how all independent variables are related to the dependent variable.

All statistical analyses were conducted using SPSS (IBM Inc., Chicago, Illinois).

3.4. RESULTS AND DISCUSSION

The first study was focussed on the development of an easy to implement methodology to estimate the tensile forces experienced by the ligament, and the differences in the ACL mechanical behaviour between genders and ages were analysed through a pilot study. This first study will allow understanding of the feasibility of manufacturing ACL implants according to patient's needs.

The second study was focussed on the comparison between 6 daily and high impact activities in order to obtain the tensile forces experienced by the ligament and with them the mechanical specification for the ACL implant.

The results of both studies were shown in the next section 3.4.1.

3.4.1. BIOMECHANICS STUDY 1

3.4.1.1. Stair negotiation

The same pattern of knee flexion/extension angle and ACL length was observed for each participant. Since an 8-step staircase was used to perform the experiment, four cycles for each leg were obtained. This model showed that the length of the ACL increased when the knee was extended and decreased as the flexion angle was increased regardless of the performed activity, this pattern is shown in Figure 3.15. Analysing the motion during climbing stairs, the maximum ACL length was recorded at full extension of the knee (stage A in Figure 3.15). The first ACL minimum length was at 90 degrees of knee flexion (stage B), then the ACL length increased at peak knee flexion due to the position of the insertion points (stage C). The second ACL minimum length was recorded at full strike (stage D) and finally the length increased again at the stance phase.

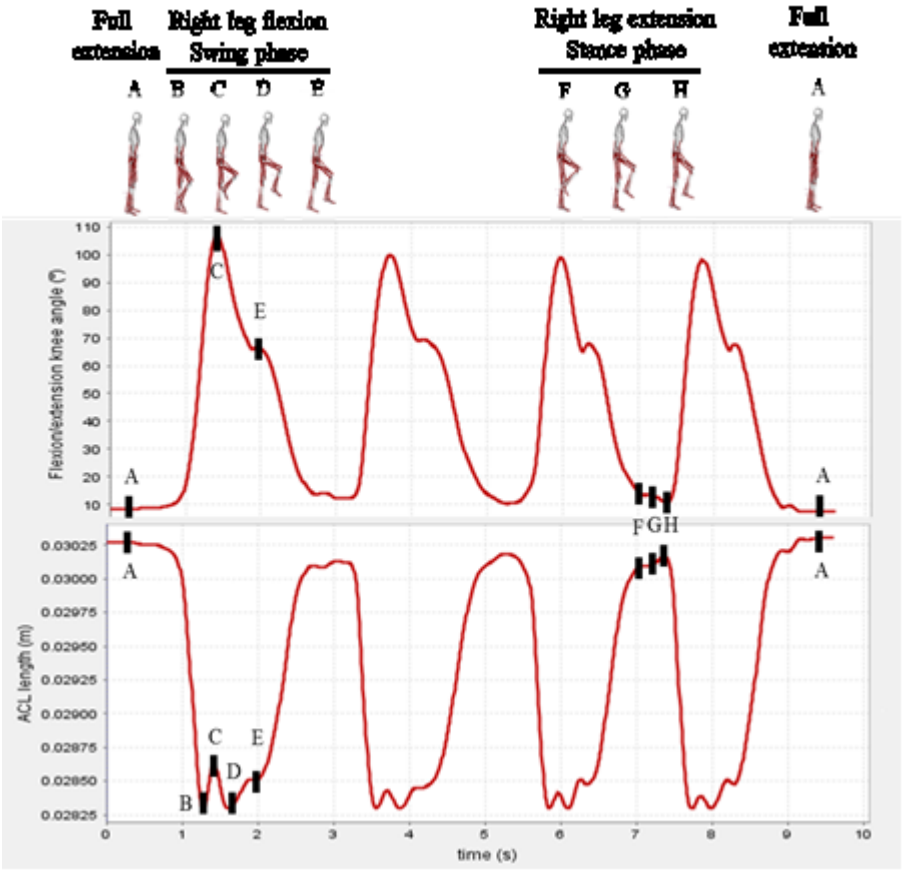

Figure 3.15 Flexion knee angle (°) versus ACL length (m) ascending stairs.

The mean of the maximum ACL length recorded was 0.0289±0.0017 m corresponding to a full extension position and the mean of the minimum ACL length was 0.027±0.0016 m. Therefore, the maximum elongation recorded was 0.0019±0.0001 m, which is approx. 19% of the reported elongation at failure of the ACL [253], [254]. Differentiating between genders, the mean ACL length for men was 0.0294±0.002 m and for women 0.0258±0.004 m.

Previous studies with 20 human cadaveric knees determined that the average of ACL length in men is 0.029±0.0025 m and in women 0.0268±0.0028 m [40]; following these findings it can be concluded that the calculated ACL length were

within the same range and therefore they could be considered as anthropometrically valid.

Analysing the ACL strain, a maximum strain of 0.084±0.0047 and a minimum strain of 0.012±0.0048 were observed.

The maximum force experienced by the ACL was observed at full extension of the knee. The average of the peak ACL force/body weight (BW) while the participant was ascending stairs was 0.409±0.058 N/BW and descending stairs was 0.416±0.089 N/BW. The peak ACL force was calculated to be 325.43 N for descending stairs, which is around 18% of the reported failure strength of the ligament [58], [59].

The most statistically significant values of force are shown in Table 3.3. Moreover, the values of peak ACL strain and forces for men versus women and young (<40 years old) versus older adults (≥40 years old) are shown in Tables 3.4 and 3.5.

Table 3.3 ACL forces during stair negotiation (mean±SD). ANOVAs for groups of sex, age and activities.

Total ACL force (N/BW)	Sex			Age			Activity		
	Men	Women	P value	Young (<40)	Older (>40)	P value	Ascending	Descending	P value
Right ACL	0.181±0.131	0.248±0.181	0.000	0.191±0.141	0.217±0.165	0.000	0.187±0.149	0.217±0.150	0.000
Left ACL	0.176±0.135	0.251±0.188	0.000	0.192±0.143	0.208±0.176	0.000	0.199±0.153	0.197±0.160	0.424

Table 3.4 Peak ACL strain and forces (mean±SD) during stair negotiation in men and women.

		Strain		Maximum Force/BW	
		Maximum	Minimum	Total Force (N/BW)	Damper Contribution Force (N/BW)
Ascending stairs	Men	0.085±0.006	0.012±0.005	0.383±0.037	0.002±0.0005
	Women	0.083±0.001	0.012±0.006	0.462±0.061	0.003±0.0007
Descending stairs	Men	0.084±0.003	0.013±0.005	0.375±0.044	0.003±0.0005
	Women	0.086±0.007	0.015±0.006	0.497±0.109	0.004±0.001

Table 3.5 Peak ACL strain and forces (mean±SD) during stair negotiation in young and older adults.

		Strain		Maximum Force/BW	
		Maximum	Minimum	Total Force (N/BW)	Damper Contribution Force (N/BW)
Ascending stairs	Young	0.081±0.001	0.011±0.005	0.415±0.049	0.0025±0.0004
	Older	0.088±0.004	0.012±0.006	0.403±0.075	0.0024±0.0009
Descending stairs	Young	0.081±0.001	0.013±0.004	0.416±0.047	0.0036±0.0012
	Older	0.089±0.004	0.017±0.003	0.416±0.135	0.0033±0.0009

From Tables 3.3, 3.4 and 3.5 the following conclusions can be deduced. Women's anterior cruciate ligaments were subjected to significantly higher tensile forces compared to men's ACLs and in general these forces were higher when the participant was descending stairs. This conclusion agrees with a previous study which reported that female athletes suffer ACL injuries from 4 to 6 more times than male athletes [17].

For this study and in order to determine how the age contributes to the ACL forces, the participants below 40 years old were considered as young people and the participants above 40 as older aged people. The ANOVA test regarding age showed that the ACL forces in both legs were significantly higher for older people compared to young people. This phenomenon can be explained since the tissue loses water and gets stiffer with increased age, therefore the ACL forces are expected to be higher as following Hooke's law, where the force is directly proportional to the stiffness.

To date there is no OpenSim model to estimate ACL force during stair negotiation. Therefore, the values of ACL force obtained in this study are difficult to compare with other models. However, some studies reported that the peak ACL forces during gait are between 0.2 N/BW and more than 1 N/BW [79].The estimation in this study was around 0.41 N/BW, therefore it was comparable to the ACL loads previously reported.

The viscoelastic contribution in the force, quantified by the ACL velocity and the damping coefficient, was negligible compared to the ACL total force. Moreover, in neither case were significant differences observed after performing different analyses of variance.

Several studies have been published to determine the ACL length and strain based on motion capture and biplanar fluoroscopic images, while certain activities such as walking and jumping are performed [75], [76]. These studies reported a peak ACL strain of up to 13%. In the present study the peak ACL strain was up to 8.9% descending stairs, therefore it can be said that this model provides a realistic calculation of ACL strain.

3.4.2. BIOMECHANICS STUDY 2

The peak ACL force and strain, position of the maximum ACL length and elongation of the ACL for each activity are presented in Table 3.6. The maximum ACL tensile force and elongation were seen during jumping with two legs.

Table 3.6 Peak right ACL tensile forces, elongation, strain and position of the maximum right ACL length for each activity (mean±SD).

Activity	Max. Force (N)	Max. Force (N)/BW	Max. Elongation (mm)	Max. Strain	Max. ACL Length Position
Walking	513.068±8.337	0.774±0.064	6.15±0.28	0.132±0.002	Heel off
Jumping with two legs	726.003±64.222	1.076±0.113	7.32±1.21	0.175±0.013	Flight phase of the jump
Running	368.243±113.627	0.624±0.216	5.28±0.05	0.097±0.002	Heel strike
Sidestep cutting	472.703±168.209	0.836±0.323	5.33±0.01	0.107±0.040	Heel strike
Crossover cutting	425.869±147.602	0.715±0.265	5.36±0.15	0.107±0.032	Heel strike
Jumping with one leg	149.352±55.474	0.243±0.092	3.86±0.17	0.047±0.016	Flight phase of the jump

Every participant exhibited a similar pattern of knee angles and ACL length when performing the same activity, therefore changes in ACL length for both sexes (considering sex as a categorical variable with 0 for men and 1 for women) can be predicted for changes in the three knee angles (quantitative variables) through multi-linear regression models. The models performed in this study were highly significant with a high Fisher's F, highly significant regression coefficients (P value < 0.001) with short confidence intervals demonstrating the precision of the calculation, a low standard error of the calculation, non-colinearity of the independent variables and normal distribution of the residuals. The signs of Pearson correlation coefficients (Table 3.7) indicate that the ACL length is longer in males, when the knee is extended, as the knee internal rotation and the valgus angle increase.

Table 3.7 Multiple linear regression parameters.

Activity	Fisher's F	Pearson Coefficients				Standard error of estimation	R^2
		Sex	Flexion	Ext. Rotation	Abduction		
Walking	615.27*	-0.446*	-0.526*	-0.483*	0.206*	0.002	0.61
Jumping with two legs	359.44*	-0.313*	-0.209*	-0.435*	0.06*	0.0028	0.3
Running	136.02*	-0.542*	-0.6*	-0.391*	0.137*	0.0025	0.36
Sidestep cutting	60.63*	-0.398*	-0.07*	-0.414*	0.083*	0.0029	0.24
Crossover cutting	91.43*	-0.469*	0.098*	-0.424*	0.221*	0.0027	0.31
Jumping with one leg	891.81*	-0.574*	-0.414*	-0.646*	0.146*	0.002	0.66

* Highly significant P value < 0.001

3.4.2.1. Walking

Analysing the walking motion, the maximum ACL length was recorded at full knee extension (stage C in Figure 3.16) at heel off. The ACL minimum length was at 50º of knee flexion (during the swing phase). A maximum was observed at maximum knee flexion (around 65º) due to a decrease of knee rotation angle.

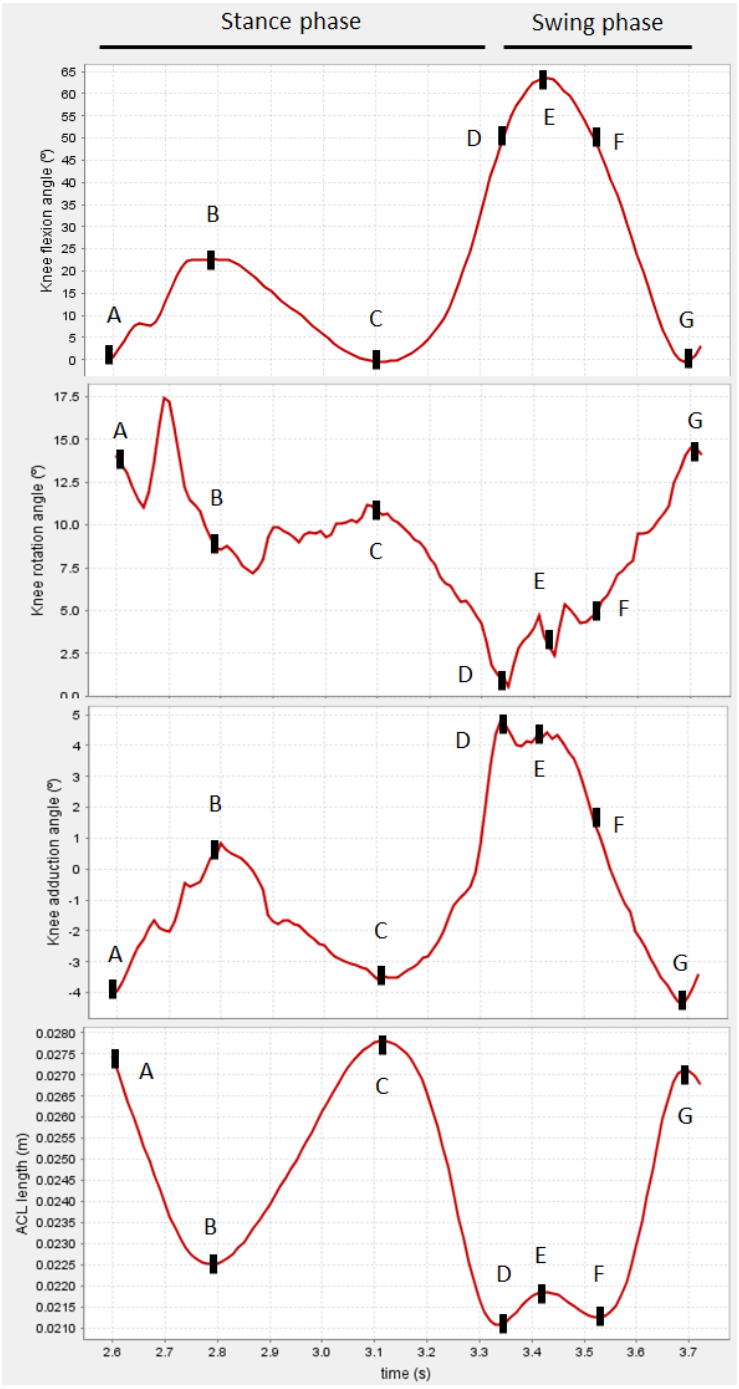

Figure 3.16 Knee angles and ACL length walking.

The following function (1) predicts the ACL length for walking.

ACL length (m) = 0.03317 – 0.002415*Sex - 0.00009*Knee flexion angle (º) - 0.000144*Knee external rotation angle (º) + 0.00006*Knee abduction angle (º) (1)

3.4.2.2. Jumping with two legs

Five ACL length peaks were found in all participants. Figure 3.17 shows the stages for this activity, where A corresponds to the moment just before reaching the force plates where the knees are extended or almost extended, B is the maximum flexion of the knee after the drop where the valgus and internal rotation angles increase, C is when the participant completely extended the knees during the jump (flight phase of the jump), D is the moment where the participant reached the highest height jumping and E is the maximum flexion of the knee after the jump.

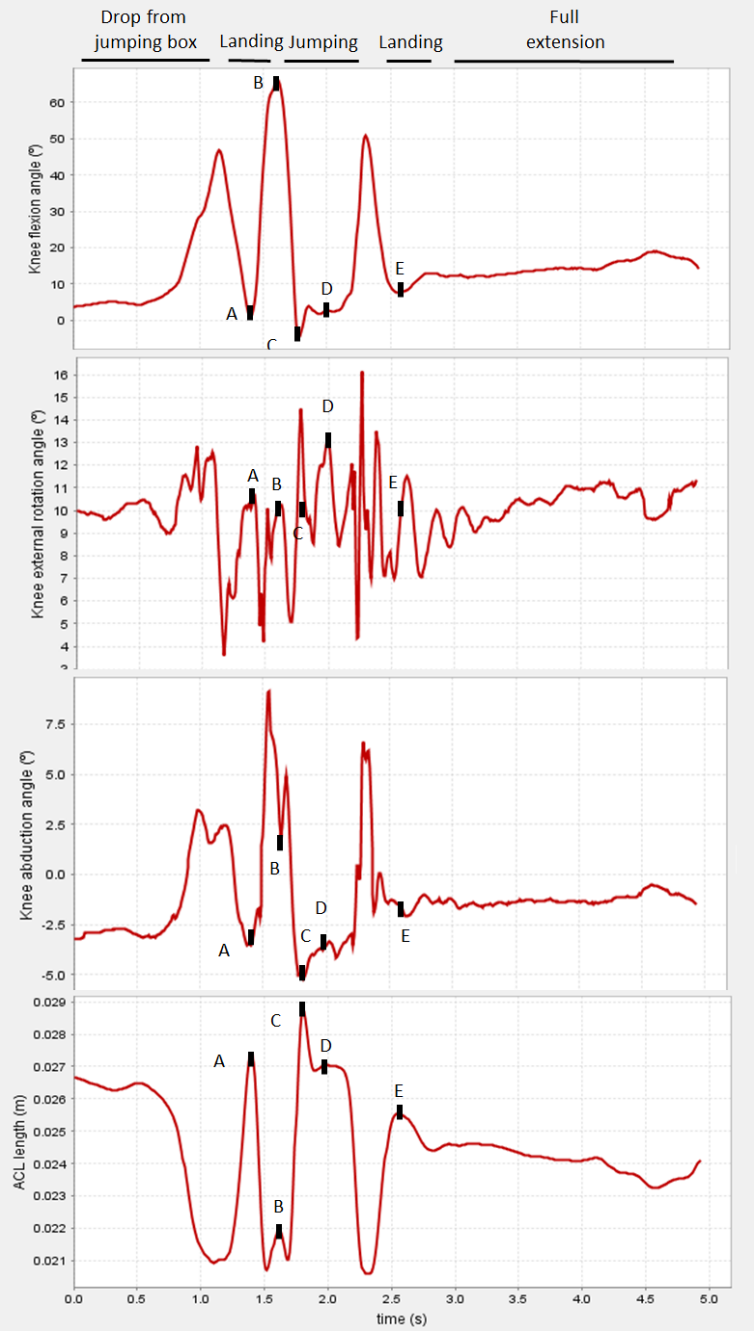

Figure 3.17 Knee angles and ACL length for jumping and landing with two legs.

Regression coefficients were used to determine the relationship (2) between gender, knee angles and ACL length at each stage for this activity:

ACL length (m) = 0.02932 – 0.000675*Sex - 0.000036*Knee flexion angle (º) - 0.000168*Knee external rotation angle (º) - 0.000054*Knee abduction angle (º) (2)

3.4.2.3. Jumping with one leg

A total of six ACL length peaks were found in all participants; the first (stage C), third (stage G) and fifth (stage J) peaks corresponded to the moment of toe off, the second (stage E), fourth (stage H) and sixth (stage K) peaks were when the participants were jumping with their leg extended. Stages F and I corresponded with the moments when the participants were landing flexing their knee. Stage B was the moment when the participant flexed the knee to gain momentum for the jump and D was the moment when the participants were jumping with the knee slightly flexed. Figure 3.18 shows all these stages for the ACL length versus the knee angles.

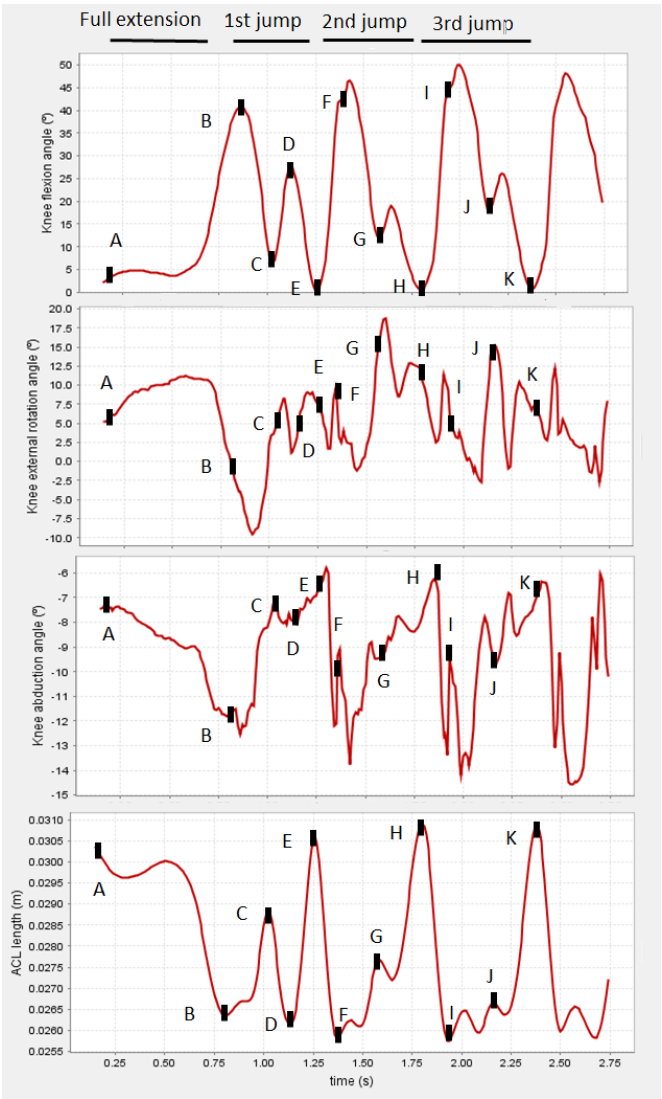

Figure 3.18 Knee angles and ACL length for jumping and landing with one leg.

The relationship between gender, knee angles and ACL length is shown in the equation (3):

ACL length (m) = 0.03149 – 0.00224*Sex - 0.000087*Knee flexion angle (º) - 0.000159*Knee external rotation angle (º) - 0.00005*Knee abduction angle (º) (3)

3.4.2.4. Running

Three ACL length peaks were found in all participants, the first peak corresponded to heel strike being the highest of the three peaks (stage A), the second peak is at toe off (stage B) and the third is at maximum knee flexion (stage C). This situation can be observed in Figure 3.19.

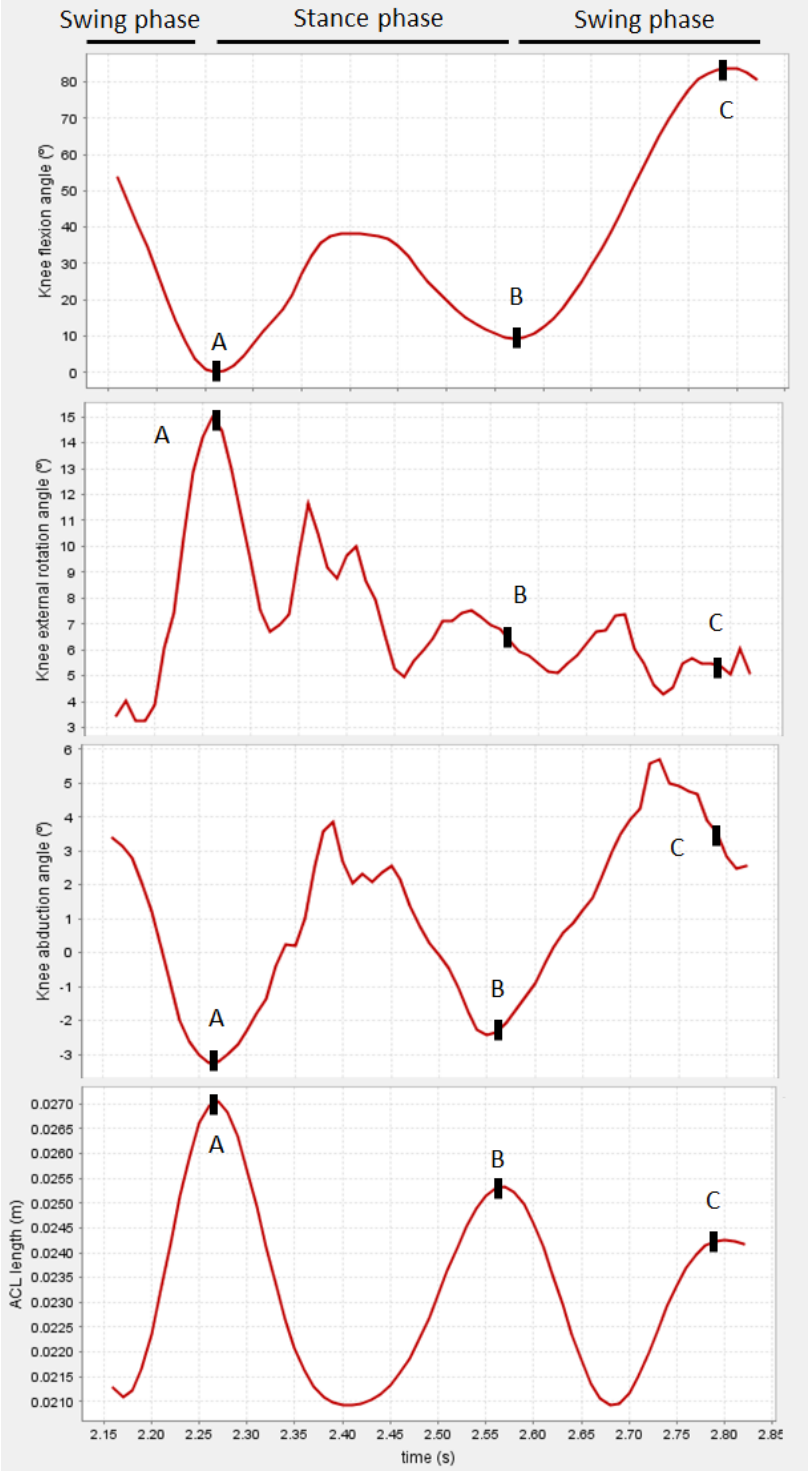

Figure 3.19 Knee angles and ACL length for running.

In the regression model for running, the constant, sex and rotation angle were highly significant; contributing to the prediction of the dependent variable. However, the coefficients of knee flexion and abduction angles were not significant (P value

0.55 and 0.18 respectively), which means that these angles do not contribute significantly to the model. The predicted function for running was:

ACL length (m) = 0.02999 – 0.00306*Sex - 0.0000019*Knee flexion angle (º) - 0.000084*Knee external rotation angle (º) - 0.000022*Knee abduction angle (º) (4)

3.4.2.5. Sidestep cutting

Similar to the previous activity (running) three ACL length peaks were found in all the participants, the first peak corresponded to heel strike (stage A), the second peak was at toe off (stage B) and the third at maximum knee flexion (stage C) (Figure 3.20).

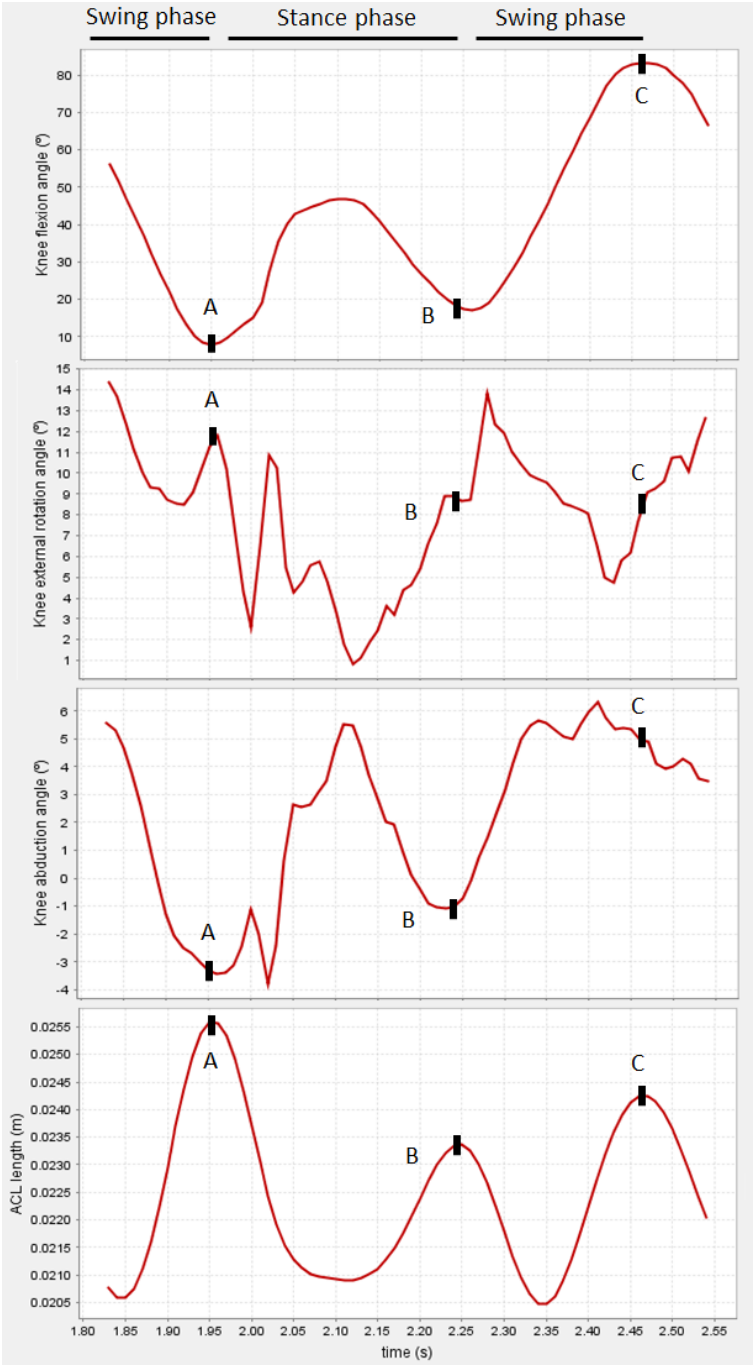

Figure 3.20 Knee angles and ACL length for sidestep cutting.

As was observed running, the constant, sex and rotation angle provided important information for predicting the dependent variable in the regression model, however the coefficients of knee flexion and abduction angles were not significant (P value 0.55 and 0.62 respectively), meaning that these angles do not contribute significantly to the model. The function model obtained was:

ACL length (m) = 0.0282 – 0.001997*Sex + 0.000002*Knee flexion angle (º) - 0.000086*Knee external rotation angle (º) - 0.0000096*Knee abduction angle (º) (5)

3.4.2.6. Crossover cutting

As observed in the activities of "running" and "sidestep cutting" the pattern of the ACL length showed three peaks for all participants in the same stages. The first peak corresponded to heel strike (stage A), the second peak is at toe off (stage B) and the third is at maximum knee flexion (stage C), as shown in Figure 3.21.

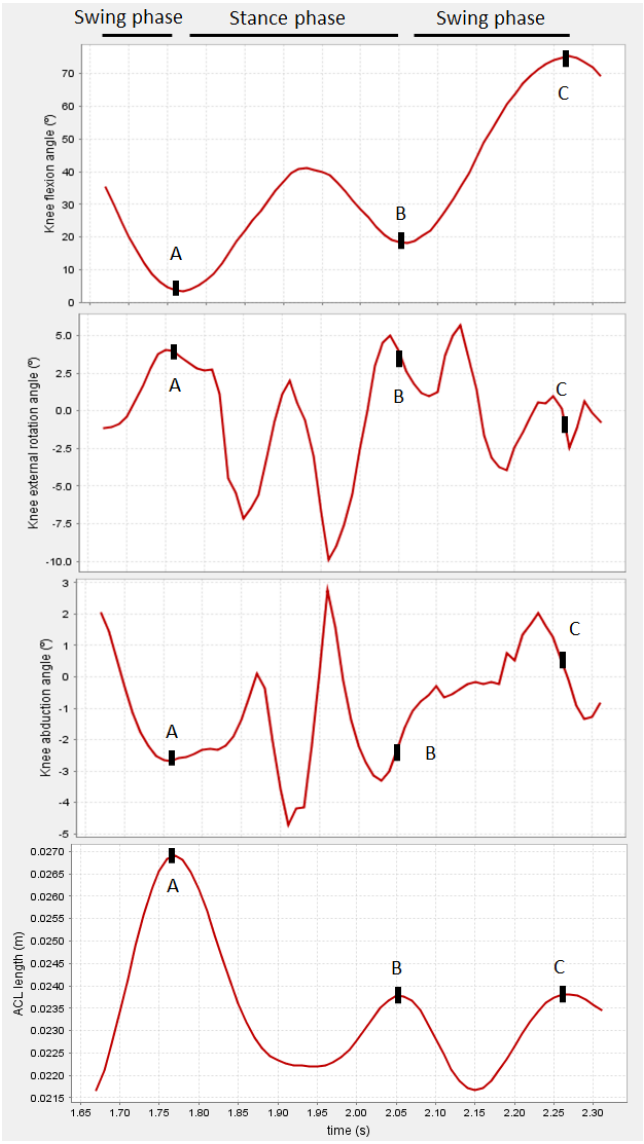

Figure 3.21 Knee angles and ACL length for crossover cutting.

The function that predicted the ACL length for crossover was:

ACL length (m) = 0.02775 -0.00239*Sex + 0.000019*Knee flexion angle (º) - 0.000666*Knee external rotation angle (º) + 0.000058*Knee abduction angle (º) (6)

The novelty of this study was the calculation of *in vivo* ACL length and tensile forces during different dynamic activities, which could provide an insight into high-risk activities for ACL injuries and rehabilitation protocols or provide mechanical specifications for ACL implants.

As was shown in section 1.2.3 the peak ACL forces were previously reported to range between 0.2 N/BW and 1 N/BW during walking [79], [102]–[104]. In biomechanics study 2 a peak ACL tensile force of 0.774±0.064 N/BW during walking was observed corresponding to 28.5% of the reported failure strength of the ACL [58], [59]. Therefore, the value reported is in the same range as the ACL loads previously reported. All these studies used computational models to calculate ACL forces; however, they exhibited different limitations that make the results non-identical. For instance, the previous studies [79], [102]–[104] developed a 1 DOF knee model; however, a 3 DOF knee model is created in biomechanics study 2, therefore the accuracy in the calculation of ACL length with this new model is higher than in previous studies.

The peak strain observed in biomechanical study 2 during walking was 13%, which agrees with a previous study based on motion capture and biplanar fluoroscopic images during the same activity [75].

The highest peak of ACL tensile force was recorded for jumping with both legs (1.076±0.113 N/BW) and their values were around 4 times higher than jumping with one leg (0.774±0.064 N/BW); the knees were more flexed during the execution of one-legged jumping in all participants, decreasing the ACL elongation and consequently the estimated ACL tensile force.

From this study (biomechanics study 2) it was observed that non-contact activities with high ACL injury rates such as crossover cutting or sidestep cutting are surprisingly associated with lower tensile forces in the ACL than daily activities such as walking. This evidence indicates that the failure mechanisms for these activities are likely due to a combination of loads, not just tensile loading. This is a novel finding not reported in the literature before. However, it was proved that the highest risk of ACL injury is when the knee is at a low degree of knee flexion (inferior to 30 degrees), in a valgus position and internal rotation with the planted foot for suddenly changing direction [117], [119]. This involves the ligament being subjected to multidirectional forces, and therefore the failure mechanisms are due to multidirectional loads.

The Pearson correlation coefficients obtained in biomechanics study 2 for cutting activities revealed a more significant linear relationship between rotation and abduction angles with the ACL length than with the flexion angle, therefore knee rotation and abduction angles contribute greatly to the elongation of the ACL for these activities as was predicted by Mc Lean *et al.* [256]. It is known that small knee flexion angles generate higher ACL tensile forces; the greater the valgus (abduction) angle the higher ACL loading is observed [77], [257], [258] and so with the greater

the rotation angle, the ACL could be subjected to a higher torsional load. Therefore, this study demonstrated for the first time that to understand the mechanical behaviour of the ACL a study of its tensile, shear and torsional loading is needed. Future work should calculate shear and torsion loads for each activity.

There are two main limitations in this Chapter. The first limitation is the assumption of having 3 DOF per knee instead of 6 DOF, in future studies a model including 6 DOF for each knee will be performed to incorporate the translation in the three axes. However, the translation of the knee joint is very small and can be negligible in comparison with the knee angles; therefore, this improvement will not greatly increase the accuracy of the model. The second limitation is that the ACL tensile forces were calculated from the ACL strain and this was calculated by tracking the coordinates of the ACL insertion points and considering the ACL as a single straight bundle; however, it is known that the fibre bundles of the ACL are twisted and wrapped around the bones. The purpose of this study was to calculate the ACL length, strain and force for healthy ACLs (with no issues of knee joint laxity), to enable development of grafts with similar characteristics; therefore, the length for the twisted bundles of the ligament was not considered and is considered to be negligible compared to the length between the insertion points of the ligament. Moreover, 3D structures based on twisted bundles of fibres were created in Chapter 6. These structures mimic the nano and micro morphology of the natural ligament, consequently this second assumption (considering the ACL as a single straight bundle) did not contribute significantly to the accuracy of the results, since the twisted structure of the ligament is taken into account in Chapter 6.

Despite the limitations of this study, the approach followed is more accurate than other studies mainly for two reasons:

- The first reason is that other studies considered the knee as a 1DOF joint [75], [76]; however this study developed a 3DOF knee model able to determine the angles not only in the sagittal plane but also in the axial and coronal planes, contributing to a more accurate of the calculation of the length of the ligament.

- Computationally checking the model uploaded in OpenSim platform [259] and published in Kar *et al.* [260], it was noticed that the scale of the model, the insertion points of the ACL and the way the ACL length had been measured were erroneous, since the model was not anatomically correct and the ACL length indicated was not physiological. However, the configuration of the scale tool, the placement of the insertion points and the measurement of the ACL length have been meticulously studied in this project and the results verified from literature.

Moreover, this study is novel given that it was the first one that aims to understand the *in vivo* ACL length, force and strain while activities such as “climbing stairs”, “jumping with maximum effort”, “run”, “crossover cutting”, “sidestep cutting”, “climbing stairs” and “jumping with one leg” were performed.

The values of maximum ACL force and strain were used as safety thresholds for the design of new ACL implants.

3.5. CONCLUSIONS

Biomechanics study 1 established a methodology to calculate *in vivo* tensile forces on the ACL during different dynamic activities. This study proved that there are significant differences between genders and ages, therefore it is feasible to create an ACL implant dependent on these variables. The forces experienced by the ACL in women and in aged people were significantly higher compared to men and young people respectively.

Biomechanics study 2 determined and compared *in vivo* ACL length and tensile forces during dynamic activities using a viscoelastic ligament model for a wide range of activities. The results of this study can inform research into ACL injury mechanisms and provide mechanical specifications for manufacturing improved ACL implants, which is the aim of the project. It established highly significant regression models between ACL lengths with respect to knee angles for the different activities enabling prediction of the behaviour of the ligament according to given angles for each activity. Finally, the peak tensile ACL force during cutting or running was lower than walking, suggesting that the failure mechanisms are due to multidirectional (including shear and torsion) loading instead of simply tensile loading in isolation. Therefore, new scaffolds have to be designed and tested to ensure they are able to bear multidirectional forces.

The results from Chapter 3 will be used as biomechanical specifications for the design and development of the scaffolds produced in Chapters 4, 5 and 6.

Chapters 4 and 5 go on to study the suitability of two different polymers (gelatin and PVA respectively) to be used for ACL replacements. To achieve the aim of these chapters, the scaffolds created were mechanically and morphologically tested. The results obtained from the mechanical tests were compared with the results found in Chapter 3 to be able to determine if those polymers would be mechanically suitable for use as ACL replacements.

Chapter 6 focusses on the study of 2D and 3D electrospun structures. The scaffolds built in this study were mechanically tested to determine which structure is more faithfully able to mimic the mechanical behaviour of the ACL.

Key Points:

1. A novel methodology was developed to calculate the *in vivo* ACL length, strain, forces and angles for a wide range of activities and allowed comparison between them.
2. This study proved that ACL failure mechanisms are due to a combination of loads and it is the first that emphasized the importance of taking into account the multidirectional loading of the ACL to develop implants able to bear the same loading as the natural ligament. Therefore, the author encourages changing the

current standard procedure for the design of ACL implants to one that incorporates multi-planar loading.

3. This study is a significant forward in the field, as to date no studies have been performed to create scaffolds that can replicate the *in vivo* loading and can bear the multi-planar loading of the natural ACL.

4. Suitability of gelatin electrospun scaffolds for the development of ligament implants from a morphological, topographical and mechanical perspective

When the *in vivo* mechanical behaviour of the ACL and the mechanical specifications for the scaffolds are known, scaffolds that morphologically, topographically and mechanically mimic the ACL can be designed and manufactured.

This chapter evaluates the suitability of gelatin electrospun scaffolds for use as ACL grafts. These scaffolds are then mechanically tested and compared with the natural ligament in order to determine their suitability for this purpose.

4.1. ABSTRACT

Electrospinning enables mimicking of the native extracellular matrix (ECM) through the creation of a nano- and micro-scale fibrous network.

Gelatin exhibits high biocompatibility and a biodegradability similar to collagen making it attractive for use in biomedical applications [215]. However, this polymer has a number of disadvantages such as poor mechanical properties or high

degradation rate, requiring the use of crosslinker agents in order to increase the stiffness and the lifespan of the material. Moreover, its easy gelation in aqueous solution complicates the manufacturing of scaffolds through the electrospinning process, making the use of harmful solvents necessary. It is well known that the ability to electrospin gelatin heavily depends on the selection of solvent and its concentration [215], [261], [262], therefore an initial study of the solvents was needed.

The novelties of this work are two-fold: to understand how changes in the solvent concentration affect the mechanical and structural properties of the scaffolds, and how the use of a crosslinker changes the morphology of the nanofibres and their network.

This chapter aims to evaluate the suitability of gelatin electrospun scaffolds for use as tissue engineered ligaments.

4.2. INTRODUCTION

Electrospinning is a manufacturing technique capable of mimicking the collagen and elastin fibres in the ECM by creating a fibrous mat with fibre diameters ranging from 1-20 μm down to approximately 10 nm. This capability makes electrospinning a suitable technique for biomedical applications and more specifically for the fabrication of tissue engineering scaffolds to be used as implants [263] with a comparable nanostructure to the natural ACL.

Biocompatibility and cell responses on scaffolds depend greatly on factors such as microstructure (fibre diameter, inter-fibre separation, void fraction and fibre orientation) and topography of the scaffold [189]. Some researchers reported that the structure and topography of the scaffold could be more important in the attachment, proliferation and gene expression than the nature of the polymer itself [264], i.e. if it is a synthetic or a natural polymer. Specifically, Ghanavati *et al.* concluded that PCL nanofibres with high surface area had better surface properties than natural collagen-chitosan film, therefore the structure and topography of a matrix seemed to be more important in wound healing than its material substance [264].

Gelatin is a natural polymer derived from the hydrolysis of collagen, the most abundant protein of the ECM. It is commonly used in biomedical, pharmaceutical and food packaging applications [265]. Its low cost, high biocompatibility, biodegradability and bioactivity make it attractive for the development of tissue engineered implants and they are essential properties for the development of scaffolds in this thesis. The original idea for the design of the scaffolds was to use a shell-core structure, where the polymer in the inner part of the fibre provides the main part of the mechanical properties to the structure and the outer part provides the biocompatibility. Due to its biocompatibility, low cost, better mechanical properties then collagen and similar degradation rate to collagen, gelatin was selected in the first instance to constitute the outer part of the scaffold.

However, despite its advantages this polymer has three main disadvantages that must be faced during its manufacturing process. The first disadvantage is the

difficulty of working with electrospun aqueous gelatin solutions at room temperature [215], [266], due to gelatin solutions with high Bloom value gelling easily at temperatures below 30ºC restricting the flow of solution through the needle and consequently the Taylor cone and fibre formation. The second disadvantage is its high degradation rate that complicates the biological characterization of the scaffold and its use as an implant. The third disadvantage is its poor mechanical properties with lower tensile stress and strain at rupture than the native ACL.

In order to overcome these limitations, two studies were performed in this chapter (Gelatin study 1 and Gelatin study 2). To avoid the gelation process during the electrospinning, different approaches with different solvents have been proposed in the literature. Fluorinated alcohols such as 2,2,2-triefluoroethanol (TFE) [266], [267] or 1,1,1,3,3,3-hexafluoro-2-propanol (HIPF) [268]; dilutions of phosphate buffer saline (PBS) in ethanol [261], [269]; carboxylic acids such as formic acid or acetic acid (HAc) [215], [270]–[275]; mixtures of different solvents such as HAc and TFE [262], HAc and dimethyl sulfoxide (DMSO) [262], HAc and ethylene glycol [262], HAc and formamide [262] or HAc and ethyl acetate [274] are the most common solvents used with gelatin. However, the use of organic solvents could affect the protein structure of the polymer; the cytotoxicity due to residual solvent in the scaffold; and the morphology, topography and mechanical properties of the scaffolds and their relation with the cell viability, response and proliferation. Therefore, after a previous investigation into the optimum solution and process parameters, the first part of the chapter (Gelatin study 1) studied how different concentrations of solvents affect the morphology, topography and mechanical properties of the scaffolds [276]–[279].

To address the limitations of having a high degradation rate and poor mechanical properties, the electrospun gelatin scaffolds must be crosslinked to create bonds between the proteins chains and provide more stability and stiffness to the material. Many chemical crosslinking agents have been investigated in the literature, including glutaraldehyde, formaldehyde, glyceraldehyde, genipin, oxygen species, carbodiimide, diepoxy compounds, diisocyanates and dextran aldehydes [280]. However, these crosslinkers reduce the number of free cell binding sites and with it the capacity of cell adhesion [281]. The second part of the Chapter (Gelatin study 2) studied how different concentrations of crosslinking agent (glutaraldehyde) affect the degradability, morphology and topography of the scaffold.

Currently, electrospun gelatin scaffolds have been developed for wound healing applications [282], [283], nervous system [284]–[286], dental applications [287], bone tissue [288]–[291] and skin tissue [292], [293], tendon implants [294] and vascular grafts [295]. However, no studies of electrospun gelatin scaffolds have been done with the purpose of manufacturing ligament implants. The only electrospun gelatin scaffolds found in the literature for tendon replacements [294] did not reach the mechanical strength needed for their application and they were far from obtaining values comparable to those exhibited for the natural ACL. That study [294] used co-electrospinning of PCL and methacrylated gelatin to manufacture tendon implants through use of 5 sheets of cell seeded aligned scaffolds. The cell growth, tensile mechanical properties and degradation were studied; however, no evidence of optimisation of the solution and process parameters nor morphological and

topographical characterization of the scaffolds to obtain biomimetic tendon implants were observed.

The novelties of this work lie in understanding how changes in the solvent concentration affect the mechanical, morphological and topographical properties of the gelatin scaffolds and so induce associated cell behaviour in order to mimic the structural, mechanical and biological properties of the natural ECM. In addition, how the use of a crosslinking agent changes the morphology of the nanofibres and their network will be evaluated to check the suitability of the polymer and crosslinker to manufacture improved connective tissue (i.e. ACL) implants.

The aim of this work was to assess the morphology, topography and mechanical behaviour of the gelatin with different solvent and crosslinker concentrations to determine its suitability to manufacture tissue engineering implants.

4.3. METHODS

4.3.1. POLYMER SOLUTION

Gelatin powder type B from bovine skin (Bloom ~ 225 g) was purchased from Sigma Aldrich (UK). Glacial acetic acid (Sigma Aldrich, UK), DMSO (Sigma Aldrich, UK) and distilled water (dH_2O) were used as solvents, dissolving the gelatin by stirring until homogenous solutions were obtained. The reasons for selecting these

solvents were: HAc enables optimisation of the electrospinning process avoiding gelation, it is not as harmful as the normal organic solvents used with gelatin and a recent study has demonstrated that the cell viability is higher than 90% [215]; and DMSO favours the creation of smoother fibres free of defects [262], able to promote cell migration.

Initial experiments performed during this thesis determined that the optimum concentration of gelatin was 25% w/v, concentrations above this value increased the viscosity of the solution making it difficult to electrospin; below this concentration, bead formation and beaded fibres were observed, reducing the mechanical properties of the scaffold and impeding cell migration. Further details about the initial experiments and their results are presented in section 4.4.1 where the optimisation of the solution and process parameters are explained.

4.3.1.1. Gelatin Study 1

For this study, nine solutions were prepared with 25% w/v of gelatin dissolved in concentrations of HAc and dH_2O of 3:1, 1:1 and 1:3, adding 0%, 5% and 10% of DMSO.

4.3.1.2. Gelatin Study 2

A gelatin solution was prepared with 25% w/v of gelatin dissolved in 1:1 HAc/ dH_2O and 5% DMSO following the mechanical results of the previous study (Gelatin study 1) [276]. The scaffolds manufactured with this solution exhibited a greater tensile strength than the scaffolds manufactured with different concentrations

of solvents; they showed an appropriate Young's modulus for tissue engineered ligament implants with comparable values as the natural ACL; and they presented fibres with uniform diameters and free of defects (all the mechanical results obtained in gelatin study 1 can be found in section 4.4.2).

4.3.2. SCAFFOLD PRODUCTION

All the scaffolds used in these two studies (Gelatin study 1 and Gelatin study 2) were fabricated with an electrospinning device (TL-01, NaBond, China) under the same set up of parameters, which allowed production of a stable Taylor cone and optimisation of the quality of the scaffold manufacturing fibres free of defects. A 10 ml syringe was loaded with the polymer to pump it with a flow rate of 2 ml/h through a 15 G needle. An electrostatic field was created applying high voltage (for this study 26 kV) between the tip of the needle and the collector. The fibres were projected from the tip of the needle over a sheet of aluminium foil attached to a 15 cm diameter rotating collector working at 1300 rpm. The distance between the needle and the collector was set up to 11 cm. Each scaffold was manufactured at room temperature (25ºC) and for 3 hours spin time.

4.3.3. CHEMICAL CROSSLINKING

Chemical crosslinking was used solely in Gelatin study 2, where two crosslinking techniques were evaluated: immersion and vapour deposition.

For crosslinking the samples by immersion, three 0.5 x 0.5 cm samples were placed in a 6 well plate with 2 ml of 25% GTA in wells for 2 hours.

For the crosslinking by vapour deposition, samples of 0.5 x 0.5 cm were cut from the scaffold manufactured for Gelatin study 2; air-dried and placed over a metallic mesh in a sealed desiccator to be crosslinked. The effect of the crosslinker over the electrospun fibres was tested with three different concentration of GTA diluted in distilled water 2.5%, 5% and 25%. 25 ml, these solutions were poured separately in a Petri dish at the bottom of the desiccator and the samples were placed over a metallic mesh on top of the Petri dish to be exposed to glutaraldehyde vapour.

4.3.4. DEGRADATION ASSAY

Two samples of each concentration of GTA were dried-air for 24 hours and the rest of the samples were placed in 6 well dishes with 4 ml of phosphate-buffered saline buffer (PBS) in each well and left in an incubator at 37ºC and 4% CO_2 in order to test their degradability with time in an environment similar to the human body. A total of 42 samples, two samples for each concentration, were left for 1, 5, 7, 14, 21 and 28 days in PBS and then dried-air for 24 hours in a fume hood. This assay was performed for Gelatin study 2.

4.3.5. SCAFFOLD/FIBRE CHARACTERIZATION

4.3.5.1. Morphology of the fibres

A SC7640 sputter coater (Quorum Technologies Ltd. Kent, UK) was used to coat the samples with gold prior to their visualization with a field emission scanning electron microscope Zeiss Supra 40 (FE-SEM, Carl Zeiss SMT Ltd., Cambridge, UK). The intensity used for coating the samples was 20 mA, the voltage 0.8 kV and the duration of the coating was 120 seconds, which provides a coating thickness of 32.6 nm, following equipment specifications. Scanning electron microscope (SEM) images were taken at approx. 6 mm working distance, 3 kV and with x 50000 magnifications. Fibre diameter (Ø fibre) and inter-fibre separation (Int.sep.) were determined with AxioVision SE64 Rel. 4.9.1 (Carl Zeiss SMT Ltd., Cambridge, UK) by measuring 20 fibres per sample for the two studies (Figure 4.1). The inter-fibre separation was defined as the maximum horizontal distance between two fibres that belong to the same pore. A pore was defined as the void space constituted by fibres (normally four fibres) that intersect one with each other and are located on the same layer of fibres.

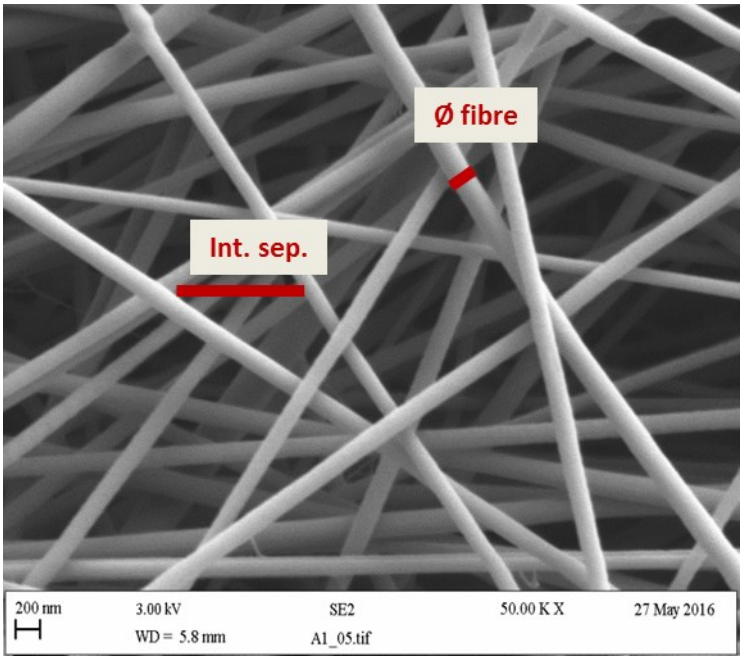

Figure 4.1 SEM image with fibre diameter (Ø fibre) and inter-fibre separation (Int. sep.).

4.3.5.2. Topography of the scaffold

The average roughness of the scaffolds was measured by taking 6 white light interferometry images per sample using an interferometer from ZeGage (Zygo Corporation, US) (Figure 4.2) following a previous study [296]. This equipment allowed high-precision 3D metrology of surface features to be obtained, determining the topography of scaffolds through measuring characteristics such as maximum peak-to-valley profile height or average roughness. The average roughness was compared between samples with different GTA concentrations and days in PBS in order to understand how the crosslinking and the incubation in PBS affected to the topography of the samples. The same procedure was followed in both studies.

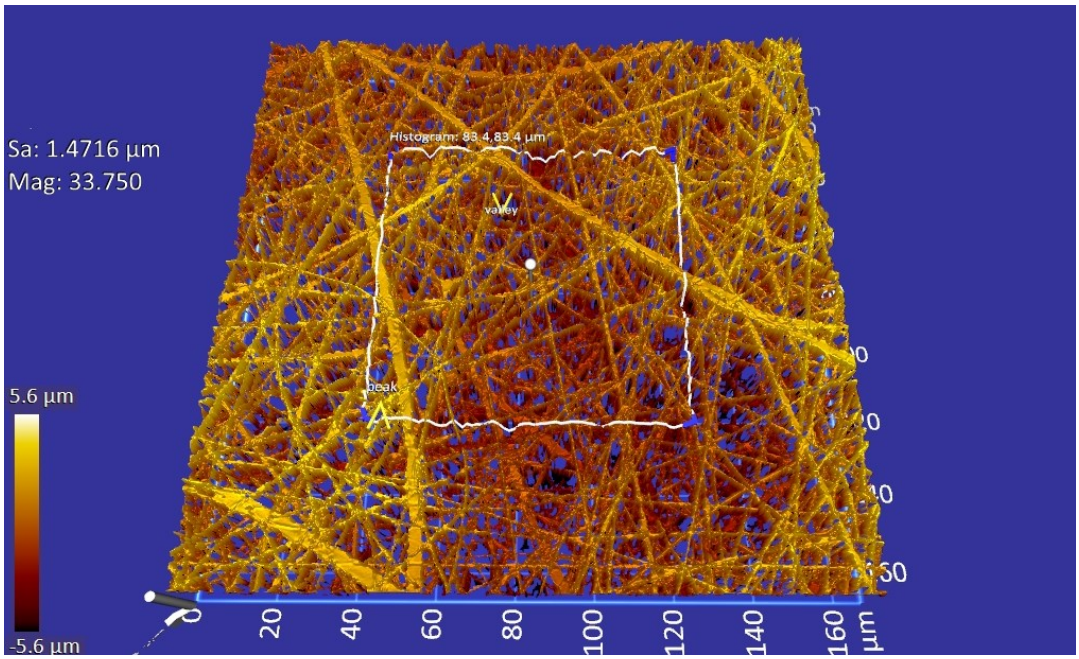

Figure 4.2 White light interferometry image showing the scaffold topography.

4.3.5.3. Mechanical behaviour of the scaffold

4 samples were mechanically analysed for each scaffold in Gelatin study 1 following a previous study [266]. The samples were removed with a dog-bone cutting die (25 x 4 mm, test length x width), and their thickness measured three times with a digital and an analogical calliper in order to check the consistency of the measurements; samples were attached to a cardboard frame to aid in the alignment of the sample in the tensometer (Instron H10KS, US) and tensile tested until failure with a 100 N load cell and 1 mm/min test speed [297]–[299]. Mechanical properties such as Young's modulus, tensile strength and strain at break were determined for each sample and statistically analysed in order to find a relationship between mechanical and morphological properties.

4.3.5.4. Chemical characterization of the scaffold

A Fourier Transform Infrared Spectrometer (PerkinElmer Spectrum two, US) was used to investigate any chemical changes in the gelatin samples. Non-significant results were observed when varying the crosslinker concentration (data shown in the appendix Figures 9.1 and 9.2).

4.3.6. STATISTICAL ANALYSIS

Mean and standard error of the mean (Std Error) were calculated for each of the structural and mechanical properties.

In order to compare these properties between scaffolds made with different solvents concentrations, one-way analysis of variance (ANOVA) with a 95% confidence was performed.

Linear regressions were performed to calculate the relationship between morphological, topographical and mechanical properties of each scaffold and solvent concentrations.

All statistical analyses were conducted using SPSS (IBM Inc, US).

4.4. RESULTS AND DISCUSSION

4.4.1. OPTIMISATION OF THE SOLUTION AND PROCESS PARAMETERS

Before the two studies were performed (Gelatin study 1 and Gelatin study 2), optimisation of the solution and process parameters was conducted. Set up of the electrospinner included determination of:

- The optimum voltage, which has to be high enough to overcome the cohesive force of the solution in order to start creating the Taylor cone for formation of the jet of fibres. If the voltage were not high enough, no fibres would be created and if the voltage is too high, beads are created. A series of experiments were performed where the voltage was varied between 15 kV and 28 kV. In this study, a stable Taylor cone and an electrospun structure free of beads were observed with 26kV.
- Flow rate: This parameter is related to the viscosity of the polymer, its concentration and the temperature of the chamber. It was observed that at higher polymer concentrations, less flow rate is needed to obtain a stable Taylor cone; the same phenomenon happened when increasing the temperature of the chamber. After a systematic series of experiments varying the flow rate from 1ml/h until 2ml/h and keeping the rest of the parameters constant, it was determined that the optimum flow rate was 2ml/h.

- Distance between collector and needle: enough distance is required to facilitate complete evaporation of the solvent; however if the distance is too high, in this case ≥ 15 cm, an unstable Taylor cone from which no fibres are projected can be observed. For the experiments performed for this study, an optimum distance of 11 cm between collector and needle was determined, which allowed creating fibres free of defects.
- Revolutions of the mandrel: Experiments with 1000, 1300, 2000, 3000, 4000, 5000 and 6000 rpm were performed in order to understand how the morphology of the scaffold changed with altered revolutions. It was observed that with revolutions of 3000 and 4000 rpm the fibres were longitudinally aligned; with lower revolutions, the fibres were randomly distributed; and with revolutions higher than 4000 rpm, the revolutions were too high increasing the vibration of the equipment and aligned fibres were not created. The rest of the experiments were performed with 1300 rpm there revolutions generating smooth fibres without defects.
- Temperature: The temperature was varied from 22º C to 30º C to obtain the ideal temperature with which to create high quality fibres with no beads. After systematic evaluations of how the temperature affected to the fibres, it was concluded that 25º C was the temperature that favoured the formation of high quality electrospun scaffolds. Below that temperature, the viscosity of the solution increased, making it difficult to spin and higher to that temperature beads were observed in the scaffolds.

- Size of the needle: Needles with 15G, 20G, 21G, 22G and 23G were evaluated to obtain an electrospun scaffold with high quality fibres and with appropriate diameter. The most optimal needle was 15G, following the criteria that it was the easiest to spin with, no occlusions were caused and smooth fibres free of beads were produced.

A resume of the optimal parameters observed is given in Table 4.1.

Table 4.1 Optimum process parameters.

Collector	Voltage	Flow rate	Distance between collector and needle	Needle	Revolutions of the mandrel
15 cm	26 kV	2 ml/h	11 cm	15G	1300 rpm

In order to optimise the solution parameters several experiments were conducted:

- Experiments to determine the ideal solvent and polymer concentration: dH_2O, PBS, ethanol 70%, HAc, fetal bovine serum (FBS) and DMSO were used as solvents. The following experiments were performed to determine the most suitable solvent and the concentration (Table 4.2).

Table 4.2 Experiments to determine the ideal solvent and concentrations.

Dissolving solution	Collector	Concentration	Voltage	Flow rate	Distance	Needle	Revolutions of the mandrel	Temperature	Time
dH_2O	Rot 15 cm	**12% Gelatin**	26 kV	2 ml/h	11 cm	15G	1300 rpm	25° C	unspinnable
dH_2O	Rot 15 cm	**9% Gelatin**	26 kV	2 ml/h	11 cm	15G	1300 rpm	25° C	unspinnable
dH_2O	Rot 15 cm	**7% Gelatin**	26 kV	2 ml/h	11 cm	15G	1300 rpm	25° C	unspinnable
dH_2O	Rot 15 cm	**5% Gelatin**	26 kV	2 ml/h	11 cm	15G	1300 rpm	25° C	unspinnable
dH_2O	Rot 15 cm	**3% Gelatin**	26 kV	2 ml/h	11 cm	15G	1300 rpm	25° C	unspinnable
PBS (x1)/IMS 70% 2:3	Rot 15 cm	**15% Gelatin**	26 kV	2 ml/h	11 cm	15G	1300 rpm	25° C	unspinnable
PBS (x1)/Ethanol 70% 2:3	Rot 15 cm	**12% Gelatin**	26 kV	2 ml/h	11 cm	15G	1300 rpm	25° C	unspinnable
PBS (x1)/Ethanol 70% 2:3	Rot 15 cm	**6% Gelatin**	26 kV	2 ml/h	11 cm	15G	1300 rpm	25° C	unspinnable
PBS (x10)/Ethanol 70% 2:3	Rot 15 cm	**12% Gelatin**	26 kV	2 ml/h	11 cm	15G	1300 rpm	25° C	unspinnable
100% Acetic acid	Rot 15 cm	**20% Gelatin**	26 kV	2 ml/h	11 cm	15G	1300 rpm	25° C	10 minutes
75% Acetic acid	Rot 15 cm	**30% Gelatin**	26 kV	2 ml/h	11 cm	15G	1300 rpm	25° C	10 minutes
50% Acetic acid	Rot 15 cm	**30% Gelatin**	26 kV	2 ml/h	11 cm	15G	1300 rpm	25° C	unspinnable
50% Acetic acid	Rot 15 cm	**25% Gelatin**	26 kV	2 ml/h	11 cm	15G	1300 rpm	25° C	10 minutes
25% Acetic acid	Rot 15 cm	**25% Gelatin**	26 kV	2 ml/h	11 cm	15G	1300 rpm	25° C	10 minutes
23.75% Acetic acid/71.25% dH_2O/DMSO 5%	Rot 15 cm	**20% Gelatin**	26 kV	2 ml/h	11 cm	15G	1300 rpm	25° C	10 minutes
47.5% Acetic acid/47.5% dH_2O/DMSO 5%	Rot 15 cm	**25% Gelatin**	26 kV	2 ml/h	11 cm	15G	1300 rpm	25° C	10 minutes
47.5% Acetic acid/47.5% dH_2O/DMSO 5%	Rot 15 cm	**25% Gelatin**	26 kV	2 ml/h	11 cm	15G	1300 rpm	25° C	10 minutes
25% Acetic acid/75% FBS	Rot 15 cm	**25% Gelatin**	26 kV	2 ml/h	11 cm	15G	1300 rpm	25° C	10 minutes
50% Acetic acid/50% FBS	Rot 15 cm	**25% Gelatin**	26 kV	2 ml/h	11 cm	15G	1300 rpm	25° C	10 minutes
75% Acetic acid/25% FBS	Rot 15 cm	**25% Gelatin**	26 kV	2 ml/h	11 cm	15G	1300 rpm	25° C	Occlusion
75% Acetic acid/25% FBS	Rot 15 cm	**25% Gelatin**	26 kV	2 ml/h	11 cm	15G	1300 rpm	25° C	10 minutes
23.75% Acetic acid/71.25% FBS/DMSO 5%	Rot 15 cm	**20% Gelatin**	26 kV	2 ml/h	11 cm	15G	1300 rpm	25° C	10 minutes
47.5% Acetic acid/47.5% FBS/DMSO 5%	Rot 15 cm	**20% Gelatin**	26 kV	2 ml/h	11 cm	15G	1300 rpm	25° C	10 minutes
71.25% Acetic acid/23.75% FBS/DMSO 5%	Rot 15 cm	**20% Gelatin**	26 kV	2 ml/h	11 cm	15G	1300 rpm	25° C	10 minutes
47.5% Acetic acid/47.5% FBS/DMSO 5%	Rot 15 cm	**25% Gelatin**	26 kV	2 ml/h	11 cm	15G	1300 rpm	25° C	10 minutes
71.25% Acetic acid/23.75% FBS/DMSO 5%	Rot 15 cm	**25% Gelatin**	26 kV	2 ml/h	11 cm	15G	1300 rpm	25° C	10 minutes
Acetic Acid	Rot 15 cm	**10% Gelatin+10% PCL**	26 kV	2 ml/h	11 cm	15G	1300 rpm	25° C	10 minutes

After experiments with 3%, 5%, 7%, 9% and 12% gelatin and distilled water at 25°C it was concluded that gelatin is not spinnable when dissolved solely in distilled water.This was due to low concentrations not having appropriate viscosity for electrospinning and higher concentrations provoking gelation of the polymer blocking the tube and needle. 15%, 12% and 6% gelatin was dissolved with PBS (x1 and x10) and ethanol 70%, but it was unspinnable in PBS and ethanol. 20%, 25% and 30% gelatin was dissolved with 100%, 75%, 50% and 25% HAc, resulting in the optimum gelatin concentration of 25%. These last experiments were also performed with FBS instead of distilled water to make the dilutions of the HAc, and fibres and ribbons with higher diameter were produced. Experiments with HAc diluted in distilled water or FBS and DMSO were then performed. Table 4.3 shows the appearance of the scaffolds depending on the solvents and polymer concentrations in order to obtain conclusions and determine which was the best scaffold in terms of its morphology.

Table 4.3 Experiments to determine the ideal solvent and concentrations.

Sample	Dissolving solution	Concentration	Bead Formation	Fibre Defects	Heterogeneous Fibres	"Ribbons"	"Spiderweb"	"Spitting"
R21	**PBS (x10)/Ethanol 70% 2:3**	**12% Gelatin**	Unspinnable					Yes
R22	**100% Acetic acid**	**20% Gelatin**	Yes	Yes	No	No	Yes	No
R23	**75% Acetic acid**	**30% Gelatin**	No	Few	No	No	Yes	No
R24	**50% Acetic acid**	**25% Gelatin**	No	Few	No	No	Yes	No
R25	**25% Acetic acid**	**25% Gelatin**	No	Few	No	No	Yes	No
R26	**23.75% Acetic acid/71.25% dH_2O/DMSO 5%**	**20% Gelatin**	Few	Few	No	No	Yes	No
R27a	**47.5% Acetic acid/47.5% dH_2O/DMSO 5%**	**25% Gelatin**	No	Few	No	No	Few	No
R27b	**47.5% Acetic acid/47.5% dH_2O/DMSO 5%**	**25% Gelatin**	No	Few	No	No	Few	No
R28	**25% Acetic acid/75% FBS**	**25% Gelatin**	No	No	Yes	No	Yes	No
R29	**50% Acetic acid/50% FBS**	**25% Gelatin**	Few	No	Yes	No	Few	No
R30a	**75% Acetic acid/25% FBS**	**25% Gelatin**	No	No	Yes	Yes	Yes	No
R30b	**75% Acetic acid/25% FBS**	**25% Gelatin**	Fused fibres		Yes	Yes	Yes	No
R31	**23.75% Acetic acid/71.25% FBS/DMSO 5%**	**20% Gelatin**	Yes	No	Yes	No	Yes	No
R32	**47.5% Acetic acid/47.5% FBS/DMSO 5%**	**20% Gelatin**	Yes	No	Yes	No	Yes	No
R33	**71.25% Acetic acid/23.75% FBS/DMSO 5%**	**20% Gelatin**	Yes	No	Yes	Yes	No	No
R34	**47.5% Acetic acid/47.5% FBS/DMSO 5%**	**25% Gelatin**	Few	No	Yes	Yes	No	No
R35	**71.25% Acetic acid/23.75% FBS/DMSO 5%**	**25% Gelatin**	Few	No	Yes	No	No	No
R36	**Acetic Acid**	**10% Gelatin+10% PCL**	No	No	Yes	No	Yes	Yes

From these initial experiments, the following general conclusions were obtained:

a) No electrospun scaffolds could be manufactured with just gelatin and distilled water, or gelatin and PBS/ethanol due to its tendency to gelate and so obstructing the tube before reaching the needle.

b) Bead formation was reduced when increasing the gelatin concentration. 25% gelatin was observed as the optimum gelatin concentration.

c) It was demonstrated that the higher the gelatin concentration, the larger the fibre diameters were observed.

d) Acetic acid was used as a solvent to avoid gelation. If the scaffolds are rinsed with PBS, prior to seeding with cells the cytotoxicity will decrease; therefore the viability of the cells would increase, and as this solvent is non-aggressive, the protein chemical structure would remain intact [215], [270], [271].

e) It was demonstrated that the higher the acetic acid (HAc) concentration, the larger the fibre diameters were observed for the same gelatin concentration.

f) The addition of DMSO increased the viscosity of the solution; therefore, it was expected to enhance the free-beads fibres formation. It was observed that when adding DMSO, the beads and “ribbons” formation decreased.

g) For the same gelatin concentration, larger fibre diameters were observed in the scaffolds through the addition of DMSO.

h) FBS was considered as a solvent because it could increase the cell viability, bio-affinity and reduce the osmotic stress [267], [300]. From these experiments, it was demonstrated that a combination of acetic acid with FBS can be used to spin gelatin fibres, however ribbons were also observed and for this reason, this solvent was initially rejected for further investigations. The fibres were more heterogeneous and with a larger diameter when the gelatin was dissolved in acetic acid/FBS comparing to acetic acid/dH_2O.

i) The addition of PCL to the gelatin can improve the degradation process of the gelatin, moreover the mechanical properties would also improve [301], [302]. It was proved that PCL can be dissolved moderately well in acetic acid [303], [304], therefore both polymers could be dissolved in acetic acid, reducing the cytotoxicity and avoiding damage in the polymer structure. Extremely heterogeneous fibres had been created with a mix of gelatin and PCL. However, an inappropriate performance of the electrospinner (no creation of a stable polymer jet) and very low fibre density were observed.

j) More experiments with 25% w/v of gelatin dissolved in concentrations of HAc and dH_2O of 3:1, 1:1 and 1:3, adding 0%, 5% and 10% of DMSO must been done in order to understand how the solvent concentration modifies the morphology, topography and mechanical properties of the scaffolds. Therefore, a second study was performed with this aim.

4.4.2. GELATIN STUDY 1: HOW DIFFERENT CONCENTRATIONS OF SOLVENTS AFFECT THE MORPHOLOGY, TOPOGRAPHY AND MECHANICAL PROPERTIES OF THE SCAFFOLDS.

After an initial study to optimise the solution and process parameters, a subsequent study to evaluate how the concentration of the solvents affect the morphology, topography and mechanical properties of the scaffolds was performed.

As described in the methods (section 4.3), nine solutions were prepared with 25% w/v of gelatin dissolved in concentrations of HAc and dH_2O of 3:1, 1:1 and 1:3, adding 0%, 5% and 10% of DMSO.

Fibre diameter, inter-fibre separation and average roughness were significantly affected by the concentration of HAc, DMSO and their interaction ($p < 0.001$), with significant differences found between scaffolds manufactured with different solvents concentrations and the scaffold parameters. Regression models revealed that fibre diameter and inter-fibre separation increased significantly ($p < 0.001$) when the concentration of HAc and DMSO increased. The concentration of HAc provides more variability than the DMSO concentration, to the dependent variable (partial $\eta^2 =$ 0.66 and 0.41 respectively); therefore, the concentration of HAc is more relevant than the concentration of DMSO in the contribution of the morphology of the scaffolds. This phenomenon can be observed in Figures 3 and 4 where the 3:1 HAc/dH_2O concentration provided greater fibre diameter and inter-fibre separation to all DMO concentration. This was also corroborated by Erencia *et al.* [215] in 2015 where solutions of gelatin with concentrations of 200, 250, 300, 350, and 400 mg/mL (kg/m3) were prepared using acetic acid at different concentrations (25, 50, and 75%

(v/v)) as solvent. Erencia *et al.* [215] proved that the viscosity of the polymer and consequently the thickness of the fibres increased when the HAc concentration was increased.

Another outcome observed from an increase of the polymer viscosity was that the fibres were more aligned when the HAc and DMSO concentration was increased.

The regression models obtained for predicting the diameter of the fibres and inter-fibre separation were:

Fibre diameter (μm) = -0.155 + 0.197 * DMSO concentration + 0.108 * HAc concentration

Inter-fibre separation (μm) = -0.693 + 0.877 * DMSO concentration + 0.487 * HAc concentration

A relationship between fibre diameter and inter-fibre separation was also observed; the greater the fibre diameter, the greater the inter-fibre separation was obtained. This fact agrees with the thesis of Joseph Lenning Lowery (Massachusetts Institute of Technology, 2009) [305] where it was proved that the packing of the fibres was more dense when the fibres were thinner.

Figures 4.3 and 4.4 show the relationship between diameter of fibres and inter-fibre separation with respect to the concentration of HAc and DMSO. The

scaffolds with the largest fibre diameter and inter-fibre separations were those manufactured with 3:1 HAc/dH$_2$O and 10% DMSO.

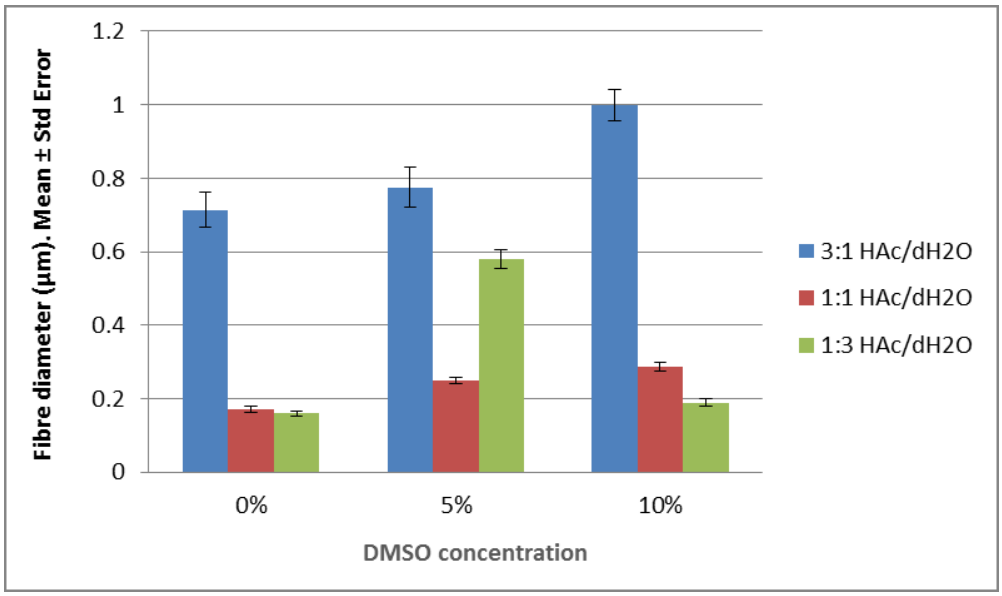

Figure 4.3 Fibre diameter (µm) for different concentrations of HAc and DMSO.

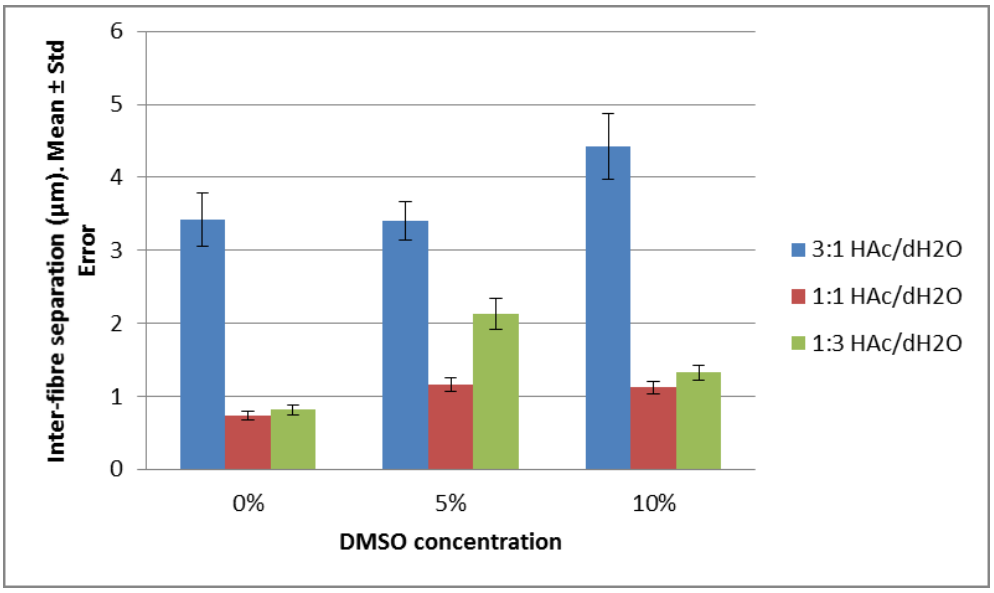

Figure 4.4 Inter-fibre separation (µm) for different concentrations of HAc and DMSO.

Analysing the roughness in relation to the acetic acid concentration, the minimum roughness was shown as 1:1 HAc/dH_2O and the maximum as 3:1 HAc/dH_2O (Figure 4.5).

The average roughness of the scaffold tended to decrease when the DMSO concentration was increased, allowing the creation of smoother fibres with an absence of beads, a fact that was also observed by Choktaweesap *et al.* [262]. Choktaweesap *et al.* [262] studied the effect of a single solvent system (glacial acetic acid) and mixed solvent systems (glacial acetic acid in combination with different solvents: 2,2,2-trifluoroethanol (TFE), dimethyl sulfoxide (DMSO), ethylene glycol (EG) and formamide (F)) on the morphology and fibre diameter. Choktaweesap *et al.* concluded that the addition of TFE, DMSO, EG, or F as co-solvent helped to improve the electrospinnability of the resulting gelatin solution. Moreover, DMSO and EG contributed to the formation of smooth gelatin fibres with reduced diameters in comparison to fibres created with acetic acid as the sole solvent.

In this case, the regression model that predicts the average roughness related to the solvent concentration was:

Average roughness (μm) = 1.756 - 0.014 * DMSO concentration - 0.242 * HAc concentration

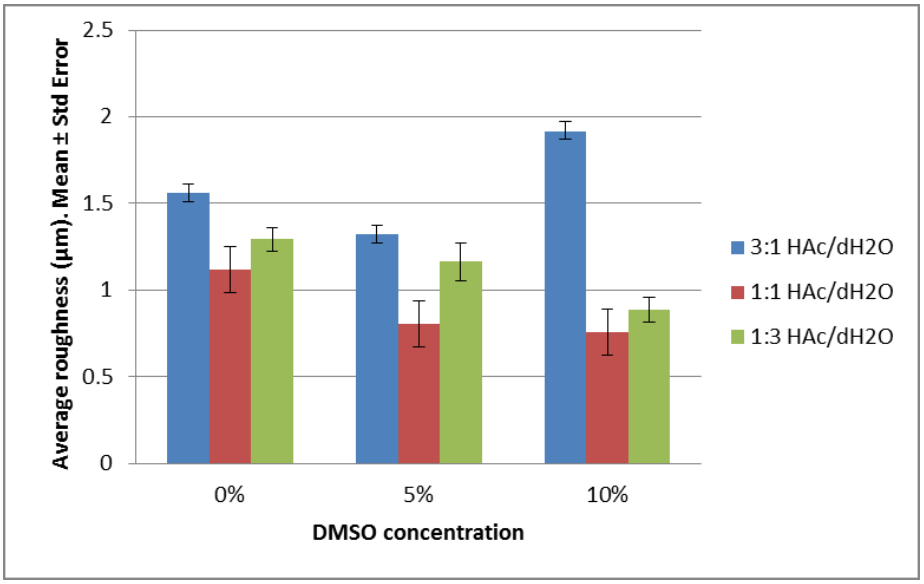

Figure 4.5 Average roughness (µm) for different concentrations of HAc and DMSO.

Mechanical properties were significantly affected by the concentration of DMSO ($p < 0.001$). Scaffolds with 1:1 HAc/ dH_2O exhibited the greatest tensile strength and strain at break at each DMSO concentration (Figure 4.6 and 4.7), due to the fact that the inter-fibre separation was the lowest allowing the creation of denser packing of fibres.

The tensile strength can be predict with the following regression model:

Tensile strength (MPa) = 2.456 - 0.166 * DMSO concentration + 0.788 * HAc concentration

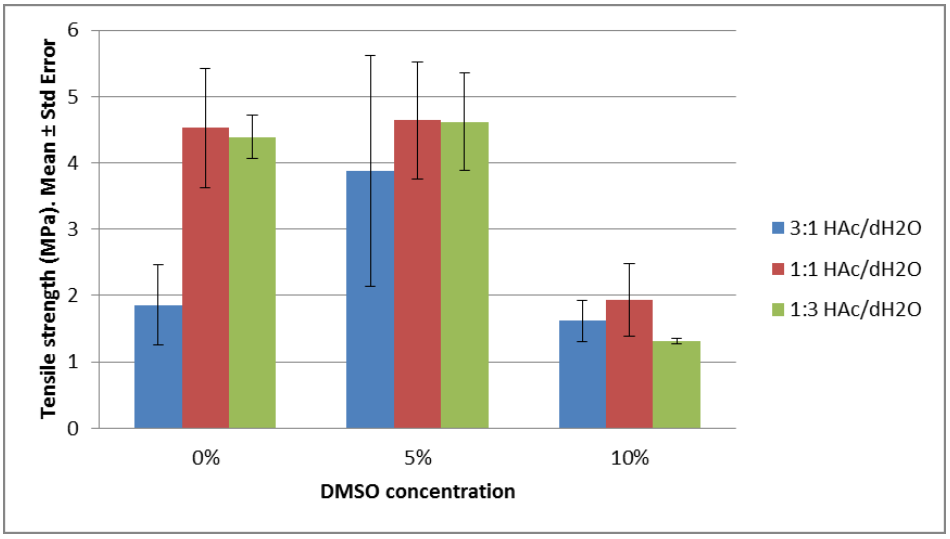

Figure 4.6 Tensile strength (MPa) for different concentrations of HAc and DMSO.

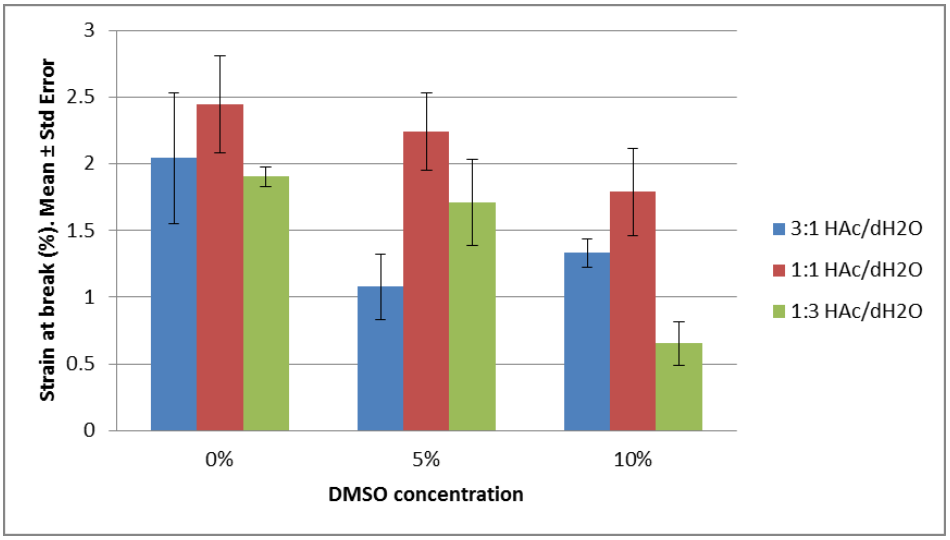

Figure 4.7 Strain at break (%) for different concentrations of HAc and DMSO.

Stress-strain curves were plotted for each tested sample. The J-shape characteristic of gelatin electrospun scaffolds [266] and biological soft tissue such as ligaments [306] was found in each sample. This J-shape is tipically shown to have a toe-region where the fibres start to straighten in the direction of the applied load and recovere their structure once load has been removed, a linear region where the

Young's modulus was calculated for each sample, and the yield region. A typical stress-strain curve shown in Figure 4.8.

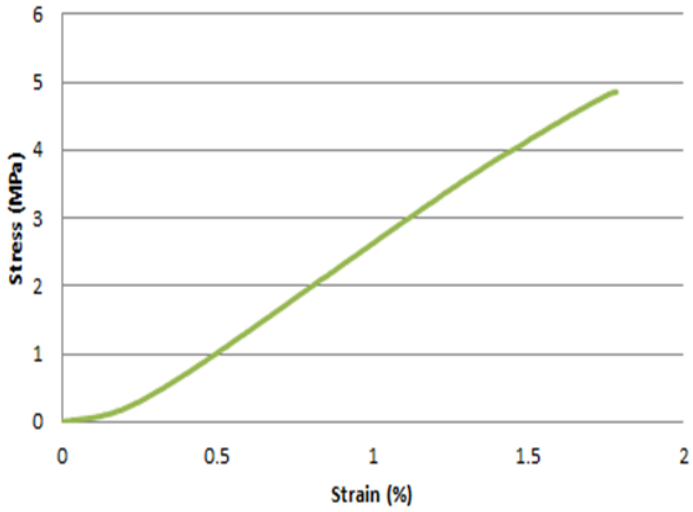

Figure 4.8 Stress-Strain curve for a 1:1 HAc/dH2O and 5% DMSO scaffold.

The natural anterior cruciate ligament (ACL) has a Young's modulus of approx. 111 MPa [59]. All scaffolds manufactured for this study exhibited a higher Young's modulus than the natural ACL but not too high to cause stress shielding once implanted into the body (as can be observed in Figure 4.9); therefore, they have an appropriate value for tissue engineered implants.

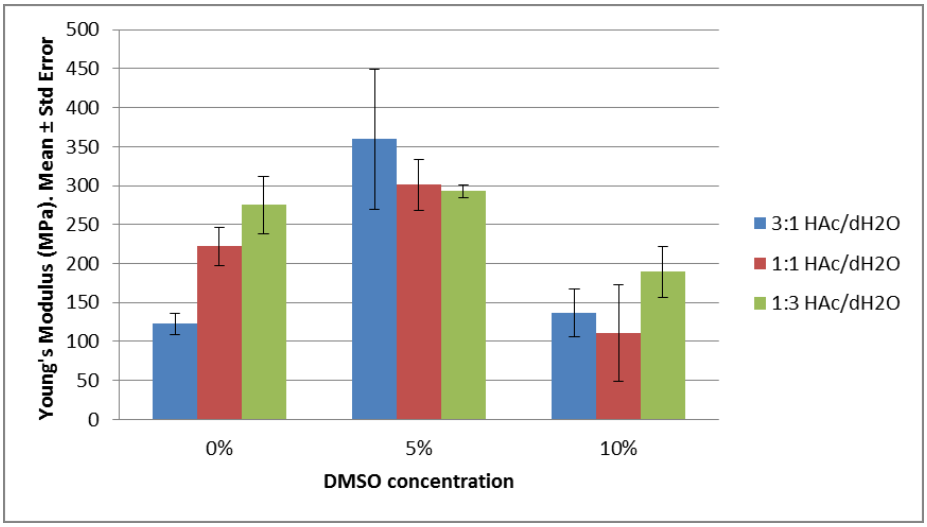

Figure 4.9 Young's modulus (MPa) for different concentrations of HAc and DMSO.

A maximum average tensile strength of 4.639±0.883 MPa, Young's Modulus of 300.961±32.603 MPa and strain at break of 2.243±0.292% were observed with tensile tests of the virgin scaffold with concentrations of 25% w/v of gelatin dissolved in 1:1 HAc (glacial acetic acid)/dH2O (distilled water) and 5% DMSO (dimethyl sulfoxide).

Previous studies revealed that the maximum tensile strength in a daily activity such as walking is approximately 17.57 MPa [237] and the maximum strain for that same activity is approx. 13% [237]. Therefore, the material properties of the gelatin electrospun scaffolds did not reach the specifications needed for daily activities such as walking.

Moreover, no significant relationships between strain at break and Young's modulus and the different concentration of solvents were obtained.

Despite not obtaining the desired mechanical properties, these values were significantly higher than the values reported in the only study for tendon replacement found in the literature [294], corroborating the importance of performing an iterative optimisation for both solution and process parameters. Yang *et al.* [294] reported values of maximum tensile strength of 1 MPa; however, in the study performed for this thesis the optimum gelatin scaffolds reached values of maximum tensile strength of 4.6 MPa. The differences between both studies lies in the type of solvent and its concentration used to perform the gelatin solution; in the case of Yang *et al.* the solvent used was TFE and its concentration 20% w/v.

Once the solvent concentration effects on the morphology of gelatin scaffolds were known, the next step was the study of the degradation of the scaffolds. As gelatin is soluble in water it is predicted that these scaffolds would be dissolved in synovial liquid existing around the knee joint, therefore a process of crosslinking has to be performed in order to slow down its biodegradation process. The following section 4.4.3 focusses on the crosslinker agent and how it affects the degradation, morphology and topography of the scaffolds.

4.4.3. GELATIN STUDY 2: HOW CROSSLINKING AFFECTS THE DEGRADABILITY OF THE SCAFFOLD, ITS MORPHOLOGY AND TOPOGRAPHY

As was explained in section 4.3.4, the degradation of 42 samples was analysed. Non-crosslinked samples exhibited total dissolution within 1 hour of incubation in PBS making the use of any biological assay and therefore the manufacturing of any implant prototype invalid. Samples crosslinked by immersion were found inviable, since they partially dissolved within two hours of immersion in GTA. Samples crosslinked by vapour deposition with 2.5% GTA were dissolved after 3 days of incubation in PBS. 5% GTA crosslinked samples (vapour deposition) lasted 7 days before being completely dissolved. Samples exposed to 25% GTA in vapour deposition remained undegraded until day 28. Figure 4.10 shows the scaffolds after being crosslinked by immersion and vapour deposition with 2.5%, 5% and 25% GTA.

Figure 4.10 Scaffolds after the crosslinking process. A) Immersion, B) Vapour deposition with 2.5% GTA, C) Vapour deposition with 5% GTA, D) Vapour deposition with 25% GTA.

Due to only the samples exposed to 25% GTA being capable of use as potential ACL implants, only those samples are presented.

The values for diameters of the fibres and inter-fibre separations for the samples exposed to 25% GTA versus the days in PBS are presented in Figures 4.11 and 4.12.

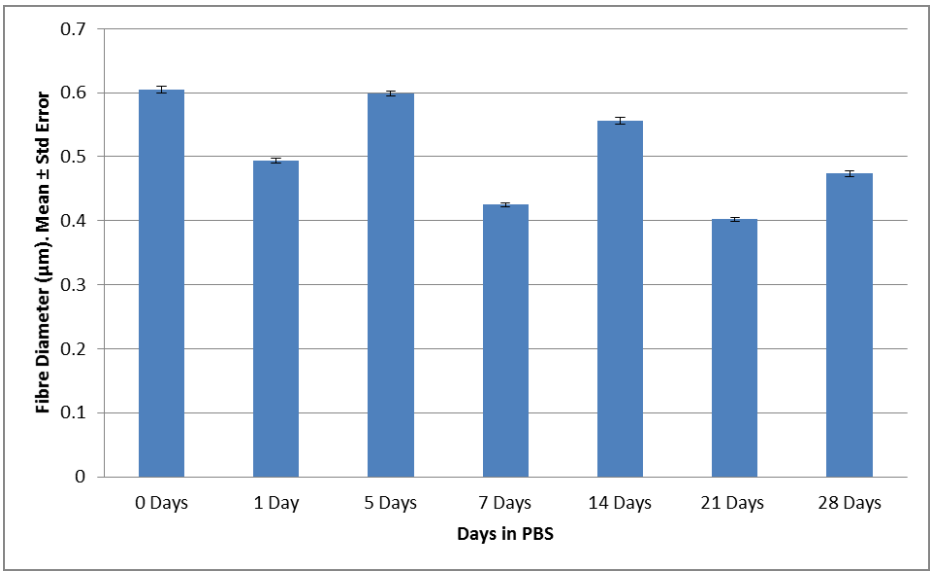

Figure 4.11 Fibre diameter (µm) with 25% GTA

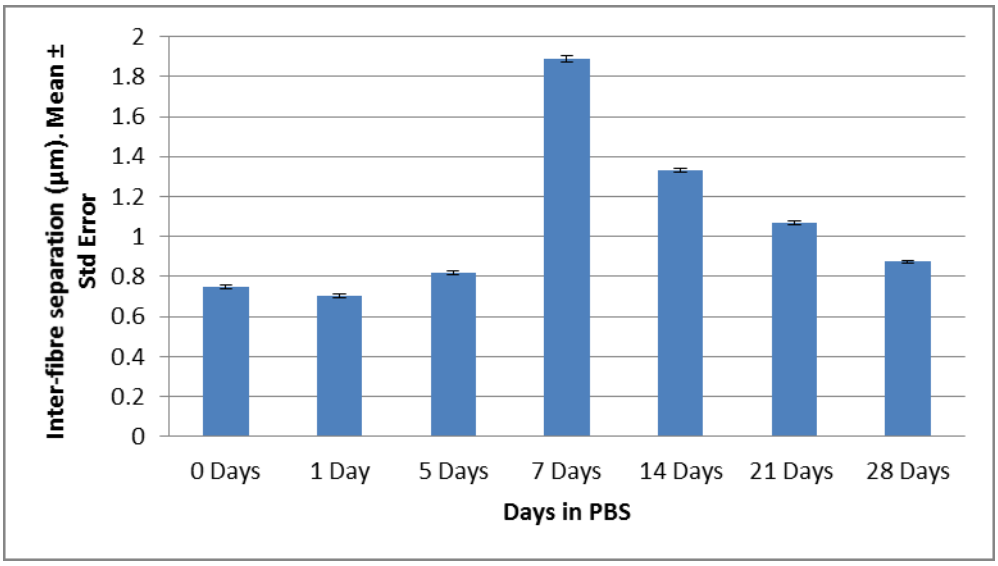

Figure 4.12 Inter-fibre separation (µm) with 25% GTA.

After a statistical analysis, it was obtained that there was a moderate negative correlation (-0.512) between the diameter of the fibres and days in PBS; therefore when the incubation days increased, the diameter of the fibre decreased. A very weak positive correlation was found between the days in PBS and the inter-fibre separation (0.1076). Regression models were performed for both parameters but neither the model nor the coefficients were significant.

The average roughness and days in PBS showed a significant positive correlation (0.8364). Therefore, the roughness of the scaffold tended to increase with the presence of PBS. The regression model between those parameters and its coefficients proved to be significant ($p < 0.05$) and it is shown below:

Average roughness (µm) = 1.423 - 0.026 * days in PBS

This phenomen could be due to the exposure of the fibres to salts dissolved in the PBS modifying their original topography. Figure 4.12 shows the values of

average roughness versus days in incubation in PBS and SEM images of each scaffold.

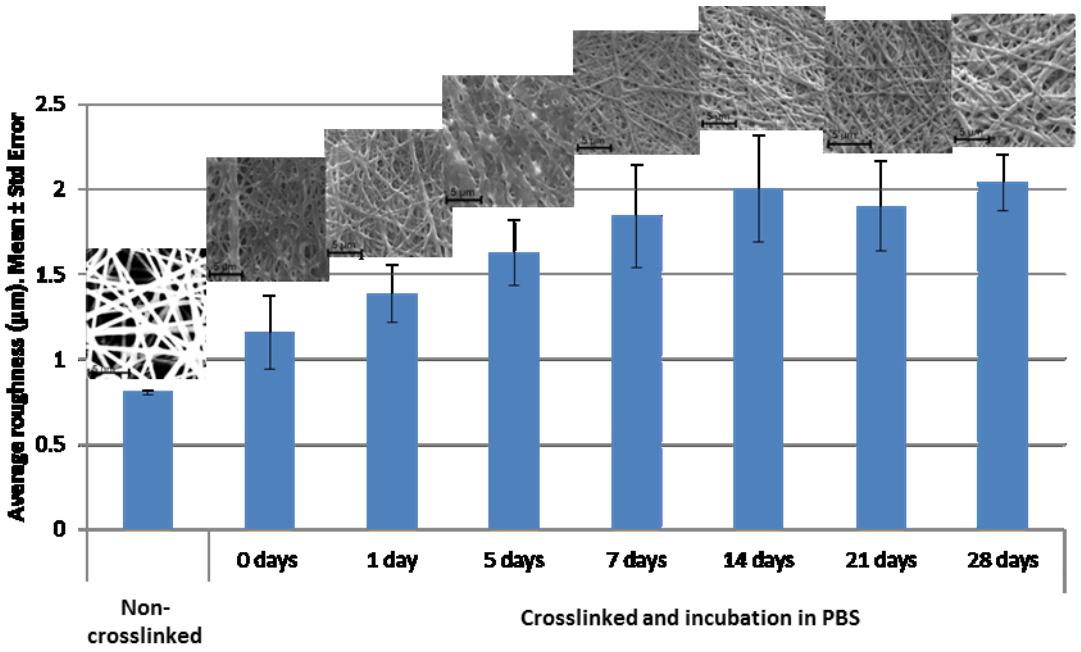

Figure 4.13 Average roughness (µm) for crosslinked scaffolds with 25% GTA.

No tensile tests were performed for crosslinked samples due to them being found to be visually more brittle and stiffer than the non-crosslinked samples (Figure 4.10), therefore it was obvious that the mechanical properties did not improve once the samples were crosslinked.

4.5. CONCLUSIONS

Acetic acid (HAc) and distilled water (dH_2O) in 3:1, 1:1 and 1:3 concentrations and dimethyl sulfoxide (DMSO) in 0%, 5% and 10% were used as solvents for electrospinning 25% w/v gelatin scaffolds.

From Gelatin study 1 it was concluded that the diameter of the fibres, inter-fibre separation, roughness and tensile strength were significantly affected by the concentration of HAc and DMSO ($p < 0.001$). The optimum concentration was found to be 25% of gelatin dissolved in 1:1 HAc and dH_2O with 5% DMSO added; the optimum parameters to create the scaffold were: 26kV, flow rate of 2 ml/h, 11 cm distance between needle and collector, 15 G of size of the needle and 1300 rpm of the mandrel.

Morphologically and topographically, it was observed that the diameter of the fibres and inter-fibre separations increased when the solvent concentration increased and the roughness decreased when the concentration of DMSO increased.

Regarding mechanical properties, despite all manufactured scaffolds exhibiting higher Young's modulus than the natural ACL, the maximum average tensile strength was 4.639±0.883 MPa and its strain at break was recorded as 2.243±0.292 %; values much lower than the native ACL (reported as having an ultimate tensile of 38 MPa and strain at failure of 44%) [59].

From Gelatin study 2, it was concluded that only the samples exposed to 25% GTA remained undegraded until day 28. However, the original morphology of the scaffolds was modified, increasing in most of the cases all the fibre parameters (diameter, inter-fibre separation and roughness) when the incubation time in PBS increased. Additionally, crosslinked samples were visually found to be more brittle and stiffer than the non-crosslinked samples, therefore their mechanical properties did not improve after the crosslinking process.

Therefore, both studies (Gelatin study 1 and Gelatin study 2) demonstrated, for the first time, that gelatin is not suitable for use as the sole polymer for the manufacture of ACL implants and further investigations must be focussed on the study of novel polymers and combinations of polymers for optimal ACL replacement.

Chapter 5 evaluates the suitability of PVA electrospun scaffolds for use as ACL replacements. The morphology, topography and mechanical behaviour of these scaffolds is studied and compared with the properties of the natural ACL.

Key points:

1. This study evaluated the suitability of gelatin electrospun scaffolds to develop biomimetic ACL grafts, since no studies with these type of scaffolds have previously been performed for the purpose of manufacturing ligament implants.

2. To date, no studies for any polymer have focussed on an iterative optimisation of solution (with different polymer and solvent concentrations) and process parameters, with the goal of achieving mechanical and morphological properties that mimic the desired biological tissue.

3. This chapter also studied how the use of crosslinking agents change the morphology of the nanofibres and their network, and how this influenced the suitability of this polymer to be used for ACL grafts.

4. The optimised gelatin scaffolds achieved mechanical properties (maximum tensile strength 4.6 MPa) significantly higher than gelatin-based electrospun scaffolds reported for tendon applications (maximum tensile strength 1 MPa [294]).

5. It was demonstrated that optimised gelatin scaffolds are not suitable to be used as the sole polymer for the manufacturing of ACL implants. This finding increases knowledge of the mechanical limitations of gelatin and moves the field forward to investigate other alternative polymers for new ACL grafts.

5. Suitability of polyvinyl alcohol (PVA) for the manufacturing of electrospun tissue engineered ligament implants: morphological, topographical and mechanical study

The lack of appropriate suitability of gelatin electrospun scaffolds for their use as ACL grafts was demonstrated in Chapter 4. Therefore, it was necessary to test the suitability of a new polymer for use as a potential ACL graft. The suitability of polyvinyl alcohol electrospun scaffolds is studied in Chapter 5 comparing the morphology, topography and mechanical behaviour of the scaffolds created in this chapter with the characteristics of the natural ACL.

5.1. ABSTRACT

Polyvinyl alcohol (PVA) is an inexpensive, biodegradable, nontoxic and biocompatible polymer [65], [217], [218], [307]. This polymer is commonly used as a baseline for experiments with other materials, because it is easily electrospinnable due to its water solubility and nontoxicity.

Recent studies used electrospun PVA mats for different applications such as food packing, tissue engineering, antibacterial, osmosis membrane, air filtration or drug delivery [307]–[312]. In these studies scaffolds were characterized in different ways (morphologically, chemically or mechanically, depending on the study) but

they were not characterized morphologically, topographically and mechanically at the same time.

The use of PVA-based electrospun scaffolds for the manufacturing of ligaments implants has not been reported to date and only one study was found where PVA-base electrospun scaffolds were used for tendon substitutes [313].

However PVA hydrogel cords were evaluated for use as ligament replacements [65], [314]–[316]. These 3D structures resulted in good biocompatibility [316] but low mechanical properties in comparison with the ACL [314].

The novelty of this work was to establish appropriate process and solution parameters in order to produce electrospun scaffolds with comparable mechanical behaviour and morphology as the native ACL.

As in the previous study with gelatin (Chapter 4), the aim of the work was to evaluate the suitability of PVA electrospun scaffolds for use in creating new tissue engineered ligaments. The results of this research will increase the understanding about the type of material needed to achieve this objective.

The work from this PhD revealed that a specific electrospinning setup could create 2D electrospun PVA scaffolds with a tensile strength of 30 ± 1 MPa close to that of the natural ligament (38 MPa [59]) and superior to 24.8 MPa reported during a jumping at maximum effort (activity which exhibited the highest tensile force) in

Chapter 3 [237]. Apart from investigating the suitability of the PVA to be used for manufacturing new tissue engineering ligaments, this study was an initial investigation to manufacture 2D scaffolds and then use them to create 3D scaffolds for ACL replacement.

5.2. INTRODUCTION

As demonstrated in the previous chapter (Chapter 4), solution and process parameters directly affect the morphology, topography and mechanical properties of the electrospun mats, therefore the optimisation of those parameters will be critical to customize the scaffolds and obtain the desired properties. This novel study focusses on a systematic optimisation of these parameters to achieve PVA electrospun scaffolds with comparable morphology and mechanical properties to the natural ACL. A number of studies reported induced changes in the morphology of the fibres from modifying solution or process parameters [217], [218], [317]; however, none of them used a consistent optimisation process to select those parameters in order to achieve the desired objective. This study optimised the process and was the basis for the development of 3D tissue-engineered ligament implants produced in the following chapter of this thesis (Chapter 6).

PVA is an inexpensive, highly hydrophilic, biodegradable, nontoxic and biocompatible polymer with excellent physical, chemical and mechanical properties. These properties make the PVA a promising polymer to create nanofibrous electrospun scaffolds for tissue engineering applications [65], [217], [218], [307] but

its use as a potential material for ligament implants still has to be proved mechanically and morphologically.

Following a literature review of the PVA-based electrospun scaffolds created for tissue engineering, it was observed that most of them were used for skin and wound dressing applications [318]–[322], as well as bone tissue [309], [323]–[326] and vascular grafts [327]–[331]. No studies were found for the development of PVA-based electrospun ligaments and only one study was found for tendons [313]; however in that article, PVA was used as sacrificial polymer with the aim of, once the PVA is dissolved in warm water, producing polyurethane hollow yarns. Therefore, the suitability of PVA electrospun scaffolds to be used for ligament implants is yet to be assessed.

PVA hydrogels are commonly studied for tissue engineered cartilage substitutes [332]–[335]. Only four articles were found with the aim of creating ligaments [65], [314]–[316]. However, none of them studied the morphology of the scaffold or assessed their mechanical behaviour under shear loading.

Bash *et al.,* used ultrahigh molecular weight polyethylene thread braided with PVA hydrogel cords to create the prototypes [65]. They reported an ultimate load in tension of their constructs of approx. 2000 N identical to the value reported for the natural ACL [58], [59]; however, they did not report any evaluation of the degradation, morphology or topography of the scaffold to be compared to the native ligament.

Cai *et al.,* studied twisted collagen I fibres with PVA hydrogel cords in order to manufacture ACL hydrogel scaffolds [314]. The maximum tensile strength reported for these constructs was 29.7 MPa, inferior to 38 MPa observed in the natural ACL.

Moreau *et al.,* (2014 and 2017) evaluated the *in vivo* influence of coating PVA hydrogel cords with hydroxyapatite to promote osteogenesis in rabbits [315], [316]. The results of these studies revealed that no bone tunnel osteolysis was observed and new bone tissue started to grow from the cortical bone [316]; however, the addition of the hydroxyapatite coating did not significantly improve the osseointegration of the implant [316].

Other studies demonstrated that crosslinked PVA hydrogels exhibited excellent biocompatibility [336] and a water-swollen network similar to the extracellular matrix of the native ligament [65]. However, they cannot mimic the morphology of the extracellular matrix and therefore non-biomimetic ligament scaffolds can be produced with hydrogels.

PVA electrospun scaffolds exhibit a network of nanofibres that mimics the extracellular matrix [337] and provides an optimum environment for cell proliferation. This polymer is easily electrospinnable due to its water solubility, nontoxicity of the solvent, the solution is ease to prepare and the production of high quality nanofibres free of defects. All of these advantages makes PVA an excellent polymer to be used as a baseline for experiments with other materials. More detail

about the advantages and disadvantages of currently used materials can be found in Section 1. 6.

The novelty of this work is in understanding how changes in the process and solution parameters affect the morphology and maximum tensile strength of PVA electrospun scaffolds. This study allowed the creation of structures with similar morphology and mechanical behaviour to the natural ACL. The relationship between the process and solution parameters that provide morphology and mechanical behaviour comparable to the ACL are not fully documented in the literature. Moreover, this study will help to determine the type of material needed to create scaffolds with comparable structure to the natural ACL and that can bear high impact loading.

As in the previous study with the gelatin (Chapter 4), the aim of this work was to assess the morphology, mechanical behaviour and degradation of the PVA electrospun scaffolds to determine its suitability to manufacture tissue-engineering implants [338].

5.3. METHODS

5.3.1. POLYMER SOLUTION

For the initial optimisation of the polymer solution, different concentrations of PVA (Sigma Aldrich, UK) diluted in distilled water (dH_2O) were prepared by

heating and stirring until a homogenous solution was achieved (see section 5.3.2.). After achieving the optimum concentration of PVA (12% w/v), different ranges of experiments with this solution were performed to determine the structure that provides the closest maximum tensile strength to the native ACL (38 MPa [59]) and that is capable of bearing a tensile strength of 24.8 MPa, reported during a jumping at maximum effort [237].

Crosslinked samples were fabricated with 25% glutaraldehyde acquired from Sigma Aldrich (UK).

5.3.2. SCAFFOLD PRODUCTION

An electrospinning device (Spraybase®, Ireland) was used to manufacture all the electrospun scaffolds. As in the last study with gelatin (section 4.4.1), it was necessary to perform an initial study (PVA study 1) to optimise the process and solution parameters, in order to produce the scaffold with the closest properties to the natural ligament. For that study different experiments were performed:

- Optimisation of the polymer concentration. Four different concentrations were studied: 10%, 12%, 14% and 16%. The rest of the parameters were fixed as shown in Table 5.1. With these first experiments, an optimum morphology of the fibres (comparable to the diameter of the collagen fibrils of the natural ACL) with appropriate diameter was obtained.

Table 5.1 Fixed process parameters to determine optimum polymer concentration.

Voltage	Flow rate	Distance between collector and needle	Needle	Revolutions of the mandrel	Temperature	Time
25 kV	1 ml/h	11 cm	18G	1000 rpm	23° C	15 min

- Optimisation of flow rate. 0.5 ml/h, 1 ml/h, 2 ml/h and 5 ml/h were tested until a stable Taylor cone was visibly obtained.

- Optimisation of voltage. The voltage was varied until a stable Taylor cone and jet was produced. The spinnability with voltages 18 kV, 20 kV, 22 kV and 25 kV was observed.

- Optimisation of the distance between needle and collector. The morphology of the fibres was studied with three different distances 50 mm, 80 mm and 110 mm. The rest of the parameters were fixed at the values shown in Table 5.2.

Table 5.2 Fixed process parameters to determine distance between needle and collector.

Concentration	Voltage	Flow rate	Revolutions of the mandrel	Needle	Time
12%	20 kV	1 ml/h	2000 rpm	18G	20 min

- Optimisation of the size of the needle. The morphology of the fibres manufactured with needle sizes of 15G, 18G, 20G, 21G, 22G and 23G in diameter were studied to determine the size that provides the best morphology (with diameter of fibres comparable to the collagen fibrils of the native ACL) with mats free of any kind of defect. Table 5.3 shows the rest of the parameters used for creating the scaffolds.

Table 5.3 Fixed process parameters to determine the size of the needle.

Concentration	Voltage	Flow rate	Distance between collector and needle	Revolutions of the mandrel	Time
12%	20 kV	1 ml/h	80 mm	2000 rpm	20 min

- Optimisation of the revolution of the mandrel. The changing orientation of the fibres was observed with different revolution speeds of the mandrel: 500 rpm, 1000 rpm, 2000 rpm and 3000 rpm. The other parameters were fixed as in Table 5.4.

Table 5.4 Fixed process parameters to determine the revolutions of the mandrel.

Concentration	Voltage	Flow rate	Distance between collector and needle	Needle	Time
12%	20 kV	1 ml/h	50 mm	18G	20 min

Once the parameters were optimised, obtaining a stable Taylor cone and scaffolds with fibres free of defects, a second study (PVA study 2) was performed to find their mechanical properties. In this study, the tensile strength and Young's modulus were evaluated for the samples with the best morphology (the most similar to the natural ACL) obtained in relation to:

- Revolution of the mandrel. 1000 rpm, 2000 rpm and 3000 rpm were studied under the conditions shown in Table 5.5.

Table 5.5 Fixed process parameters varying the revolutions of the mandrel.

Concentration	Voltage	Flow rate	Distance between collector and needle	Needle	Time
12%	20 kV	1 ml/h	80 mm	18G	2 h

- Size of the needle. 18G and 21G were studied performing the experiments with the following set up (Table 5.6).

Table 5.6 Fixed process parameters varying the size of the needle.

Concentration	Voltage	Flow rate	Distance between collector and needle	Revolutions of the mandrel	Time
12%	20 kV	1 ml/h	80 mm	2000 rpm	2 h

The third study (PVA study 3) was focussed on the degradation of the selected scaffold shown to have the morphology and mechanical properties closest to the natural ligament. This scaffold was manufactured with 10 ml of 12% polymer solution pumped with a flow rate of 1 ml/h through an 18 G needle. The voltage between the tip of the needle and the collector was set up at 20 kV. The fibres were projected from the tip of the needle over a sheet of aluminium foil attached to a 9.65 cm diameter rotating collector working at 2000 rpm, in order to obtain aligned fibres and a maximum tensile strength similar to the natural ACL. The distance between the needle and the collector was set up 8 cm. The scaffolds were manufactured at room temperature and for 2 hours spin time. Prior to performing the degradation study, the samples were crosslinked following the procedure explained in the next section (5.3.3).

5.3.3. CHEMICAL CROSSLINKING

PVA is soluble in water and in any other biological solution [339]. This fact would directly affect the viability of the scaffold in a culture medium, to grow cells on it in order to obtain a tissue-engineered scaffold, and inside the body once the scaffold is implanted. Therefore, to slow down the degradation of the PVA scaffolds a crosslinking process of the samples has to be performed.

Two crosslinking techniques were evaluated: immersion and vapour deposition. For crosslinking the samples by immersion, glutaraldehyde (GTA) and methanol were studied. For this technique, six samples were placed in 6 well plates

with 2 ml of ≥ 99.6% methanol in three of the wells and 2 ml of 25% GTA in the other three wells for 2 hours.

The crosslinking by vapour deposition was performed by pouring 25 ml of 25% GTA in a Petri dish at the bottom of a sealed desiccator. 16 samples (created for PVA Study 3) were placed over a metallic mesh on top of the Petri dish and exposed to glutaraldehyde vapour for a 24 hour period inside the desiccator. After the vapour deposition crosslinking process, the samples were dried under a fume hood for 24 hours in order to remove the moisture and reduce the toxicity of the samples due to the GTA. Two samples were reserved for topographical characterization after being crosslinked, an additional two samples were rinsed in PBS for 30 seconds and dried under a fume hood for 24 hours, and the remainder (12 samples) were used for the degradation assay explained in the next section (5.3.4).

Moreover, 16 samples were crosslinked to be mechanically characterized in PVA Study 2 and dried under a fume hood for 24 hours.

5.3.4. DEGRADATION ASSAY

Twelve samples of the scaffold created with the optimum solution and process parameters were air-dried for 24 hours and placed in 6 well plates (2 samples per well) with 4 ml of PBS in each well. These samples were then left in an incubator at 37ºC and 4% CO_2 in order to test their degradability over time in temperature conditions similar to human body conditions. These samples were left in PBS for 1,

5, 7, 14, 21 and 28 days. Before topographical characterization of the samples, they were air-dried for 24 hours in a fume hood to remove the moisture.

5.3.5. SCAFFOLD/FIBRE CHARACTERIZATION

5.3.5.1. Fibre morphology

Fibre morphology was analysed for all scaffolds manufactured in PVA studies 1 and 2; this parameter was not fully evaluated for PVA study 3 due to the difficulty of measuring swollen electrospun fibres, this was explained in more depth in section 5.4.3.

As in the previous study with gelatin (Chapter 4), a SC7640 sputter coater (Quorum Technologies Ltd. Kent, UK) was used to coat the samples with gold prior to their visualization with a field emission scanning electron microscope (Zeiss Supra 40, FE-SEM, Carl Zeiss SMT Ltd., Cambridge, UK). The intensity used for coating the samples was 20 mA, the voltage 0.8 kV and the duration of the coating was 120 seconds. SEM images of each sample created with the different set ups were taken at around 6 mm working distance, with a voltage of 2 kV and with magnifications of 1000x, 2000x and 3000x. Fibre diameters and inter-fibre separations were determined with AxioVision SE64 Rel. 4.9.1 (Carl Zeiss SMT Ltd., Cambridge, UK) by measuring 20 fibres per sample. Two samples (replicates) were measured for each different scaffold and two scaffolds (repeats) were produced for each configuration (16 different set ups) to guarantee the repeatability of the results, therefore a total of 64 samples was analysed.

5.3.5.2. Scaffold topography

Scaffold topography was evaluated for PVA study 3. 6 white light interferometry images were taken per sample using an interferometer from ZeGage (Zygo Corporation). A total of 108 images were analysed for this study. The average roughness was compared between crosslinked samples (16 crosslinked samples) with different times in PBS and the initial non-crosslinked samples (2 non-crosslinked samples)

5.3.5.3. Mechanical behaviour of the scaffolds

A total of 76 samples were mechanically characterized. The mechanical behaviour of 5 different non-crosslinked scaffolds and 1 crosslinked scaffold (created with the optimum solution and process parameters) were analysed. From each non-crosslinked scaffold, 6 longitudinal and 6 transverse samples were tested and for the crosslinked scaffold, 8 longitudinal and 8 transverse samples were mechanically characterized. Longitudinal samples were called to the samples with the fibres orientated longitudinally to the applied load during the tensile test. Transverse samples were the ones with their fibres orientated transversally to the applied load.

The samples were removed from the mats with a dog-bone cutting die (25 x 4 mm, test length x width). Their thickness was measured three times with a digital and an analogical calliper in order to check the consistency of the measurements. They were attached on a cardboard frame to help the alignment of the sample in the tensometer (Instron H10KS) and they were tensile tested until failure with a 100 N

load cell and 1 mm/min test speed. Tensile strength was determined for each sample and statistically analysed in order to evaluate the relationship between this mechanical property and the morphological properties.

5.3.6. STATISTICAL ANALYSIS

Mean and standard error of the mean (Std Error) were calculated for all quantitative structural and mechanical properties.

Pearson coefficient of correlation and simple linear regressions were used to estimate the relationship between process and solvent parameters and the morphology, topography and mechanical properties of the scaffolds.

All statistical analyses were conducted using SPSS (IBM Inc, Chicago, Illinois).

5.4. RESULTS AND DISCUSSION

5.4.1. PVA STUDY 1: OPTIMISATION OF THE SOLUTION AND PROCESS PARAMETERS

5.4.1.1. Optimisation of polymer concentration

Four concentrations of PVA with distilled water were considered in this experiment: 10%, 12%, 14% and 16%. Due to the high viscosity of the 16% solution, no scaffold could be manufactured with that concentration.

Scaffolds with beads were produced with concentrations below 12% (Figure 5.1 A) and the viscosity of the solution caused difficulties in electrospinning with concentrations above 12%. SEM images of scaffolds produced with 10%, 12% and 14% solutions are shown in Figure 5.1.

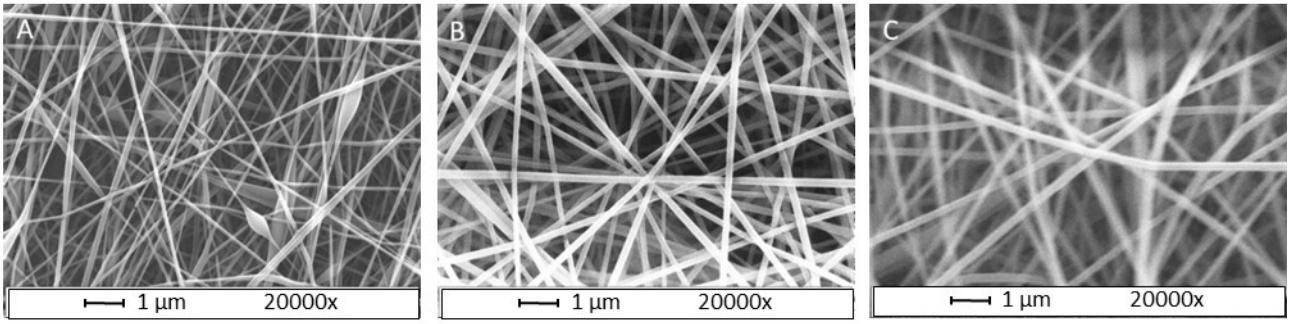

Figure 5.1 PVA scaffolds with A) 10% B) 12% and C) 14% polymer concentration.

Studying the morphology of the scaffolds, it was observed that the diameter of the fibres increased with increased percentage of polymer solution as shown in Figure 5.2. The correlation between both parameters follows a perfect positive linear association with 0.999. In addition, the regression model follows the expression below:

Diameter of the fibres (µm) = -0.191 + 2.7625 * concentration of the polymer (%)

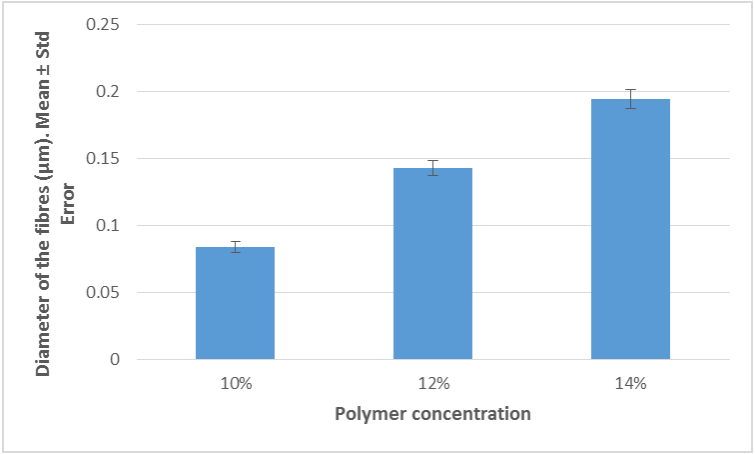

Figure 5.2 Diameter of the fibres versus concentration of polymer

There are two different groups of collagen fibrils in the native ligament, a group of fibrils with diameters between 40 and 75 nm and other group with diameters between 100 nm and 150 nm [33], [45]–[47], [209]. Due to 12% PVA being determined as the concentration that created the average diameter of the fibres most comparable to the fibrils (10%: 84±3.9 nm, 12%: 143±5.6 nm, 14%: 194±6.9nm) and the ease of electrospinning PVA with that concentration, 12% was considered as the optimum concentration of polymer. Therefore, the rest of the experiments were set up with 12% PVA.

5.4.1.2. Optimisation of flow rate

The flow rate was modified from 0.5 ml/h, 1 ml/h, 2 ml/h to 5 ml/h until a stable Taylor cone and jet were obtained. Continuous drops were observed (not allowing the creation of a stable Taylor cone) with rates of 2 ml/h and 5 ml/h. At 0.5 ml/h the flow was not high enough in speed to maintain a stable jet. A flow rate of 1 ml/h created a stable jet without the presence of continuous drops, so this was determined to be optimum.

5.4.1.3. Optimisation of voltage

Once the polymer concentration and the flow rate were set up to 12% PVA and 1ml/h, the voltage was varied from 18 kV, 20kV, 22 kV to 25 kV until the electrostatic force overcame the cohesive force of the solution and a charged jet was visible. This was observed to occur from 20 kV. This phenomenon was also observed with 22 kV and 25 kV; however, due to the risk of static shock for the user and the

risk of damaging the electrospinner (higher risks as the voltage is increased) it was decided to set the electrospinner at the lowest voltage possible.

5.4.1.4. Optimisation of the distance between needle and collector

Three different distances were considered: 50 mm, 80 mm and 110 mm. Figure 5.3 shows the diameter of the fibres and the inter-fibre separations in relation to the distance between the needle and collector.

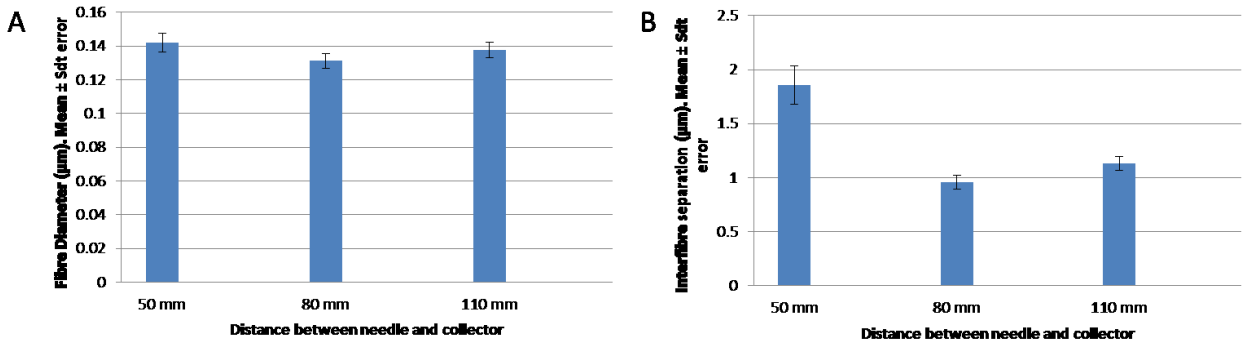

Figure 5.3 A) Diameter of the fibres and B) Inter-fibre separation versus distance between needle and collector

The diameters of the fibres and the inter-fibre separations were analysed statistically with respect to the distance between the needle and the collector. No significant linear regression between diameter of the fibre and this distance or inter-fibre separation and the distance were observed. The Pearson coefficients between diameter and distance was -0.39 and between inter-fibre separation and distance was -0.76. The morphology of the three scaffolds can be observed in Figure 5.4.

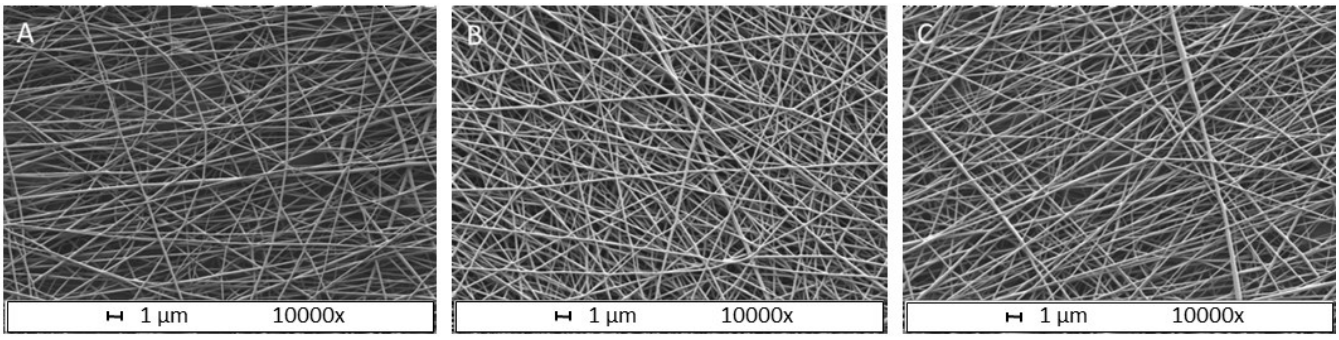

Figure 5.4 Scaffolds fabricated with A) 50 mm distance between needle and collector, B) 80 mm and C) 110 mm.

As no significant differences were determined for the morphology of the fibres against the distance between the needle and the collector, it was decided to set an optimum value of 80 mm distance. This decision was made based on two aspects: the total evaporation of the solvent and the productivity of the manufacturing process. Scaffold made with 50 mm distance between needle and collector exhibited problems of solvent evaporation. The production of scaffolds made with 110 mm distance were slower than with 80 mm distance between the needle and the collector, reducing the productivity.

5.4.1.5. Optimisation of size of the needle

The morphology of the scaffolds was studied using five needles with different sizes: 15G, 18G, 20G, 21G and 22G. Figure 5.5 shows the diameter of the fibres and the inter-fibre separation versus the size of the needle.

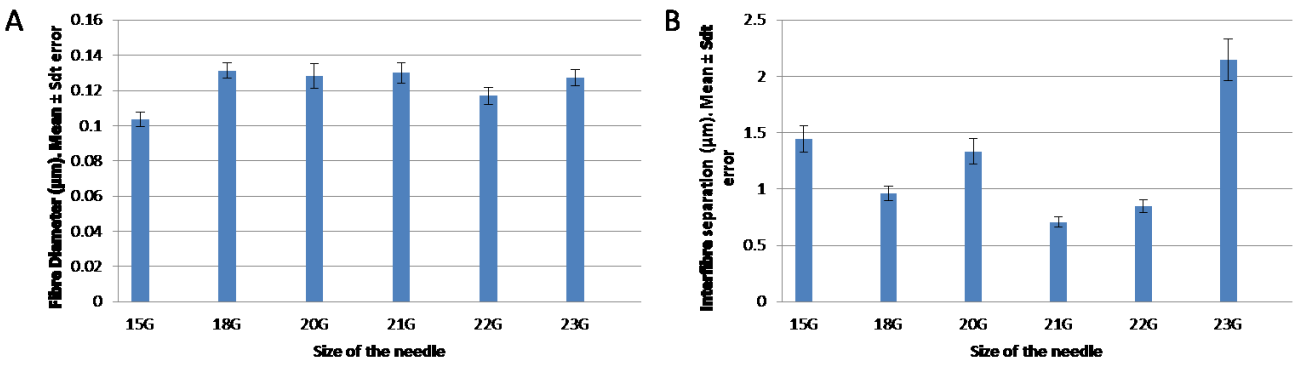

Figure 5.5 A) Diameter of the fibres and B) Inter-fibre separation versus size of the needle

Statistically analysing both of these parameters against the size of the needle, it was observed that neither significant correlations nor significant regression models were obtained, therefore the selection of the size of the needle was taken through a manufacturing perspective. It was observed that a very small diameter of the needle (22G and 23G) produced thin scaffolds, due to the density of the fibres projected over the collector being low (Figure 5.6 E and F); therefore the time to create thicker scaffolds increased significantly and the productivity of the process was decreased. Electrospun scaffolds produced with the needle with the biggest diameter also produced a thin electrospun scaffold (observed inter-fibre separation for 15G in Figure 5.5 B), decreasing the productivity. Another aspect to take into consideration was the ease of obtaining a stable Taylor cone. It was easier to spin with a needle of 18G diameter rather than smaller diameter needles, since it is less likely to block the needle and obtain a stable Taylor cone if the needle has a bigger diameter. For these reasons, and for the next experiment (section 5.4.1.6. Optimisation of the revolutions of the mandrel), it was considered that the optimum needle size was 18G. However, mechanical tests were performed to compare the maximum tensile strength for scaffolds created with 18G and 21G to corroborate that the assumption made in this

experiment was valid. Figure 5.6 shows the different scaffolds produced with the different needle sizes.

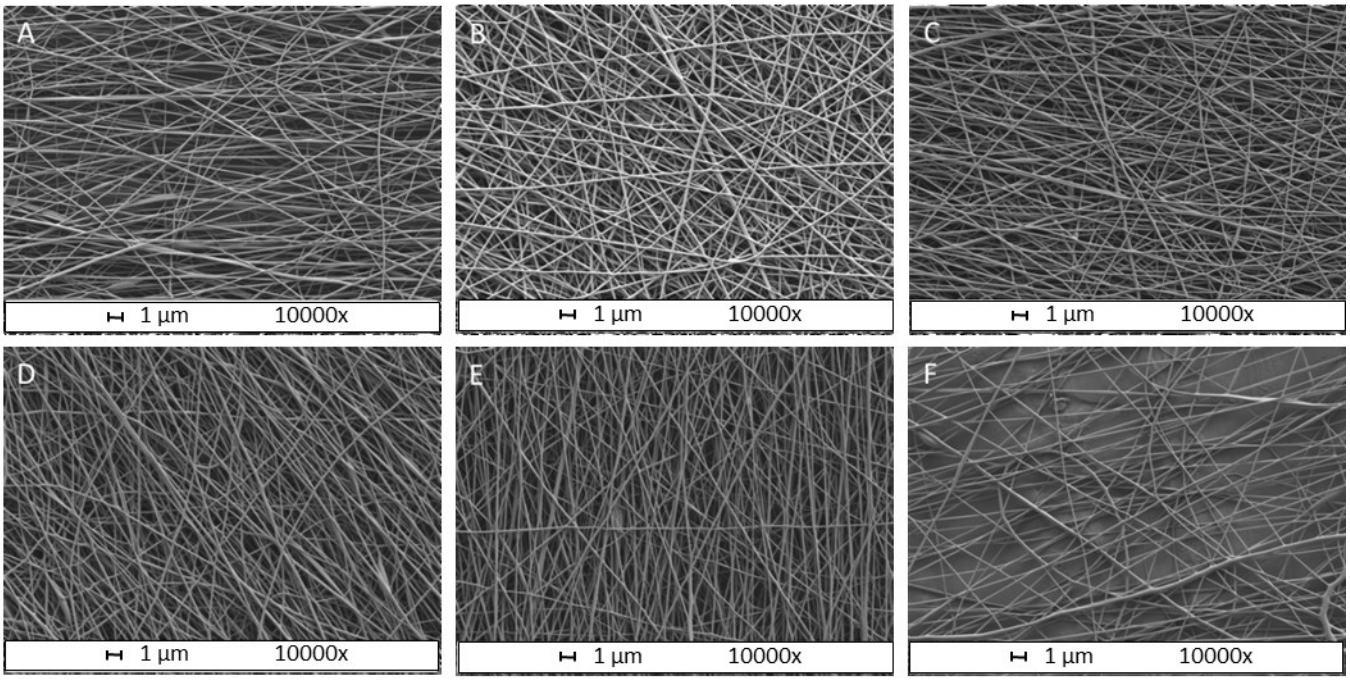

Figure 5.6 Scaffolds fabricated with size of the needle of A) 15G, B) 18G, C) 20G, D) 21G, E) 22G and F) 23G

5.4.1.6. Optimisation of revolutions of the mandrel

The morphology of the fibres was studied as a result of changing the revolutions of the mandrel. 500 rpm, 1000 rpm, 2000 rpm and 3000 rpm were evaluated. Figure 5.7 shows the diameter of the fibres and the inter-fibre separations in relation to the revolutions of the collector. As was observed from the graphs (Figure 5.7 A and B), all of the scaffolds presented fibre diameters between 100 nm and 150 nm, comparable to the diameter of the collagen fibrils in the natural ACL [33], [45]–[47], [209]. The higher inter-fibre separation was observed for scaffolds made with mandrel revolutions of 2000 rpm, this is a key point since scaffolds with higher inter-fibre separation would promote more cellular migration inside the

scaffold than scaffolds with low inter-fibre separation. This was observed in Ionescu *et al.* [340], where higher porosity scaffolds were better infiltrated and exhibited a more uniform matrix deposition of proteoglycan and collagen.

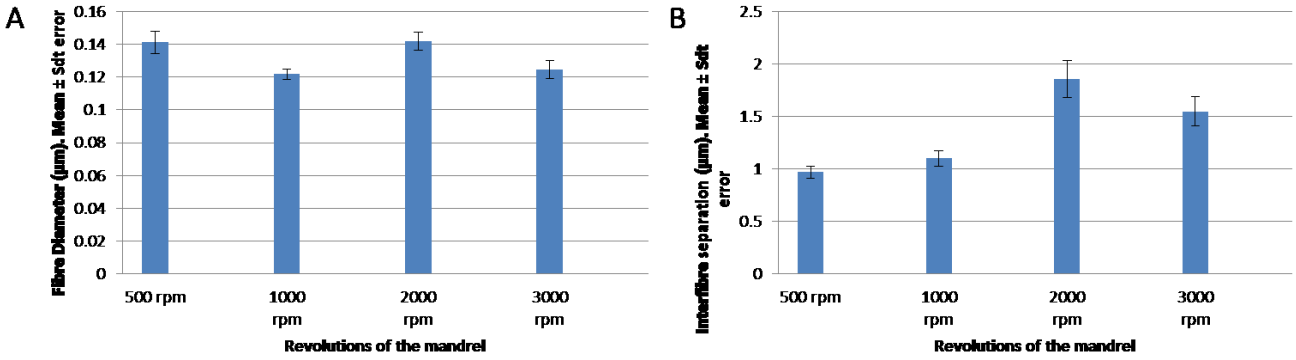

Figure 5.7 A) Diameter of the fibres and B) Inter-fibre separations versus revolutions of the mandrel

As in the last section (5.4.1.5), neither significant correlations nor significant regression models were obtained after statistical analysis. Therefore, the optimum mandrel revolution was determined by observing which scaffold had the highest inter-fibre separation and which presented more aligned fibres. It is known that the collagen fibres are parallel and longitudinally orientated in the natural ACL, therefore, in terms of morphological structure of the scaffolds, the best revolution would be the one that produced aligned fibres free of defects comparable to the natural ACL. In the next section (5.4.2. PVA Study 2) different scaffolds created with different speeds were mechanically tested to corroborate whether scaffolds with aligned fibres produced higher maximum tensile strength than randomly orientated fibres. The different scaffolds produced by varying the revolutions can be observed in Figure 5.8.

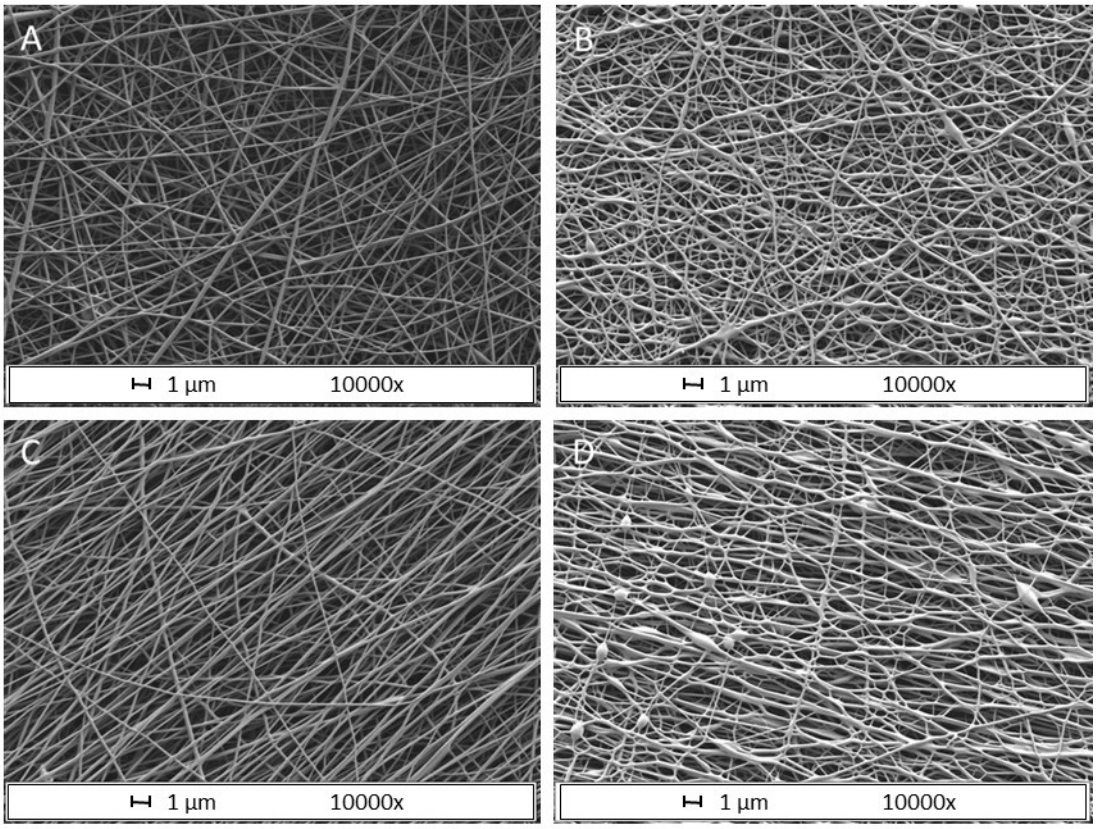

Figure 5.8 Scaffolds fabricated with A) 500 rpm, B) 1000 rpm, C) 2000 rpm, and D) 3000 rpm

Examining the scaffolds created, it was observed that values below 2000 rpm did not produce aligned electrospun mats and above 2000 rpm beads were produced, due to the vibration caused by the high revolutions of the mandrel. Therefore, 2000 rpm was considered at this stage as optimum, because the fibres created with this setting exhibited higher inter-fibre separation, did not present any defect and were aligned mimicking the natural ACL.

5.4.2. PVA STUDY 2: MECHANICAL CHARACTERIZATION

After the initial study (PVA Study 1) to obtain the optimum solution and process parameters that provided a stable Taylor cone and optimum fibre morphology, a second study (PVA Study 2) was performed to evaluate the

mechanical properties of 6 different scaffolds. This second study was performed to corroborate whether the scaffolds created with the optimum solution and process parameters obtained in PVA Study 1 exhibited a maximum tensile strength comparable to the value observed in the natural ligament (38 MPa [59]). From the initial morphological study, it was determined that the optimum process and solution parameters were (Table 5.7):

Table 5.7 Optimum process and solution parameters.

Concentration	Voltage	Flow rate	Distance between collector and needle	Revolutions of the mandrel	Needle	Time
12%	20 kV	1 ml/h	80 mm	2000 rpm	18G	2 h

In this study, the influence of the mandrel revolution and the size of the needle against the maximum longitudinal and transverse tensile strength were analysed. For this study, 5 thicker scaffolds were produced to enable securing them in the grips without rupture due to stress concentrations; therefore 2 hours of electrospinning was necessary to create thick enough scaffolds.

5.4.2.1. Revolution of the mandrel

5.4.2.1.1. Maximum tensile strength parallel to the direction of the fibres

As was predicted the scaffold that provided higher tensile strength parallel to the direction of the fibres was generated with a mandrel speed of 2000 rpm, because the fibres in that scaffold were more aligned than with other revolutions and were free of beads that weaken the scaffold. The fact that more aligned fibres generated higher maximum tensile strength was also observed by Bosworth *et al.* [263], where scaffolds with randomly distributed and aligned fibres were created with a mandrel

speed of 50 rpm and 600 rpm respectively. The results obtained for maximum tensile strength for 1000, 2000 and 3000 rpm are shown in Figure 5.9.

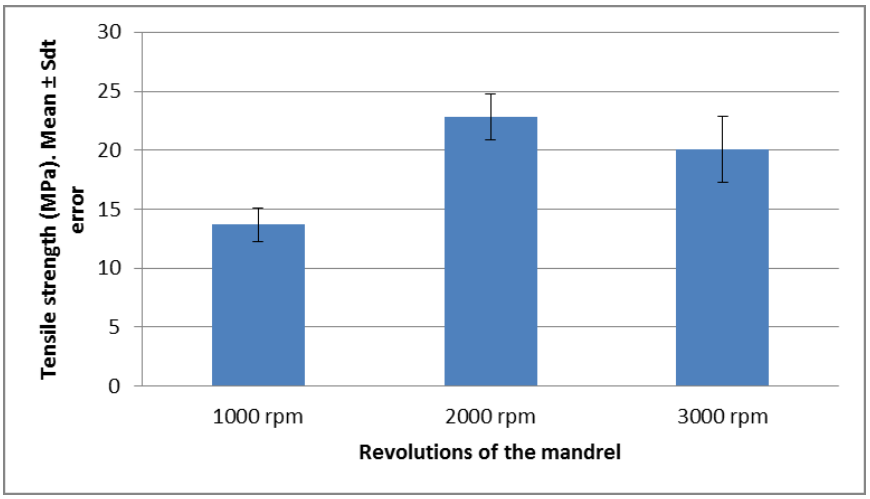

Figure 5.9 Maximum tensile strength in the parallel direction of the fibres versus revolution of the mandrel

For 2000 rpm a maximum tensile strength of 22.823 ± 1.978 MPa was obtained. Studies developed in Chapter 3 showed that the maximum tensile strength observed for jumping at maximum effort was 24.8 MPa and in walking was 17.57 MPa [237]. The maximum tensile strength exhibited after tensile testing human ACL was 38 MPa [59]. Therefore, these results were comparable to the mechanical properties needed for an implant for ACL replacement. In order to increase the tensile strength and reduce the degradation rate, experiments with crosslinked samples were performed and they are shown in section 5.3.3.

Moreover, the morphology of the fibres after being tensile tested and the morphology of a damaged ACL appeared similar as observed in Figure 5.10.

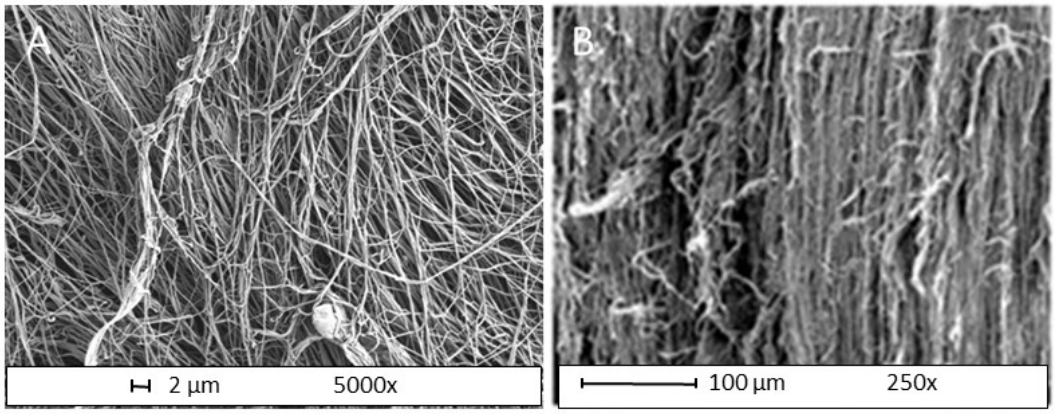

Figure 5.10 A) Morphology of the scaffold after being tested B) Damaged ACL **[48]**

The previous figure (Figure 5.10 A) shows that the fibres maintained their alignment and crimp pattern after being tensile tested, this alignment and pattern also existed in damaged ligaments as can be observed in Figure 5.10 B.

After this analysis it was verified that 2000 rpm was the optimum revolution to provide a tensile strength and morphology comparable to the natural ACL.

5.4.2.1.2. Maximum tensile strength perpendicular to the direction of the fibres

The maximum tensile strength in the perpendicular direction of the fibres was also analysed to detect which structure better resisted under a transverse load. This is important to bear shear forces, as it was proved in Chapter 3 that failure mechanisms are due to multidirectional loading, how the scaffolds mechanically behave under tensile, shear and torsion loading therefore has to be analysed [236], [237]. Figure 5.11 shows the values of the maximum tensile strength against the mandrel revolutions.

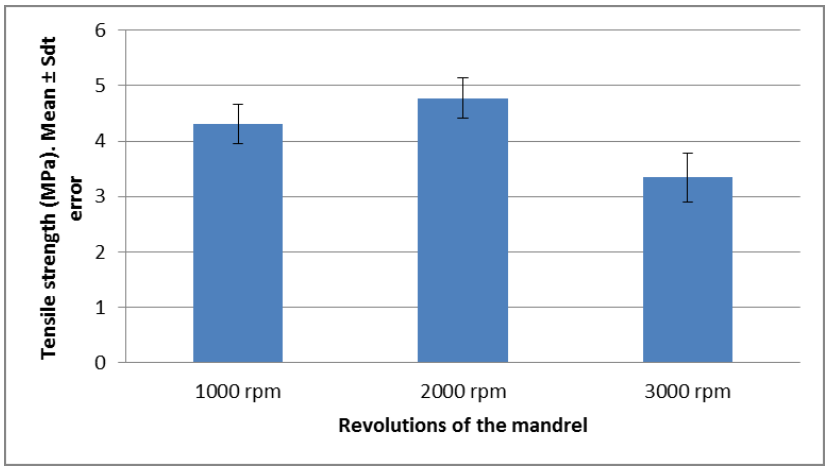

Figure 5.11 Maximum tensile strength in the perpendicular direction of the fibres versus revolution of the mandrel

As was expected the maximum tensile strength in the perpendicular direction of the fibres was considerable lower than in the parallel direction. However, this study showed that the highest maximum tensile strength in the perpendicular direction of the fibres was obtained with 2000 rpm of the mandrel. How the scaffolds created with this configuration behaved under shear loading was evaluated in Chapter 6. Future work should be focussed on the study of testing the natural ACL under shear loading and compared to the results observed in this thesis.

The following figure (Figure 5.12) shows the morphology of the fibres after being tensile tested perpendicular to the direction of the fibres.

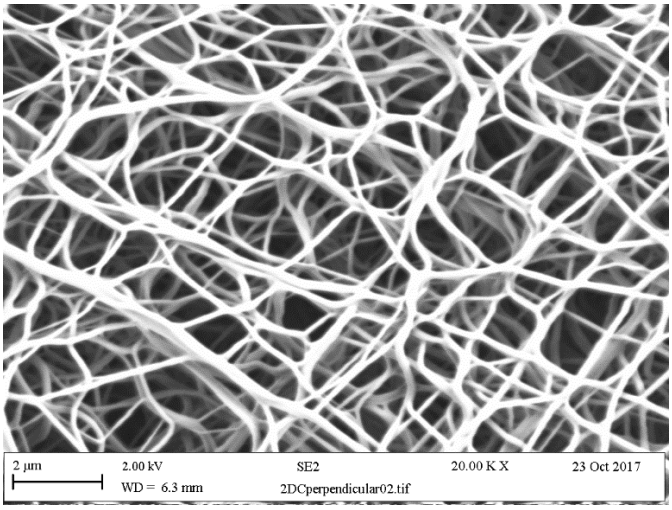

Figure 5.12 Morphology of the scaffold after being tested perpendicular to the direction of the fibres.

In this case, the porosity of the scaffold increased as the fibres were separated.

5.4.2.2. Size of the needle

The same study as in section 5.4.1.5 was performed with two different needle sizes: 18G and 21G due to both providing aligned fibres free of defects and no significant relationship between fibre morphology and needle size being observed in section 5.4.1.5.

5.4.2.2.1. Maximum tensile strength parallel to the direction of the fibres

After tensile testing the scaffolds in the parallel fibre direction, it was determined that 18G was the size of the needle that provided the highest maximum tensile strength, as shown in Figure 5.13.

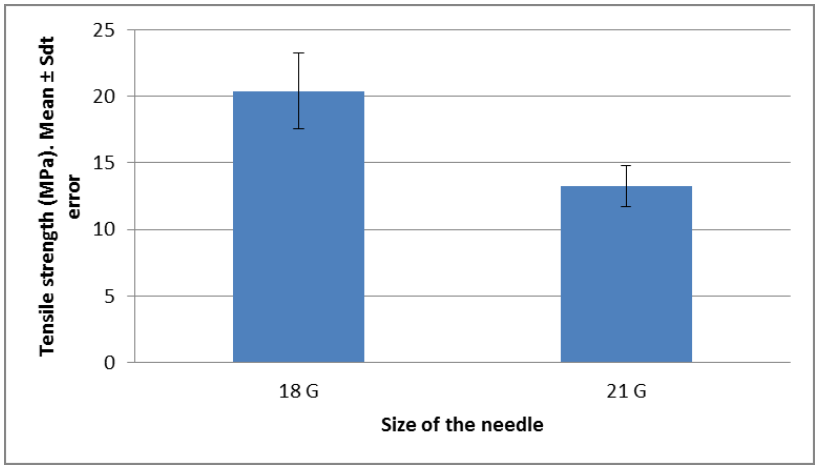

Figure 5.13 Maximum tensile strength parallel to the direction of the fibres versus size of the needle

Figure 5.14 shows the morphology of the scaffolds produced with 18G and 21G needles. It was observed that the scaffolds manufactured with 18G needle size had more uniform fibres and were free of beads; however, the scaffolds created with 21G needle showed some beads and heterogeneous fibres reducing the tensile strength compared to the scaffolds fabricated with the 18G needle.

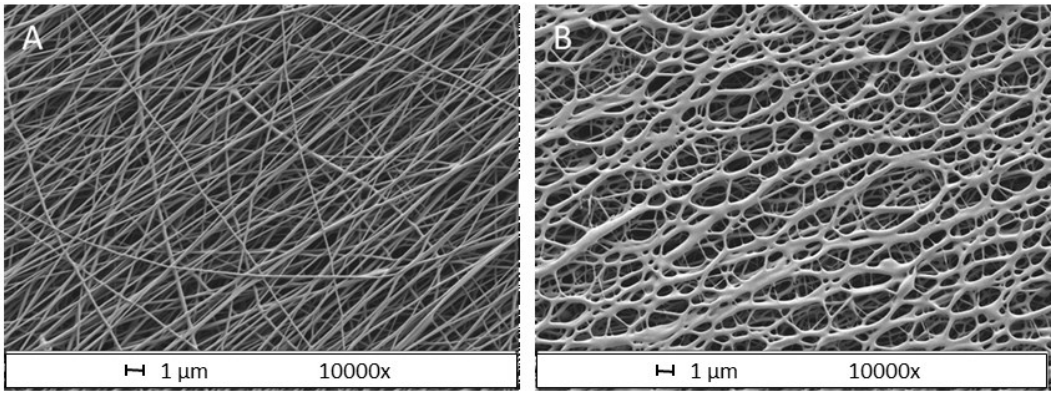

Figure 5.14 Scaffolds manufactured with needle size A) 18G and B) 21G

5.4.2.2.2. Maximum tensile strength perpendicular to the direction of the fibres

The maximum tensile strength in the perpendicular direction to the fibres was higher for the scaffold manufactured with 18G needles compared to 21G needles, as observed in Figure 5.15.

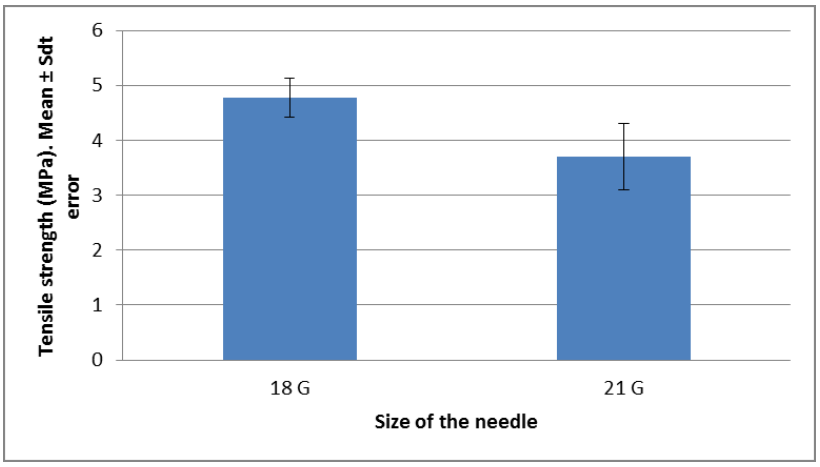

Figure 5.15 Maximum tensile strength perpendicular to the direction of the fibres versus size of the needle

Therefore, it was confirmed that the optimum parameters to provide improved morphology and mechanical properties were as shown in Table 5.7: 12% PVA concentration, 20 kV, 1ml/h flow rate, 80 mm distance between needle and collector, 2000 rpm and diameter of the needle of 18G.

5.4.2.3. Crosslinked samples of the scaffold manufactured with the optimum solution and process parameters

As previously explained (section 5.3.3), PVA is a soluble polymer, therefore to slow down its degradation process it was necessary to crosslink the scaffolds and characterize the new crosslinked samples. In this section, the scaffold that showed the highest maximum tensile strength and that was produced with the optimum solution and process parameters was crosslinked. The maximum tensile strength (longitudinal and transverse to the direction of the fibres) was calculated for this crosslinked scaffold, which remained stable and undegraded along the timeframe of the mechanical, morphological and topographical characterization. The comparison between non-crosslinked samples and crosslinked samples is shown in Figure 5.16.

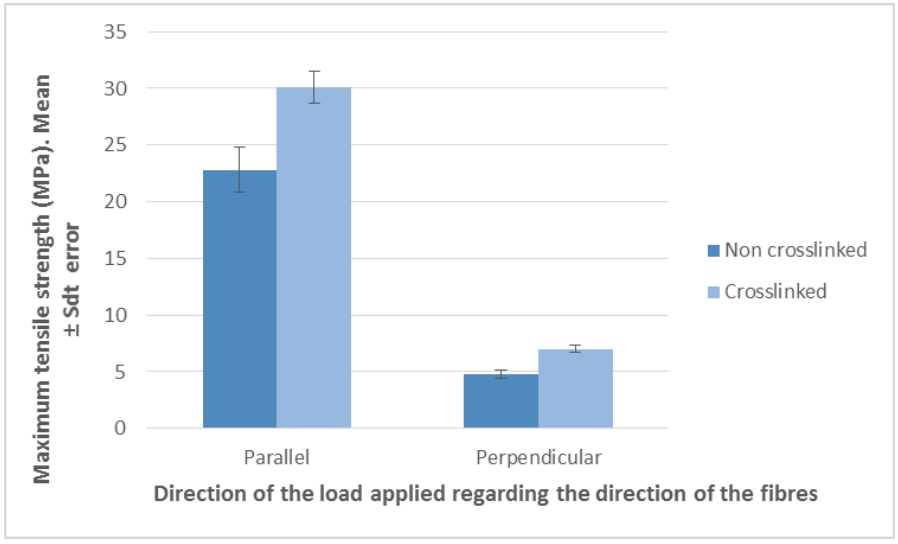

Figure 5.16 Maximum tensile strength parallel and perpendicular to the direction of the fibres for non-crosslinked and crosslinked samples produced with the optimum set up.

From the results obtained, it was observed that the crosslinked samples increased their maximum tensile strength from 22 ± 1 MPa to 30 ± 1 MPa when the load was applied parallel to the direction of the fibres and reached 7 MPa for the crosslinked samples in the perpendicular direction of the fibres. Therefore, the maximum tensile strength for crosslinked samples was approximatly the maximum tensile strength of the native ACL (38 MPa [59]) and superior to the maximum tensile strength observed during jumping at maximum effort where it was recorded as 24.8 MPa [237]. Further studies modifying the geometry of the scaffolds to create 3D scaffolds were mechanically characterised in Chapter 6 to verify if 3D PVA scaffolds could reach the appropriate tensile strength and could be considered for use as ACL implants.

5.4.3. PVA STUDY 3: DEGRADATION STUDY

Two different techniques were considered to crosslink the samples: immersion in methanol and in GTA and vapour deposition in GTA. After performing the crosslinking, only the samples crosslinked by vapour deposition could be used for further studies; the samples treated by immersion dissolved after a few minutes of use of this technique.

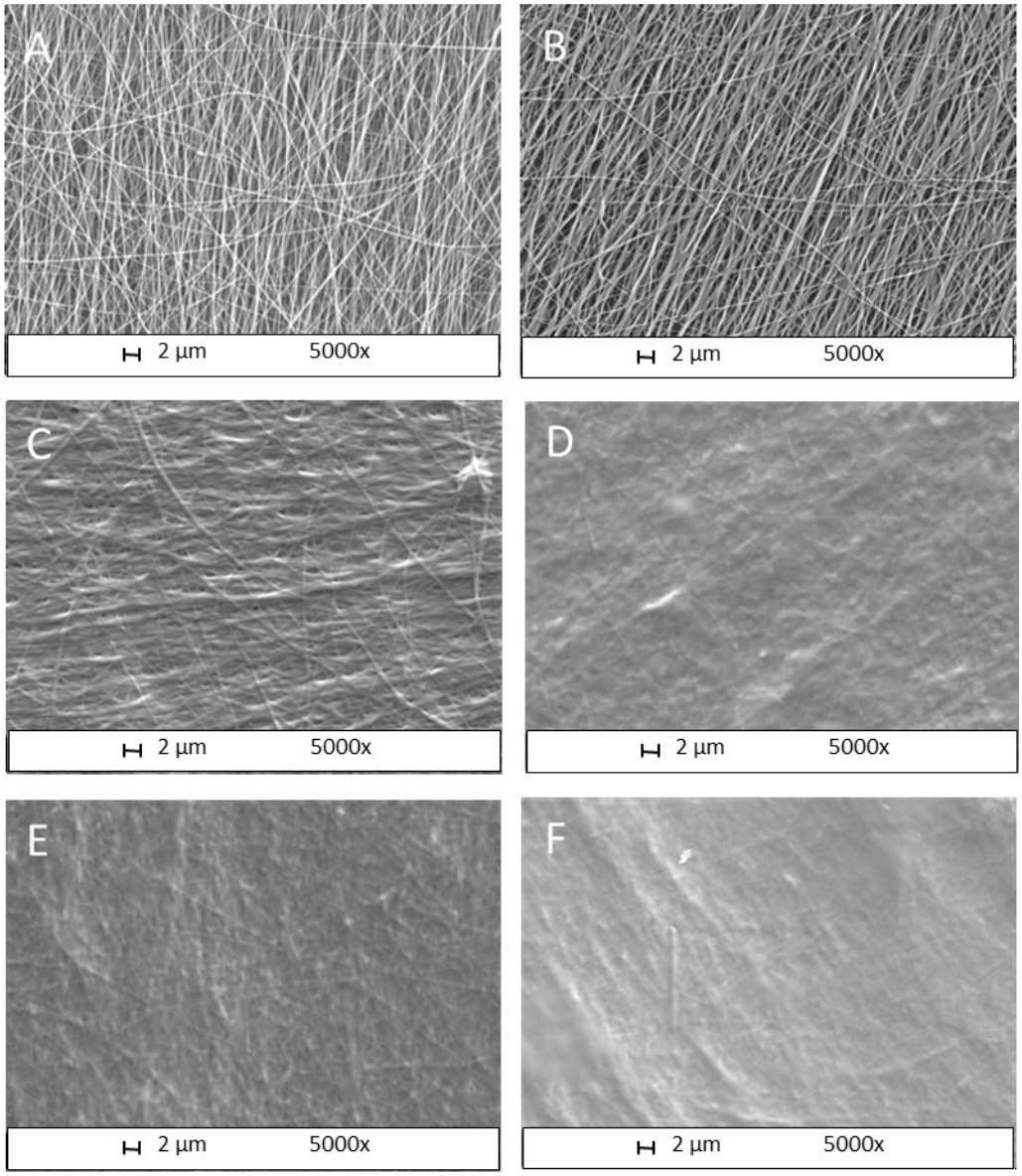

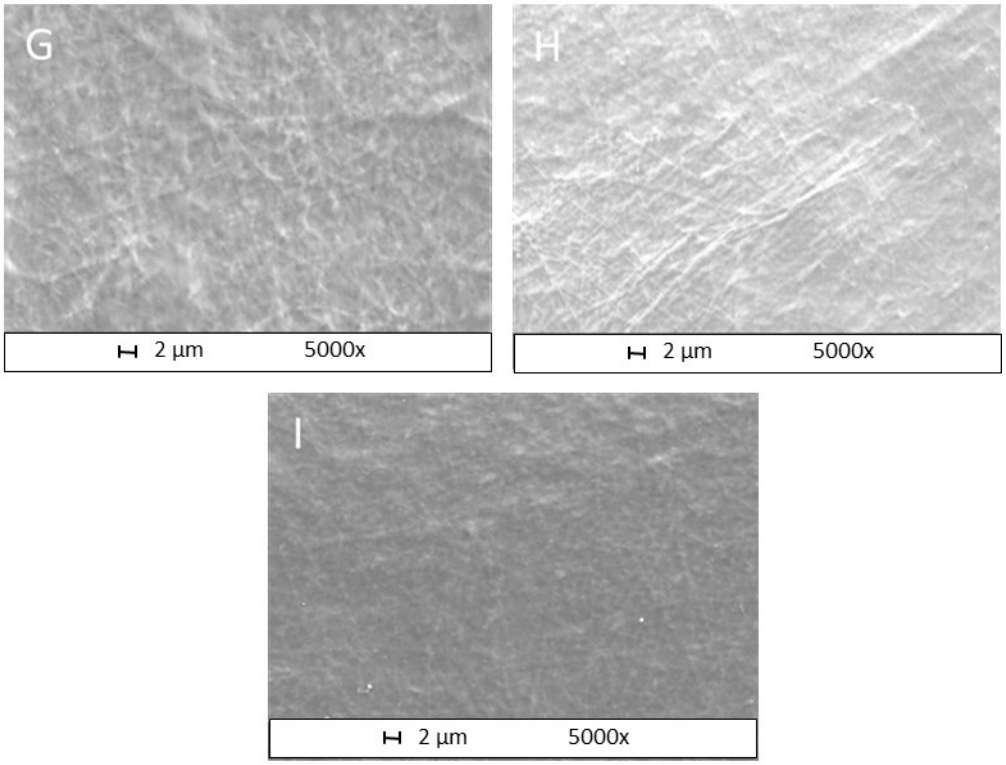

Figure 5.17 Degradation of PVA samples examined under SEM A) non-crosslinked B) crosslinked C) crosslinked and rinsed D) 1 day E) 5 days F) 7 days G) 14 days H) 21 days I) 28 days of incubation in PBS.

Figure 5.17 shows PVA samples under the following conditions: non-crosslinked; dried after crosslinking; rinsed and dried after crosslinking; and dried after 1, 5, 7, 14, 21 and 28 days in incubation in PBS at 37°C and 4% CO_2. Once the samples were soaked in PBS, the fibres of the scaffolds were difficult to visualize and to measure using an SEM. This is due to PVA behaving as a hydrogel when it was immersed in an aqueous liquid, and its fibres swelln. However, it was visually shown that the fibres remained, imitating the extracellular matrix, and that the crosslinked PVA electrospun scaffolds did not degrade after 28 days of incubation immersed in PBS (Figures 5.17 and 5.18); therefore they can be used in future cell culture experiments to investigate their attachment, proliferation or cell orientation, as was performed by other research groups [327], [341], [342].

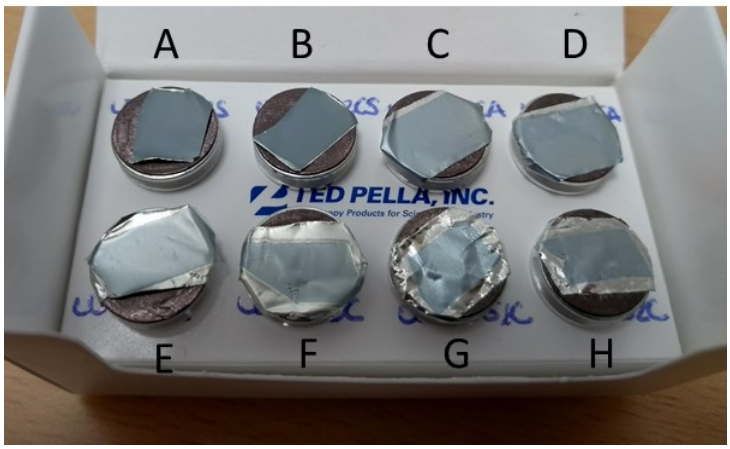

Figure 5.18 Degradation of PVA samples A) crosslinked B) crosslinked and rinsed C) 1 day D) 5 days E) 7 days F) 14 days G) 21 days H) 28 days of incubation in PBS.

Despite the difficulties in measuring the fibres, 20 measurements (per sample) of fibre diameter were performed after 1 and 28 days of being immersed in PBS, resulting fibre diameters of 461 ± 4 nm and 453 ± 3 nm respectively. Although these values showed a swelling of the nanofibres, the cell behaviour would not be compromised, since previous studies with PVA electrospun scaffolds reported excellent cell adhesion and proliferation with values of fibre diameter between 379 ± 37 nm and 524 ± 31 nm [324].

Moreover, it was demonstrated that crosslinked PVA hydrogels exhibited excellent biocompatibility [65], [217]–[219], [309], [318], [320], [323], [326], [327], [329], [330] and a water-swollen network similar to the extracellular matrix of the native ligament [65].

The average roughness of the scaffolds was analysed, in order to check if the crosslinking process and the incubation in PBS changed the topography of the

samples. Andrews *et al.* [189] reported that cellular behaviour is influenced by the scaffold topography. Moreover, values of roughness between 0.3 µm and 1.2 µm exhibited high percentage of cell coverage and cell spreading after 28 days of being seeded. These results induces to think that the scaffolds produced with roughness about 0.6 µm in this Chapter 5, would achieve comparable results of cell behaviour as the results reported. Figure 5.19 shows the roughness results of the present study.

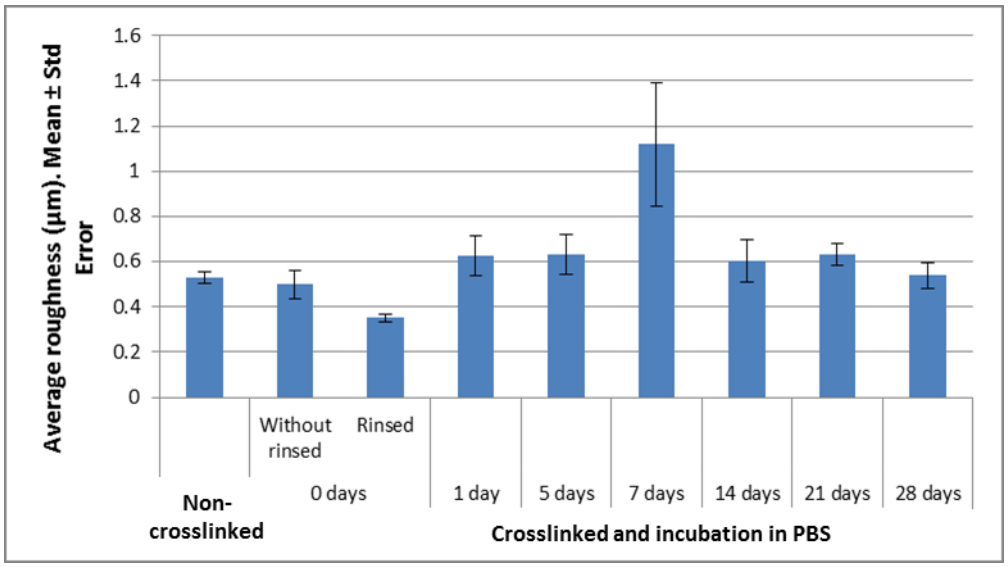

Figure 5.19 Roughness of the sample after being crosslinked and immersed in PBS

After statistical analysis, the correlation between average roughness of the scaffold and days in PBS was a null negative correlation (-0.054). The ANOVA and regression model were not significant. Therefore, the roughness did not change either with the crosslinking or with the incubation in PBS, proving that those treatments did not affect the topography of the scaffolds.

5.5. CONCLUSIONS

This study analysed the suitability of PVA electrospun scaffolds to be used as ACL implants. The first step of this study was focussed on finding the optimum process and solution parameters with which to manufacture scaffolds with morphology and mechanical strength similar to the native ligament. Once the optimum parameters were determined, scaffolds with those parameters were manufactured and their mechanical properties and degradation studied.

The maximum tensile strength was calculated for non-crosslinked and crosslinked samples, recording values of 22 ± 1 MPa for the non-crosslinked samples and 30 ± 1 MPa for crosslinked samples, when the load was applied parallel to the direction of the fibres. The crosslinked samples exhibited values of maximum tensile strength similar to the native ACL (38 MPa [59]) and higher than the maximum tensile strength observed during jumping at maximum effort (24.8 MPa [237]) reported in Chapter 3; therefore these samples showed potential for use as ACL replacements, when considering just the maximum tensile strength.

The scaffolds exposed to 25% glutaraldehyde remained undegraded and with an intact topography after 28 days of incubation in phosphate-buffered saline (PBS). Further studies should be performed in order to understand its degradation rate and "lifespan" in PBS. However, it can be concluded from the results that PVA electrospun scaffolds can be used to grow cells on them and therefore manufacture tissue-engineered implants in future work.

This study demonstrated that PVA scaffolds have a great potential to be used to manufacture ACL implants, since they exhibited excellent mechanical, morphological and topographical properties. Chapter 6 investigates the possibility of manufacturing 3D electrospun PVA scaffolds to enable full functionality for ACL implantable medical devices.

Key points:

1. This study evaluated for the first time the suitability of PVA electrospun scaffolds to produce biomimetic ACL implants.
2. Before the development of Chapters 4 and 5, no studies for any polymer had focussed on an iterative optimisation of solution and process parameters, with the goal of achieving mechanical and morphological properties that mimic the desired biological tissue.
3. The optimised PVA crosslinked scaffolds reached a maximum tensile strength of 30 MPa, comparable to the native ACL.
4. The topography of the scaffolds produced remained unaltered after being exposed to 25% GTA and 28 days of incubation in PBS.
5. The scaffolds showed values of fibre diameter between 120 and 140 nm, comparable to the values of the collagen fibrils in the extracellular matrix.
6. It was demonstrated that 2D PVA electrospun scaffolds exhibited excellent mechanical, morphological and topographical properties for use in the manufacture of ACL implants, and they formed the baseline to produce 3D structures.

6. Evaluation of 2D and 3D PVA electrospun structures

The significant potential of PVA electropun scaffolds for use as ACL implants was demonstrated in Chapter 5. In Chapter 6, the mechanical and morphological properties of different 2D and 3D PVA electrospun structures is tested to evaluate their suitability for use as ACL grafts.

6.1. ABSTRACT

The ACL has the highest rate of injury in the knee. Currently, autografts are used in 90% of the surgeries to replace the damaged ACL and recover the stability of the joint. However, these grafts present donor-site morbidity and long postoperative rehabilitation. In order to reduce these disadvantages, tissue engineered electrospun grafts were proposed in this study.

A range of 2D and 3D PVA electrospun scaffolds was studied to evaluate their suitability for use as ACL grafts. To this end, 2D electrospun scaffolds, one twisted filament scaffolds, 3 twisted filaments scaffolds and 3 twisted/braided filaments scaffolds were characterized morphologically and mechanically. It was assumed that similar fibre networks to the extra-cellular matrix would promote tissue ingrowth; and morphological structure and mechanical behaviour comparable to the natural ACL would provide the mechanical properties required. The final aim of this

chapter was to determine which electrospun structure would provide the closest morphology and mechanical properties to the natural ligament, in dry and wet environments and under tensile and shear loading.

6.2. INTRODUCTION

The ACL rupture is the most common injury in the knee joint. Due to its low vascularization, this ligament has very poor healing mechanisms, making the use of ACL grafts necessary for its reconstruction or replacement [343].

Nowadays, the gold standards for ACL replacement are the patella-tendon, hamstring-tendon and quadriceps-tendon autografts [343]. However, the autografts exhibit various disadvantages, such as donor site morbidity, long rehabilitation time or lack of availability, potentially solved through the implantation of tissue engineered grafts [344].

An ideal tissue engineered ligament should be biocompatible (able to perform with an appropriate host response in a specific application), promote tissue ingrowth with an appropriate porosity, degrade at the same rate as the host tissue is growing and exhibit mechanical behaviour similar to the natural ligament [343], [345], with toe, linear and failure regions. The maximum tensile stress should be approximately 38 MPa [59], the Young's modulus approximately 111 MPa [59] and the shear modulus approximately 68 MPa [346]. The structure of the implant ideally

should be similar to the hierarchical structure of the ligament, hence mimicking the extracellular matrix and so promoting cell proliferation, and imitating the mechanical response. Therefore, the fibres should be between 40 and 150 nm in diameter mimicking the collagen fibrils in the ACL, the bundle of fibres approx. 1 to 20 μm, and the filaments between 360 and 1500 μm in diameter simulating the fascicles of the natural ACL.

Polymers such as collagen [347], silk fibroin [344], poly L-lactic acid [345], [347], poly-caprolactone [263], polyvinyl alcohol or polyethylene [65] have been used to manufacture tissue engineered scaffolds for tendon and ligament replacement.

As shown in Chapter 5, PVA is an inexpensive polymer with excellent physical, chemical and mechanical properties. Currently PVA nanofibrous electrospun scaffolds are used in tissue engineering applications due to PVA being a highly hydrophilic, biodegradable, nontoxic and biocompatible polymer [65], [218], [219] and as the scaffolds present a network of nanofibres that mimics the extracellular matrix, characteristic of electrospun scaffolds. Due to its water solubility and nontoxicity, PVA is easily manageable since it is not necessary to use any mechanism of extraction of toxic vapours. Moreover, optimising the solution and process parameters, tuneable and free from beads nanofibres can be produced with this polymer. All of these advantages enable PVA to be used as a baseline polymer for other experiments.

However, independent of the material used and focussing on the manufacturing process, there is a lack of studies to assess 3D tissue engineered

ligaments, especially those produced by the electrospinning technique. Currently there are different techniques to create tissue engineered ligaments: twisting, braiding, weaving, knitting and combinations of the above-mentioned [345]. It is known that by modifying the geometrical pattern of the structure its mechanical properties can be changed [345], [348]. Braided structures are designed to transfer large loads, bearing axial and shear loads and provide torsion stability [345], [349]. Twisted fibres are used to improve the abrasion resistance and flexibility [345], [348]. Microfibres of the polymers previously mentioned were purchased and then twisted [344], [345], [350], [351], braided [345], [352], [353] and a combination of both [345] forming bundles of fibres simulating the ligamentous or tendinous structures.

The electrospinning technique allows the creation of a network of nanofibres similar to the extracellular matrix of soft tissue. To the author's knowledge, just two studies with one filament twisted electrospun scaffolds have been performed to date to produce tendon implants [263], [347] and no studies of this specific structure were performed for the ACL. Bosworth *et al.,* investigated the mechanical behaviour between 2D PCL electrospun scaffolds with randomly and aligned distributed fibres and 3D PCL twisted electrospun scaffolds [263]. The conclusions of that study were that 3D electrospun bundles exhibited ten times more ultimate tensile stress than 2D electrospun scaffolds with randomly distributed fibres, and 2D electrospun scaffolds with aligned fibres showed three times more ultimate tensile stress than the same scaffold but with randomly distributed fibres. However, the *in-vitro* results obtained were far from the mechanical properties of the native ACL (maximum tensile stress 38 MPa and Young's modulus 111 MPa [59]),

reporting a Young's modulus of 14.11 MPa and an ultimate tensile stress of 4.74 MPa [263]. Sensini A *et al.,* mechanically evaluated one filament twisted electrospun scaffolds manufactured with PLLA/Coll-75/25, PLLA/Coll-50/50 and pure PLLA in dry and wet conditions, concluding that dry PLLA/Coll-75/25 samples exhibited the highest ultimate tensile stress of 15 MPa [347], inferior to the natural ACL that exhibits an ultimate tensile stress of 38 MPa. Mounthy *et al.,* developed a 3D electrospun structure by manually twisting four filaments of polydioxanone (PDO) together, obtaining ultimate tensile stress between 45 and 48 MPa [354], superior to the natural ACL (38 MPa); however Young's modulus between 60 and 80 MPa, inferior to the 111 MPa exhibited by the natural ACL, corresponding to laxity problems of the structure. Rothrauff *et al.,* studied the mechanical properties of PCL and PLLA braided and stacked electrospun scaffolds [355]. In that study, the highest ultimate tensile stress was 20 MPa, found in PCL braided electrospun scaffolds, but this was inferior to the natural ACL.

Therefore, only four comparative studies have been performed to date. Moreover, none of them studied the morphology of the scaffold compared with the morphology of the extracellular matrix of the ACL. They also did not investigate any comparison between 2D electrospun structures and multiple 3D electrospun structures under cyclic tensile and shear loading and in wet and dry environments. Therefore, a study of potential 2D and 3D electrospun structures must be performed in order to determine the most appropriate structure in terms of morphology and mechanical properties that could mimic the natural ACL.

Many studies have been performed to determine the function of the ACL. An important number of those studies analysed the shear force experienced by the ligament during anterior tibial translation, since the ACL restrains the anterior translation of the tibia and the posterior translation of the femur [85], [101], [124], [356]–[362]. These studies have established predictive models to estimate the anterior tibial shear force in relation to knee angles or muscle forces. These models were based on *in vivo* motion capture technique in combination with computational models and statistical analysis. Due to the relevance of these studies and the results of the biomechanical study (Chapter 3) [236], [237], where it was demonstrated that the ACL is subjected to multidirectional loading, it was considered important to study the behaviour of different structures under shear loading to determine which structure could bear a comparable shear loading to the native ACL. This study brings a novel point of view in the mechanical testing of ligament implants, since the majority of the tests are developed under tensile load and the shear load is not considered in the design of the ligament implants.

The aim of this final study was to determine the suitability of different PVA electrospun structures for use as ACL replacements. In order to achieve that goal, crosslinked and non-crosslinked 2D and 3D structures were mechanically analysed, in dry and wet conditions under cyclic tensile and shear forces, and their morphology was studied and compared to the natural ACL [363], [364].

6.3. MATERIALS AND METHODS

6.3.1. MATERIALS

As in Chapter 5, PVA purchased from Sigma Aldrich (UK) was diluted in distilled water (dH_2O) by heating and stirring until a homogenous solution was achieved. From Chapter 5 it was determined that the optimum concentration of PVA was 12% w/v, concentrations above this increased the viscosity of the solution making it difficult to electrospun, and below this bead formation and beaded fibres were observed, reducing the mechanical properties of the scaffold.

Crosslinked samples were manufactured using 25% gluteraldehyde acquired from Sigma Aldrich (UK).

6.3.2. MANUFACTURING PROCESS

Crosslinked and non-crosslinked 2D and 3D electrospun structures were created to study their morphology and mechanical behaviour in order to determine which structure would be more suitable for an ACL replacement.

6.3.2.1. Fabrication of the 2D electrospun scaffolds

All the scaffolds were manufactured following the optimum set up found for PVA, described in the last chapter (Chapter 5). The scaffolds created with this set-up showed diameter of the fibres of 143 ± 5 nm (close to the diameter of the collagen fibrils of 100-150 nm [33], [45]–[47], [124]) and a maximum tensile strength of 30 ± 1 MPa (close to the natural ligament 38 MPa [59]). An electrospinning device (Spraybase®, Ireland) was used to fabricate the electrospun meshes. A 20 ml syringe was loaded with 10 ml of polymer solution and it pumped with a flow rate of 1 ml/h through a 18 G needle. An electrostatic field was created applying high voltage of 20 kV between the tip of the needle and the collector. The fibres were projected from the tip of the needle over a sheet of aluminium foil attached to a 9.65 cm diameter rotating collector working at 2000 rpm, in order to obtain aligned fibres and a maximum tensile strength similar to the natural ACL. The distance between the needle and the collector was set up to 8 cm. The scaffolds were manufactured at room temperature and for 3 hours spin time. Non-crosslinked 2D structures were fabricated by cutting the electrospun mesh in a dog-bone shape in order to test them mechanically and compare the mechanical behaviour to the 3D electrospun structures. Crosslinked 2D samples were manufactured and studied in the same way but they were exposed to a crosslinker agent for 24 hours, this procedure will be explain in section 6.3.3.

6.3.2.2. Fabrication of the 3D electrospun structures

The 2D electrospun meshes were cut into rectangles of 2 x 15 cm, pealed carefully from the aluminium foil and manually twisted clockwise to form a packed filament. The four first images in Figure 6.1 show the process to manufacture the filaments. Each filament was then cut in half to optimise the sample size to be tested and three different types of scaffolds were created with those filaments: one filament scaffolds, 3 twisted filaments scaffolds and 3 twisted/braided filaments scaffolds.

a) One twisted filament scaffolds were created by manually twisting the 2D electrospun scaffolds as explained above. A sample of this structure is shown in Figure 6.1 A).

b) 3 twisted filaments scaffolds were fabricated by twisting together three of the one filament scaffolds. The three filaments were twisted together, in a clockwise manner, until a packed and stable structure was created. A structure was considered packed and stable when it could not be manually twisted anyfurther and kept the created shape. In order to create a homogeneous structure the three filaments were selected with similar diameter. An example of this kind of 3D structure is shown in image B) of Figure 6.1.

c) 3 twisted/braided filaments scaffolds were manufactured by manually braiding three twisted filaments with similar diameters. As with the other

two structures, the braid was manufactured in as tight form as possible (until the braid kept its shape) in order to create a packed and stable structure. This structure is shown in image C) of Figure 6.1.

Crosslinked 3D samples were manufactured and exposed to glutaraldehyde in order to avoid degradation of the polymer (this method is explained in section 6.3.3.). However, the fabrication procedure and the subsequent analyses are identical to the non-crosslinked scaffolds.

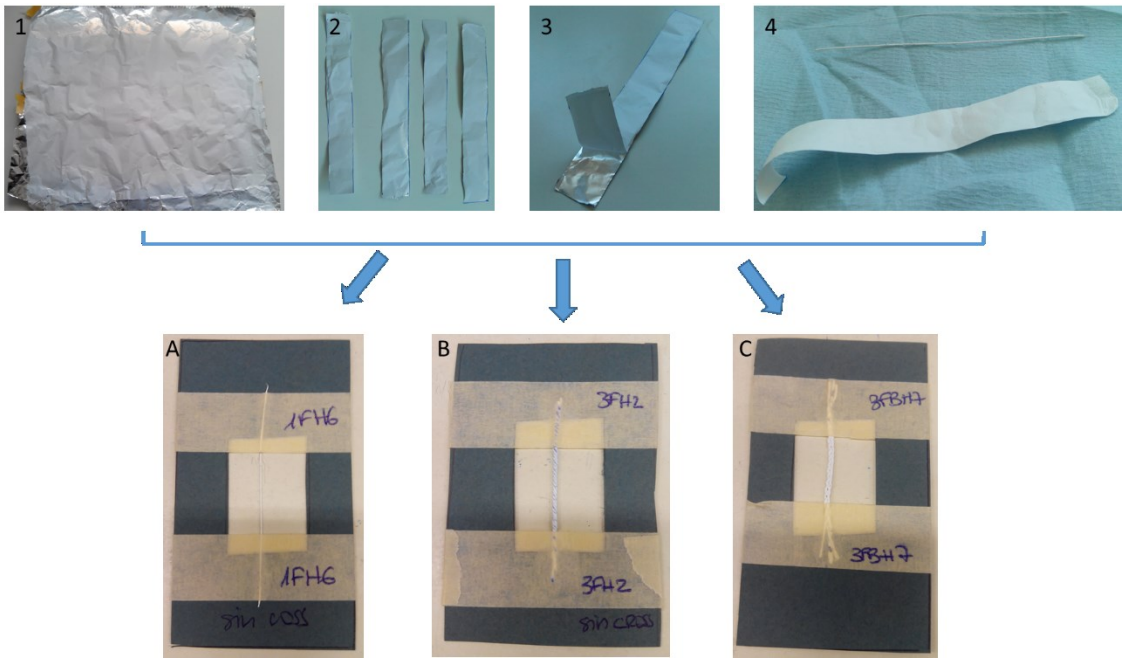

Figure 6.1 1) PVA electrospun scaffold. 2) 2 x 15 cm rectangular PVA meshes. 3) Peeled scaffold. 4) Twisted filament scaffold. A) 1 twisted filament scaffold. B) 3 twisted filaments scaffold. C) 3 twisted/braided filaments scaffold.

6.3.3. CROSSLINKING PROCESS

PVA is easily dissolved in water, and therefore in serum or culture medium. In order to avoid degradation of the PVA scaffolds a crosslinking process had to be performedcon the samples.

Two crosslinking techniques were evaluated in the last chapter (Chapter 5, section 5.3.3.). Following that evaluation, vapour deposition was found to be the most suitable technique for avoiding degradation and damage to the network of the electrospun scaffolds, demonstrating that the scaffolds remained stable and with similar topography for at least 28 days (Chapter 5, section 5.4.3.). In the same study, the concentration of crosslinker agent was analysed and 25% glutaraldehyde (GTA) was determined as the optimum percentage for completely crosslinking the polymer.

As described in Chapter 5 (section 5.3.3.), 25 ml of 25% GTA was poured into a Petri dish at the bottom of the desiccator, then the air-dried samples to be crosslinked were placed over a metallic mesh on top of the Petri dish and the desiccator sealed. The samples were exposed to glutaraldehyde vapour for 24 hours inside the desiccator. After the crosslinking process, the samples were dried under a fume hood for 24 hours in order to remove the moisture and reduce the toxicity of the samples.

6.3.4. MECHANICAL CHARACTERIZATION

Three different mechanical assays were performed to evaluate the mechanical behaviour of the 2D and 3D structures created: Cyclic tensile tests with dry samples, cyclic tensile test with wet samples and cyclic shear tests with dry samples. No cyclic shear tests were performed with wet samples due to the difficulty of obtaining comparable data for native ACL. Future work should compare the mechanical behaviour of these structures to the natural ACL under torsion and shear loading in dry and wet conditions.

The 2D samples were prepared by cutting the scaffold mesh with a dog-bone cutting die (25 x 4 mm, test length x width). The 3D samples were manufactured as described in a previous section (Chapter 6 section 6.2.2.2.). 92 samples were separately attached on cardboard frames to maintain the sample alignment in the tensometer (Instron H10KS, US). One image of each 3D structure over a cardboard frame is shown in Figure 6.1. The samples to be crosslinked were introduced with the cardboard frame into a sealed desiccator to be treated with GTA vapour as was explained in the last section (Chapter 6 section 6.3.3.). These samples were crosslinked with the cardboard frame to avoid any deformation of the scaffolds, as crosslinker agents tend to shrink the samples and makes handling difficult.

The thickness of each sample was measured three times with a digital calliper, an analogue calliper and through SEM images in order to compare the measurements and check if the results of the three methods are consistent. These

measurements were used to calculate the cross sectional area of each scaffold and with it be able to calculate the stress and normalize the mechanical results.

All samples were tested under cyclic loading. As the number of loading and unloading cycles increases, the stress / strain curves of each cycle are getting closer. Therefore, these tests enable checking the laxity of the sample and determining the number of loops needed to preload the sample until no significant differences between stress / strain curves are obtained. Although three different mechanical tests were performed to evaluate different conditions, the set up for the tensometer was identical for all experiments. Each sample was subjected to ten loading cycles and then tested to failure. The determination of the number of cycles was shown and explained in section 6.3.4.1. Each cycle stretched the sample up to 13% strain, since the maximum % strain in a gait cycle was found to be 13%, following previous studies performed by this and other research groups [75], [237]. All the tests were performed with a 100 N load cell and 5 mm/min test speed.

Mechanical properties including Young's modulus in the 1st and in the 21st curve (each load had a loading curve and an unloading curve. The 21st curve corresponded to the test to failure), tensile strength and strain at break were calculated for each sample and compared with crosslinked and non-crosslinked samples of the four different structures studied.

6.3.4.1. Cyclic tensile tests in dry conditions

In order to determine the optimum hysteresis test, a study of the number of cycles was performed. For this study 2D non-crosslinked samples were used. These

samples were subjected to load cycles of 3, 5, 10 and 20 cycles. One sample was used for each condition. The proximity of the curves and their gradient (Young's modulus) were evaluated.

Once the number of loops were defined (in this case 10 cycles up to 13% strain and then failure), a total of 64 samples (8 crosslinked samples and 8 non-crosslinked samples for each 2D and 3D structure, i.e. 4 structures in total), were tested to determine the Young's modulus in the 1st and in the 21st curve (corresponding to the 1st and 10th cycle), tensile strength and strain at break. The Young's modulus for these two curves was evaluated to understand the changes in the mechanical behaviour of the scaffolds when the number of cycles increased. The mechanical properties of the samples were compared to the properties of the natural ACL, since the purpose of these experiments was to evaluate the different structures to determine which exhibited mechanical properties similar to the natural ACL under dry conditions.

6.3.4.2. Cyclic tensile tests in wet conditions

It is well known that the material properties change if the scaffolds are tested in dry or in wet conditions, reducing the maximum tensile stress of the scaffold when it is tested in a wet environment [347]. The ACL is surrounded by the synovial membrane of the knee joint, which makes the ligament extrasynovial although in an intraarticular position [34]. Even though the ACL is not immersed in synovial liquid since the synovial membrane envelopes it, it is placed in a wet environment. Therefore, the designed implants should be able to withstand adequate load in wet conditions in order to function as the natural ligament.

For this second experiment (cyclic tensile tests in wet conditions) a study of the mechanical behaviour of the scaffold immersed in PBS (phosphate-buffered saline) for different periods of time was previously performed. This initial study helped to determine which period of time was optimum to perform the rest of the experiments. For this previous experiment, 1 twisted filament scaffolds were immersed in PBS for periods of 1 minute, 5 minutes, 15 minutes and 1 hour and the Young's modulus in the 1st and in the 21st curve, tensile strength and strain at break were calculated to determine the optimum time period.

After the initial experiment a total of 12 samples, 3 samples of each of the crosslinked 2D and 3D structures, were analysed after being immersed for 1 minute in PBS. The purpose of these experiments was to evaluate which structure was the most appropriate under wet conditions, in order to produce the most similar characteristics to the natural ACL. Two examples of the different wet structures can be observed in Figure 6.2.

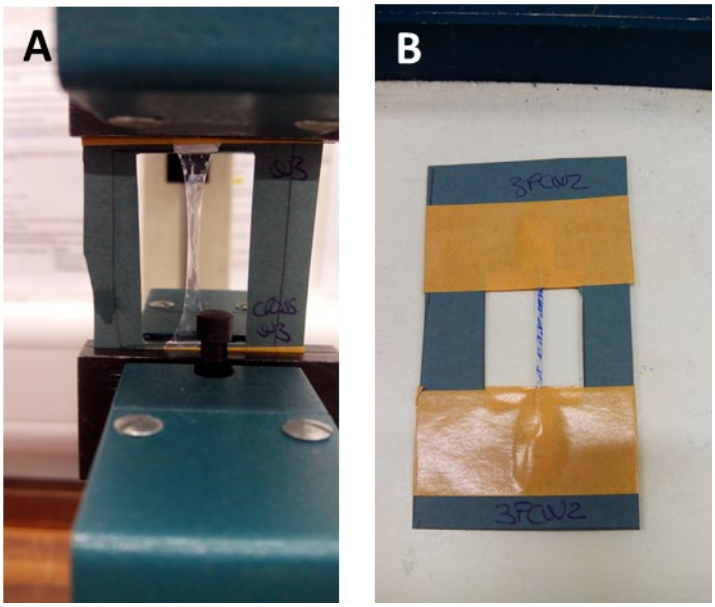

Figure 6.2 A) PVA 2D crosslinked wet electrospun scaffold. B) 3 twisted filaments crosslinked wet scaffold.

It should be noted that all experiments in wet conditions were performed under the same set up used in the experiments in dry conditions. However, due to the elastic character of the PVA in wet conditions a preload of 0.1N was added to fully align the sample in the tensometer.

As for the experiments in dry conditions the Young's modulus in the 1st and in the 21st curve, tensile strength and strain at break were calculated for each sample.

6.3.4.3. Cyclic shear tests

Different papers have been reviewed in order to obtain the angle of inclination of the ACL in the sagittal plane [365]–[367]. Following this review, it was determined that the angle of the ACL in the sagittal plane was approximately 50° (the angles varies between 51.6° ± 3.3° and 46.9° ± 4.9°). Images A and B of

Figure 6.3 show two MRIs of the knee with the sagittal angle and the direction of the shear force. The shear force was mimicked with a tensometer (Instron H10KS), placing the samples in a cardboard frame to facilitate the alignment of the sample, and with the sagittal angle of the native ACL, as shown in images D and E of Figure 6.3.

As in the last section (6.3.4.2), all experiments to calculate the maximum shear stress were performed under the same set-up as previously, with a tensometer (Instron H10KS, US), 10 cycles of load to 13% strain and then to failure, 100 N load cell and 5 mm/min test speed. The difference in this case lies in the orientation of the sample, as the goal is to measure the shear force instead of the tensile force. To develop this experiment a total of 12 samples, 3 samples of each crosslinked 2D and 3D structures were tested. The purpose of these experiments was to evaluate which structure was most appropriate under shear loading, i.e. demostranting the most similar characteristics to the natural ACL.

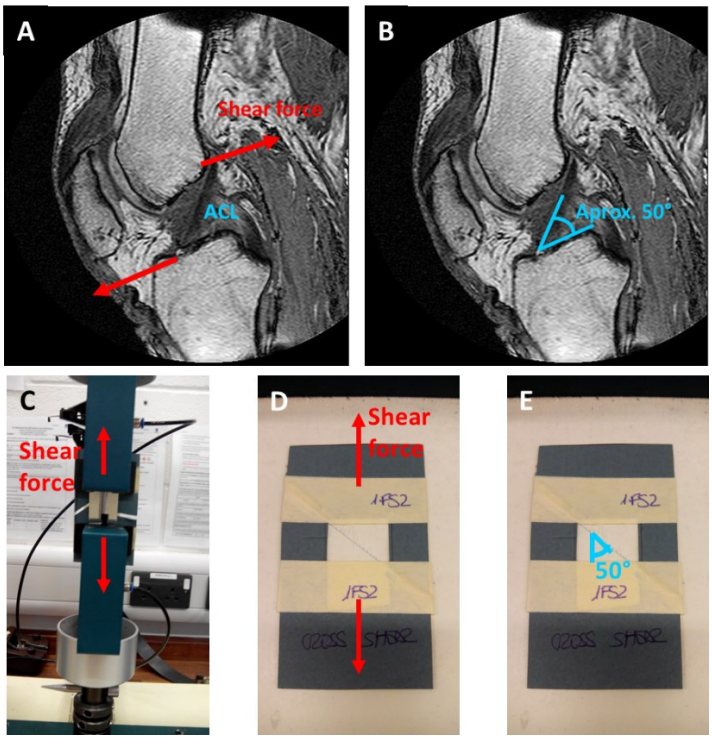

Figure 6.3 A) MRI of the right knee showing the shear force. Modified from **[368]**. B) ACL angle in the sagittal plane. Modified from **[368]**. C) Applied force in a tensometer. D) Shear force experienced by 1 twisted crosslinked filament scaffold in a tensometer. E) Orientation

6.3.5. MORPHOLOGICAL CHARACTERIZATION

A SC7640 sputter coater (Quorum Technologies Ltd. Kent, UK) was used to coat the samples with gold prior to their visualization with a field emission scanning electron microscope, Zeiss Supra 40 (FE-SEM, Carl Zeiss SMT Ltd., Cambridge, UK). The intensity used for coating the samples was 20 mA, the voltage 0.8 kV and the duration of the coating was 120 seconds, which provided a coating thickness of 32.6 nm following equipment specifications. SEM images were taken between 5 and 6 mm working distance, at 2 kV and with magnifications of 100x, 1000x, 5000x and 20000x in order to measure the nanofibres, the bundle of fibres and fascicles. Two images for each magnification and scaffold were taken and two scaffolds for each 3D structure and each set of testing conditions were analysed. Fibre diameter and

thickness of the bundles of fibres and fascicles were determined with AxioVision SE64 Rel. 4.9.1 software (Carl Zeiss SMT Ltd., Cambridge, UK) by measuring 20 fibres/image in two 20000x magnification SEM images, 3 bundles of fibres/image in two 5000x magnification SEM images and the fascicles of each sample in two 100x magnification SEM images, for each 3D structure and each set of testing conditions. The created filaments were considered as fascicles, since their diameters were comparable. Figure 6.1 shows how the fibres, bundle of fibres and fascicles were measured.

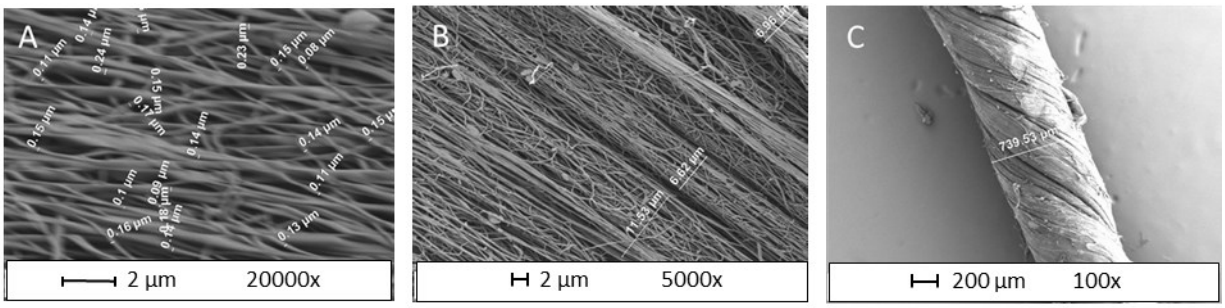

Figure 6.4 A) Diameter of the fibres. B) Dimension of groups of fibres. C) Diameter of the fascicle.

The dimensions of the fibres, bundles and fascicles of the scaffolds were compared with the dimensions of the fibrils, fibres and fascicles of collagen in the native ACL found in the literature.

6.3.6. DATA ANALYSIS

Mean and standard error of the mean (Std Error) were calculated for each of the structural and mechanical properties for all 2D and 3D crosslinked and non-crosslinked structures.

In order to compare these properties between the 2D and 3D scaffolds and testing conditions, one-way analysis of variance (ANOVA) with a 95% confidence was performed. Moreover, two one-way ANOVAs were performed to determine the optimum number of cycles for the cyclic mechanical tests, and to determine the time of the samples immersed in PBS for the wet condition tests.

All statistical analyses were conducted using SPSS (IBM Inc, US).

6.4. RESULTS AND DISCUSSION

This section 6.4 analyses the mechanical behaviour and the morphology of the 2D and 3D structures. Once the scaffolds were characterized, they were compared against data from the literature on the natural ligament and its collagen fibres, in order to determine the best solution for consideration as an ACL implant.

6.4.1. MECHANICAL CHARACTERIZATION

6.4.1.1. Cyclic tensile tests in dry conditions

In this experiment the mechanical properties of dry samples were evaluated. These hysteresis tensile tests were developed in order to determine the preload necessary in the implant prior to being placed into the knee. As the samples were loaded the loading curves were getting closer together and the stiffness of the polymer was more and more comparable. Therefore, an initial study evaluating the

number of cycles perfomed in the hysteresis test was required prior to the mechanical characterization of the different structures.

After this test, the Young's modulus in the 1st and 21st curve, the maximum tensile stress and the strain at break were calculated for each 2D and 3D structure.

6.4.1.1.1. Study of the number of cycles

For this test, the mechanical behaviour of 2D non-crosslinked scaffolds was studied under different numbers of load cycles: 3, 5, 10 and 20 cycles and then tested to failure. The choice of performing this initial test with 2D non-crosslinked scaffolds was to simplify the test in terms of time and resources used. Therefore, it was assumed that the results obtained with 2D non-crosslinked samples could be extrapolated to the 3D structures.

For the correct understanding of the rest of this section, it is noteworthy to clarify that each cycle consists of two curves, the loading curve and the unloading curve. Therefore, the hysteresis test of 3 loading cycles had 6 loading/unloading curves plus the last curve to break; hence, the 3 cycles test had 7 curves, the 5 cycles test had 15, the 10 cycles test had 21 curves and the 20 cycles hysteresis test 41 curves.

Figure 6.5 shows the "Force (N) / Extension (mm)" curves for 3, 5, 10 and 20 hysteresis cycles in four 2D non-crosslinked samples. From this figure it was easily observed that the loading curves were getting closer and closer together as the number of cycles was increased, and also that the Young's modulus values calculated

from the different loading curves were increasingly comparable; therefore it could be concluded that the samples behaved in a similar way after a certain number of cycle were reached.

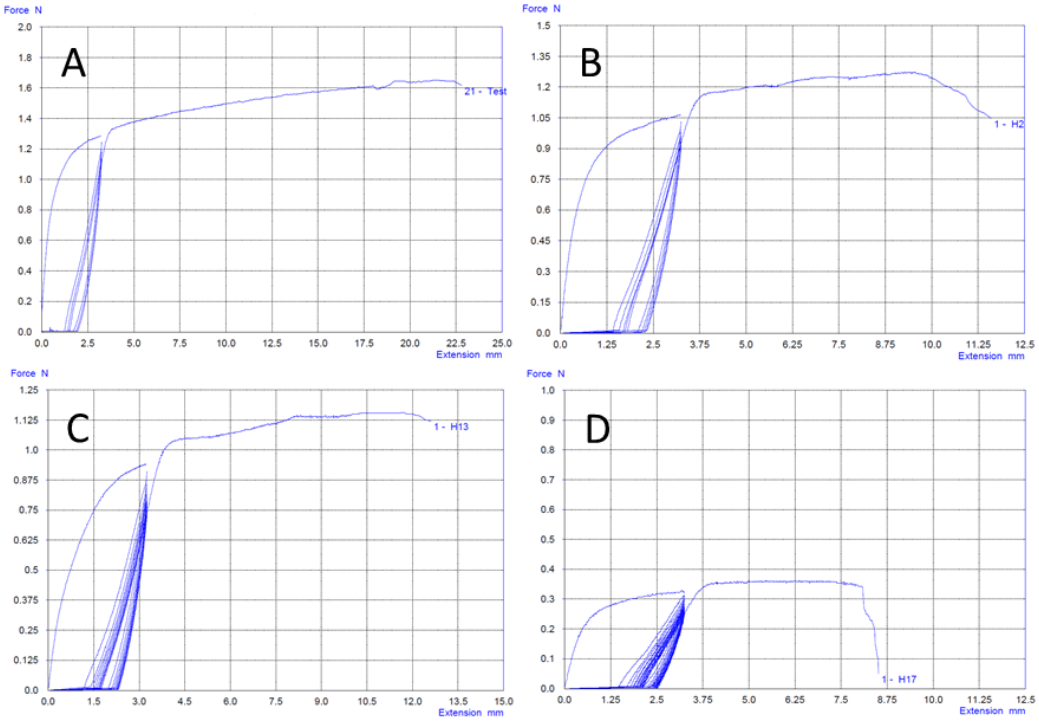

Figure 6.5 A) 3 hysteresis cycles. B) 5 hysteresis cycles. C) 10 hysteresis cycles. D) 20 hysteresis cycles

Table 6.1 shows Young's Modulus of the different curves calculated from a 2D non-crosslinked sample under 20 loading cycles.

Table 6.1 Young's modulus from different loading curves for a 2D non-crosslinked sample

	Young's Modulus (MPa)
Curve 5	321
Curve 7	314
Curve 9	321
Curve 11	321
Curve 19	341
Curve 21	341
Curve 37	341
Curve 39	341
Curve 41	341

From Figure 6.5 it was determined that the optimum number of cycles was 10, since the last loading curves of numbers 19 and 21 were not significantly different ($p > 0.05$). This fact can be also observed in Table 6.1 where the Young's modulus calculated from 11% to 12% strain was constant from curve 19 until 41. Therefore, the rest of the cyclic tests were performed with 10 loading cycles.

6.4.1.1.2. Mechanical properties of dry 2D and 3D scaffolds

In this section the maximum tensile stress in MPa, and the Young's Modulus in the 1st and 21st curves are calculated and compared, for each crosslinked and non-crosslinked structure.

a) Maximum tensile stress:

Table 6.2 shows the maximum tensile stress after 10 loading cycles of the 8 samples analysed for each crosslinked and non-crosslinked structure. The mean, standard deviation and standard error of the mean were also calculated and used to plot a graph where all structures were compared (Figure 6.6).

Table 6.2 Maximum tensile stress for 2D and 3D samples

	2D samples		1 twisted filament samples		3 twisted filaments samples		3 twisted/braided filaments samples	
	Non-crosslinked	Crosslinked	Non-crosslinked	Crosslinked	Non-crosslinked	Crosslinked	Non-crosslinked	Crosslinked
	41	20	57	39	18	19	32	38
	38	23	28	44	15	27	27	42
	27	21	38	50	17	11	25	51
	18	21	37	46	19	24	32	47
	20	25	39	40	23	15	33	32
	14	33	21	49	17	17	16	31
	33	30	32	150	19	32	25	38
	25	28	47	15	15	21	26	25
Mean (MPa)	**27**	**25**	**37**	**54**	**18**	**21**	**27**	**38**
SD	**10**	**5**	**11**	**40**	**3**	**7**	**5**	**9**
±Std Error	**3**	**2**	**4**	**14**	**1**	**2**	**2**	**3**

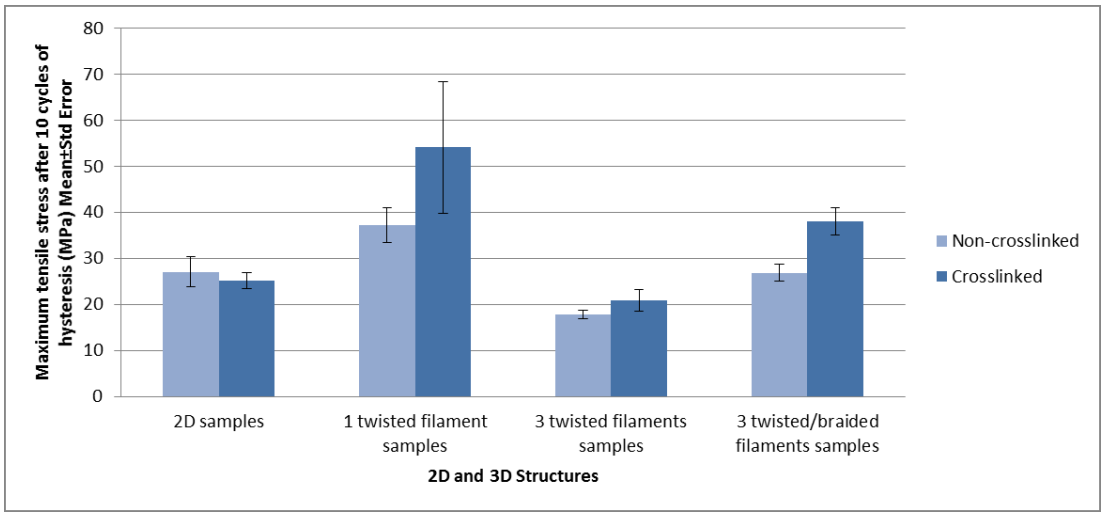

Figure 6.6 Maximum tensile stress after 10 loading cycles

It was known that the maximum tensile stress for the natural ACL is approx. 38 MPa [59] and it was calculated in Chapter 3, that the maximum tensile stress for jumping at maximum effort was 24.8 MPa and for walking was 17.57 MPa [237]. These values were considered, along with other parameters such as Young's modulus or the morphology of the scaffolds, to determine which structures would be the most appropriate for use as an ACL substitute.

It can be observed in Table 6.1 and Figure 6.6 that the structure with the highest maximum tensile stress was the one twisted filament scaffold, with 37 ± 4

MPa for the non-crosslinked samples and 54 ± 14 MPa for the crosslinked samples. However, the 3 twisted/braided filaments crosslinked samples with 38 ± 3 MPa also reached the necessary tensile stress required for the ligament; therefore, both structures were studied to determine which one was the most suitable for an ACL replacement.

The fact that the 1 twisted filament structure exhibited a higher tensile stress compared to the 3 twisted/braided filaments is due to the 3 filaments each being different. If all of the filaments of the structure were loaded identically, the resultant strength would be the sum of the strength of each filament. In order to maximize the tensile properties each filament should be equally loaded. However, in twisted/braided structures, the tension exerted in each filament, while the tensile test was performed, was different and resulted in a weaker and less stiff implant as it was also observed in Kim D. H. *et al.* [369], where the effect of twisting and braiding human hamstring tendon grafts resulted in a reduction of tensile strength and stiffness. Hearle J.W.S *et al.* [370] affirmed that the act of twisting or braiding fibres contributes to increasing the flexibility and handiness of a fabric. The manufacturing of 3D structures based on twisting and braiding filaments was used in this study to reduce the stiffness and improve the handling and the flexibility of the scaffolds, as was demonstrated in the studies cited above [369], [370].

b) Young's modulus:

This section has the purpose of drawing conclusions about the stiffness of the 2D and 3D scaffolds when they are pre-loaded. To this end, a comparison

between the Young's modulus calculated from the 1st and the 21st curve of the 2D structures and the different three 3D structures was performed. This comparison aided understanding of how the PVA scaffolds mechanically behave under cyclic tensile tests and their stiffness.

Young's modulus was calculated in order to gain information about how the polymer behaves after a certain loading cycles until 13% strain, which is the maximum % strain that the ligament exhibits during a daily task as during walking. It was calculated from the 1st and the 21st loading curves and between 11% and 12% strain of the 8 samples analysed for each crosslinked and non-crosslinked structure. This property was crucial to choose the most suitable 3D structure for use as an ACL replacement, since the implant would be subjected to continuous loading cycles once implanted into the knee.

Tables 6.3 and 6.4 show Young's modulus from the 1st and 21st loading curves.

Table 6.3 Young's modulus from the 1st curve for 2D and 3D samples

	2D samples		1 twisted filament samples		3 twisted filaments samples		3 twisted/braided filaments samples	
	Non-crosslinked	Crosslinked	Non-crosslinked	Crosslinked	Non-crosslinked	Crosslinked	Non-crosslinked	Crosslinked
	862	507	471	235	46	18	115	97
	1174	663	241	297	67	31	53	101
	713	289	336	362	33	26	94	214
	419	434	393	294	46	38	156	148
	404	384	372	249	61	100	81	55
	397	658	158	426	60	111	72	177
	966	564	174	641	78	198	40	136
	838	486	370	108	58	135	66	135
Mean (MPa)	**722**	**498**	**315**	**326**	**56**	**82**	**85**	**133**
SD	**292**	**130**	**112**	**158**	**14**	**64**	**37**	**49**
±Std Error	**103**	**46**	**39**	**56**	**5**	**23**	**13**	**17**

Table 6.4 Young's modulus from the 21st curve for 2D and 3D samples

	2D samples		1 twisted filament samples		3 twisted filaments samples		3 twisted/braided filaments samples	
	Non-crosslinked	Crosslinked	Non-crosslinked	Crosslinked	Non-crosslinked	Crosslinked	Non-crosslinked	Crosslinked
	413	225	272	234	85	28	167	120
	459	138	232	303	71	50	110	130
	310	213	322	373	72	32	135	212
	195	247	364	286	90	60	189	172
	228	365	361	250	98	91	147	94
	802	301	146	424	68	102	95	173
	176	289	178	710	109	187	77	154
	423	971	340	106	91	123	112	135
Mean (MPa)	**376**	**344**	**277**	**336**	**85**	**84**	**129**	**149**
SD	**204**	**262**	**84**	**178**	**15**	**54**	**37**	**37**
±Std Error	**72**	**93**	**30**	**63**	**5**	**19**	**13**	**13**

The mean, standard deviation and standard error of the mean were also calculated and used to plot a graph where all structures were compared. Figure 6.7 shows the Young's modulus (Mean ± Std Error) calculated from the 1st and 21st curves for all of the scaffolds.

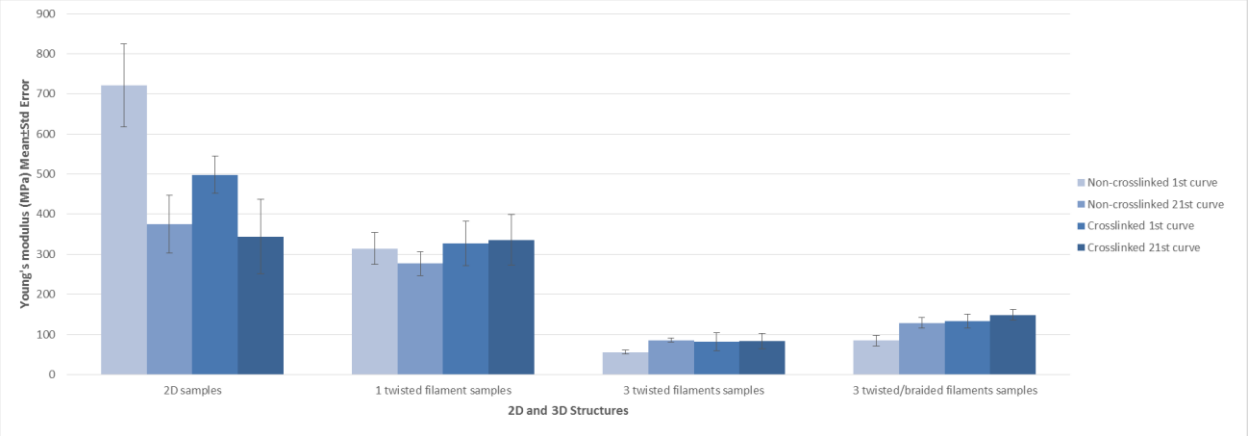

Figure 6.7 Young's modulus of 1st and 21st curves for 2D and 3D samples

The Young's modulus of the ACL is approximately 111MPa [59]. The structures that were closer to that value were the 3 twisted/braided filaments samples with a Young's modulus of 133 MPa calculated from the 1st curve for crosslinked samples and 129 MPa calculated from the 21st curve for non-crosslinked samples.

This structure exhibited the closest values of Young's modulus to the natural ACL in all its variations (in the 1st and 21st curve and non-crosslinked and crosslinked).

Moreover, from this graph it was observed that all 3D structures behave more consistently than the 2D structures. This fact is surprising since the author expected to add more variation with the manual process used to manufacture the 3D scaffolds. However, the 3D samples behaved better mechanically and with less variability, as was observed from the similar values of mean and standard error of the mean for these structures.

Moreover, the 3D structures behaved as expected. Crosslinked samples were stiffer than the non-crosslinked samples from the same structure, demonstrated through higher values of Young's modulus. This was predictable, since the crosslinking process creates bonds to link one polymer chain to another, increasing the stiffness of the structure.

Additionaly, the values of Young's modulus for the 21st curves were higher than for the 1st curves in the 3 twisted and 3 twisted/braided filaments samples. This was due to the dry PVA scaffolds starting to deform plastically before the 13% strain, increasing their stiffness. This means that the implant would not recover its original shape after cycles of load comparable to walking and therefore these PVA structures would show laxity issues in a dry environment.

However, it was assumed that wet samples would behave more elastically than dry samples. For this reason, and because the ACL implant would be in a wet

environment inside the body, experiments with wet samples are presented in section 6.4.1.2. Therefore, although the values of Young's modulus and maximum tensile stress for 3 twisted/braided filaments samples were very similar to the natural ligament, its mechanical behaviour was not identical to the ACL and should be improved, evaluating its elasticity under wet conditions.

The time for the total degradation of 2D PVA electrospun scaffolds was one hour. Therefore, it is necessary to crosslink the PVA scaffolds in order to slow down the degradation once the scaffold is implanted in the body. For this reason, although the closest value of Young's modulus was obtained with non-crosslinked scaffolds, only stable crosslinked samples were considered as suitable scaffolds for its implantation in the body, and only those samples were tested in the rest of the experiments performed.

6.4.1.1.3. Hysteresis curves for the different 3D structures in dry conditions

This purpose of this section is to study the laxity of the 2D and 3D scaffolds when they are pre-loaded. The "Force (N) / Extension (mm)" of the different 3D structures with non-crosslinked and crosslinked structures was analysed through the chapter. Again, from Figures 6.8 - 6.10 it was determined that the crosslinked samples were stiffer than the non-crosslinked samples, since the gradient of the curves were steeper. In addition, the non-crosslinked samples elongated more than the crosslinked samples for the same group of structures; graphs B in Figures 6.8 - 6.10 exhibited lower values of extension (and therefore strain at beak) than graphs A in the respective figures.

As previously explained, dry PVA scaffolds started to deform plastically before 13% strain. As these scaffolds were plastically deformed, they did not recovered their original length; therefore, their length and laxity increased after being tested.

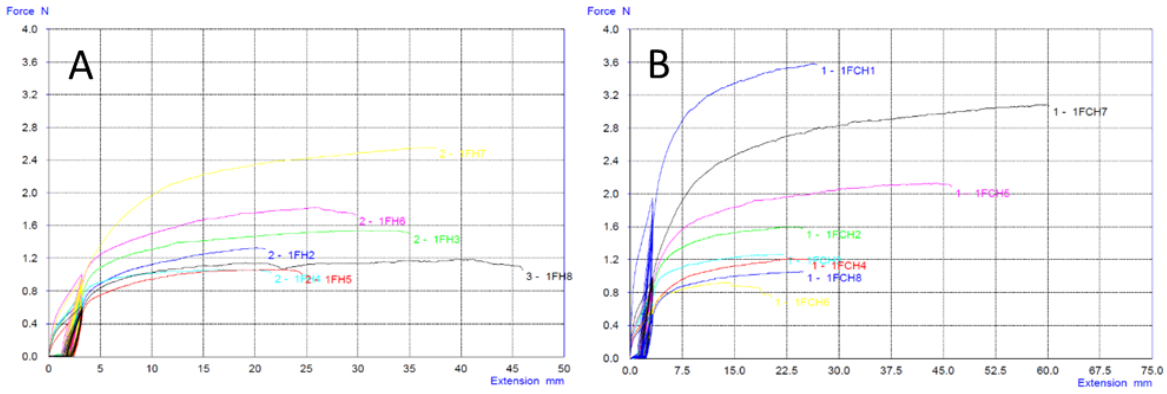

Figure 6.8 Force (N) / Extension (mm) in 1 twisted filament samples A) Non-crosslinked B) Crosslinked

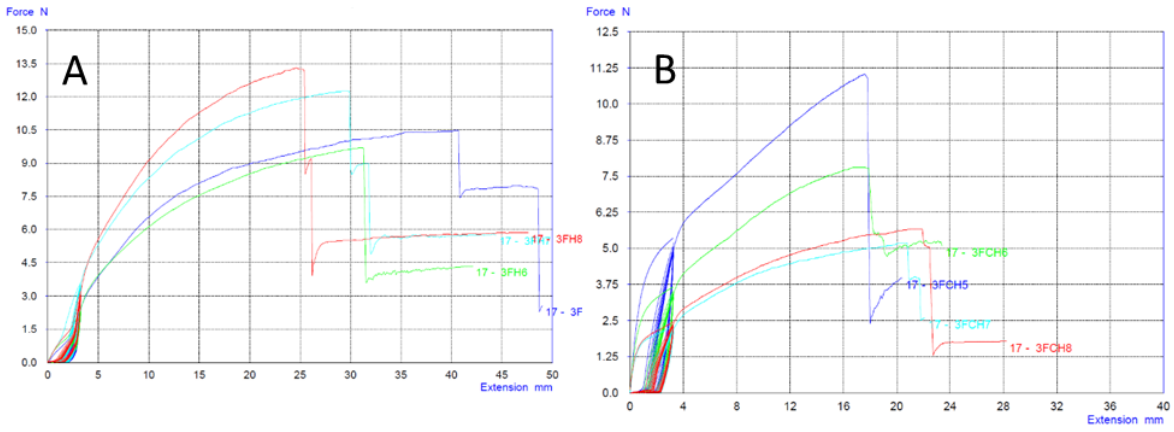

Figure 6.9 Force (N) / Extension (mm) in 3 twisted filaments samples A) Non-crosslinked B) Crosslinked

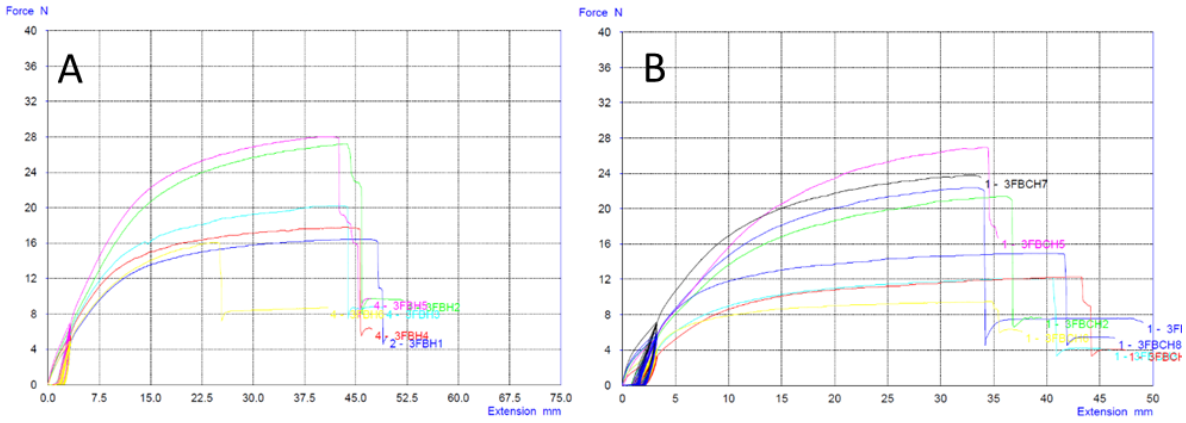

Figure 6.10 Force (N) / Extension (mm) in 3 twisted/braided filaments samples A) Non-crosslinked B) Crosslinked

Key Points from Cyclic Tensile Tests in Dry Conditions:

1. 10 pre-loading cycles was determined as the optimum.

2. The maximum tensile stress closest to the natural ACL (38 MPa [59]) was observed for the 3 twisted/braided filaments crosslinked samples, which exhibited a maximum tensile stress of 38 ± 3 MPa. This value was the most similar to the value of the natural ACL reported in the field.

3. 3 twisted/braided filaments samples exhibited values of Young's modulus, calculated from the 1st and 21st curves, comparable to the natural ACL (111MPa [59]). Values of 133 MPa for 3 twisted/braided filaments crosslinked samples calculated from the 1st curve and 129 MPa for 3 twisted/braided filaments non-crosslinked samples calculated from the 21 st curve were observed.

4. 3D structures exhibited more consistent mechanical behaviour than 2D samples.

5. Crosslinked samples were stiffer than non-crosslinked samples.

6. Dry samples exhibited laxity issues due to their plastic mechanical behaviour.

6.4.1.2. Cyclic tensile tests in wet conditions

The same experiments under the same parameters as performed in a dry environment were performed in wet conditions. However, in this case an initial study had to be performed in order to determine the time during which the scaffolds should be immersed in PBS. For this experiment and as mentioned in the methods (section 6.3.4.2.), four 1 twisted filament crosslinked samples were immersed in PBS for 1, 5, 15 and 60 minutes and the mechanical properties of each sample were determined. The results of this experiment will be explained in section 6.4.1.2.1.

Once the immersion time in PBS was decided, the same tensile parameters specified for the dry samples were used with the wet samples to calculate the mechanical properties of the different scaffolds. The results of these experiments will be presented in the second section below (6.4.1.2.2.).

6.4.1.2.1. Determination of sample immersion time in PBS.

a) Maximum tensile stress:

Table 6.5 and Figure 6.11 show the maximum tensile stress in MPa of 1 twisted filament crosslinked samples after being immersed for specific periods of time in PBS.

As was appreciable from the results and a one-way ANOVA no significant differences were observed ($p > 0.05$). Therefore, in terms of the maximum tensile

stress there was not any significant difference in testing the samples after 1 minute of being immersed in PBS or after 1 hour.

Table 6.5 Maximum tensile stress of 1 twisted crosslinked filament samples after being immersed in PBS.

Maximum tensile stress (MPa)	Time in PBS
12	1 min
14	5 min
13	15 min
12	60 min

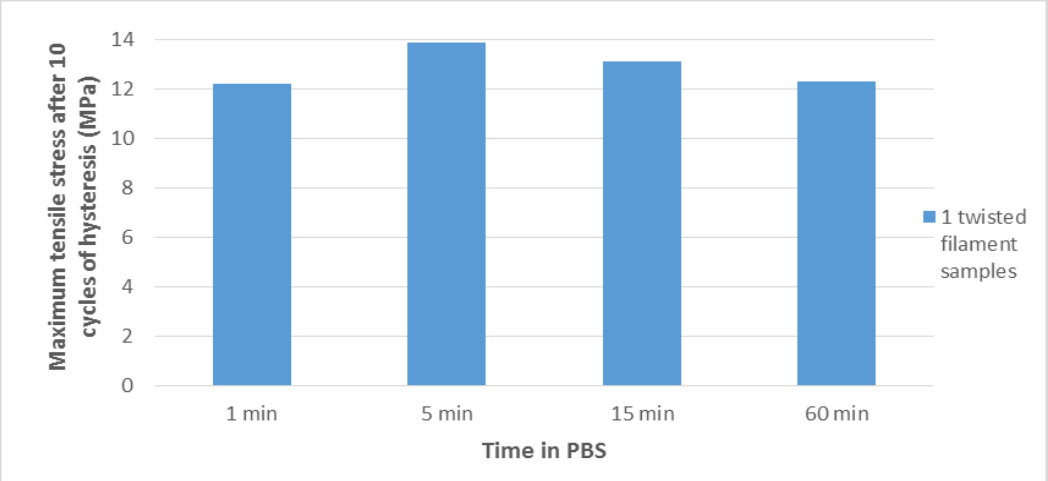

Figure 6.11 Maximum tensile stress after 10 loading cycles in 1 twisted filament crosslinked samples immersed in PBS

The time of the scaffolds immersed in PBS was also determined through the calculation of the Young's modulus from the first loading curve. The results are presented below.

b) Young's modulus:

Table 6.6 and Figure 6.12 show the Young's modulus (MPa) calculated from the first loading curve of 1 twisted filament crosslinked samples after being immersed for specific periods of time in PBS.

In this case no significant differences were observed for periods of time between 1 minute and 60 minutes. However, the Young's modulus dropped slightly after 1 hour of immersion. Hence, in order to speed up the process of the experiments and due to a lack of significant differences in the mechanical properties with respect to immersion time, the decision was taken to immerse the samples in PBS for 1 minute to perform the rest of the experiments.

Table 6.6 Young's modulus from the 1st curve of 1 twisted filament crosslinked samples after being immersed in PBS.

Young's modulus (MPa)	Time in PBS
20	1 min
20	5 min
21	15 min
16	60 min

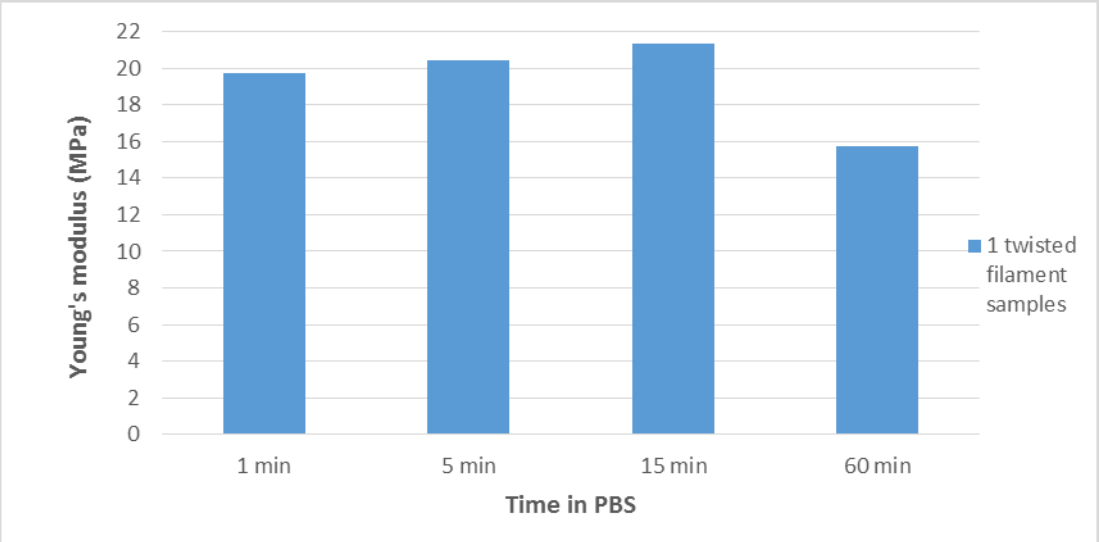

Figure 6.12 Young's modulus (MPa) of the first curve of loading in 1 twisted filament crosslinked samples immersed in PBS

6.4.1.2.2. Mechanical properties of wet 2D and 3D scaffolds

Once the time in PBS of each sample was determined, the next step was to test each type of 2D and 3D crosslinked structures after 1 minute in PBS to evaluate their material properties (maximum tensile stress and Young's modulus in the 1st and 21st curves). To develop this experiment three samples of each structure were studied.

a) Maximum tensile stress:

Table 6.7 and Figure 6.13 show the maximum tensile stress in MPa for all the 2D and 3D crosslinked samples tested after being immersed for 1 minute in PBS.

Table 6.7 Maximum tensile stress of 2D and 3D crosslinked samples after being immersed for 1 min. in PBS.

	2D samples	1 twisted filament samples	3 twisted filaments samples	3 twisted/braided filaments samples
		39	10	10
		12	8	9
	1	25	9	8
Mean (MPa)	**1**	**25**	**9**	**9**
SD		**13**	**1**	**1**
±Std Error		**9**	**1**	**1**

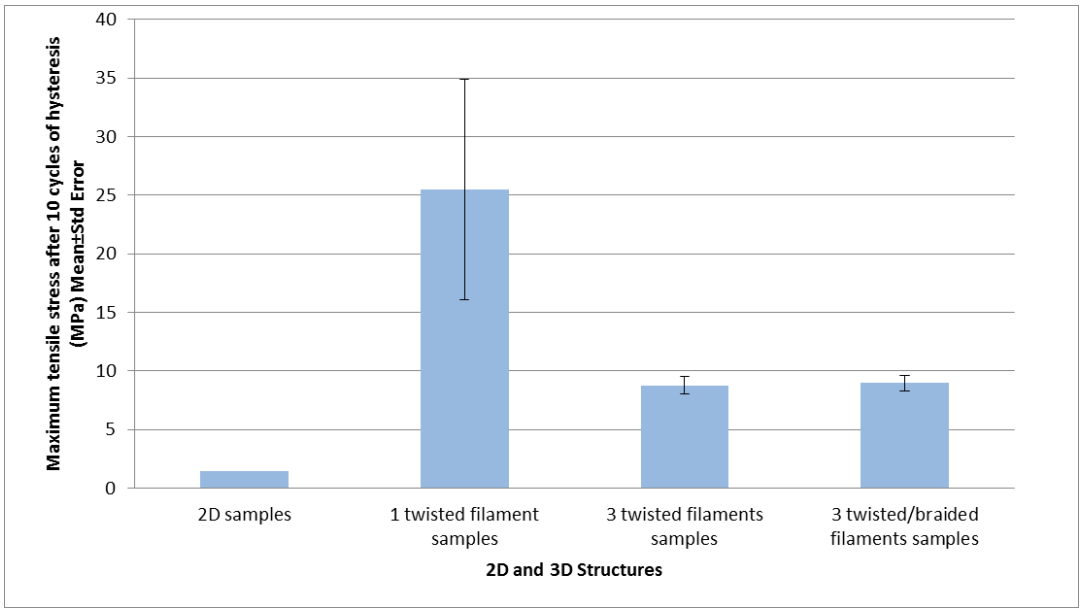

Figure 6.13 Maximum tensile stress (MPa) after 10 loading cycles in 2D and 3D samples immersed in PBS

Examining the results, it can be concluded that the structure with the highest maximum tensile stress was the 1 twisted filament; however, this structure exhibited a high variability in the results, larger than the other 3D crosslinked structures. Therefore, more robust structures, such as 3 twisted filaments scaffolds or 3 twisted/braided filaments scaffolds, showed more consistent mechanical properties than thinner structures. This phenomenon was also observed in the tensile tests in dry conditions (Tables 6.2 - 6.4) and it was a factor in the selection of the most suitable structure.

Moreover, the 1 twisted filament structure could bear the maximum loading required during a high impact activity, such as jumping at maximum effort (24 MPa) [237]; however it did not reach the maximum tensile stress observed in the natural ACL (38 MPa [59]). Therefore, other materials or the combination of several materials should be studied mechanically under wet conditions in order to reach an

approximate value of maximum tensile stress comparable to the natural ACL. Further investigations will be focussed in this direction.

The crosslinking process tended to deform the scaffolds reducing their size. In order to avoid a huge deformation of the sample and to be able to test it properly, the samples were placed on a cardboard frame before being crosslinked. However, when the 2D samples were immersed in PBS, the pressure of the PBS column above the sample broke the sample. To be able to test the 2D samples in a wet environment, instead of immersing the samples in the PBS for 1 minute, a few drops of PBS were placed over the sample to reduce the pressure of PBS column. However, due to the extreme fragility of the 2D samples, only one out of three 2D samples could be tested in wet conditions.

It was noteworthy that although the maximum tensile stress dropped significantly compared to the dry samples for all type of structures, all samples tested failed next to the lower grip (Figure 6.14), due to the high stress concentration in that part of the sample caused by the clamp. Many trials were performed with different pneumatic clamps, tapes to hold the sample and level of pressure in the clamps; however, the samples still broke due to the stress concentration created by the clamp. Therefore, the author expects that with improved gripping techniques for elastic polymers these results will be increased.

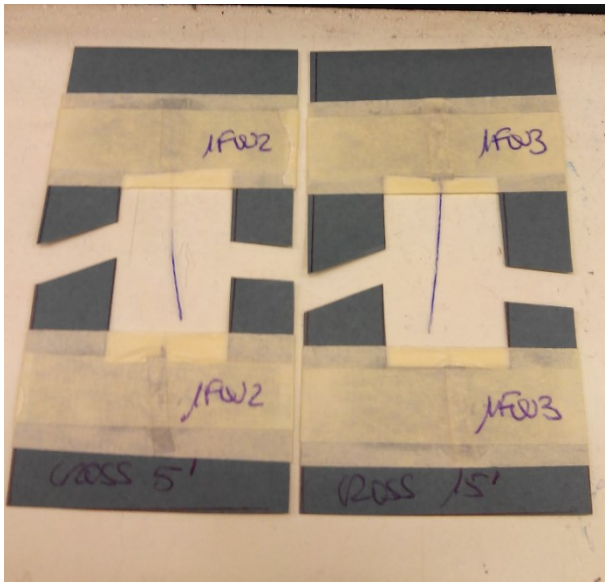

Figure 6.14 Example of wet samples after being mechanically tested

In the next section the Young's modulus calculated from the 1st and 21st curves and a comparison between both are presented.

b) Young's modulus:

Table 6.8 shows the values of Young's modulus calculated from the 1st and 21st loading curves and between 11% and 12% strain. These values were calculated in three crosslinked samples of each type of structure and after being immersed in PBS for 1 min. The mean, standard deviation and standard error of the mean were also calculated and used to plot a graph where all structures were compared (Figure 6.15).

Table 6.8 Young's modulus from the 1st and 21st curves of 2D and 3D crosslinked samples after being immersed for 1 min. in PBS.

	2D samples	1 twisted filament samples	3 twisted filaments samples	3 twisted/braided filaments samples
		66	9	11
		52	8	15
	42	45	7	12
Mean (MPa)	**42**	**54**	**8**	**12**
SD		**11**	**1**	**2**
±Std Error		**8**	**1**	**1**

As explained in section a) above, due to the extreme fragility of the 2D samples only one 2D sample could be tested in wet conditions. For this reason neither the standard deviation nor the standard error of the mean were calculated for that structure.

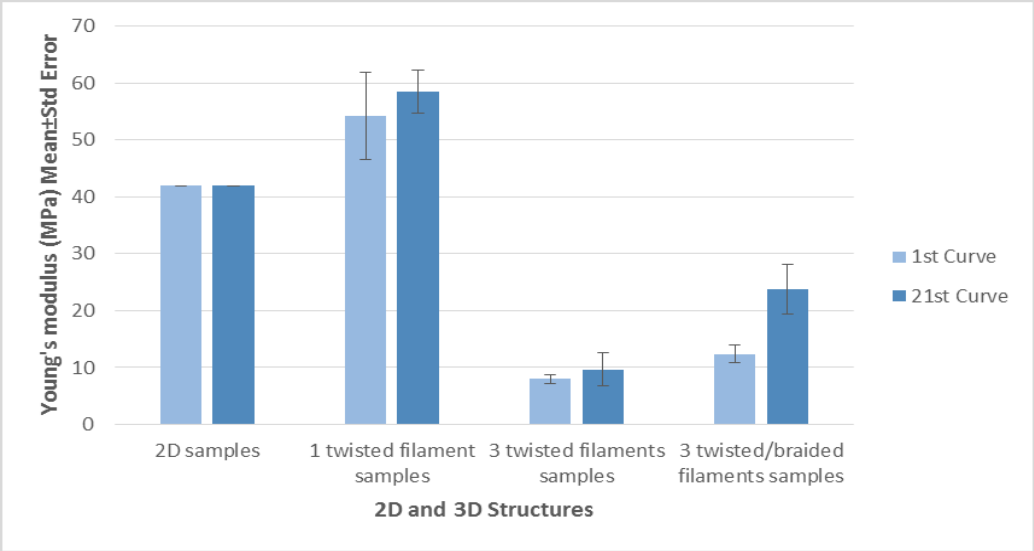

Figure 6.15 Young's modulus (MPa) of the 1st and 21st curves of loading for 2D and 3D samples immersed in PBS

Observing the values obtained for Young's modulus calculated from the 1st curve, there was not any structure with values of Young's modulus close to the natural ligament (close to 111 MPa). The highest value was observed with 1 twisted filament samples with a mean of Young's modulus of 54.24 MPa; however, as with the maximum tensile stress, the standard deviation and consequently the standard

error of the mean were higher than in the other 3D structures. This implied that the 1 twisted filament structure did not provide consistent results, and therefore other 3D structure such as the 3 twisted/braided filaments structure would be a better solution in terms of the manufacturing process for fabricating an ACL replacement.

The results obtained from Young's modulus from the 21st curve did not change qualitatively from the results obtained from the first curve. The highest Young's modulus from the 21st curve was observed in 1 twisted filament scaffolds and the lowest value was observed for 3 twisted filaments samples. However, it was observed that the results were more consistent in the 21st curve for 1 twisted filament scaffolds than the results calculated from the first curve; and all samples exhibited higher Young's modulus when calculating it from the 21st curve.

Although this experiment showed lower mechanical properties than the natural ACL, it is still worth looking at how the different structures behave, to adopt the most suitable design in future experiments with materials that could reach the appropriate Young's modulus.

As was expected from the results obtained in dry conditions, the highest Young's modulus was observed in 1 twisted crosslinked samples followed by the 3 twisted/braided filaments crosslinked scaffolds. As in dry conditions the Young's moduli calculated from the 21st curves were higher than the Young's moduli calculated from the 1st curves, however there were no significant differences found between them. The mechanical behaviour of all wet samples was elastic and all of them recovered their original shape after a load was applied and then removed.

Following the results and the discussion for dry and wet conditions, it can concluded that the 3 twisted/braided filaments crosslinked structure would be the best solution for use as an ACL replacement in order to obtain the most comparable mechanical properties to the natural ACL. Therefore, the next section 6.4.1.2.3 focusses on the mechanical behaviour of these scaffolds.

6.4.1.2.3. Hysteresis curves of 3 twisted/braided filaments crosslinked structures in wet conditions

Figure 6.16 shows the "Force (N) / Extension (mm)" of the most suitable structure for an ACL replacement, the 3 twisted/braided filaments crosslinked scaffolds.

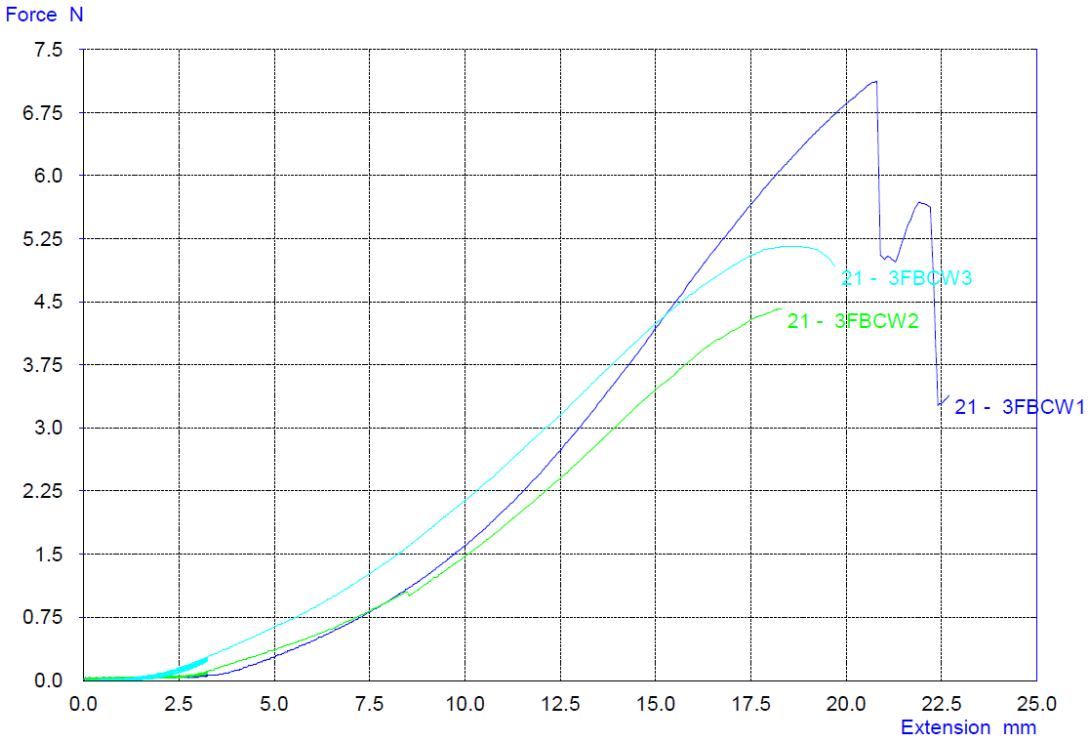

Figure 6.16 Force (N) / Extension (mm) in 3 twisted/braided filaments crosslinked samples

What is more surprising and beneficial in order to be considered as a potential ACL implant is its elastic character and the toe region observed in every wet sample. In this study, it was demonstrated that the dry PVA electrospun scaffolds behaved plastically and no toe region was observed when a tensile test was performed; this fact was also observed in Merkle V.M *et al.* [327], where mechanical properties of PVA, gelatin and PVA/Gelatin core/shell scaffolds were investigated. However, the wet PVA scaffolds behaved elastically and all of them exhibited a well-defined toe region, as observed in Figure 6.16. This is due to the capacity of PVA to absorb water; PVA is a highly hydrophilic polymer that behaves as a hydrogel in aqueous solution. PVA hydrogels have the characteristic of showing a large elongation with low levels of tensile force giving rise to a toe region followed by an elastic region as observed in Zhang Y. *et al.* [371], where different concentrations of PVA hydrogels (1 wt%, 2 wt%, 4 wt%, 6 wt%) were tensile tested.

Therefore, these wet structures did not exhibit any problems with laxity, due to their ability to recover their original shape and length after being deformed.

However as demonstrated in Chapter 3, the failure mechanisms of the ACL are not due to just tensile force, therefore the study of the implants under a shear force has to be performed. This study is presented in section 6.4.1.3.

Key Points from Cyclic Tensile Tests in Wet Conditions:

1. There were no significant differences between Young's modulus of samples after 1 minute in PBS or after 60 minutes.

2. The maximum tensile stress closest to the natural ACL (38 MPa [59]) was observed for the 1 twisted crosslinked samples, which exhibited a maximum tensile stress of 38 ± 25 MPa. However, these structures showed a high variability in the results compared to other structures.

3. The closest value of Young's modulus to the natural ACL (111MPa [59]) was observed for 1 twisted filament samples. Values of 54 MPa calculated from the 1st curve and 58 MPa calculated from the 21st curve were observed. However, as previously mentioned these structures showed a high variability compared to other structures.

4. More robust structures such as 3 twisted/braided filaments and 3 twisted filaments samples exhibited more consistent mechanical behaviour than 2D samples or 1 twisted filament structures. Therefore, they are preferable to the thinner structures.

5. Wet samples exhibited an elastic character with a well-defined toe region. Therefore, they showed a mechanical behaviour comparable to the native ACL.

6. Wet samples did not present laxity issues due to their elastic behaviour.

6.4.1.3. Cyclic shear tests

2D and 3D scaffolds were tested under shear load, mimicking the anterior/posterior shear force experienced by the ACL during sudden stops or

changes of direction, that normaly occur during high impact activities such as cutting.

A tensometer (Instron H10KS) was used to experimentally test these shear forces. This equipment is designed to exert a tensile force on the sample; therefore, in order to mimic the shear force the sample must be positioned at a specific angle as explained in section 6.3.4.3.

As in previous experiments (cyclic tensile tests in dry and wet conditions, sections 6.4.1.1 and 6.4.1.2), the 2D and 3D crosslinked samples were subjected to 10 loading cycles under dry conditions. The maximum shear stress and the Young's modulus in curves 1 and 21 were calculated. Three samples were manufactured and tested for each 2D and 3D structure; however, just two 2D samples were considered in the study due to the great variability of the results obtained with the third sample. Therefore the results of that sample were considered as outlier and they were excluded from the study.

6.4.1.3.1. Mechanical properties of dry 2D and 3D scaffolds under shear loading

a) Maximum shear stress:

Table 6.9. and Figure 6.17 show the maximum shear stress in MPa for all 2D and 3D crosslinked samples tested in dry conditions.

Table 6.9 Maximum shear stress (MPa) of all 2D and 3D crosslinked samples

	2D samples	1 twisted filament samples	3 twisted filaments samples	3 twisted/braided filaments samples
		60	21	98
	12	43	16	124
	7	31	14	101
Mean (MPa)	**10**	**44**	**17**	**108**
SD	**3**	**14**	**3**	**14**
±Std Error	**2**	**8**	**2**	**8**

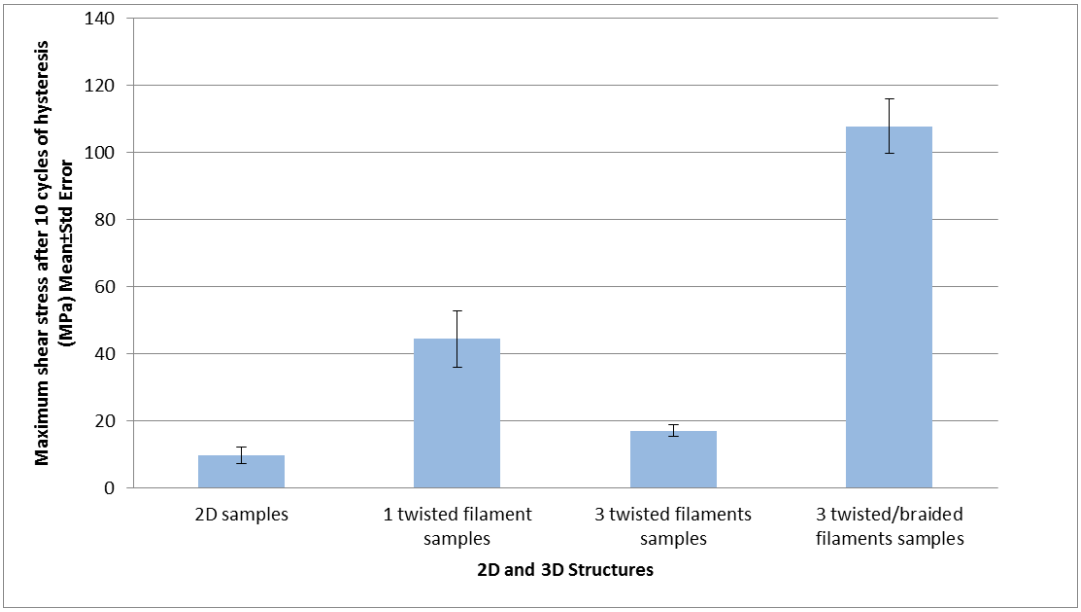

Figure 6.17 Maximum shear stress (Mean ± Std Error) of the 2D and 3D crosslinked scaffolds

The 3 twisted/braided filaments crosslinked structure exhibited the highest maximum shear stress compared with the other structures, allowing the samples to bear higher shear loads than the rest of the structures. This fact is in agrement with the studies performed by Kawabata and Walters [372], [373] where it was demonstrated that braiding techniques can bear and transfer axial loads, improving shear resistance and providing mechanical reinforcement.

b) Shear modulus:

Table 6.10 and Figure 6.18 show the shear modulus calculated from the 1st and 21st curves, between 11% and 12% strain, for all the 2D and 3D crosslinked samples tested in dry conditions.

Table 6.10 Shear modulus calculated from the 1st and 21st curves (MPa) of all 2D and 3D crosslinked samples

	2D samples		1 twisted filament samples		3 twisted filaments samples		3 twisted/braided samples	
	1st Curve	21st Curve	1st Curve	21st Curve	1st Curve	21st Curve	1st Curve	21st Curve
			70	101	12	27	99	155
	298	139	64	87	9	17	117	180
	183	99	27	47	8	12	70	99
Mean (MPa)	**241**	**119**	**54**	**78**	**10**	**19**	**95**	**145**
SD	**81**	**29**	**24**	**28**	**2**	**8**	**24**	**42**
±Std Error	**58**	**20**	**14**	**16**	**1**	**5**	**14**	**24**

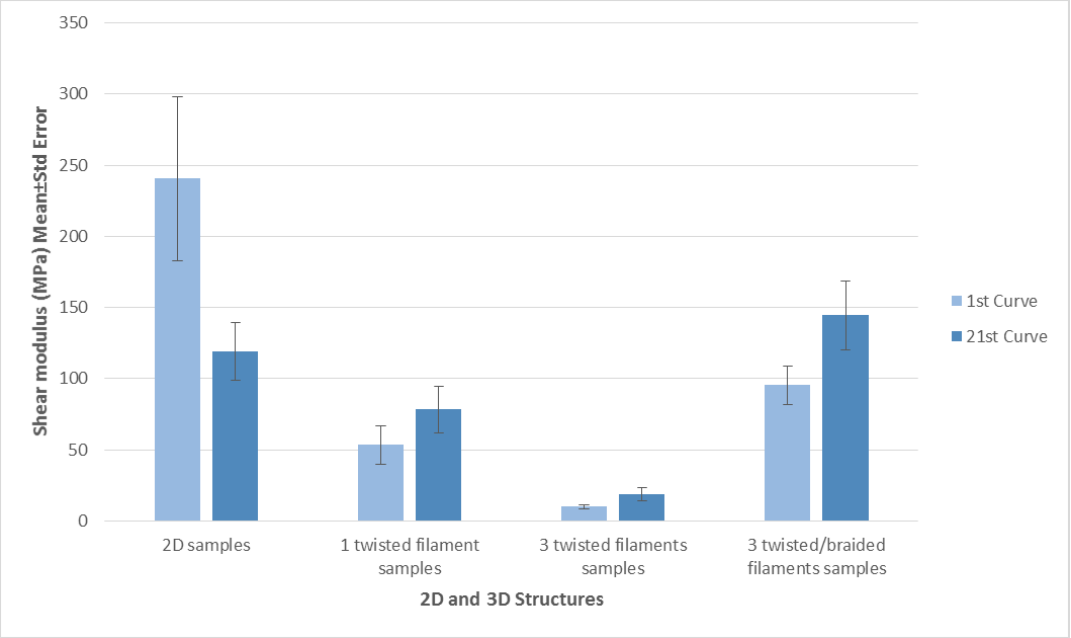

Figure 6.18 Shear modulus calculated from the 1st and 21st curves (Mean ± Std Error) of the 2D and 3D crosslinked scaffolds

The highest shear modulus calculated from the first curve was observed in 2D samples with a value of 240 MPa and the minimum value for the 3 twisted filaments crosslinked samples with a mean value of 10 MPa.

The highest shear modulus calculated from the 21st curve was observed in 3 twisted/braided filaments crosslinked samples with a value of 144 MPa and the minimum value for the 3 twisted filaments crosslinked samples with a mean value of 18 MPa.

As the tensile test also showed, the shear moduli calculated from the 21st curves of the samples were higher than the moduli calculated from the first curves in all 3D structures analysed. This was because the dry samples deformed permanently before 13% strain was reached.

Due to the fact that the ACL is normally mechanically characterized through measuring its reaction under axial loads, very few studies have been done to calculate the shear modulus of the natural ACL. However, one computational study found that the short-term shear modulus of the ACL was 68 MPa and the long-term shear modulus was 45 MPa [346]. Following these data, the closest structure to those values was the 1 twisted crosslinked filament; however, the mechanical behaviour of this structure was quite far from the behaviour expected for the natural ACL in the tensile experiments under dry and wet conditions. Therefore, the 1 twisted crosslinked filament was rejected as a possible ACL implant.

The next structure most comparable to the shear modulus value obtained in the literature was the 3 twisted/braided filaments crosslinked scaffolds. Therefore, considering the results obtained from all tensile and shear tests performed on the different scaffolds, it was concluded that the best structure to use as an ACL implant would be the 3 twisted/braided filaments crosslinked scaffolds. The next section 6.4.1.3.2 will show the force/extension curves obtained after the shear tests for this type of scaffolds.

6.4.1.3.2. Hysteresis curves of 3 twisted/braided filaments crosslinked structures in dry conditions and under a shear load

Figure 6.19 shows the "Shear force (N) / Extension (mm)" of the most suitable structure for an ACL replacement, the 3 twisted/braided filaments crosslinked scaffolds.

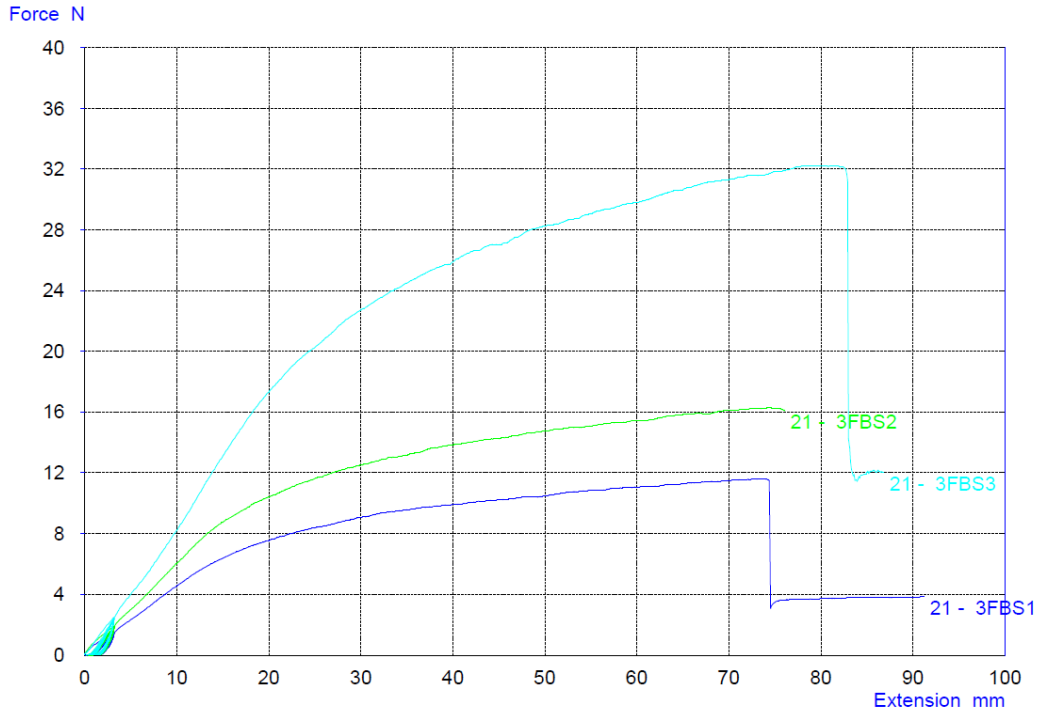

Figure 6.19 Shear force (N) / Extension (mm) in 3 twisted/braided filaments crosslinked samples

As observed in the tensile tests with dry PVA samples, when the samples were tested under shear loads, all structures behaved plastically and no toe region was observed. To the author's knowledge, to date there is no shear data from natural ACL to compare to experimental data from the scaffolds. Future work should be focussed on mechanically characterizing the natural ACL under shear forces and torsion.

Key Points from Cyclic Shear Tests in Dry Conditions:

1. 3 twisted/braided filaments crosslinked samples exhibited the highest maximum shear stress of 107 MPa.

2. The highest shear modulus calculated from the 21st curve was found in 3 twisted/braided filaments crosslinked samples, at 145 MPa.

3. To date, there is a shortage of natural ACL shear data. Future work should be focussed on charaterizing the native ACL under shear and torsion.

6.4.2. MORPHOLOGICAL CHARACTERIZATION

The natural ACL consists of collagen fibrils of 40-150 nm in diameter, these fibrils are organized in groups forming fibres with diameters between 1 and 20 μm; simultaneously the collagen fibres are arranged in groups creating fascicles of 360-1500 μm in diameter [33], [45]–[47], [124]. An SEM image of the fibres of collagen in the ACL is shown in Figure 6.20.

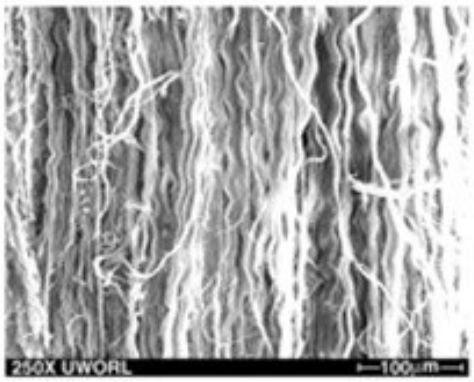

Figure 6.20 Collagen fibres of a natural ACL **[48]**.

A morphological characterization of the scaffolds was performed in order to finalize the decision on which 3D structure would be the most suitable to be used as an ACL replacement. To this end, PVA fibrils, fibres and fascicles of similar dimensions as the natural ligament were created, since it was assumed that these structures would mimic the mechanical and biological properties of the natural

ligament. Moreover, a study of the influence of chemical, environmental and mechanical conditions on the morphology of the 3D scaffolds was performed.

The morphological characterization of the 3D scaffolds was focussed on four different points:

- The morphology of the original 3D structures (prior to any other treatment).
- How the crosslinking technique modified the morphology of the scaffolds.
- Influence of wet conditions on the morphology of crosslinked scaffolds.
- Influence of tensile and shear forces on the morphology of the scaffolds.

6.4.2.1. Morphological characterization of 3D non-crosslinked structures

As shown in Chapter 5 wherein PVA electrospun scaffolds were studied, the production of 2D electrospun scaffolds generated a homogeneous network of fibres. The manufacturing of 3D structures allowed the creation of bundles of fibres and fascicles that were not present in the 2D structures, mimicking the morphology of the natural ACL.

As explained in the methodology (section 6.3.5), four SEM images with different magnifications were taken from each 3D structure in order to determine the

diameter of the PVA fibres, the diameter of the groups of fibres and the diameter of the fascicles.

Figures 6.21-6.23 show the morphology of 1 twisted filament non-crosslinked samples, 3 twisted filaments non-crosslinked samples and 3 twisted/braided filaments non-crosslinked samples respectively. For each 3D structure three different magnifications are presented below (100x, 5000x and 20000x magnifications) in order to demostrate the macro, micro and nano structures of the three types of 3D scaffolds. At the same time, these images were used to measure the diameter of the fibres, the bundles of fibres and the fascicles.

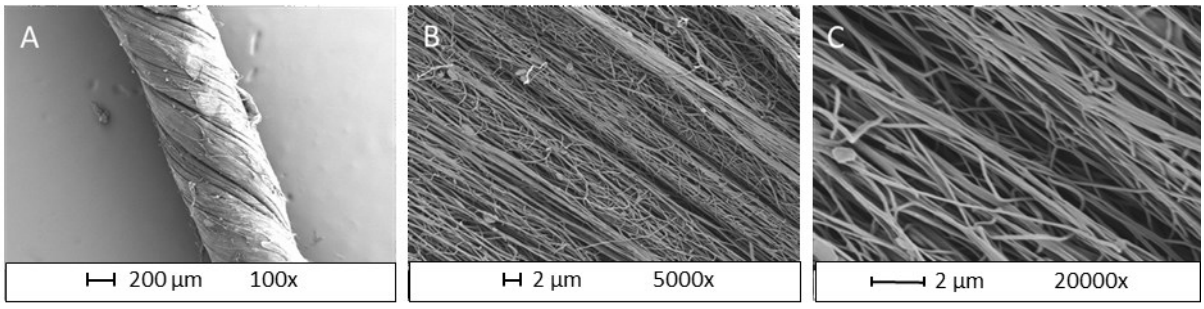

Figure 6.21 1 twisted filament non-crosslinked samples A) 100x B) 5000x C) 20000x

The diameter of the PVA fibres in the 1 twisted filament structure was 97 ± 5 nm, the thickness of the bundle of fibres was 8 ± 1µm and the size of the fascicles was 711 ± 19 µm.

Contrasting these values with the diameter of the fibrils, fibres and fascicles of the natural ACL, it was observed that all were statistically comparable and no significant difference was observed between them.

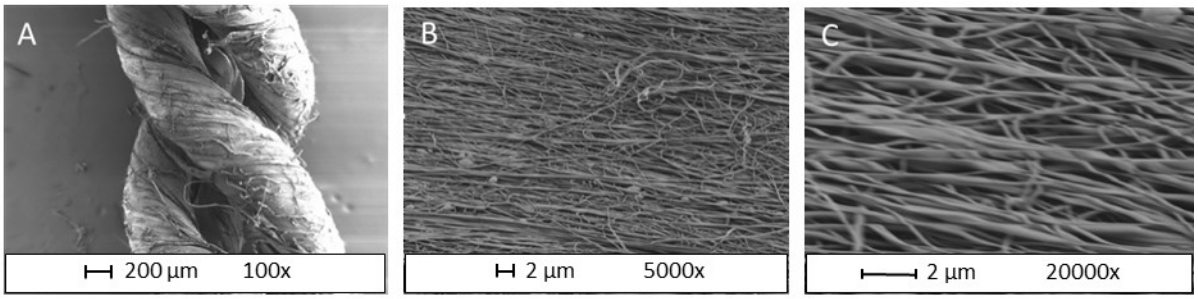

Figure 6.22 3 twisted filaments non-crosslinked samples A) 100x B) 5000x C) 20000x

The diameter of the fibres, the dimension of the bundles of fibres and the diameter of the fascicles were also measured for the 3 twisted filaments structure. The diameter of PVA fibres was 146 ± 8 nm, the thickness of the group of fibres was 25 ± 5 µm and the diameter of the fascicles was 614 ± 64 µm. As in the previous structure, none of these values showed any significant difference with the dimensions of fibres, bundles of fibres and fascicles of the natural ACL, i.e. they were statistically comparable.

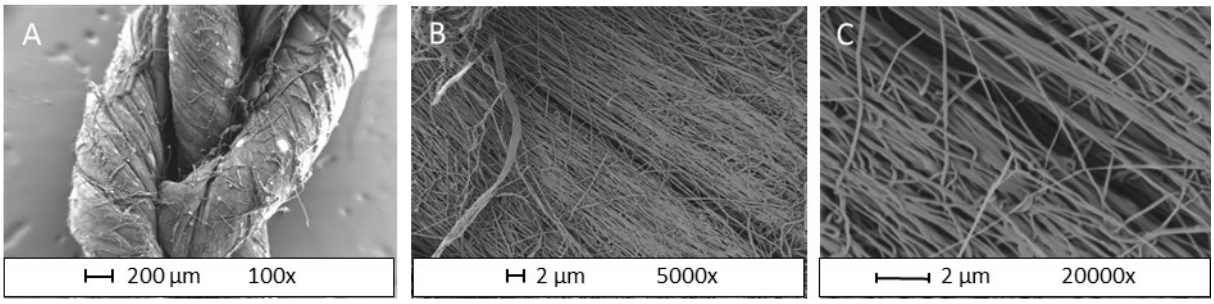

Figure 6.23 3 twisted/braided filaments non-crosslinked samples A) 100x B) 5000x C) 20000x

In the case of the 3 twisted/braided filaments structure, the mean diameter of the PVA fibres was 121 ± 6 nm, the thickness of the group of fibres was 18 ± 5 µm and the diameter of the fascicles was 593 ± 27 µm.

If these measurements were compared with the diameters of the collagen fibrils, fibres and fascicules of the natural ACL, it was observed that all measurements were in the same range of dimension as the structure of the collagen in the natural ligament and no significant differences were observed. The diameters of the PVA fibres were in the range of values for collagen fibrils diameters, the thickness of the group of fibres were in the range of the values for collagen fibres diameters and the size of the fascicules of the PVA fibres were in the range of values of the fascicules of collagen in the ACL.

In this study, it was also demonstrated that the nanofibres were not damaged in the manufacturing process and their diameter of the fibres and alignment were unmodified compared to the 2D electrospun scaffolds.

6.4.2.2. Influence of the crosslinking agent on the morphology of 3D structures

From the mechanical study, it was determined that the most suitable 3D structure was the 3 twisted/braided filaments structure, therefore the rest of this section will solely focus on this type of structure (Figure 6.24).

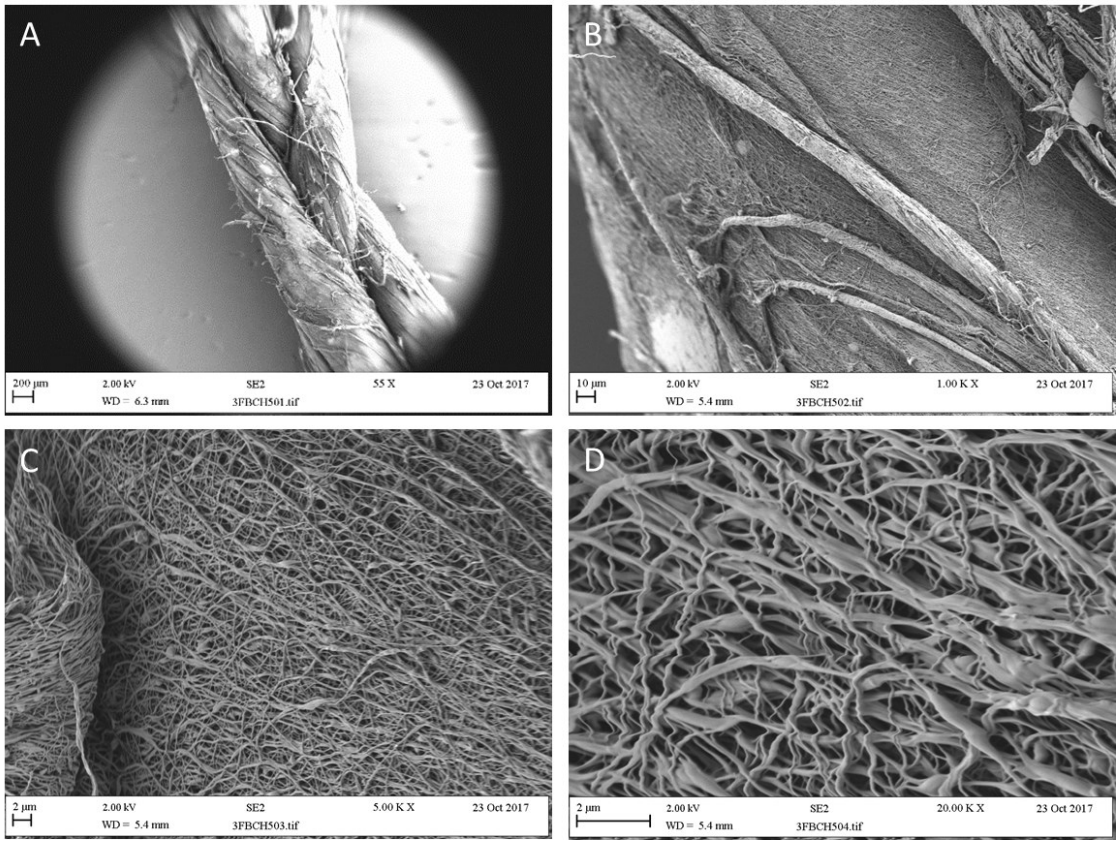

Figure 6.24 3 twisted/braided filaments crosslinked sample A) 55x B) 1000x C) 5000x D) 20000x

The mean diameter of the crosslinked PVA fibres in the 3 twisted/braided filaments structure was 177 ± 19 nm, the thickness of the group of fibres was 18 ± 4 µm and the size of the fascicles was 675 ± 48 µm.

Comparing the crosslinked structure with the non-crosslinked, it was observed that the diameter of the fibres increased with the crosslinking. This was predictable since the crosslinking process creates bonds between the fibres increasing their diameters. This was also observed in Kishan A.P. *et al.* [374], where an increase of 24% in the diameter of the fibres was reported after crosslinking the scaffolds with gluteraldehyde.

6.4.2.3. Influence of a wet environment on the morphology of 3D structures

Figure 6.25 shows a 3 twisted/braided filaments sample after immersion in PBS for 1 minute.

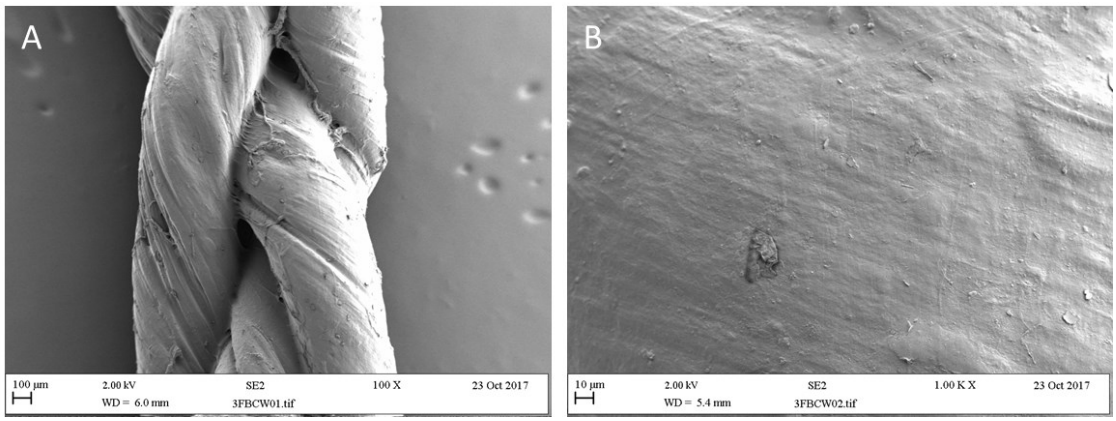

Figure 6.25 3 twisted/braided filaments crosslinked sample in wet conditions A) 100x B) 1000x

For wet conditions, only the diameter of the fascicles could be determined, being 569 ± 9 µm for the 3 twisted/braided filaments structure. Once the samples were soaked in PBS the dimensions of the groups of fibres and fibres were difficult to measure, since it is not possible to observed the surface of wet samples under the SEM. However, it was proved in the last study (section 5.4.3.) that the crosslinked PVA electrospun scaffolds were not degraded after 28 days of incubation in PBS, therefore PVA structures would be suitable for *in vivo* use as was demonstrated by other researchers [336], [375]–[378]. Moreover, crosslinked PVA hydrogels exhibited excellent biocompatibility [336], [375] and a water-swollen network similar to the extracellular matrix of the native ligament [65]. Future studies will focus on investigation of the adhesion, proliferation and orientation of human primary fibroblasts on the 3D electrospun scaffolds.

6.4.2.4. Influence of mechanical forces on the morphology of 3D structures

Visually comparing the collagen fibres from a damaged ACL (Figure 6.26) and one of the 3 twisted/braided filaments structures post tensile testing (Figure 6.27), it was observed that they had similarities in the disorganization of the fibres; previously the fibres were aligned and after tensile testing they had no preferential orientation.

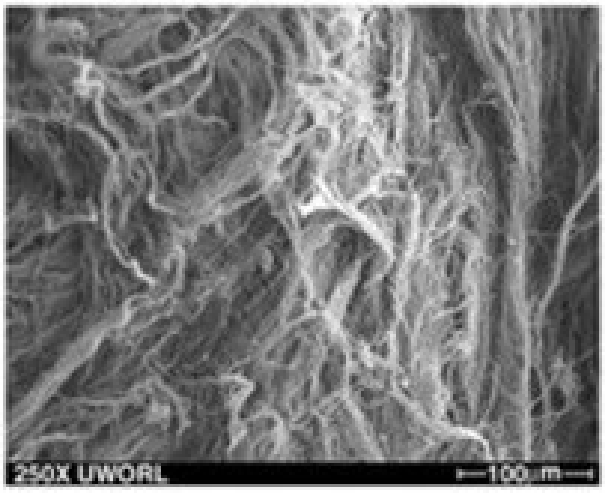

Figure 6.26 Collagen fibres of a damaged natural ACL **[48]**.

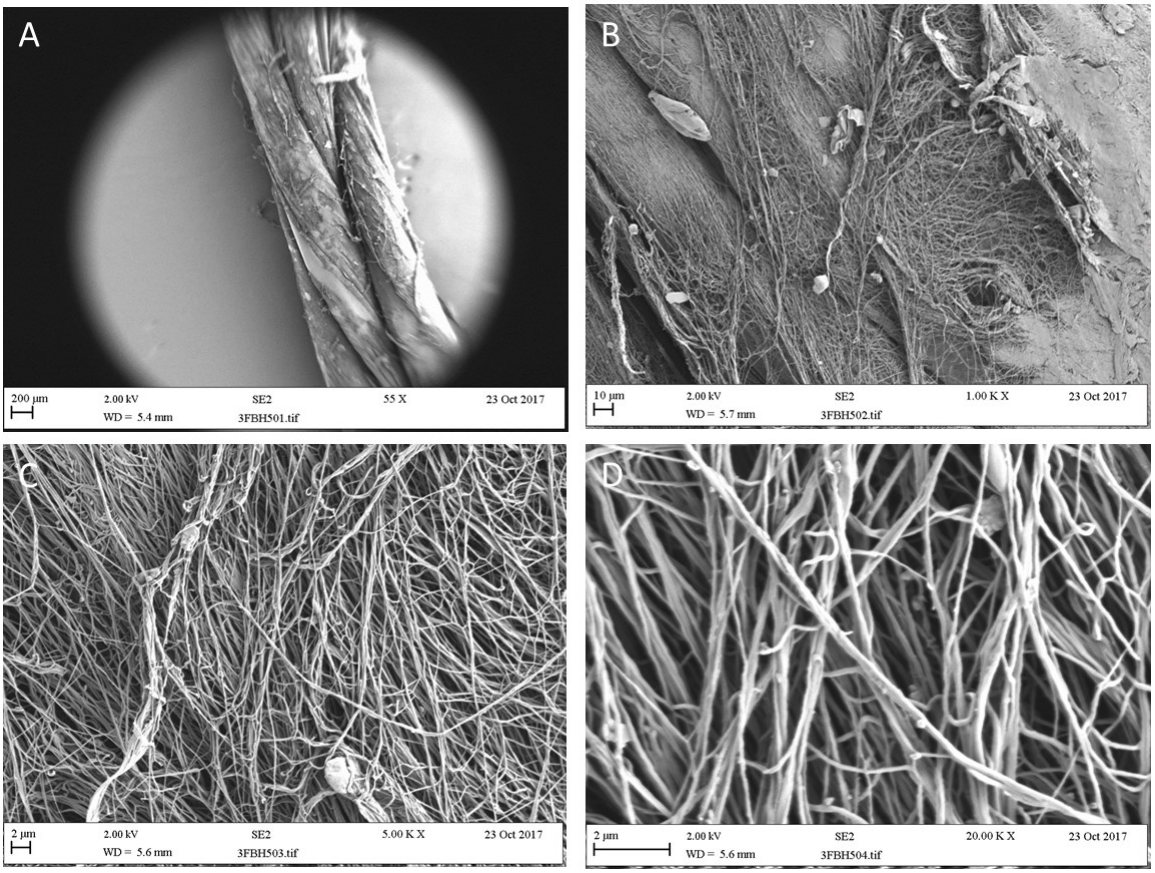

Figure 6.27 3 twisted/braided filaments non-crosslinked sample after tensile testing A) 55x B) 1000x C) 5000x D) 20000x

In the case of the 3 twisted/braided filaments structures already tensile tested, the mean diameter of the PVA fibres was 110 ± 9 nm, the thickness of the group of fibres was 28 ± 8 µm and the diameter of the fascicles was 496 ± 22 µm.

A 3 twisted/braided filaments structure after being tested under shear load was also morphologically characterized (Figure 6.28).

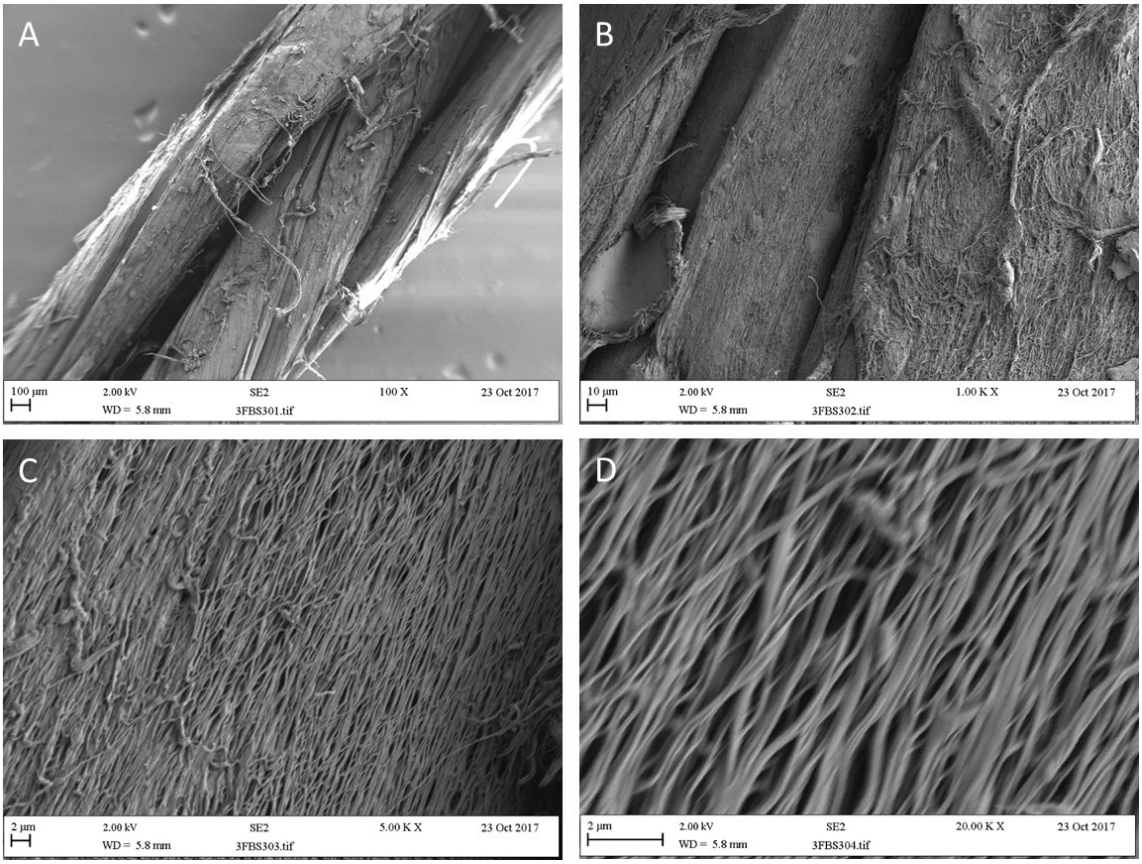

Figure 6.28 3 twisted/braided filaments non-crosslinked sample after being tested under shear load A) 100x B) 1000x C) 5000x D) 20000x

After shear loading, the mean diameter of the PVA fibres was 103 ± 6 nm, the thickness of the group of fibres was 20 ± 3 µm and the diameter of the fascicles was 506 ± 46 µm.

In this last study it was observed that the diameter of the fibres and the diameter of the fascicules were reduced in the tested samples. This was due to the fascicles and fibres being stretched during the tensile and shear tests, reducing their diameters. However, the thickness of the group of fibres increased after being tested, this was because the groups of fibres after the test were closer to one each other, increasing the thickness of the group of fibres.

6.5. CONCLUSIONS

The principal goal for Chapter 6 was to determine which 3D electrospun scaffold would be the most suitable for an ACL replacement, as a result of exhibiting the most similarities to the natural ACL. To reach this aim multiples variables (mechanical: maximum tensile strength, Young's modulus, shear stress, laxity, repeatability of force/elongation behaviour; and morphological: diameter of the fibres, bundle of fibres and fascicles) were studied and compared to the natural ACL in dry and wet conditions under load cycles.

In dry conditions, the 3 twisted/braided filaments crosslinked structure demonstrated the most similar mechanical properties to the natural ACL. This structure produced a maximum tensile stress of 38 ± 3 MPa and a Young's modulus after 10 loading cycles of 149 ± 13 MPa. The principal disadvantage was that dry electrospun PVA scaffolds had a plastic behaviour, therefore these scaffolds did not recover their shape after deformation and they exhibited laxity issues. Moreover, the stress/strain curve for dry samples did not exhibit any toe-region characteristic of the mechanical behaviour of soft tissue and more specifically the ACL. In order to solve these issues and mimic the environment inside the knee joint, wet samples were characterized.

It was observed that when wet PVA were tested scaffolds they behaved elastically and all of them exhibited a well-defined toe region, as was found in the natural ACL. They did not show any laxity issue, since all samples recovered their

original length after being unloaded. However, the mechanical properties reduced significantly for all structures studied. As an example, the 3 twisted/braided filaments crosslinked structure, the most suitable structure under dry conditions, produced a maximum tensile stress of 9 ± 1 MPa and a Young's modulus after 10 loading cycles of 24 ± 4 MPa in wet conditions. Nevertheless, these values were lower than they should be; since all samples tested in wet conditions failed due to the clamp causing high stress concentrations near to the lower grip. In spite of this inconvenience, which only occurred in the tensile tests in wet conditions, it could be affirmed that the results were qualitatively valid and allowed the comparison between the different structures. Future work should be directed to the study of new gripping techniques for elastic polymers in wet conditions to be able to increase the accuracy of the results.

As demonstrated in the gait analysis study (Chapter 3) not only the tensile properties have to be considered. The failure mechanics of the ACL were due to multidirectional loading; therefore, it was also important to determine how the scaffolds behaved under shear loading. After shear testing, it was shown that the 3 twisted/braided filaments crosslinked scaffolds exhibited the highest maximum shear stress compared with the other structures, allowing the samples to bear higher shear loads than the rest of the structures.

After these three mechanical studies, performed with 2D and 3D structures, it was concluded that the most suitable structure to be considered as ACL replacement was the 3 twisted/braided filaments crosslinked structure, with the

closest values to the mechanical properties of the ACL in dry conditions and bearing higher shear loading.

In terms of morphology, it was demonstrated that the manufacturing process did not damage the nanofibres and their nano-morphology and alignment were not modified. However, this process affected the distribution of the PVA fibres, creating bundles of fibres easily measurable with a SEM. Moreover, the dimension of the PVA fibres, bundle of fibres and fascicles agreed with the diameters of the collagen fibrils, fibres and fascicles in the natural ligament. After a tensile test to failure, the morphology of the 3D structure was visually comparable to the morphology of the collagen fibres of a damaged ACL.

In conclusion, within the current confines of this study, it was demostrated that the 3 twisted/braided filaments scaffolds is the most suitable structure to be used as a replacement for the ACL. Future work should be focussed on the biological characterization of this specific structure analysing aspects such as cellular adhesion, proliferation and orientation.

A discussion of all of the studies performed in this thesis with their limitations and the potential for future work is covered in the next chapter (Chapter 7).

Key points:

1. This study, for the fist time, evaluated and compared 2D and multiple 3D electrospun structures with the aim of determining which structure reproduced more closely reproduced the mechanical behaviour and morphology of the natural ACL.

2. Cyclic tensile and shear loading under dry and wet conditions had not been previously analysed for 3D electrospun scaffolds.

3. Neither 2D nor 3D PVA electrospun structures had been previously studied for ligament replacement.

4. 3 twisted/braided filaments scaffolds in dry conditions exhibited a maximum tensile stress of 38 MPa identical to the native ACL and a Young's modulus of 129 MPa comparable to the 111 MPa [59] reported for the natural ACL.

5. More robust structures exhibited more consistent mechanical properties than thinner structures, a finding not reported before in the field.

6. Wet samples exhibited an elastic character with a well-defined toe region comparable to the natural ACL. Moreover, they did not show any laxity issue.

7. 3 twisted/braided filaments scaffolds exhibited the highest mechanical properties under shear loading.

8. No significant differences were observed between the diameter of fibre, bundles of fibres and fascicles created and the diameter of collagen fibrils, bundles of fibres and fascicles of the natural ACL.

9. This study demonstrated that the nanofibres were not damaged in the manufacturing process and their diameter and alignment were not modified compared to the 2D electrospun scaffolds.

7. Discussion

The ACL is one of the ligaments with higher injuries rate in professionals and amateurs athletes [1] and the most commonly injured (49%) ligament in the knee [2]. More than 200,000 patients are diagnosed with ACL rupture each year in the United States, of which 175,000 cases require surgery [22]. The high number of surgeries is because this ligament can not regenerate it, due to its ver poor content of fibroblasts. Currently biological and synthetic scaffolds are used for ACL replacements. However, the grafts and ligament implants currently available exhibit a number of different disadvantages that have to be solved to develop the appropriate mobility and stability of the knee. One alternative to the current grafts is to develop tissue-engineered ligaments, avoiding rejection of the implant and providing biological and mechanical properties comparable to the natural ligament.

The overall goal of this project was to create 3D electrospun scaffolds morphologically and mechanically comparable to the native ACL to use as ligament replacements. To achieve that goal, the first step was to analyse ACL *in vivo* mechanical behaviour in order to mimic it and propose improvements for the design of new ligament implants to replace the native ACL. A second step was to evaluate the suitability of two materials to fabricate ligament prototypes through use of the electrospinning technique. Finally, 3D electrospun structures were created and their mechanical behaviour analysed in order to determine the optimum scaffold, achieving the most comparable morphology and mechanical properties (maximum tensile strength, Young's modulus and shear modulus) to the natural ACL.

This Chapter 7 has the objective of providing a general discussion of each study performed with their contribution to knowledge and limitations.

7.1. BIOMECHANICAL SPECIFICATIONS FOR DESIGNING ACL IMPLANTS

The mechanical behaviour of the ACL has been studied through many techniques to date. Some studies used cadaveric knees [40] subjected to different loads but these studies exhibited limitations mimicking the *in vivo* mechanical behaviour of the ACL. Other techniques used video and motion capture [70], [71] to understand ACL injury mechanisms; these techniques studied the joint kinematics, however ACL length, strain or force were not addressed. Some studies calculated the *in vitro* ACL strain [72] and *in vivo* ACL strain during cycling and squatting [73], [74] using strain gauges, but this technique requires surgery to implant the gauge and only records the strain in small locations not across the whole ligament. Other techniques used motion capture and biplanar fluoroscopy [75], [76] and motion capture and musculoskeletal simulations [77]–[79] to determine ACL length and strain during walking and jumping with both legs but activities with a high injury rates such as jumping with one leg or cutting have not been evaluated.

There are discrepancies in the results calculating *in vivo* ACL strain and force because of the different techniques and their limitations. For instance, some studies reported ACL forces of 0.2 N/BW [102] during walking and other researchers

with the same task reported 1 N/BW [103], [104]. Therefore, in order to compare between activities and to have mechanical specifications to design ACL ligaments, it was necessary to build a novel, reliable, reproducible and easy methodology to investigate the *in vivo* mechanical behaviour of the ACL during different activities in just one study.

Moreover, the mechanical characterization of tissue engineered ligament implants are based on tensile loading and the calculation of Young's modulus, ultimate tensile strain or tensile stress at yield. Up to now, no ligament implants have been designed considering shear loading; however, it was demonstrated in Chapter 3 that ACL failure mechanisms are due to multidirectional loading and not solely tensile loading; therefore, the current ACL implants are not designed to bear multi-planar loading and consequently do not guarantee to bear the real loading in all space planes that the native ligament does. Moreover, the *in vivo* mechanical behaviour of the ACL had not been considered for the design and development of new ligament implants. Therefore the design of the current ligament implants is not focussed on replicating the *in vivo* mechanical behaviour, and consequently the current ACL implants cannot accurately reproduce the *in vivo* mechanical behaviour of the ACL .

7.1.1. CONTRIBUTIONS TO KNOWLEDGE IN THE FIELD

The gait analysis studies showed a novel method to evaluate the *in vivo* ACL length, tensile forces, strain and knee angles during 7 activities (climbing stairs, jumping with maximum effort, run, crossover cutting, sidestep cutting, walking and jumping with one leg), and allowed the comparison of those values between the

different activities. This was a significant advancement because, as was explained previously, the wide range of techniques available to determine those parameters and the limitations associated with the techniques, produced large variations in the results for the same activity; therefore, the comparison between activities with different calculation methods was invalid.

Nowadays all ligament implants are solely mechanically characterized under tensile loading; however, this study indicated that ACL failure mechanisms are due to a combination of loads. Therefore, in order to mimic the mechanical behaviour of the ACL it is necessary to understand the performance under tensile, shear and torsional loading. This study is the first that emphasized the importance of multidirectional loading of the ACL to develop implants that can bear the accurate loading of the natural ACL. Therefore, to create more accurate biomimetic implants it is necessary to change the standard procedure for the design of this ligament.

In this PhD, the manufactured ACL prototypes were not solely assessed under cyclic tensile loading but under cyclic shear loading and in dry and wet conditions, to ensure that the prototypes can bear the same loading and under the same conditions as the natural ACL.

Two further improvements have been made compared to other gait studies in the field. The first improvement was related to the degrees of freedom of the knee model. Most of the studies considered the knee as a 1DOF joint [75], [76]; however, a 3DOF knee model was developed in this thesis. This model was able to determine the angles not only in the sagittal plane but also in the axial and coronal planes,

contributing to calculating the length of ligament more accurately. In certain studies [260] the location of the insertion points of the ACL, the scale of the model and therefore the measurement of the ACL length are incorrect. However, the configuration of the scale tool, the placement of the insertion points and the measurement of the ACL length have been meticulously studied in this project and the results verified from literature, as shown in Chapter 3.

The 3DOF knee model developed in this study could help not only to design biomimetic ligament implants (since this model allows us to know the *in vivo* mechanical behaviour of the ACL and therefore the strain and forces during different tasks), but to prevent injury risks (since it calculates the *in vivo* ACL loading and can identify the activities with high risks of injury), improve rehabilitation protocols (recognising the activities or exercises that can strengthen certain muscles to enhance the stability of the knee without overloading the ACL), study graft insertion points in order to reduce failure rates (since the behaviour of the ACL graft against different locations of its insertion points can be studied with the model and the placement optimised), or design ligaments according to patient's needs (since it was proved that age and gender affects the ACL loading, therefore requiring the ACL graft to bear different loads).

The novelty of this study was the development of a methodology to calculate *in vivo* ACL length, strain and tensile forces during different dynamic activities, in order to be able to design and manufacture biomimetic ACL grafts. These grafts can replicate the *in vivo* mechanical behaviour and so bear the same loading as the natural ACL. This methodology is a great step forward in the field, since to date no

studies have been performed to create scaffolds that can mimic the *in vivo* loading and can bear the multi-planar loading of the natural ACL.

7.1.2. LIMITATIONS

Some limitations are linked to this methodology. The first limitation is the assumption of having 3 DOF per knee instead of 6 DOF. However, the translations of the knee joint in the model are negligible compared to the angles in the knee, therefore these displacements do not significantly affect the accuracy of the results. Moreover, the use of these 3DOF is easier and less time consuming than working with a 6DOF knee model and therefore more useful to study the *in vivo* mechanical behaviour of the ACL in other activities.

The second limitation is associated with the fact that the ACL tensile forces were calculated from the ACL strain and this in turn was calculated by tracking the coordinates of the ACL insertion points and considering the ACL as a single straight bundle; however, it is known that the fibre bundles of the ACL are twisted and wrapped around the bones. This study evaluated the ACL length, strain and force for healthy ACLs with no issues of laxity in order to be able to mimic this behaviour in new grafts; therefore, the length for the twisted bundles of the ligament is negligible compared to the length between the insertion points of the ligament, moreover the final 3D structures created showed twisted bundles mimicking the nano and micro morphology of the natural ligament, consequently this assumption did not contribute significantly to the accuracy of the results.

The third limitation is related to the calculation of the unloaded length of the ACL. This value is unknown, since the only way to measure it is to remove the ACL from the participants of the study, and therefore it was calculated from well-established reference lengths and strains [308]. In modelling, there are always some assumptions that are needed in order to achieve an outcome.

7.2. SUITABILITY OF GELATIN ELECTROSPUN SCAFFOLDS IN THE DEVELOPMENT OF LIGAMENT IMPLANTS UNDER A MORPHOLOGICAL, TOPOGRAPHICAL AND MECHANICAL PERSPECTIVE

Gelatin has been used for many applications such as pharmaceutical, biomedical or food packaging [304], [307]–[310], [312] due to its low cost, biodegradability, non-toxicity and biocompatibility. Moreover, gelatin is a natural polymer derivated from collagen; therefore, this polymer seems to be ideal to mimic the mechanical and biological properties of the collagen, the most abundant protein of the extracellular matrix of the soft tissue and specifically ligaments.

Although this polymer is commonly used, it has shown three main disadvantages for the manufacturing of ligament implants through the electrospinning technique and its subsequent implantation in the body. The first disadvantage is the difficulty of working with electrospun aqueous gelatin solutions at room temperature [215], [266], due to the tendency of gelatin solutions to jell at temperature below 30ºC preventing the solution from flowing properly through the

needle. The second disadvantage is related to its high degradation rate; this polymer dissolves in biological medium in a few hours, complicating its biological characterization and use as an implant. The third disadvantage is its poor mechanical properties with low tensile stress and strain at break.

However, all of these disadvantages can be addressed to enhance its use for tissue engineering applications. To date, no studies have focussed on the optimisation of process and solution parameters to face these problems and so produce gelatin electrospun scaffolds more comparable to the natural ACL. Currently, electrospun gelatin scaffolds have been developed for wound healing applications [282], [283], nerve [284]–[286], dental [287], bone [288]–[291] and skin tissue [292], [293], tendon [294] and vascular grafts [295]. However, no studies of electrospun gelatin scaffolds have been performed with the purpose of manufacturing ligament implants. Moreover, the electrospun gelatin scaffolds performed for tendon replacements did not reach the mechanical strength needed for their application and they were far from obtaining values comparable to those exhibited for the ACL.

7.2.1. CONTRIBUTIONS TO KNOWLEDGE IN THE FIELD

The aim of this work was to evaluate the suitability of gelatin electrospun scaffolds for use as ACL tissue engineered implants.

This study has a number of different novelties. The first novelty was the aim of the study itself, to evaluate the suitability of gelatin electrospun scaffolds for use as ACL replacements. This polymer has been studied for other applications but never

for ACL implants. The second novelty was to optimise the process and solution parameters to obtain a scaffold with the morphology, topography and mechanical properties more comparable to the native ACL, in order to create biomimetic ACL grafts. To that end, the study of how the solvent concentration affected the mechanical, morphological and topographical properties of the gelatin scaffolds was performed. The final novelty lay in the understanding of how the use of a crosslinking agent changes the morphology of the nanofibres and their network, and how this affects the suitability of this polymer to constitute ACL grafts.

Moreover, the optimised scaffolds developed in this thesis demostrated mechanical properties significantly higher than the electrospun studies reported for tendon applications, demonstrating the importance of optimise in both solution and process parameters. As an example, the scaffolds created in this study (Chapter 4) reached maximum tensile strength of 4.6 MPa, however the maximum tensile strength, with the same polymer (gelatin), reported for tendon replacement was 1 MPa [294].

Another positive outcome from this study was that it showed that gelatin is not suitable to be used as the sole polymer for the manufacture of ACL implants even after being optimised. This finding increased knowledge of the mechanical limitations of gelatin and moves the field forward to investigate other alternative polymers for new ACL prototypes.

7.2.2. LIMITATIONS

Gelatin electrospun scaffolds exhibited low mechanical properties. After the process and the solution parameters were optimised, a maximum average tensile strength of 4±1 MPa and 2 % of strain at break were recorded. Those values were significantly lower than native ACL that showed 38 MPa of maximum tensile strength and 44 % of strain at break.

Moreover, the morphology and topography of gelatin scaffolds were modified after performing a degradation study, demonstrating that gelatin electrospun scaffolds are not stable enough to performe cell tests

However, they allow better understanding of the mechanical behaviour and degradation process for use of gelatin in other possible applications and move the field forward to research another alternative polymer that can achieve the properties needed for consideration in the development of ACL replacements.

7.3. SUITABILITY OF POLYVINYL ALCOHOL (PVA) IN THE MANUFACTURING OF ELECTROSPUN TISSUE ENGINEERED LIGAMENT IMPLANTS: MORPHOLOGICAL, TOPOGRAPHICAL AND MECHANICAL STUDY

PVA is an expensive, biocompatible, hydrophilic, biodegradable and nontoxic polymer [65], [217]–[219]. Besides, this polymer is easily electrospinnable, able to be diluted in water and to produce nanofibres free of defects. All these

characteristics enable PVA to be used as a baseline for experiments with other materials.

Previous studies have been performed to understand how the process and solution parameters affected the morphology of the scaffold [217], [218]; however, none of them studied how these factors influence the mechanical properties of the scaffolds, nor optimised these parameters to achieve the properties needed for an specific application. Chapter 5 studied the optimisation of solution and process parameters to create biomimetic ACL prototypes with morphology and mechanical behaviour comparable to the natural ACL; moreover, the degradation of the optimum scaffold was also evaluated.

A number of studies demonstrated that crosslinked PVA hydrogels exhibited excellent biocompatibility [336], a water-swollen network similar to the extracellular matrix of the native ligament [65] and in combination with ultrahigh molecular weight polyethylene (UHMWPE) can produce an appropriate mechanical performance comparable to the natural ACL [65]. However, its use as electrospun scaffolds and as a potential sole material for ligament implants still has to be proved mechanically and morphologically.

7.3.1. CONTRIBUTIONS TO KNOWLEDGE IN THE FIELD

Electrospinning is commonly known as a technique that produces scaffolds with low mechanical properties. However, this study proved that through optimising the process and solution parameters the production of implants with morphology and

mechanical properties comparable to the native soft tissue is possible. This is the first time that a progressive optimisation process has been performed for any electrospun polymer with the aim of achieving mechanical and morphological properties that mimics the desired biological tissue (i.e. ligaments).

Chapter 5 studied and proved for the first time the suitability of PVA electrospun scaffolds to be used for the manufacture of ACL grafts, reporting excellent values of maximum tensile strength (30 ± 1 MPa) comparable to 38 MPa exhibited in the native ACL [48], and an unaltered topography after being exposed to 25% GTA and left for 28 days of incubation in PBS. Moreover, the scaffolds showed values of fibre diameter between 120 and 140 nm comparable to the values of the collagen fibrils in the extracellular matrix.

Therefore, this study demonstrated that PVA scaffolds exhibited excellent mechanical and morphological properties to be used for the manufacturing of ACL implants and they were the baseline to produce 3D structures, moving the field forward towards the goal of creating biomimetic ACL prototypes.

7.3.2. LIMITATIONS

The main limitation was not to have evaluated the scaffolds biologically. However, the history of good biocompatibility of PVA in biomedical applications such as wound healing, tissue engineered bone, skin or vascular tissue [65], [217]–[219], [309], [318], [320], [323], [326], [327], [329], [330] and the fact that the scaffolds mimic the morphology of the extracellular matrix of the ACL, provide

good expectations about cell growth on the created scaffolds. As described in the future work section (section 7.5.), the cells proliferation and the capacity of cell to create extracellular matrix will be evaluated in further experiments.

The other limitation of this study was the difficulty of measuring PVA electrospun fibres after the degradation study. Although the topography of the scaffolds was proved to be unmodified and the nanofibres maintained imitation of the extracellular matrix during the incubation time, the morphology of the scaffolds was difficult to characterize after being immersed in PBS. This phenomenon may be due to the fact that PVA is a high hydrophilic polymer that could keep the water inside the fibre network even after 24 hours of being dried in a fume hood and so complicating scaffold visualization with SEM. However, as was reported in Chapter 5, 20 measurements (per sample) of fibre diameter were performed after 1 and 28 days of being immersed in PBS, producing fibres diameter of 461 ± 4 nm and 453 ± 3 nm respectively. These values showed a swelling of the nanofibres, however the cell behaviour would not be compromised, since previous studies reported excellent cell adhesion and proliferation with values of fibre diameter between 379.14±37 nm and 524±31 nm [324]. Moreover, to have water-swollen nanofibres network is not a limitation itself, given that similar behaviour was observed with the collagen of the extracellular matrix of the native ligament [65]. Moreover, it was widely reported that aspects such as cellular adhesion, movement or orientation, critical to develop ligament implants that require aligned fibroblasts along the scaffold, is significantly dependent on the type and size of the surface topography [379], and this remain similar after the degradation study. Further research must be done into increasing the incubation periods in order to evaluate the lifespan of the scaffold.

7.4. EVALUATION OF 2D AND 3D PVA STRUCTURES

Currently 90% of ACL replacements are made from autografts [184]; however, this technique shows disadvantages such as muscle weakness at the donor site, graft site morbidity, knee pain, infection, loss of sensitivity due to nerve damage and long operation and rehabilitation time.

Allografts and xenografts also exhibit drawbacks associated with the possibility of transmitting diseases and risk of immunogenic response, limitations in the availability of donor tissue and difficulties with the sterilization of the graft.

Commercial synthetic ligament implants have the advantage of eliminating issues such as donor site morbidity, transfer of diseases and long operation times. However, implants such as Gore-Tex, Dacron or LARS have shown poor biocompatibility causing infection and synovitis and although they exhibit good mechanical behaviour in the short-term, they failed in the long-term due to an increase of the laxity, stiffness, mechanical failure and rerupture of the graft [25], [28].

Tissue engineered implants aim to eliminate all the disadvantageous characteristics of synthetic commercial grafts allowing cell growth on them, biodegrading the polymer at the same time as new ligamentous tissue is created and mimicking the mechanical properties of the natural ACL.

The idea of developing electrospun tissue engineered ligament implants lies in the possibility of reproducing the extracellular matrix through the electrospinning technique eliminating all issues caused by autografts, allografts, xenografts and current commercial ACL implants shown above.

7.4.1. CONTRIBUTIONS TO KNOWLEDGE IN THE FIELD

This study evaluated and compared for the first time 2D and multiple 3D electrospun structures with the goal of determining which structure reproduces more faithfully the functionality of the natural ACL in dry and wet environments and under tensile and shear loading.

Some studies with individual twisted electrospun scaffolds have previously been performed [263], [347], [355], [380], however this study is the first that compares between different structures (2D structures, 3D structures such as 1 twisted filament, 3 twisted filaments and 3 twisted/braided filaments) under cyclic tensile and shear loading and in wet and dry environments.

This study stablished the fundaments to evaluate the new implants under shear load, implementing a novel and easy methodology to test the scaffolds under these loading mechanisms. This novel methodology is a step forward for testing new implants and ligaments contributing to the design and evaluation of new ACL implants.

Moreover, neither 2D nor 3D PVA electrospun structures had been studied for ligament replacement previously, therefore the study of those structures was a novelty itself.

Regarding the mechanical results obtained: 3 twisted/braided ligaments scaffolds in dry conditions exhibited a maximum tensile stress of 38 MPa identical to the native ACL [59] and a Young's modulus of 129 MPa comparable to 111 MPa reported for the natural ACL [59]. Moreover, wet samples exhibited an elastic behaviour with a well-defined toe region comparable to the natural ACL and they did not show any laxity issues. 3 twisted/braided filaments scaffolds exhibited the highest mechanical properties under shear loading. Moreover, it was observed that more robust structures exhibited, more consistent mechanical properties than thinner structures, a finding not previously reported in the field.

Analysing the morphology of the scaffolds: no significant differences were observed between the diameter of fibres, bundle of fibres and fascicles created and the diameter of collagen fibrils, bundle of fibres and fascicles of the natural ACL. Moreover, this study demonstrated that the nanofibres were not damaged in the manufacturing process and their diameter and alignment were not modified compared to the 2D electrospun scaffolds.

7.4.2. LIMITATIONS

Electrospun PVA scaffolds showed excellent morphology and mechanical properties (Young's modulus and maximum tensile stress) comparable to the native ACL and better than the other four comparable studies performed in the field [263], [347], [355], [380]. However, a plastic behaviour was observed in the scaffolds created, potentially causing laxity issues once the scaffold was implanted in the knee.

Wet PVA scaffolds behaved elastically, they do not exhibit any laxity issues and all of them showed a well-defined toe region comparable to the natural ACL. However, the mechanical properties of wet samples are lower than in dry conditions. Part of these low results is due to the grip technique, since the clamp caused high stress concentrations near to the lower grip and all samples tested in a wet environment failed near to the clamp. Further investigation is needed to produce an improved gripping technique for elastic polymers to obtain more accurate and reproducible results.

A great step forward in the field has been achieved in testing the electrospun scaffolds under tensile and shear loading; however to test the samples under torsion is extremely challenging and is beyond the scope of many facilities, for these reasons the scaffolds produced during this thesis were not tested under torsion. Future studies must address the *in vivo* shear and torsion of the ligament and develop techniques to test ligament implants under torsion, as was explained in the first study (Chapter 3), in that ACL failure mechanisms are likely due to a combination of multidirectional

loads. Therefore new ACL implants should be designed to bear different loading mechanisms, not solely tensile loading as currently happens.

The last limitation is related to the manual fabrication technique. All samples were braided or twisted manually; therefore, they were not as homogeneous as they could be if they had been manufactured with automated braiding or twisting machines. However, 3D scaffolds showed a standard deviation and standard error of the mean for Young's modulus and maximum tensile strength significantly lower than 2D scaffolds, demonstrating that more robust samples (3D structures) exhibited more consistent and reproducible mechanical properties than 2D structures, and therefore the manual manufacturing technique contributed positively to the mechanical reproducibility of the scaffolds.

The next section (section 7.2) will show the further work needed to create a tissue-engineered ACL graft suitable to be implanted.

7.5. FUTURE PERSPECTIVES

Further work must be performed before the tissue-engineered scaffolds developed in this thesis could move forward towards eventual clinical use. The most important future studies are presented below:

a) From the biomechanical study, it was demonstrated that failure mechanisms are due to multidirectional loading. Therefore, the first step

would be to calculate the *in vivo* shear force and torsion of the ACL to be able to design ACL implants that could bear those values; this has not been investigated in the literature to date. Some initial calculations of the shear force have been performed following the expression: $F = G*\theta/S$. Where G is the shear modulus (G = 45 MPa [346]), θ the abduction/adduction angle in radians and S the cross sectional area of the ligament (S = 29.2 mm^2 [41]). Appling this equation to each participant and each activity, the following maximum shear force for men, women and the average between them were obtained (Figure 7.1).

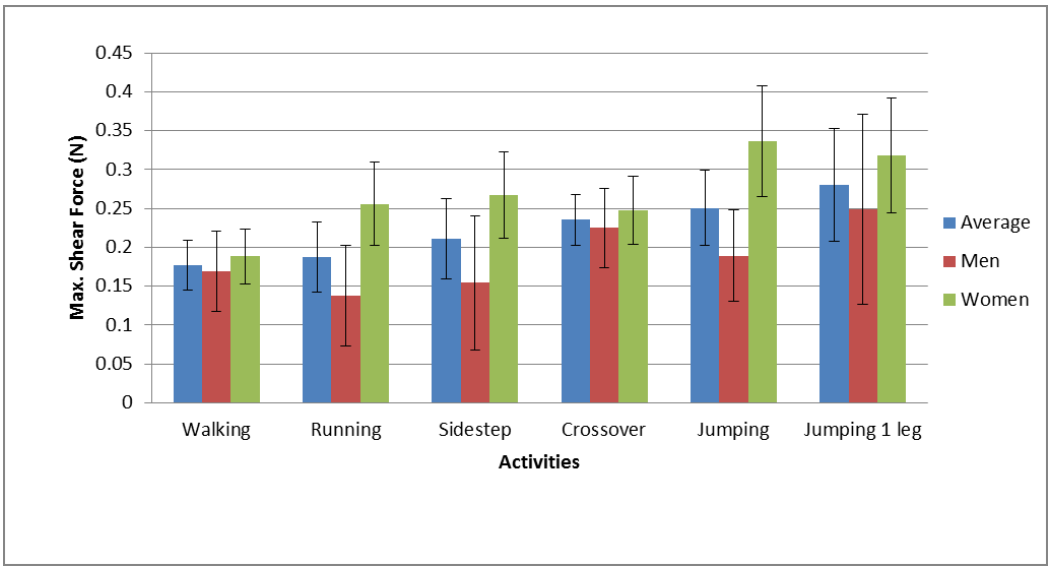

Figure 7.1 Maximum shear force for men, women and the average between them.

Some calculations of the torsion were also performed following the expression: $T = G*\theta*J/L$. Where T is the torque, G is the shear modulus (45 MPa [346]), θ the rotation angle in radians, J polar moment of inertia ($J = \pi*d^4/32$, with d = 6.1 mm diameter of the ACL) and L the length of the ligament. Applying this last equation to each participant and each activity, the

maximum torque in Nmm for women, men and the average between both while they were performing the different activities were obtained (Figure 7.2).

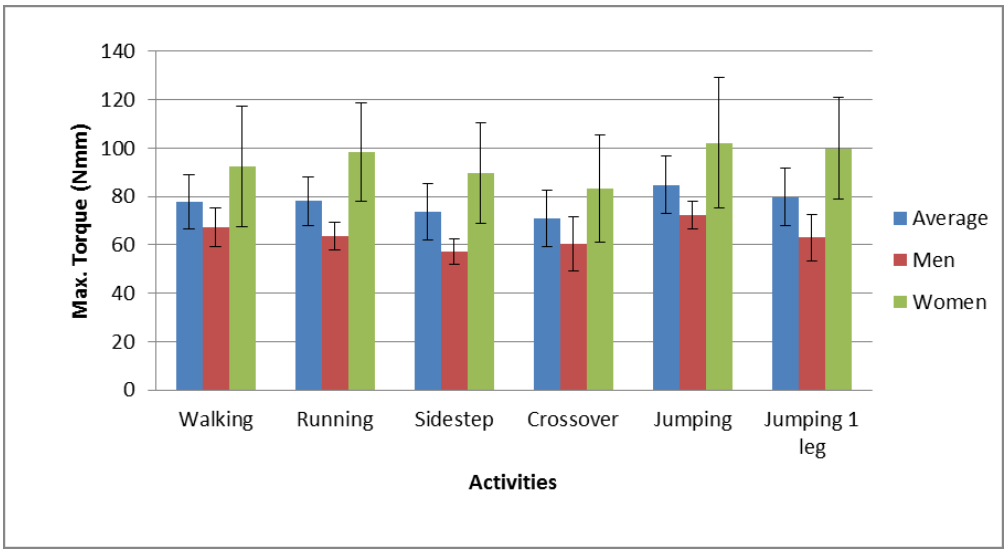

Figure 7.2 Maximum torsion for men, women and the average between them.

Although some initial calculations have been done, a more accurate model should be developed based on finite elements analysis, since these initial estimations cannot faithfully simulate the mechanical behaviour for large deformations that any biological soft tissue exhibits.

b) Once the mechanical specifications for shear and torsion are determined, the scaffolds must be tested under torsion to compare the results with the estimated values. The methodology to test the samples under shear has been explained in Chapter 6; however, how to test the samples under torsion has to be studied. This study will allow the design, manufacture and

testing of ACL implants with comparable mechanical properties to the natural ACL.

c) The mechanical properties of wet PVA samples were lower than the mechanical properties of the ACL. Therefore, another polymer or a composition of several polymers must be studied to reach the same mechanical behaviour as the natural ACL in wet conditions. Moreover, all wet samples failed due to the high stress concentration caused by the clamps, therefore different gripping techniques for elastic polymers must be studied.

d) Once the mechanical properties are achieved, biological characterization of the scaffold has to be performed, evaluating aspects such as cellular viability and morphology, cellular adhesion, cellular proliferation, the capacity of the seeded fibroblast to produce collagen and generate the new extracellular matrix, and cell migration. This step would be essential in the development of a future tissue engineered ACL implant.

e) Aspects such as degradation rate, lifespan of the implant and behaviour under fatigue must also be considerated before any animal trails are performed. These topics have been initially studied during this thesis with degradation assays of 28 days and 10 tensile and shear loading cycles; however, a degradation assay longer than 28 days calculating the degradation rate and the evaluation of loading cycles until failure would be necessary to determine the life cycle of the scaffold and its suitability to be implanted.

f) Further studies will be focussed on the fixation of the implant in animal and subsequently human knees and their recovery process. These first steps would be necessary for its development: to perform a literature review of all fixation methods currently available with their advantages and disadvantages; study the healing process and how to promote osteosyntesis at the ligament enthesis; investigate the operative procedure for implantation; evaluate the use of sutures and the prevention of high stree concentrations; finally implant the graft in an animal model and test its mechanical and biological behaviour.

8. Conclusion

The ACL presents the highest ligament injury rates in both recreational and professional athletes. Currently the gold standard for ACL reconstruction is using autografts; however this technique exhibits deficiencies such as muscle weakness at the donor site and graft site morbidity, therefore other alternatives must be studied.

This PhD aims to produce proof of concept for the design and manufacture of 3D electrospun prototypes with comparable mechanical properties and morphology to native ACL. In order to achieve this goal a literature review was first done with a description of the ligament and current implants. An *in vivo* mechanical study of the ACL was then performed to obtain the mechanical specifications, necessary for the scaffold design. The next step was to assess the suitability of a biological and a synthetic polymer to be used as ACL replacements. Finally, once one of the polymers was determined to have potential for use as ligament implants, different 3D structures were evaluated to obtain a prototype with comparable morphological and mechanical properties to the natural ACL.

From the biomechanical study, a novel methodology to calculate the *in vivo* ACL length and tensile forces during different dynamic activities was established. It was proved that significant differences between genders and ages exists, with the force experienced by the women's ACL significantly higher compared to men's and the ACL tensile force in aged people significantly higher compared to young people. Moreover, novel regression models for ACL lengths with respect to knee angles for

the different activities were calculated enabling prediction of the mechanical behaviour of the ligament. One of the most unexpected and relevant findings in this study was that peak tensile ACL force during cutting or running was lower than walking; this determined that failure mechanisms are due to multidirectional (including shear and torsion) loading instead of simply tensile loading. Therefore, future implants have to be designed and tested to bear multidirectional forces, not solely tensile loads as for current ACL implants.

The electrospinning technique was selected to create the scaffolds for this thesis, due to this manufacturing process best mimicking the morphology of the extracellular matrix of soft tissue. Gelatin and PVA were studied for their great potential for manufacturing ligament implants, because both are inexpensive, nontoxic, biocompatible, biodegradable and easy to electrospin. Moreover, these polymers have never been investigated or used as electrospun structures for the manufacture of ligament implants.

From the study of gelatin electrospun scaffolds, it was concluded that the solvents and their concentrations significantly affected the morphology, topography and mechanical behaviour of the scaffolds. Therefore, it is necessary to optimise the solution and process parameters to be able to replicate the morphology, topography and mechanical properties of the natural ACL. This step is essential and it is not reported in the literature related to development of tendon/ligament electrospun implants. The diameter of the fibres and inter-fibre separations increased when the solvent concentration increased and the roughness decreased when the concentration of DMSO increased. Once the solvent concentration was optimised, a maximum

average tensile strength of 4 ±1 MPa and 2 % of strain at break was recorded, these values being much lower than native ACL. Moreover, after performing a degradation study a modification of the original morphology of the scaffold was observed. Therefore, this study demonstrated that gelatin is not suitable to be used as the sole polymer for the manufacturing of ACL implants, which increases the knowledge of the mechanical limitations of gelatin and moves the field forward to investigate other alternative polymers for new ACL prototypes.

The suitability of PVA electrospun scaffolds to be used as ACL implants was also assessed. This study was focussed on the optimisation of the process to manufacture scaffolds with morphology and mechanical strength comparable to the native ligament. Crosslinked scaffolds exhibited a maximum tensile strength of 30 ± 1 MPa, a value very close to the maximum tensile strength of the native ACL (approx. 38 MPa). Moreover, scaffolds exposed to 25% GTA remained undegraded and with an intact topography after 28 days of incubation in PBS. Therefore, after having fully characterised the PVA scaffolds, it can be concluded that these scaffolds produced better behaviour than that previously investigated by the field demostrating comparable mechanical properties values as the values for the ACL. Therefore, it was shown that PVA electrospun scaffolds are suitable for the development of ligament implants and so could form the baseline to produce 3D structures.

Finally, 2D and 3D electrospun scaffolds were studied to determine which structure was the most suitable for an ACL replacement. Only 4 researchers had previously focussed on 3D electrospun scaffolds; however, non of them compared multiple structures mechanically and morphologically and they were far from achieving mechanical properties comparable to the natural ACL. The results from

Chapter 6 revealed that the 3 twisted/braided filaments crosslinked structure provided a maximum tensile stress of 38 ± 3 MPa and a Young's modulus after 10 loading cycles of 148 ± 13 MPa in dry conditions. This was shown to be the structure with the mechanical properties closest to the natural ACL (38 MPa of maximum tensile stress and 111 MPa Young's modulus). Wet PVA scaffolds exhibited an elastic mechanical behaviour with a well-defined toe region, as appears in the natural ACL. However, the maximum tensile stress and Young's modulus after 10 loading cycles dropped to 9 ± 1 MPa and 24 ± 4 MPa respectively. Although these values are lower than values of the natural ACL, they are higher than the values reported by other researchers in the field. After shear tests, the 3 twisted/braided filaments crosslinked structure was found to exhibit the highest maximum shear stress, allowing the samples to bear higher shear loads than the other structures studied. Due to the lack of previous experiments to quantify this mechanical property, the selection of the 3D structure was based on the similarity of the shear modulus observed in each structure with the value in the natural ACL. The fact that the maximum shear strength and modulus were considered as a design parameter was unique in the field and necessary as was proved in Chapter 3. Analysing the morphology of the 3D scaffolds, it was demonstrated that the manufacturing process did not damage the nanofibres nor their nano-morphology and alignment. Moreover, the dimension of the PVA fibres, bundle of fibres and fascicles agreed with the diameters of the collagen fibrils, fibres and fascicles in the natural ligament. In conclusion and following the findings of this last study, it is recommended that the 3 twisted/braided filaments scaffolds are the most suitable structure to be used as a replacement for the ACL.

This thesis demonstrated that to be able to design and develop ACL implants with mechanical and morphological properties comparable to the natural ACL, it is necessary to consider tensile and shear loading and optimise the solution and process parameters; this was novel and not reported in the literature of the field. Moreover, the suitability of produced electrospun prototypes with excellent mechanical and morphological properties comparable to the natural ACL was demonstrated. 3 twisted/braided filaments scaffolds should be taken for further investigation with cell testing, animal models and finally clinical trials.

Figure 8.1 summarizes the aim, novelties and conclusions of each study performed in this thesis.

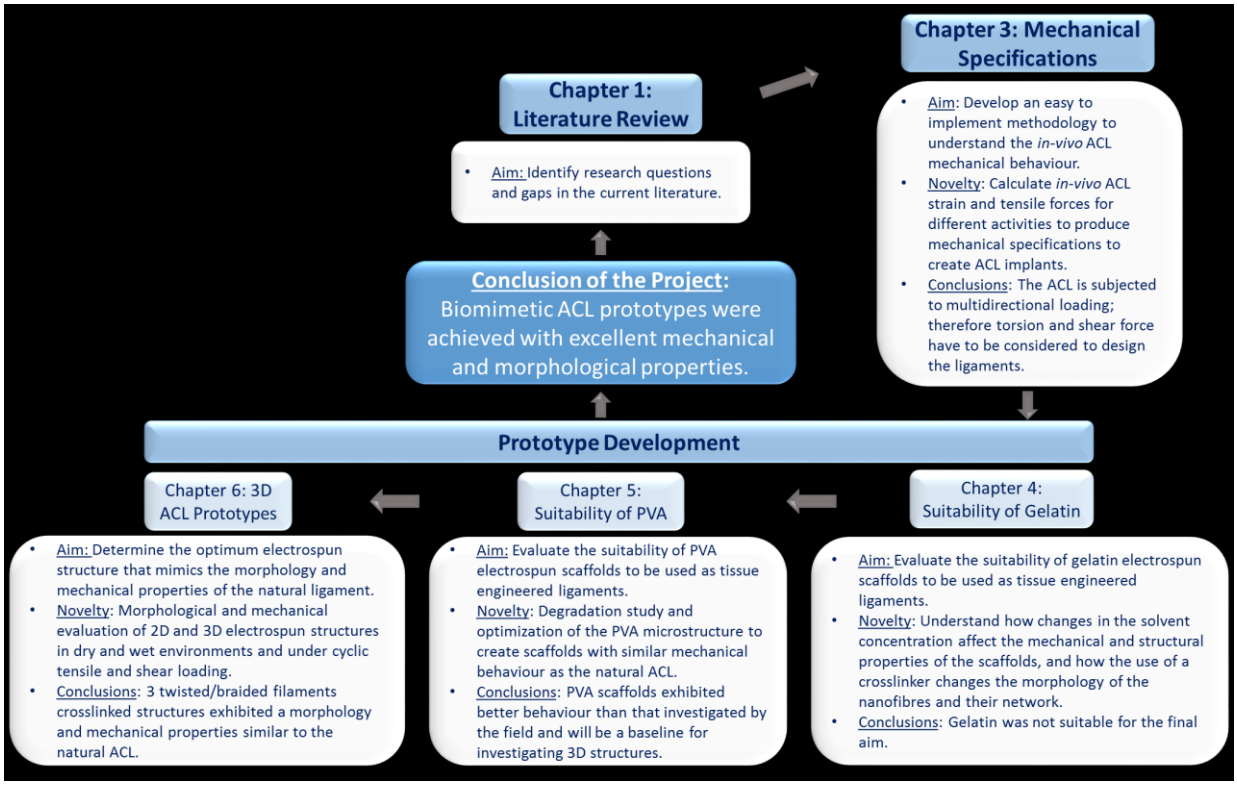

Figure 8.1 Aims, novelties and conclusions of each study performed in this thesis.

9. References

[1] J. Dargel, M. Gotter, K. Mader, D. Pennig, J. Koebke, and R. Schmidt-Wiethoff, 'Biomechanics of the anterior cruciate ligament and implications for surgical reconstruction', *Strateg. Trauma Limb Reconstr.,* vol. 2, no. 1, pp. 1–12, 2007.

[2] 'Synopsis of causation: knee (ligament damage) - GOV.UK'. [Online]. Available: https://www.gov.uk/government/publications/synopsis-of-causation-knee-ligament-damage. [Accessed: 22-Mar-2018].

[3] A. M. Joseph, C. L. Collins, N. M. Henke, E. E. Yard, S. K. Fields, and R. D. Comstock, 'A Multisport Epidemiologic Comparison of Anterior Cruciate Ligament Injuries in High School Athletics', *J. Athl. Train.*, vol. 48, no. 6, pp. 810–817, 2013.

[4] E. Arendt and R. Dick, 'Knee injury patterns among men and women in collegiate basketball and soccer. NCAA data and review of literature', *Am J Sports Med*, vol. 23, no. 6, pp. 694–701, 1995.

[5] T. Nessler, L. Denney, and J. Sampley, 'ACL Injury Prevention: What Does Research Tell Us?' *Curr. Rev. Musculoskelet. Med.*, vol. 10, no. 3, pp. 281–288, 2017.

[6] A. J. Wiggins, R. K. Grandhi, D. K. Schneider, D. Stanfield, K. E. Webster, and G. D. Myer, 'Risk of Secondary Injury in Younger Athletes After Anterior Cruciate Ligament Reconstruction: A Systematic Review and Meta-analysis', *Am. J. Sports Med.*, vol. 44, no. 7, pp. 1861–1876, 2016.

[7] C. M. Rugg, D. Wang, P. Sulzicki, and S. L. Hame, ‘Effects of prior knee surgery on subsequent injury, imaging, and surgery in NCAA collegiate athletes’, *Am. J. Sports Med.*, vol. 42, no. 4, pp. 959–964, 2014.

[8] D. N. Giugliano and J. L. Solomon, ‘ACL tears in female athletes’, *Phys. Med. Rehabil. Clin. N. Am.*, vol. 18, no. 3, pp. 417–438, 2007.

[9] D. Gehring, M. Melnyk, and A. Gollhofer, ‘Gender and fatigue have influence on knee joint control strategies during landing’, *Clin. Biomech. Bristol Avon*, vol. 24, no. 1, pp. 82–87, 2009.

[10] A. P. Toth and F. A. Cordasco, ‘Anterior cruciate ligament injuries in the female athlete’, *J. Gend.-Specif. Med. JGSM Off. J. Partnersh. Womens Health Columbia*, vol. 4, no. 4, pp. 25–34, 2001.

[11] S. Sarafrazi, R. T. B. Abdulah, and M. Amiri-Khorasani, ‘Kinematic analysis of hip and knee angles during landing after imagery in female athletes’, *J. Strength Cond. Res.*, vol. 26, no. 9, pp. 2356–2363, 2012.

[12] S. B. Mountcastle, M. Posner, J. F. Kragh, and D. C. Taylor, ‘Gender differences in anterior cruciate ligament injury vary with activity: epidemiology of anterior cruciate ligament injuries in a young, athletic population’, *Am. J. Sports Med.*, vol. 35, no. 10, pp. 1635–1642, 2007.

[13] M. de Loës, L. J. Dahlstedt, and R. Thomée, ‘A 7-year study on risks and costs of knee injuries in male and female youth participants in 12 sports’, *Scand. J. Med. Sci. Sports*, vol. 10, no. 2, pp. 90–97, 2000.

[14] T. E. Hewett, T. N. Lindenfeld, J. V. Riccobene, and F. R. Noyes, ‘The effect of neuromuscular training on the incidence of knee injury in female athletes. A prospective study’, *Am. J. Sports Med.*, vol. 27, no. 6, pp. 699–706, 1999.

[15] L. J. DiStefano, D. A. Padua, M. J. DiStefano, and S. W. Marshall, 'Influence of age, sex, technique, and exercise program on movement patterns after an anterior cruciate ligament injury prevention program in youth soccer players', *Am. J. Sports Med.*, vol. 37, no. 3, pp. 495–505, 2009.

[16] M. R. Hutchinson and M. L. Ireland, 'Knee injuries in female athletes', *Sports Med. Auckl. NZ*, vol. 19, no. 4, pp. 288–302, 1995.

[17] J. Agel, E. A. Arendt, and B. Bershadsky, 'Anterior cruciate ligament injury in national collegiate athletic association basketball and soccer: a 13-year review', *Am J Sports Med*, vol. 33, no. 4, pp. 524–530, 2005.

[18] J. G. Ingram, S. K. Fields, E. E. Yard, and R. D. Comstock, 'Epidemiology of knee injuries among boys and girls in US high school athletics', *Am. J. Sports Med.*, vol. 36, no. 6, pp. 1116–1122, 2008.

[19] 'New device could revolutionise major knee surgery | News | The University of Aberdeen'. [Online]. Available: https://www.abdn.ac.uk/news/4068/. [Accessed: 15-Mar-2018].

[20] Miller RH, *Knee injuries*, In: Canale ST, Editor. Campbell's Operative Orthopaedics. 10th ed. London: Mosby. 2003.

[21] 'How much does a private cruciate knee ligament surgery cost in the UK? Private Healthcare UK'. [Online]. Available:https://www.privatehealth.co.uk/conditions-and-treatments/cruciate-knee-ligament-surgery/costs/. [Accessed: 15 Mar. 2018].

[22] N. L. Leong, F. A. Petrigliano, and D. R. McAllister, 'Current tissue engineering strategies in anterior cruciate ligament reconstruction', *J Biomed Mater Res A*, vol. 102, no. 5, pp. 1614–1624, 2014.

[23] S. Lyman, P. Koulouvaris, S. Sherman, H. Do, L. A. Mandl, and R. G. Marx, 'Epidemiology of anterior cruciate ligament reconstruction: trends, readmissions, and subsequent knee surgery', *J. Bone Joint Surg. Am.*, vol. 91, no. 10, pp. 2321–2328, 2009.

[24] L. T. Buller, M. J. Best, M. G. Baraga, and L. D. Kaplan, 'Trends in Anterior Cruciate Ligament Reconstruction in the United States', *Orthop. J. Sports Med.*, vol. 3, no. 1, 2014.

[25] Aranque MC, *Desarrollo de una prótesis regenerativa de tendón*, Universidad Politécnica de Valencia, 2013.

[26] K. R. Stone, U. M. Abdel-Motal, A. W. Walgenbach, T. J. Turek, and U. Galili, 'Replacement of human anterior cruciate ligaments with pig ligaments: a model for anti-non-gal antibody response in long-term xenotransplantation', *Transplantation*, vol. 83, no. 2, pp. 211–219, 2007.

[27] S. Zaffagnini, A. Grassi, G. M. Marcheggiani Muccioli, T. Roberti Di Sarsina, F. Raggi, A. Benzi, M. Marcacci, 'Anterior cruciate ligament reconstruction with a novel porcine xenograft: the initial Italian experience', *Joints*, vol. 3, no. 2, pp. 85–90, 2015.

[28] J. Chen, J. Xu, A. Wang, and M. Zheng, 'Scaffolds for tendon and ligament repair: review of the efficacy of commercial products', *Expert Rev Med Devices*, vol. 6, no. 1, pp. 61–73, 2009.

[29] S. Rathbone, N. Maffulli, and S. H. Cartmell, 'Most British Surgeons Would Consider Using a Tissue-Engineered Anterior Cruciate Ligament: A Questionnaire Study', *Stem Cells Int.*, vol. 2012, 2012.

[30] 'Patel Hospital'. [Online]. Available: http://www.patelhospital.co.in/articles. [Accessed: 22 Mar. 2018].

[31] J. K. Lee, S. Lee, S. C. Seong, and M. C. Lee, 'Anatomy of the anterior cruciate ligament insertion sites: comparison of plain radiography and three-dimensional computed tomographic imaging to anatomic dissection', Knee Surg Sports Traumatol Arthrosc, vol. 23, no. 8, pp. 2297–2305, 2015.

[32] G. A. Compeán-Martínez, F.Vilchez-Cavazos, C.Acosta-Oscar F. Mendoza-Lemus, O. de la Garza-Castro1, R. I. Guzmán, R. E. Elizondo-Omaña and S. Guzmán López, 'Anthropometric references for reconstruction of the anterior cruciate ligament in the anatomical position', Eur. J. Anat., vol. 17, no. 3, pp. 176–181, 2018.

[33] K. Shino, B. W. Oakes, S. Horibe, K. Nakata, and N. Nakamura, 'Collagen fibril populations in human anterior cruciate ligament allografts. Electron microscopic analysis', *Am. J. Sports Med.*, vol. 23, no. 2, pp. 203–208; discussion 209, 1995.

[34] G. G. Arliani, G.G. Arliani, D.C. Astur, E. R. Moraes, C.C. Kaleka, W. Jalikjian, P. Golano, M. Cohen, 'Three dimensional anatomy of the anterior cruciate ligament: a new approach in anatomical orthopedic studies and a literature review', *Open Access J. Sports Med.*, vol. 3, pp. 183–188, 2012.

[35] C. B. Frank, D. A. Hart, and N. G. Shrive, 'Molecular biology and biomechanics of normal and healing ligaments a review', *Osteoarthritis Cartilage*, vol. 7, no. 1, pp. 130–140, 1999.

[36] C. N. Nagineni, D. Amiel, M. H. Green, M. Berchuck, and W. H. Akeson, 'Characterization of the intrinsic properties of the anterior cruciate and medial collateral ligament cells: an *in vitro* cell culture study', *J. Orthop. Res. Off. Publ. Orthop. Res. Soc.*, vol. 10, no. 4, pp. 465–475, 1992.

[37] D. Amiel, C. N. Nagineni, S. H. Choi, and J. Lee, 'Intrinsic properties of ACL and MCL cells and their responses to growth factors', *Med. Sci. Sports Exerc.*, vol. 27, no. 6, pp. 844–851, 1995.

[38] V. S. Alfonso and F. G. Sancho, 'Anatomía descriptiva y funcional del ligamento cruzado anterior. Implicaciones clínico-quirúrgicas', p. 10, 1992.

[39] 'Anatomic Single- and Double-Bundle Anterior Cruciate Ligament (ACL) Reconstruction| Department of Orthopaedic Surgery | University of Pittsburgh University of Pittsburgh 2011'. [Online]. Available: http://www.orthonet.pitt.edu/content/doublebundle.htm. [Accessed: 01 Sep. 2015].

[40] J. Hashemi, H. Mansouri, N. Chandrashekar, J. R. Slauterbeck, D. M. Hardy, and B. D. Beynnon, 'Age, sex, body anthropometry, and ACL size predict the structural properties of the human anterior cruciate ligament', *J Orthop Res*, vol. 29, no. 7, pp. 993–1001, 2011.

[41] N. Pujol, S. Queinnec, P. Boisrenoult, A. Maqdes, and P. Beaufils, 'Anatomy of the anterior cruciate ligament related to hamstring tendon grafts. A cadaveric study', *Knee*, vol. 20, no. 6, pp. 511–514, 2013.

[42] P. Kannus, 'Structure of the tendon connective tissue', *Scand. J. Med. Sci. Sports*, vol. 10, no. 6, pp. 312–320, 2000.

[43] R. Sandoval, D. A. G. Alvarado, and L. M. P. Cortés, 'Mechanobiology of ligament repair', *Rev. Cuba. Investig. Biomed.*, vol. 29, pp. 155–169, 2010.

[44] S. A. Sell, M. J. McClure, C. E. Ayres, D. G. Simpson, and G. L. Bowlin, 'Preliminary Investigation of Airgap Electrospun Silk-Fibroin-Based Structures for Ligament Analogue Engineering', *J Biomater Sci Polym Ed*, vol. 22, no. 10, pp. 1253–1273, 2010.

[45] H. D. Moeller, U. Bosch, and B. Decker, 'Collagen fibril diameter distribution in patellar tendon autografts after posterior cruciate ligament reconstruction in sheep: changes over time.', *J. Anat.*, vol. 187, no. Pt 1, pp. 161–167, 1995.

[46] S. Bancelin, C. Aimé, I. Gusachenko, L. Kowalczuk, G. Latour, T. Coradin, M. C. Schanne-Klein, 'Determination of collagen fibril size via absolute measurements of second-harmonic generation signals', *Nat. Commun.*, vol. 5, 2014.

[47] R. Strocchi, V. De Pasquale, A. Facchini, M. Raspanti, S. Zaffagnini, and M. Marcacci, 'Age-related changes in human anterior cruciate ligament (ACL) collagen fibrils', *Ital. J. Anat. Embryol. Arch. Ital. Anat. Ed Embriologia*, vol. 101, no. 4, pp. 213–220, 1996.

[48] P. P. Provenzano, D. A. Martinez, R. E. Grindeland, K. W. Dwyer, J. Turner, A. C. Vailas, R. J. Vanderby, 'Hindlimb unloading alters ligament healing', *J. Appl. Physiol. Bethesda Md 1985*, vol. 94, no. 1, pp. 314–324, 2003.

[49] P. Sharma and N. Maffulli, 'Tendon injury and tendinopathy: healing and repair', *J Bone Jt. Surg Am*, vol. 87, no. 1, pp. 187–202, 2005.

[50] R. James, G. Kesturu, G. Balian, and A. B. Chhabra, 'Tendon: biology, biomechanics, repair, growth factors, and evolving treatment options', *J Hand Surg Am*, vol. 33, no. 1, pp. 102–12, 2008.

[51] 'Tendon Healing Mechanobiology | ShoulderDoc by Prof. Lennard Funk'. [Online]. Available: https://www.shoulderdoc.co.uk/article/1029. [Accessed: 22 Mar. 2018].

[52] Calvo B, *Modelado del comportamiento de tejidos biológicos blandos*. Universidad de Zaragoza, 2011.

[53] K. Robi, N. Jakob, K. Matevz, and V. Matjaz, 'The Physiology of Sports Injuries and Repair Processes', *Curr. Issues Sports Exerc. Med.*, 2013.

[54] F. R. Noyes, J. L. DeLucas, and P. J. Torvik, 'Biomechanics of anterior cruciate ligament failure: an analysis of strain-rate sensitivity and mechanisms of failure in primates', *J Bone Jt. Surg Am*, vol. 56, no. 2, pp. 236–253, 1974.

[55] D. L. Butler, E. S. Grood, F. R. Noyes, and R. F. Zernicke, 'Biomechanics of ligaments and tendons', *Exerc. Sport Sci. Rev.*, vol. 6, pp. 125–181, 1978.

[56] 'Cartilage Indentation - Cartilage Bioengineering Laboratory'. [Online]. Available: http://www.me.udel.edu/research_groups/lu/indentation.htm. [Accessed: 22 Mar. 2018].

[57] 'BME 332: Ligament/Tendon Structure-Function'. [Online]. Available: http://www.umich.edu/~bme332/ch10ligten/bme332ligamenttendon.htm. [Accessed: 22 Mar. 2018].

[58] S. L. Woo, J. M. Hollis, D. J. Adams, R. M. Lyon, and S. Takai, 'Tensile properties of the human femur-anterior cruciate ligament-tibia complex. The effects of specimen age and orientation', *Am J Sports Med*, vol. 19, no. 3, pp. 217–225, 1991.

[59] F. R. Noyes and E. S. Grood, 'The strength of the anterior cruciate ligament in humans and Rhesus monkeys', *J Bone Jt. Surg Am*, vol. 58, no. 8, pp. 1074–1082, 1976.

[60] N. Chandrashekar, H. Mansouri, J. Slauterbeck, and J. Hashemi, 'Sex-based differences in the tensile properties of the human anterior cruciate ligament', *J Biomech*, vol. 39, no. 16, pp. 2943–50, 2006.

[61] T. Zhou, P. N. Grimshaw, and C. Jones, ‘A biomechanical investigation of the anteromedial and posterolateral bands of the porcine anterior cruciate ligament’, *Proc. Inst. Mech. Eng. [H]*, vol. 223, no. 6, pp. 767–775, 2009.

[62] S. G. McLean, K. F. Mallett, and E. M. Arruda, ‘Deconstructing the anterior cruciate ligament: what we know and do not know about function, material properties, and injury mechanics’, *J. Biomech. Eng.*, vol. 137, no. 2, 2015.

[63] Z. Ge, F. Yang, J. C. H. Goh, S. Ramakrishna, and E. H. Lee, ‘Biomaterials and scaffolds for ligament tissue engineering’, *J. Biomed. Mater. Res. A*, vol. 77A, no. 3, pp. 639–652, 2006.

[64] T. Blair, *Biomedical Textiles for Orthopaedic and Surgical Applications: Fundamentals, Applications and Tissue Engineering*. Elsevier, 2015.

[65] J. S. Bach, F. Detrez, M. Cherkaoui, S. Cantournet, D. N. Ku, and L. Corté, ‘Hydrogel fibres for ACL prosthesis: Design and mechanical evaluation of PVA and PVA/UHMWPE fibre constructs’, *J. Biomech.*, vol. 46, no. 8, pp. 1463–1470, 2013.

[66] J. S. Bach, *Design and evaluation of prosthetic anterior cruciate ligament replacement medical device*. Georgia Institute of Technology, 2012.

[67] H. Abe, K. Hayashi, and M. Sato, *Data Book on Mechanical Properties of Living Cells, Tissues, and Organs*. Springer Science & Business Media, 2013.

[68] V. C. Mow, A. Ratcliffe, and S. L.-Y. Woo, *Biomechanics of Diarthrodial Joints*. Springer Science & Business Media, 2012.

[69] S. Nukavarapu, J. Freeman, and C. Laurencin, *Regenerative Engineering of Musculoskeletal Tissues and Interfaces*. Woodhead Publishing, 2015.

[70] T. E. Hewett, J. S. Torg, and B. P. Boden, ‘Video analysis of trunk and knee motion during non-contact anterior cruciate ligament injury in female athletes: lateral

trunk and knee abduction motion are combined components of the injury mechanism', *Br J Sports Med*, vol. 43, no. 6, pp. 417–422, 2009.

[71] T. Krosshaug, A. Nakamae, B. P. Boden, L. Engebretsen, G. Smith, J. R. Slauterbeck, T. E. Hewett, R. Bahr, 'Mechanisms of anterior cruciate ligament injury in basketball: video analysis of 39 cases', *Am J Sports Med*, vol. 35, no. 3, pp. 359–367, 2007.

[72] J. T. Weinhandl, M. C. Hoch, S. Y. Bawab, and S. I. Ringleb, 'Comparison of ACL strain estimated via a data-driven model with *in vitro* measurements', *Comput. Methods Biomech. Biomed. Engin.*, vol. 19, no. 14, pp. 1550–1556, 2016.

[73] B. C. Fleming, B. D. Beynnon, P. A. Renstrom, G. D. Peura, C. E. Nichols, and R. J. Johnson, 'The strain behaviour of the anterior cruciate ligament during bicycling. An *in vivo* study', *Am. J. Sports Med.*, vol. 26, no. 1, pp. 109–118, 1998.

[74] B. D. Beynnon, R. J. Johnson, B. C. Fleming, C. J. Stankewich, P. A. Renström, and C. E. Nichols, 'The Strain Behaviour of the Anterior Cruciate Ligament During Squatting and Active Flexion-Extension: A Comparison of an Open and a Closed Kinetic Chain Exercise', *Am. J. Sports Med.*, vol. 25, no. 6, pp. 823–829, 1997.

[75] K. A. Taylor, H. C. Cutcliffe, R. M. Queen, G. M. Utturkar, C. E. Spritzer, W. E. Garrett, L. E. DeFrate, '*In vivo* measurement of ACL length and relative strain during walking', *J Biomech*, vol. 46, no. 3, pp. 478–483, 2013.

[76] K. A. Taylor, M. E. Terry, G. M. Utturkar, C. E. Spritzer, R. M. Queen, L. A. Irribarra, W. E. Garrett, L. E. DeFrate, 'Measurement of *in vivo* anterior cruciate ligament strain during dynamic jump landing', *J Biomech*, vol. 44, no. 3, pp. 365–371, 2011.

[77] J. Kar and P. M. Quesada, ‘A Musculoskeletal Modeling Approach for Estimating Anterior Cruciate Ligament Strains and Knee Anterior–Posterior Shear Forces in Stop-Jumps Performed by Young Recreational Female Athletes’, *Ann. Biomed. Eng.*, vol. 41, no. 2, pp. 338–348, 2013.

[78] H. Xu, D. Bloswick, and A. Merryweather, ‘An improved OpenSim gait model with multiple degrees of freedom knee joint and knee ligaments’, *Comput Methods Biomech Biomed Engin*, vol. 18, no. 11, pp. 1217–1224, 2015.

[79] K. B. Shelburne, M. R. Torry, and M. G. Pandy, ‘Muscle, ligament, and joint-contact forces at the knee during walking’, *Med Sci Sports Exerc*, vol. 37, no. 11, pp. 1948–1956, 2005.

[80] R. F. Escamilla, G. S. Fleisig, N. Zheng, S. W. Barrentine, K. E. Wilk, and J. R. Andrews, ‘Biomechanics of the knee during closed kinetic chain and open kinetic chain exercises’, *Med. Sci. Sports Exerc.*, vol. 30, no. 4, pp. 556–569, 1998.

[81] R. F. Escamilla, N. Zheng, R. Imamura, T. D. Macleod, W. B. Edwards, A. Hreljac, G. S. Fleisig, K. E. Wilk, C. T. Moorman, J. R. Andrews, ‘Cruciate ligament force during the wall squat and the one-leg squat’, *Med. Sci. Sports Exerc.*, vol. 41, no. 2, pp. 408–417, 2009.

[82] R. F. Escamilla, N. Zheng, T. D. Macleod, R. Imamura, W.B. Edwards, A. Hreljac, G. S. Fleisig, K. E. Wilk, C. T. Moorman, L. Paulos, J. R. Andrews, ‘Cruciate ligament forces between short-step and long-step forward lunge’, *Med. Sci. Sports Exerc.*, vol. 42, no. 10, pp. 1932–1942, 2010.

[83] R. F. Escamilla, N. Zheng, T. D. Macleod, R. Imamura, W.B. Edwards, A. Hreljac, G. S. Fleisig, K. E. Wilk, C. T. Moorman, L. Paulos, J. R. Andrews, ‘Cruciate ligament tensile forces during the forward and side lunge’, *Clin. Biomech. Bristol Avon*, vol. 25, no. 3, pp. 213–221, 2010.

[84] A. Heijne, B. C. Fleming, P. A. Renstrom, G. D. Peura, B. D. Beynnon, and S. Werner, 'Strain on the anterior cruciate ligament during closed kinetic chain exercises', *Med. Sci. Sports Exerc.*, vol. 36, no. 6, pp. 935–941, 2004.

[85] T. Nagura, H. Matsumoto, Y. Kiriyama, A. Chaudhari, and T. P. Andriacchi, 'Tibiofemoral joint contact force in deep knee flexion and its consideration in knee osteoarthritis and joint replacement', *J. Appl. Biomech.*, vol. 22, no. 4, pp. 305–313, 2006.

[86] K. B. Shelburne and M. G. Pandy, 'A dynamic model of the knee and lower limb for simulating rising movements', *Comput. Methods Biomech. Biomed. Engin.*, vol. 5, no. 2, pp. 149–159, 2002.

[87] C. S. Shin, A. M. Chaudhari, and T. P. Andriacchi, 'The influence of deceleration forces on ACL strain during single-leg landing: a simulation study', *J. Biomech.*, vol. 40, no. 5, pp. 1145–1152, 2007.

[88] Y. K. Oh, D. B. Lipps, J. A. Ashton-Miller, and E. M. Wojtys, 'What strains the anterior cruciate ligament during a pivot landing?', *Am. J. Sports Med.*, vol. 40, no. 3, pp. 574–583, 2012.

[89] A. Kanamori, S. L. Woo, C. B. Ma, J. Zeminski, T. W. Rudy, G. Li, G. A. Livesay, 'The forces in the anterior cruciate ligament and knee kinematics during a simulated pivot shift test: A human cadaveric study using robotic technology', *Arthrosc. J. Arthrosc. Relat. Surg. Off. Publ. Arthrosc. Assoc. N. Am. Int. Arthrosc. Assoc.*, vol. 16, no. 6, pp. 633–639, 2000.

[90] H. Fujie, K. Mabuchi, S. L. Woo, G. A. Livesay, S. Arai, and Y. Tsukamoto, 'The use of robotics technology to study human joint kinematics: a new methodology', *J. Biomech. Eng.*, vol. 115, no. 3, pp. 211–217, 1993.

[91] H. Fujie, G. A. Livesay, M. Fujita, and S. L. Woo, 'Forces and moments in six-DOF at the human knee joint: mathematical description for control', *J. Biomech.*, vol. 29, no. 12, pp. 1577–1585, 1996.

[92] H. Fujie, G. A. Livesay, S. L. Woo, S. Kashiwaguchi, and G. Blomstrom, 'The use of a universal force-moment sensor to determine in-situ forces in ligaments: a new methodology', *J. Biomech. Eng.*, vol. 117, no. 1, pp. 1–7, 1995.

[93] S. P. Darcy, R. H. P. Kilger, S. L.-Y. Woo, and R. E. Debski, 'Estimation of ACL forces by reproducing knee kinematics between sets of knees: A novel non-invasive methodology', *J. Biomech.*, vol. 39, no. 13, pp. 2371–2377, 2006.

[94] A. Hosseini, T. J. Gill, S. K. Van de Velde, and G. Li, 'Estimation of *in vivo* ACL force changes in response to increased weightbearing', *J. Biomech. Eng.*, vol. 133, no. 5, 2011.

[95] H. Koga, T. Muneta, R. Bahr, L. Engebretsen, and T. Krosshaug, 'ACL Injury Mechanisms: Lessons Learned from Video Analysis', in *Rotatory Knee Instability*, Springer, Cham, pp. 27–36, 2017.

[96] V. R. Carlson, F. T. Sheehan, and B. P. Boden, 'Video Analysis of Anterior Cruciate Ligament (ACL) Injuries: A Systematic Review', *JBJS Rev.*, vol. 4, no. 11, 2016.

[97] B. P. Boden, J. S. Torg, S. B. Knowles, and T. E. Hewett, 'Video analysis of anterior cruciate ligament injury: abnormalities in hip and ankle kinematics', *Am. J. Sports Med.*, vol. 37, no. 2, pp. 252–259, 2009.

[98] K. B. Shelburne, M. G. Pandy, F. C. Anderson, and M. R. Torry, 'Pattern of anterior cruciate ligament force in normal walking', *J. Biomech.*, vol. 37, no. 6, pp. 797–805, 2004.

[99] N. Zheng, G. S. Fleisig, R. F. Escamilla, and S. W. Barrentine, 'An analytical model of the knee for estimation of internal forces during exercise', *J. Biomech.*, vol. 31, no. 10, pp. 963–967, 1998.

[100] D. E. Toutoungi, T. W. Lu, A. Leardini, F. Catani, and J. J. O'Connor, 'Cruciate ligament forces in the human knee during rehabilitation exercises', *Clin. Biomech. Bristol Avon*, vol. 15, no. 3, pp. 176–187, 2000.

[101] M. A. Pflum, K. B. Shelburne, M. R. Torry, M. J. Decker, and M. G. Pandy, 'Model prediction of anterior cruciate ligament force during drop-landings', *Med. Sci. Sports Exerc.*, vol. 36, no. 11, pp. 1949–1958, 2004.

[102] J. B. Morrison, 'The mechanics of the knee joint in relation to normal walking', *J. Biomech.*, vol. 3, no. 1, pp. 51–61, 1970.

[103] J. J. Collins, 'The redundant nature of locomotor optimisation laws', *J. Biomech.*, vol. 28, no. 3, pp. 251–267, 1995.

[104] J. J. Collins and J. J. O'Connor, 'Muscle-ligament interactions at the knee during walking', *Proc. Inst. Mech. Eng. [H]*, vol. 205, no. 1, pp. 11–18, 1991.

[105] S. L.-Y. Woo, R. E. Debski, A. J. Vangura, J. D. Withrow, T. M. Vogrin, E. K. Wong, F. H. Fu, 'Use of robotic technology to study the biomechanics of ligaments and their replacements', *Oper. Tech. Orthop.*, vol. 10, no. 1, pp. 87–91, 2000.

[106] B. C. Fleming, B. D. Beynnon, P. A. Renstrom, R. J. Johnson, C. E. Nichols, G. D. Peura, B. S. Uh, 'The strain behaviour of the anterior cruciate ligament during stair climbing: an *in vivo* study', *Arthrosc. J. Arthrosc. Relat. Surg. Off. Publ. Arthrosc. Assoc. N. Am. Int. Arthrosc. Assoc.*, vol. 15, no. 2, pp. 185–191, 1999.

[107] 'Documentation home - Documentation home - Documentation | VICON'. [Online]. Available: https://docs.vicon.com/. [Accessed: 21 Mar. 2018].

[108] Trew, M., T, *Measuring and analysing human movement. Everett eds. Human movement*. 5th ed. London: Elsevier Churchill Livingstone.

[109] 'Collecting Experimental Data - OpenSim Documentation'. [Online]. Available: https://simtk-confluence.stanford.edu/display/OpenSim/Collecting+Experimental+Data. [Accessed: 21 Mar. 2018].

[110] 'How Scaling Works - OpenSim Documentation'. [Online]. Available: https://simtk-confluence.stanford.edu/display/OpenSim/How+Scaling+Works. [Accessed: 23 Mar. 2018].

[111] 'How Inverse Kinematics Works - OpenSim Documentation'. [Online]. Available: https://simtk-confluence.stanford.edu/display/OpenSim/How+Inverse+Kinematics+Works. [Accessed: 23 Mar. 2018].

[112] 'How Inverse Dynamics Works - OpenSim Documentation'. [Online]. Available: https://simtk-confluence.stanford.edu/display/OpenSim/How+Inverse+Dynamics+Works. [Accessed: 23 Mar. 2018].

[113] 'How Static Optimisation Works - OpenSim Documentation'. [Online]. Available: https://simtk-confluence.stanford.edu/display/OpenSim/How+Static+Optimisation+Works. [Accessed: 23 Mar. 2018].

[114] 'Analyses - OpenSim Documentation'. [Online]. Available: https://simtk-confluence.stanford.edu/display/OpenSim/Analyses. [Accessed: 23 Mar. 2018].

[115] D. G. Thelen, 'Adjustment of muscle mechanics model parameters to simulate dynamic contractions in older adults', *J Biomech Eng*, vol. 125, no. 1, pp. 70–77, 2003.

[116] A. M. Ahmed, A. Hyder, D. L. Burke, and K. H. Chan, '*In-vitro* ligament tension pattern in the flexed knee in passive loading', *J. Orthop. Res. Off. Publ. Orthop. Res. Soc.*, vol. 5, no. 2, pp. 217–230, 1987.

[117] O.-E. Olsen, G. Myklebust, L. Engebretsen, and R. Bahr, 'Injury mechanisms for anterior cruciate ligament injuries in team handball: a systematic video analysis', *Am. J. Sports Med.*, vol. 32, no. 4, pp. 1002–1012, 2004.

[118] L. Y. Griffin, J. Agel, M. J. Albohm, E. A. Arendt, R. W. Dick, W. E. Garrett, J. G. Garrick, Timothy Hewett, L. Huston, M. L. Ireland, R. J. Johnson, W. B. Kibler, S. Lephart, J. L. Lewis, T. N. Lindenfeld, B. R. Mandelbaum, P. Marchak, C. C. Teitz, E. M. Wojtys, 'Noncontact anterior cruciate ligament injuries: risk factors and prevention strategies', *J. Am. Acad. Orthop. Surg.*, vol. 8, no. 3, pp. 141–150, 2000.

[119] J. Hashemi, N. Chandrashekar, T. Jang, F. Karpat, M. Oseto, and S. Ekwaro-Osire, 'An Alternative Mechanism of Non-contact Anterior Cruciate Ligament Injury During Jump-landing: *In-vitro* Simulation', *Exp. Mech.*, vol. 47, pp. 347–354, 2007.

[120] K. G. Harmon and M. L. Ireland, 'Gender differences in noncontact anterior cruciate ligament injuries', *Clin. Sports Med.*, vol. 19, no. 2, pp. 287–302, 2000.

[121] T. E. Hewett, 'Anterior Cruciate Ligament Injuries in Female Athletes: Part 1, Mechanisms and Risk Factors', *Am. J. Sports Med.*, vol. 34, no. 2, pp. 299–311, 2006.

[122] L. Y. Griffin, M. J. Albohm, E. A. Arendt, R. Bahr, B. D. Beynnon, M. Demaio, R. W. Dick, L. Engebretsen, W. E. Jr. Garrett, J. A. Hannafin, T. E. Hewett, L. J. Huston, M. L. Ireland, R. J. Johnson, S. Lephart, B. R. Mandelbaum, B. J. Mann, P. H. Marks, S. W. Marshall, G. Myklebust, F. R. Noyes, C. Powers, C. Jr. Shields, S. J. Shultz, H. Silvers, J. Slauterbeck, D. C. Taylor, C. C. Teitz, E. M. Wojtys, B. Yu, 'Understanding and preventing noncontact anterior cruciate ligament injuries: a review of the Hunt Valley II meeting, January 2005', *Am. J. Sports Med.*, vol. 34, no. 9, pp. 1512–1532, 2006.

[123] J. D. Chappell, B. Yu, D. T. Kirkendall, and W. E. Garrett, 'A comparison of knee kinetics between male and female recreational athletes in stop-jump tasks', *Am. J. Sports Med.*, vol. 30, no. 2, pp. 261–267, 2002.

[124] T. C. Sell, C. M. Ferris, J. P. Abt, Y. S. Tsai, J. B. Myers, F. H. Fu, S. M. Lephart, 'Predictors of proximal tibia anterior shear force during a vertical stop-jump', *J. Orthop. Res. Off. Publ. Orthop. Res. Soc.*, vol. 25, no. 12, pp. 1589–1597, 2007.

[125] R. A. Malinzak, S. M. Colby, D. T. Kirkendall, B. Yu, and W. E. Garrett, 'A comparison of knee joint motion patterns between men and women in selected athletic tasks', *Clin. Biomech. Bristol Avon*, vol. 16, no. 5, pp. 438–445, 2001.

[126] H. C. Smith, P. Vacek, R. J. Johnson, J. R. Slauterbeck, J. Hashemi, S. Shultz, B. D. Beynnon, 'Risk Factors for Anterior Cruciate Ligament Injury: A Review of the Literature–Part 2: Hormonal, Genetic, Cognitive Function, Previous Injury, and Extrinsic Risk Factors', *Sports Health Multidiscip. Approach*, vol. 4, no. 2, pp. 155–161, 2012.

[127] K. Estes, B. Cheruvu, M. Lawless, R. Laughlin, and T. Goswami, 'Risk assessment for anterior cruciate ligament injury', *Arch. Orthop. Trauma Surg.*, vol. 135, no. 10, pp. 1437–1443, 2015.

[128] C.-F. Lin, M. Gross, C. Ji, D.Padua, P. Weinhold, W. E. Garrett, B.Yu, 'A stochastic biomechanical model for risk and risk factors of non-contact anterior cruciate ligament injuries', *J. Biomech.*, vol. 42, no. 4, pp. 418–423, 2009.

[129] A. D. Mazzocca, C. W. Nissen, M. Geary, and D. J. Adams, 'Valgus medial collateral ligament rupture causes concomitant loading and damage of the anterior cruciate ligament', *J. Knee Surg.*, vol. 16, no. 3, pp. 148–151, 2003.

[130] ‘Anterior Cruciate Ligament (ACL) Injury’, *Physiopedia*. [Online]. Available: https://www.physio-pedia.com/Anterior_Cruciate_Ligament_(ACL)_Injury. [Accessed: 23 Mar. 2018].

[131] S. H. Hong, J.-Y. Choi, G. K. Lee, J.-A. Choi, H. W. Chung, and H. S. Kang, ‘Grading of anterior cruciate ligament injury. Diagnostic efficacy of oblique coronal magnetic resonance imaging of the knee’, *J. Comput. Assist. Tomogr.*, vol. 27, no. 5, pp. 814–819, 2003.

[132] T. O. Souryal and T. R. Freeman, ‘Intercondylar notch size and anterior cruciate ligament injuries in athletes. A prospective study’, *Am. J. Sports Med.*, vol. 21, no. 4, pp. 535–539, 1993.

[133] D. A. Shaerf, ‘Anterior cruciate ligament reconstruction best practice: A review of graft choice’, *World J. Orthop.*, vol. 5, no. 1, p. 23, 2014.

[134] J. W. F. and A. L. Kwansa, ‘Recent Advancements in Ligament Tissue Engineering: The Use of Various Techniques and Materials for ACL Repair’, *Recent Patents on Biomedical Engineering (Discontinued)*, 31-Dec-2007. [Online]. Available: http://www.eurekaselect.com/95052/article. [Accessed: 23 Mar. 2018].

[135] B. P. Conrad, M. Rappé, M. Horodyski, K. W. Farmer, and P. A. Indelicato, ‘The effect of sterilization on mechanical properties of soft tissue allografts’, *Cell Tissue Bank.*, vol. 14, no. 3, pp. 359–366, 2013.

[136] R. Singh, D. Singh, and A. Singh, ‘Radiation sterilization of tissue allografts: A review’, *World J. Radiol.*, vol. 8, no. 4, pp. 355–369, 2016.

[137] M. S. Binnet, B. Akan, and A. Kaya, ‘Lyophilised medial meniscus transplantations in ACL-deficient knees: a 19-year follow-up’, *Knee Surg. Sports Traumatol. Arthrosc. Off. J. ESSKA*, vol. 20, no. 1, pp. 109–113, 2012.

[138] O. Cornu, X. Banse, P. L. Docquier, S. Luyckx, and C. Delloye, 'Effect of freeze-drying and gamma irradiation on the mechanical properties of human cancellous bone', *J. Orthop. Res. Off. Publ. Orthop. Res. Soc.*, vol. 18, no. 3, pp. 426–431, 2000.

[139] G. A. Godette, J. A. Kopta, and D. M. Egle, 'Biomechanical effects of gamma irradiation on fresh frozen allografts *in vivo*', *Orthopedics*, vol. 19, no. 8, pp. 649–653, 1996.

[140] A. J. Bailey, 'Effect of ionizing radiation on connective tissue components', *Int. Rev. Connect. Tissue Res.*, vol. 4, pp. 233–281, 1968.

[141] A. Maslennikova, M. Kochueva, N. Ignatieva, A. Vitkin, O. Zakharkina, V. Kamensky, E. Sergeeva, E. Kiseleva and V. Bagratashvili, 'Effects of gamma irradiation on collagen damage and remodeling', *Int. J. Radiat. Biol.*, vol. 91, no. 3, pp. 240–247, 2015.

[142] H. E. Schwartz, M. J. Matava, F. S. Proch, C. A. Butler, A. Ratcliffe, M. Levy, D. L. Butler, 'The effect of gamma irradiation on anterior cruciate ligament allograft biomechanical and biochemical properties in the caprine model at time zero and at 6 months after surgery', *Am. J. Sports Med.*, vol. 34, no. 11, pp. 1747–1755, 2006.

[143] P. A. Indelicato, M. G. Ciccotti, J. Boyd, L. D. Higgins, B. S. Shaffer, and C. T. Vangsness, 'Aseptically processed and chemically sterilized BTB allografts for anterior cruciate ligament reconstruction: a prospective randomized study', *Knee Surg. Sports Traumatol. Arthrosc.*, vol. 21, no. 9, pp. 2107–2112, 2013.

[144] J. A. Fishman, 'Assessment of infectious risk in clinical xenotransplantation: the lessons for clinical allotransplantation', *Xenotransplantation*, vol. 21, no. 4, pp. 307–308, 2014.

[145] C. R. Associates, ‘Aperion Biologics, Inc. | Independent Equity Research | Crystal Research Associates, LLC’. [Online]. Available: https://www.crystalra.com/research-library/aperion. [Accessed: 23 Mar. 2018].

[146] N. Davarinos, B. J. O’Neill, and W. Curtin, ‘A Brief History of Anterior Cruciate Ligament Reconstruction’, *Advances in Orthopedic Surgery*, 2014. [Online]. Available: https://www.hindawi.com/journals/aos/2014/706042/. [Accessed: 23 Mar. 2018].

[147] T. Chen, J. Jiang, and S. Chen, ‘Status and headway of the clinical application of artificial ligaments’, *Asia-Pac. J. Sports Med. Arthrosc. Rehabil. Technol.*, vol. 2, no. 1, pp. 15–26, 2015.

[148] C. Legnani, A. Ventura, C. Terzaghi, E. Borgo, and W. Albisetti, ‘Anterior cruciate ligament reconstruction with synthetic grafts. A review of literature’, *Int. Orthop.*, vol. 34, no. 4, pp. 465–471, 2010.

[149] N. Rushton, D. J. Dandy, and C. P. Naylor, ‘The clinical, arthroscopic and histological findings after replacement of the anterior cruciate ligament with carbon-fibre’, *J. Bone Joint Surg. Br.*, vol. 65, no. 3, pp. 308–309, 1983.

[150] E. Haque, E. Preston, B. C. Fleming, A. Amendola, J. T. Andrish, J. A. Bergfeld, W. R. Dunn, C. Kaeding, J. E. Kuhn, R. G. Marx, E. C. McCarty, R. C. Parker, K. P. Spindler, M. Wolcott, B. R. Wolf, G. N. Williams, ‘A Systematic Review for Anterior Cruciate Ligament Reconstruction’, *J. Anesth. Surg.*, vol. 3, no. 1, 2016.

[151] M. F. Guidoin, Y. Marois, J. Bejui, N. Poddevin, M. W. King, and R. Guidoin, ‘Analysis of retrieved polymer fibre based replacements for the ACL’, *Biomaterials*, vol. 21, no. 23, pp. 2461–2474, 2000.

[152] T. Fukubayashi and K. Ikeda, ‘Follow-up study of Gore-Tex artificial ligament--special emphasis on tunnel osteolysis’, *J. Long. Term Eff. Med. Implants*, vol. 10, no. 4, pp. 267–277, 2000.

[153] A. W. Murray and M. F. Macnicol, ‘10-16 year results of Leeds-Keio anterior cruciate ligament reconstruction’, *The Knee*, vol. 11, no. 1, pp. 9–14, 2004.

[154] A. P. Jones, S. Sidhom, and G. Sefton, ‘Long-term clinical review (10-20 years) after reconstruction of the anterior cruciate ligament using the Leeds-Keio synthetic ligament’, *J. Long. Term Eff. Med. Implants*, vol. 17, no. 1, pp. 59–69, 2007.

[155] P. D. Parchi, C. Gianluca, L. Dolfi, A. Baluganti, N. Piolanti, F. Chiellini, M. Lisanti, ‘Anterior cruciate ligament reconstruction with LARS^{TM} artificial ligament results at a mean follow-up of eight years’, *Int. Orthop.*, vol. 37, no. 8, pp. 1567–1574, 2013.

[156] A. Steel, ‘Orthopaedic implants | Sports, Medicine, & Orthopaedic | Neoligaments Leeds-Keio’, *Neoligaments*. [Online]. Available: https://www.neoligaments.com/. [Accessed: 23 Mar. 2018].

[157] A. Cazenave, D. Baert, and P. E. Ridoux, ‘Reconstruction of the anterior cruciate ligament with artificial ligament (Ligastic). Clinical results in 72 patients’, *Rev. Chir. Orthop. Reparatrice Appar. Mot.*, vol. 80, no. 5, pp. 413–419, 1994.

[158] T. M. Tiefenboeck, E. Thurmaier, M. M. Tiefenboeck, R. C. Ostermann, J. Joestl, M. Winnisch, M. Schurz, S. Hajdu, M. Hofbauer, ‘Clinical and functional outcome after anterior cruciate ligament reconstruction using the LARS^{TM} system at a minimum follow-up of 10 years’, *Knee*, vol. 22, no. 6, pp. 565–568, 2015.

[159] G. W. Bowyer and S. J. Matthews, ‘Anterior cruciate ligament reconstruction using the Gore-tex ligament’, *J. R. Army Med. Corps*, vol. 137, no. 2, pp. 69–75, 1991.

[160] T. M. McGrath, G. Waddington, J. M. Scarvell, N. Ball, R. Creer, K. Woods, D. Smith, R. Adams, ‘An ecological study of anterior cruciate ligament reconstruction, part 2: Functional performance tests correlate with return-to-sport outcomes’, *Orthop. J. Sports Med.*, vol. 5, no. 2, 2017.

[161] D. P. Iliadis, D. N. Bourlos, D. S. Mastrokalos, E. Chronopoulos, and G. C. Babis, ‘LARS Artificial Ligament Versus ABC Purely Polyester Ligament for Anterior Cruciate Ligament Reconstruction’, *Orthop. J. Sports Med.*, vol. 4, no. 6, 2016.

[162] A. V. Lukianov, J. C. Richmond, G. R. Barrett, and J. Gillquist, ‘A multicenter study on the results of anterior cruciate ligament reconstruction using a Dacron ligament prosthesis in “salvage” cases.’, *Am. J. Sports Med.*, vol. 17, no. 3, pp. 380–385; discussion 385, 1989.

[163] S. Zaffagnini, G. M. Marcheggiani Muccioli, V. Chatrath, A. Bondi, V. De Pasquale, D. Martini, B. Bacchelli, M. Marcacci, ‘Histological and ultrastructural evaluation of Leeds-Keio ligament 20 years after implant: A case report’, *Knee Surg. Sports Traumatol. Arthrosc.*, vol. 16, no. 11, pp. 1026–1029, 2008.

[164] F. H. Silver, A. J. Tria, J. P. Zawadsky, and M. G. Dunn, ‘Anterior cruciate ligament replacement: a review’, *J. Long. Term Eff. Med. Implants*, vol. 1, no. 2, pp. 135–154, 1991.

[165] A. A. Schepsis and J. Greenleaf, ‘Prosthetic materials for anterior cruciate ligament reconstruction’, *Orthop. Rev.*, vol. 19, no. 11, pp. 984–991, 1990.

[166] D. J. Zoltan, C. Reinecke, and P. A. Indelicato, 'Synthetic and allograft anterior cruciate ligament reconstruction', *Clin. Sports Med.*, vol. 7, no. 4, pp. 773–784, 1988.

[167] 'Repair and Regeneration of Ligaments, Tendons, and Joint Capsule - Google Libros'. [Online]. Available: https://books.google.co.uk/books?id=j7qNAPK8fbcC&pg=PA279&lpg=PA279&dq=Repair+and+Regeneration+of+Ligaments,+Tendons,+and+Joint+Capsule.&source=bl&ots=gHVtdbUWyq&sig=mDHs_XdM8spMKlNsiiVVSpld-IM&hl=es&sa=X&ved=0ahUKEwjk683VhoPaAhUdOsAKHd76AK4Q6AEIZDAI#v=onepage&q=Repair%20and%20Regeneration%20of%20Ligaments%2C%20Tendons%2C%20and%20Joint%20Capsule.&f=false. [Accessed: 23 Mar.2018].

[168] W. K. Krudwig, 'Reconstruction of Cruciate Ligaments Using a Synthetic Ligament of Polyethylene Terephthalate (Trevira Ligament)', in *Ligaments and Ligamentoplasties*, Springer, Berlin, Heidelberg, 1997, pp. 245–253.

[169] 'Telos Medical USA - Austin & Associates - Quality Orthopaedic & Podiatry Products'. [Online]. Available: http://www.telosmedical.com/trevira-synthetic-ligament. [Accessed: 23 Mar. 2018].

[170] G. W. Woods, C. A. Homsy, J. M. Prewitt, and H. S. Tullos, 'Proplast leader for use in cruciate ligament reconstruction', *Am. J. Sports Med.*, vol. 7, no. 6, pp. 314–320, 1979.

[171] K. P. Schulitz, H. Krahl, and W. H. Stein, Eds., *Late Reconstructions of Injured Ligaments of the Knee*. Berlin Heidelberg: Springer-Verlag, 1978.

[172] L. A. Pruitt and A. M. Chakravartula, *Mechanics of Biomaterials: Fundamental Principles for Implant Design*. Cambridge University Press, 2011.

[173] W. Müller and W. Hackenbruch, *Surgery and Arthroscopy of the Knee: Second European Congress of Knee Surgery and Arthroscopy Basel, Switzerland, 29.Sept.-4.Oct.1986*. Springer Science & Business Media, 2012.

[174] H. Seitz, S. Marlovits, I. Schwendenwein, E. Müller, and V. Vécsei, 'Biocompatibility of polyethylene terephthalate (Trevira hochfest) augmentation device in repair of the anterior cruciate ligament', *Biomaterials*, vol. 19, no. 1–3, pp. 189–196, 1998.

[175] K. Healy, D. W. Hutmacher, D. W. Grainger, and C. J. Kirkpatrick, *Comprehensive Biomaterials II*. Elsevier, 2017.

[176] 'Artificial ligaments LIGASTIC® – Orthomed'. [Online]. Available: https://www.orthomed.fr/index.php/products/sutures-and-ligaments/artificial-ligaments/. [Accessed: 23 Mar. 2018].

[177] B. D. Ratner, A. S. Hoffman, and F. J. Schoen, *Biomaterials Science: An Introduction to Materials in Medicine*. Elsevier, 1996.

[178] L. Yahia, Hagemeister, Drouin, M. Sati, and C. Rivard, 'Conceptual Design of Prosthetic Anterior Cruciate Ligaments: the Need for a Biomimetical Approach.', *Biomimetics*, vol. 2, pp. 309-330, 1994.

[179] 'ACL Prosthesis | Biotextiles 2017'. [Online]. Available: https://biotextiles2017blog.wordpress.com/team-2/. [Accessed: 23 Mar. 2018].

[180] Y.-X. Wang, J. L. Robertson, W. B. Spillman, and R. O. Claus, 'Effects of the chemical structure and the surface properties of polymeric biomaterials on their biocompatibility', *Pharm. Res.*, vol. 21, no. 8, pp. 1362–1373, 2004.

[181] H.-J. Sung, C. Meredith, C. Johnson, and Z. S. Galis, 'The effect of scaffold degradation rate on three-dimensional cell growth and angiogenesis', *Biomaterials*, vol. 25, no. 26, pp. 5735–5742, 2004.

[182] B. P. Chan and K. W. Leong, 'Scaffolding in tissue engineering: general approaches and tissue-specific considerations', *Eur. Spine J.*, vol. 17, no. Suppl 4, pp. 467–479, 2008.

[183] R. Vaishya, A. K. Agarwal, S. Ingole, and V. Vijay, 'Current Trends in Anterior Cruciate Ligament Reconstruction: A Review', *Cureus*, vol. 7, no. 11, 2015.

[184] R. Mascarenhas and P. B. MacDonald, 'Anterior cruciate ligament reconstruction: a look at prosthetics - past, present and possible future', *McGill J. Med. MJM*, vol. 11, no. 1, pp. 29–37, 2008.

[185] U. G. T. M. Sampath, Y. C. Ching, C. H. Chuah, J. J. Sabariah, and P.-C. Lin, 'Fabrication of Porous Materials from Natural/Synthetic Biopolymers and Their Composites', *Materials*, vol. 9, no. 12, 2016.

[186] N. Sultana, M. I. Hassan, and M. M. Lim, 'Scaffold Fabrication Protocols', in *Composite Synthetic Scaffolds for Tissue Engineering and Regenerative Medicine*, Springer, Cham, pp. 13–24, 2015.

[187] P. X. Ma, 'Scaffolds for tissue fabrication', *Mater. Today*, vol. 7, no. 5, pp. 30–40, 2004.

[188] V. Karageorgiou and D. Kaplan, 'Porosity of 3D biomaterial scaffolds and osteogenesis', *Biomaterials*, vol. 26, no. 27, pp. 5474–5491, 2005.

[189] K. D. Andrews and J. A. Hunt, 'Upregulation of matrix and adhesion molecules induced by controlled topography', *J. Mater. Sci. Mater. Med.*, vol. 19, no. 4, pp. 1601–1608, 2008.

[190] S. M. Peltola, F. P. W. Melchels, D. W. Grijpma, and M. Kellomäki, 'A review of rapid prototyping techniques for tissue engineering purposes', *Ann. Med.*, vol. 40, no. 4, pp. 268–280, 2008.

[191] A. Haider, S. Haider, and I.-K. Kang, 'A comprehensive review summarizing the effect of electrospinning parameters and potential applications of nanofibres in biomedical and biotechnology', *Arab. J. Chem.*, 2015.

[192] X. C. Zhang, *Science and Principles of Biodegradable and Bioresorbable Medical Polymers: Materials and Properties*. Woodhead Publishing, 2016.

[193] M. Boffito, S. Sartori, and G. Ciardelli, 'Polymeric scaffolds for cardiac tissue engineering: requirements and fabrication technologies', *Polym. Int.*, vol. 63, no. 1, pp. 2–11, 2014.

[194] H. Chen, R. K. Truckenmüller, C. van Blitterswijk, and L. Moroni, 'Fabrication of nanofibrous scaffolds for tissue engineering applications', *Nanomater. Tissue Eng. Fabr. Appl.*, 2013.

[195] Tucker, 'The History of the Science and Technology of Electrospinning from 1600 to 1995', vol. 7, pp. 63–73, 2012.

[196] M. Li, M. J. Mondrinos, M. R. Gandhi, F. K. Ko, A. S. Weiss, and P. I. Lelkes, 'Electrospun protein fibres as matrices for tissue engineering', *Biomaterials*, vol. 26, no. 30, pp. 5999–6008, 2005.

[197] Y.-F. Goh, I. Shakir, and R. Hussain, 'Electrospun fibres for tissue engineering, drug delivery, and wound dressing', *J. Mater. Sci.*, vol. 48, no. 8, pp. 3027–3054, 2013.

[198] 'electrospinning'. [Online]. Available: http://www.che.vt.edu/Faculty/Wilkes/GLW/electrospinning/electrspinning.html. [Accessed: 04 Mar. 2018].

[199] W. J. Li and R. S. Tuan, 'Fabrication and application of nanofibrous scaffolds in tissue engineering', *Curr Protoc Cell Biol*, vol. 25, 2009.

[200] Q. P. Pham, U. Sharma, and A. G. Mikos, 'Electrospinning of polymeric nanofibres for tissue engineering applications: A review', *Tissue Eng.*, vol. 12, no. 5, pp. 1197–1211, 2006.

[201] M. R. Ladd, T. K. Hill, J. J. Yoo, and S. J. Lee, 'Electrospun Nanofibres in Tissue Engineering', *Nanofibres - Prod. Prop. Funct. Appl.*, 2011.

[202] L. M. D. Sánchez, Leonardo Rodriguez, and Marcos López, 'Electrospinning: la era de las nanofibras', *Rev. Iberoam. Polímeros*, vol. 14, no. 1, pp. 10–27, 2014.

[203] G. Liu, Z. Gu, Y. Hong, L. Cheng, and C. Li, 'Electrospun starch nanofibres: Recent advances, challenges, and strategies for potential pharmaceutical applications', *J. Controlled Release*, vol. 252, pp. 95–107, 2017.

[204] B. Tarus, N. Fadel, A. Al-Oufy, and M. El-Messiry, 'Effect of polymer concentration on the morphology and mechanical characteristics of electrospun cellulose acetate and poly (vinyl chloride) nanofibre mats', *Alex. Eng. J.*, vol. 55, no. 3, pp. 2975–2984, 2016.

[205] J. L. Chen, C. R. Allen, T. E. Stephens, A. K. Haas, L. J. Huston, R. W. Wright, B. T. Feeley, 'Differences in Mechanisms of Failure, Intraoperative Findings, and Surgical Characteristics Between Single- and Multiple-Revision ACL Reconstructions', *Am. J. Sports Med.*, vol. 41, no. 7, pp. 1571–1578, 2013.

[206] H. Janik and M. Marzec, 'A review: fabrication of porous polyurethane scaffolds', *Mater. Sci. Eng. C Mater. Biol. Appl.*, vol. 48, pp. 586–591, 2015.

[207] L. D. Muiznieks and F. W. Keeley, 'Molecular assembly and mechanical properties of the extracellular matrix: A fibrous protein perspective', *Biochim. Biophys. Acta BBA - Mol. Basis Dis.*, vol. 1832, no. 7, pp. 866–875, 2013.

[208] C. Frantz, K. M. Stewart, and V. M. Weaver, 'The extracellular matrix at a glance', *J. Cell Sci.*, vol. 123, no. 24, pp. 4195–4200, 2010.

[209] S. A. Sell, P. S. Wolfe, K. Garg, J. M. McCool, I. A. Rodriguez, and G. L. Bowlin, 'The Use of Natural Polymers in Tissue Engineering: A Focus on Electrospun Extracellular Matrix Analogues', *Polymers*, vol. 2, no. 4, pp. 522–553, 2010.

[210] P. Gunatillake and R. Adhikari, 'Biodegradable synthetic polymers for tissue engineering', *Eur. Cell. Mater.*, vol. 5, pp. 1–16, 2003.

[211] G. BaoLin and P. X. MA, 'Synthetic biodegradable functional polymers for tissue engineering: a brief review', *Sci. China Chem.*, vol. 57, no. 4, pp. 490–500, 2014.

[212] M. Guthold, W. Liu, E. A. Sparks, L. M. Jawerth, L. Peng, M. Falvo, R. Superfine, R. R. Hantgan, S. T. Lord, 'A Comparison of the Mechanical and Structural Properties of Fibrin Fibres with Other Protein Fibres', *Cell Biochem. Biophys.*, vol. 49, no. 3, pp. 165–181, 2007.

[213] M. Jafari-Sabet, H. Nasiri, and R. Ataee, 'The Effect of Cross-Linking Agents and Collagen Concentrations on Properties of Collagen Scaffolds', *J. Arch. Mil. Med.*, vol. 4, no. 4, 2016.

[214] H. M. Pauly, D. J. Kelly, K. C. Popat, N. A. Trujillo, N. J. Dunne, H. O. McCarthy, T. L. Haut Donahue, 'Mechanical properties and cellular response of novel electrospun nanofibres for ligament tissue engineering: Effects of orientation and geometry', *J. Mech. Behav. Biomed. Mater.*, vol. 61, pp. 258–270, 2016.

[215] M. Erencia, F. Cano, J. A. Tornero, M. M. Fernandes, T. Tzanov, J. Macanás, F. Carrillo, 'Electrospinning of gelatin fibres using solutions with low acetic acid concentration: Effect of solvent composition on both diameter of electrospun fibres and cytotoxicity', *J. Appl. Polym. Sci.*, vol. 132, no. 25, 2015.

[216] J. S. Bach, F. Detrez, M. Cherkaoui, S. Cantournet, D. N. Ku, and L. Corté, 'Hydrogel fibres for ACL prosthesis: design and mechanical evaluation of PVA and PVA/UHMWPE fibre constructs', *J. Biomech.*, vol. 46, no. 8, pp. 1463–1470, 2013.

[217] C. Zhang, X. Yuan, L. Wu, Y. Han, and J. Sheng, 'Study on morphology of electrospun poly(vinyl alcohol) mats', *Eur. Polym. J.*, vol. 41, no. 3, pp. 423–432, 2005.

[218] P. Supaphol and S. Chuangchote, 'On the electrospinning of poly(vinyl alcohol) nanofibre mats: A revisit', *J. Appl. Polym. Sci.*, vol. 108, no. 2, pp. 969–978, 2008.

[219] J.-C. Park, T. Ito, K.-O. Kim, K.-W. Kim, B.-S. Kim, M.-S. Khil, H.-Y. Kim and I.-S. Kim, 'Electrospun poly(vinyl alcohol) nanofibres: effects of degree of hydrolysis and enhanced water stability', *Polym. J.*, vol. 42, no. 3, pp. 273–276, 2010.

[220] A. C. Gurlek, B. Sevinc, E. Bayrak, and C. Erisken, 'Synthesis and characterization of polycaprolactone for anterior cruciate ligament regeneration', *Mater. Sci. Eng. C*, vol. 71, pp. 820–826, 2017.

[221] N. L. Leong, N. M. Kabir, A. Arshi, A. N. Nazemi, J. Jiang, B. M. Wu, F. A. Petrigliano, D. R. Mcallister, 'Use of ultra-high molecular weight polycaprolactone scaffolds for ACL reconstruction', *J. Orthop. Res. Off. Publ. Orthop. Res. Soc.*, vol. 34, no. 5, pp. 828–835, 2016.

[222] N. L. Leong, A. Arshi, N. Kabir, A. Nazemi, F. A. Petrigliano, B. M. Wu, D. R. McAllister, '*In vitro* and *in vivo* evaluation of heparin mediated growth factor release from tissue-engineered constructs for anterior cruciate ligament reconstruction', *J. Orthop. Res. Off. Publ. Orthop. Res. Soc.*, vol. 33, no. 2, pp. 229–236, 2015.

[223] F. A. Petrigliano, G. A. Arom, A. N. Nazemi, M. G. Yeranosian, B. M. Wu, and D. R. McAllister, '*In Vivo* Evaluation of Electrospun Polycaprolactone Graft for Anterior Cruciate Ligament Engineering', *Tissue Eng. Part A*, vol. 21, no. 7–8, pp. 1228–1236, 2015.

[224] F. Chen, J. W. S. Hayami, and B. G. Amsden, 'Electrospun poly(L-lactide-co-acryloyl carbonate) fibre scaffolds with a mechanically stable crimp structure for ligament tissue engineering', *Biomacromolecules*, vol. 15, no. 5, pp. 1593–1601, 2014.

[225] Z. Mardina, N. Fitriana, R. Siswanto, O. Oktavina, N. Zahra, P. Widiyanti, D. Rudyarjo, E. Indarto, R. Langenati, 'The Influence of Braiding Angle Variation in Braided-Twisted Fibre Scaffold Based Poly L-Lactic Acid for Anterior Cruciate Ligament Reconstruction Application', *Adv. Mater. Res.*, vol. 845, pp. 925–928, 2013.

[226] C. E. da Silveira Franciozi, S. J. M. Ingham, G. C. Gracitelli, M. V. M. Luzo, F. H. Fu, and R. J. Abdalla, 'Updates in biological therapies for knee injuries: anterior cruciate ligament', *Curr. Rev. Musculoskelet. Med.*, vol. 7, no. 3, pp. 228–238, 2014.

[227] J. Zhu, X. Zhang, Z. Shao, L. Dai, L. Li, X. Hu, X. Wang, C. Zhou, and Y. Ao, '*In Vivo* Study of Ligament-Bone Healing after Anterior Cruciate Ligament Reconstruction Using Autologous Tendons with Mesenchymal Stem Cells Affinity Peptide Conjugated Electrospun Nanofibrous Scaffold', *Journal of Nanomaterials*, 2013. [Online]. Available: https://www.hindawi.com/journals/ jnm/2013/831873/. [Accessed: 04 Mar. 2018].

[228] '(567a) Electrospun Degradable Segmented Polyurethane Elastomers for Ligament Tissue Engineering | AIChE Academy'. [Online]. Available:

https://www.aiche.org/conferences/aiche-annual- meeting/2005/proceeding/paper/567a-electrospun-degradable-segmented-polyurethane-elastomers-ligament-tissue-engineering-0. [Accessed: 04 Mar. 2018].

[229] C. H. Lee, H. J. Shin, I. H. Cho, Y.-M. Kang, I. A. Kim, K.-D. Park, J.-W. Shin, 'Nanofibre alignment and direction of mechanical strain affect the ECM production of human ACL fibroblast', *Biomaterials*, vol. 26, no. 11, pp. 1261–1270, 2005.

[230] S. M. Full, C. Delman, J. M. Gluck, R. Abdmaulen, R. J. Shemin, and S. Heydarkhan-Hagvall, 'Effect of fibre orientation of collagen-based electrospun meshes on human fibroblasts for ligament tissue engineering applications', *J. Biomed. Mater. Res. B Appl. Biomater.*, vol. 103, no. 1, pp. 39–46, 2015.

[231] P. S. Thayer, A. F. Dimling, D. S. Plessl, M. R. Hahn, S. A. Guelcher, L. A. Dahlgren, and A. S. Goldstein, 'Cellularized cylindrical fibre/hydrogel composites for ligament tissue engineering', *Biomacromolecules*, vol. 15, no. 1, pp. 75–83, 2014.

[232] J. He, N. Jiang, T. Qin, W. Zhang, Z. Liu, Y. Liua and D. Lia, 'Microfibre-reinforced nanofibrous scaffolds with structural and material gradients to mimic ligament-to-bone interface', *J. Mater. Chem. B*, vol. 5, no. 43, pp. 8579–8590, 2017.

[233] D. C. Surrao, S. D. Waldman, and B. G. Amsden, 'Biomimetic poly(lactide) based fibrous scaffolds for ligament tissue engineering', *Acta Biomater.*, vol. 8, no. 11, pp. 3997–4006, 2012.

[234] F. R. Noyes and S. Barber-Westin, *ACL Injuries in the Female Athlete: Causes, Impacts, and Conditioning Programs*. Springer Science & Business Media, 2013.

[235] T. E. Hewett, 'Neuromuscular and hormonal factors associated with knee injuries in female athletes. Strategies for intervention', *Sports Med. Auckl. NZ*, vol. 29, no. 5, pp. 313–327, 2000.

[236] E. Roldán, N. D. Reeves, G. Cooper, and K. Andrews, 'Design Consideration for ACL Implants based on Mechanical Loading', *Procedia CIRP*, vol. 49, pp. 133–138, 2016.

[237] E. Roldán, N. D. Reeves, G. Cooper, and K. Andrews, '*In vivo* mechanical behaviour of the anterior cruciate ligament: A study of six daily and high impact activities', *Gait Posture*, vol. 58, pp. 201–207, 2017.

[238] E. Roldán, N. D. Reeves, G. Cooper, and K. Andrews, 'Study of *in vivo* mechanical behaviour of ACL to design improved tissue engineered implants', presented at the The 8th MMU Postgraduate Research Conference 'Innovation', Manchester, UK, 2015.

[239] E. Roldán, N. D. Reeves, G. Cooper, and K. Andrews, 'Mechanical specifications for the design of ACL implants through the investigation of the *in vivo* mechanical behaviour in daily and high impact activities', presented at the 28th European Conference on Biomaterials, Athens, Greece, 2017.

[240] L. Blankevoort and R. Huiskes, 'Ligament-bone interaction in a three-dimensional model of the knee', *J Biomech Eng*, vol. 113, no. 3, pp. 263–269, 1991.

[241] P. D. B. Price, C. Gissane, and D. J. Cleather, 'Reliability and minimal detectable change values for predictions of knee forces during gait and stair ascent derived from the FreeBody musculoskeletal model of the lower limb', *Front. Bioeng. Biotechnol.*, vol. 5, 2017.

[242] M. Hajizadeh, A. Hashemi Oskouei, F. Ghalichi, and G. Sole, 'Knee Kinematics and Joint Moments During Stair Negotiation in Participants With

Anterior Cruciate Ligament Deficiency and Reconstruction: A Systematic Review and Meta-Analysis', *PM R*, vol. 8, no. 6, pp. 563-579, 2016.

[243] H.-Y. Tseng and B.-S. Liu, 'Effects of load carrying methods and stair slopes on physiological response and postures during stairs ascending and descending', *Ind. Health*, vol. 49, no. 1, pp. 30–36, 2011.

[244] D. M. Hooper, M. C. Morrissey, R. Crookenden, J. Ireland, and J. P. Beacon, 'Gait adaptations in patients with chronic posterior instability of the knee', *Clin. Biomech.*, vol. 17, no. 3, pp. 227–233, 2002.

[245] M. E. Zabala, J. Favre, S. F. Scanlan, J. Donahue, and T. P. Andriacchi, 'Three-dimensional knee moments of ACL reconstructed and control subjects during gait, stair ascent, and stair descent', *J. Biomech.*, vol. 46, no. 3, pp. 515–520, 2013.

[246] W. R. Taylor, M. O. Heller, G. Bergmann, and G. N. Duda, 'Tibio-femoral loading during human gait and stair climbing', *J. Orthop. Res. Off. Publ. Orthop. Res. Soc.*, vol. 22, no. 3, pp. 625–632, 2004.

[247] B. Gao, M. L. Cordova, and N. N. Zheng, 'Three-dimensional joint kinematics of ACL-deficient and ACL-reconstructed knees during stair ascent and descent', *Hum. Mov. Sci.*, vol. 31, no. 1, pp. 222–235, 2012.

[248] M. Hall, C. A. Stevermer, and J. C. Gillette, 'Gait analysis post anterior cruciate ligament reconstruction: knee osteoarthritis perspective', *Gait Posture*, vol. 36, no. 1, pp. 56–60, 2012.

[249] 'Gait 2392 and 2354 Models - OpenSim Documentation'. [Online]. Available: https://simtk-confluence.stanford.edu/display/OpenSim/Gait+2392+and+2354+Models. [Accessed: 21 Mar. 2018].

[250] J. M. Winters, 'Hill-Based Muscle Models: A Systems Engineering Perspective', in *Multiple Muscle Systems*, Springer, New York, NY, pp. 69–93, 1990.

[251] S. S. Jordan, L. E. DeFrate, K. W. Nha, R. Papannagari, T. J. Gill, and G. Li, 'The *in vivo* kinematics of the anteromedial and posterolateral bundles of the anterior cruciate ligament during weightbearing knee flexion', *Am J Sports Med*, vol. 35, no. 4, pp. 547–554, 2007.

[252] J. L. Wu, A. Hosseini, M. Kozanek, H. R. Gadikota, T. J. th Gill, and G. Li, 'Kinematics of the anterior cruciate ligament during gait', *Am J Sports Med*, vol. 38, no. 7, pp. 1475–1482, 2010.

[253] D. P. Pioletti, 'Viscoelastic properties of soft tissues', Ecole Polytechnique Federale de Lausanne, 1997.

[254] K. H. Bloemker, T. M. Guess, L. Maletsky, and K. Dodd, 'Computational knee ligament modeling using experimentally determined zero-load lengths', *Open Biomed Eng J*, vol. 6, pp. 33–41, 2012.

[255] S. P. D. Richard E. Debski, S. L. Y. W. R. E. Debski, P. D. Shon, and L. Y. W. Savio, 'Experimental and Computational Modeling of Joint and Ligament Mechanics', *J. Appl. Biomech.*, vol. 20, pp. 450–474, 2004.

[256] S. G. McLean, X. Huang, and A. J. van den Bogert, 'Investigating isolated neuromuscular control contributions to non-contact anterior cruciate ligament injury risk via computer simulation methods', *Clin. Biomech.*, vol. 23, no. 7, pp. 926–936, 2008.

[257] K. L. Markolf, D. M. Burchfield, M. M. Shapiro, M. F. Shepard, G. A. Finerman, and J. L. Slauterbeck, 'Combined knee loading states that generate high anterior cruciate ligament forces', *J. Orthop. Res. Off. Publ. Orthop. Res. Soc.*, vol. 13, no. 6, pp. 930–935, 1995.

[258] Y. Shimokochi and S. J. Shultz, 'Mechanisms of Noncontact Anterior Cruciate Ligament Injury', *J. Athl. Train.*, vol. 43, no. 4, pp. 396–408, 2008.

[259] ‘SimTK: Studying Anterior Cruciate Ligament Strains in Young Female Athletes: Project Home’. [Online]. Available: https://simtk.org/projects/acl_biomech. [Accessed: 05 Dec. 2018].

[260] J. Kar, ‘A forward dynamics simulation study of increasing load on the anterior cruciate ligament of the knee, for young women performing recreational drop jump activities.’, *Electron. Theses Diss.*, 2011.

[261] M. Erencia, F. Cano, J. A. Tornero, J. Macanás, and F. Carrillo, ‘Preparation of electrospun nanofibres from solutions of different gelatin types using a benign solvent mixture composed of water/PBS/ethanol: Electrospinning of Different Gelatin Types Using Water/PBS/Ethanol’, *Polym. Adv. Technol.*, vol. 27, no. 3, pp. 382–392, 2016.

[262] N. Choktaweesap, K. Arayanarakul, D. Aht-ong, C. Meechaisue, and P. Supaphol, ‘Electrospun Gelatin Fibres: Effect of Solvent System on Morphology and Fibre Diameters’, *Polym. J.*, vol. 39, no. 6, pp. 622–631, 2007.

[263] L. A. Bosworth, N. Alam, J. K. Wong, and S. Downes, ‘Investigation of 2D and 3D electrospun scaffolds intended for tendon repair’, *J. Mater. Sci. Mater. Med.*, vol. 24, no. 6, pp. 1605–1614, 2013.

[264] Z. Ghanavati, N. Neisi, V. Bayati, and M. Makvandi, ‘The influence of substrate topography and biomaterial substance on skin wound healing’, *Anat. Cell Biol.*, vol. 48, no. 4, pp. 251–257, 2015.

[265] S. Farris, J. Song, and Q. Huang, ‘Alternative Reaction Mechanism for the Cross-Linking of Gelatin with Glutaraldehyde’, *J. Agric. Food Chem.*, vol. 58, no. 2, pp. 998–1003, 2010.

[266] Z.-M. Huang, Y. Z. Zhang, S. Ramakrishna, and C. T. Lim, 'Electrospinning and mechanical characterization of gelatin nanofibres', *Polymer*, vol. 45, no. 15, pp. 5361–5368, 2004.

[267] Y. H. Kim, D.-H. Kim, J. Hwang, H.-S. Kim, G. Young, L. Zae, Y. Ryoo, S.-U. Choi, S. Lee, 'The inclusion of fetal bovine serum in gelatin/PCL electrospun scaffolds reduces short-term osmotic stress in HEK 293 cells caused by scaffold components', *J. Appl. Polym. Sci.*, vol. 129, no. 6, pp. 3273–3281, 2013.

[268] C. B. Horner, G. Ico, J. Johnson, Y. Zhao, and J. Nam, 'Microstructure-dependent mechanical properties of electrospun core–shell scaffolds at multi-scale levels', *J. Mech. Behav. Biomed. Mater.*, vol. 59, pp. 207–219, 2016.

[269] Z. Zha, W. Teng, V. Markle, Z. Dai, and X. Wu, 'Fabrication of gelatin nanofibrous scaffolds using ethanol/phosphate buffer saline as a benign solvent', *Biopolymers*, vol. 97, no. 12, pp. 1026–1036, 2012.

[270] L. Maleknia and Z. Majdi, 'Electrospinning of Gelatin Nanofibre for biomedical Application', *Orient. J. Chem.*, vol. 30, no. 4, pp. 2043–2048, 2014.

[271] M. Erencia, F. Cano, J. A. Tornero, J. Macanás, and F. Carrillo, 'Resolving the Electrospinnability Zones and Diameter Prediction for the Electrospinning of the Gelatin/Water/Acetic Acid System', *Langmuir*, vol. 30, no. 24, pp. 7198–7205, 2014.

[272] I. Steyaert, H. Rahier, S. Van Vlierberghe, J. Olijve, and K. De Clerck, 'Gelatin nanofibres: Analysis of triple helix dissociation temperature and cold-water-solubility', *Food Hydrocoll.*, vol. 57, pp. 200–208, 2016.

[273] N. Okutan, P. Terzi, and F. Altay, 'Affecting parameters on electrospinning process and characterization of electrospun gelatin nanofibres', *Food Hydrocoll.*, vol. 39, pp. 19–26, 2014.

[274] J.-H. Song, H.-E. Kim, and H.-W. Kim, 'Production of electrospun gelatin nanofibre by water-based co-solvent approach', *J. Mater. Sci. Mater. Med.*, vol. 19, no. 1, pp. 95–102, 2008.

[275] K. Siimon, H. Siimon, and M. Järvekülg, 'Mechanical characterization of electrospun gelatin scaffolds cross-linked by glucose', *J. Mater. Sci. Mater. Med.*, vol. 26, no. 1, 2015.

[276] E. Roldán, N. D. Reeves, G. Cooper, and K. Andrews, 'Influence of solvent concentration on morphology, topography and mechanical properties of gelatin electrospun nanofibres: Analysis of induced cell behaviour', *ECM Meet. Abstr.*, no. 5, p. 62, 2016.

[277] E. Roldán, N. D. Reeves, G. Cooper, and K. Andrews, 'Suitability of gelatin electrospun scaffolds for use in the development of ligament implants: a morphological, topographical and mechanical perspective', presented at the 28th European Conference on Biomaterials, Athens, Greece, 2017.

[278] E. Roldán, N. D. Reeves, G. Cooper, and K. Andrews, 'Effects of solvent concentration on the morphology, topography and mechanical behaviour of gelatin electrospun nanofibres for use in tissue engineering implants', presented at the MMU Science & Engineering Research Symposium, Manchester, UK, 2016.

[279] E. Roldán, N. D. Reeves, G. Cooper, and K. Andrews, 'Study of the morphology, topography and mechanical properties of gelatin electrospun nanofibres based on solvent concentration', presented at the ManBioMat. Biomaterials and tissue engineering conference, Manchester, UK, 2016.

[280] R. N. Kale and A. N. Bajaj, 'Ultraviolet Spectrophotometric Method for Determination of Gelatin Crosslinking in the Presence of Amino Groups', *J. Young Pharm.*, vol. 2, no. 1, pp. 90–94, 2010.

[281] C. N. Grover, J. H. Gwynne, N. Pugh, S. W. Hamaia, R. W. Farndale, S. M. Best, R. E. Cameron, 'Crosslinking and composition influence the surface properties, mechanical stiffness and cell reactivity of collagen-based films', *Acta Biomater.*, vol. 8, no. 8, pp. 3080–3090, 2012.

[282] E. J. Chong, T. T. Phan, I. J. Lim, Y. Z. Zhang, B. H. Bay, S. Ramakrishna, C. T. Lim, 'Evaluation of electrospun PCL/gelatin nanofibrous scaffold for wound healing and layered dermal reconstitution', *Acta Biomater.*, vol. 3, no. 3, pp. 321–330, 2007.

[283] S. E. Kim, D. N. Heo, J. B. Lee, J. R. Kim, S. H. Park, S. H. Jeon and I. K. Kwon, 'Electrospun gelatin/polyurethane blended nanofibres for wound healing', *Biomed. Mater. Bristol Engl.*, vol. 4, no. 4, 2009.

[284] D. Gupta, J. Venugopal, M. P. Prabhakaran, V. R. G. Dev, S. Low, A. T. Choon, S. Ramakrishna, 'Aligned and random nanofibrous substrate for the *in vitro* culture of Schwann cells for neural tissue engineering', *Acta Biomater.*, vol. 5, no. 7, pp. 2560–2569, 2009.

[285] L. Ghasemi-Mobarakeh, M. P. Prabhakaran, M. Morshed, M. H. Nasr-Esfahani, and S. Ramakrishna, 'Electrical stimulation of nerve cells using conductive nanofibrous scaffolds for nerve tissue engineering', *Tissue Eng. Part A*, vol. 15, no. 11, pp. 3605–3619, 2009.

[286] L. Ghasemi-Mobarakeh, M. P. Prabhakaran, M. Morshed, M.-H. Nasr-Esfahani, and S. Ramakrishna, 'Electrospun poly(epsilon-caprolactone)/gelatin nanofibrous scaffolds for nerve tissue engineering', *Biomaterials*, vol. 29, no. 34, pp. 4532–4539, 2008.

[287] K. Ohkawa, S. Hayashi, N. Kameyama, H. Yamamoto, M. Yamaguchi, S. Kimoto, S. Kurata, H. Shinji, 'Synthesis of collagen-like sequential polypeptides

containing O-phospho-L-hydroxyproline and preparation of electrospun composite fibres for possible dental application', *Macromol. Biosci.*, vol. 9, no. 1, pp. 79–92, 2009.

[288] L. Francis, J. Venugopal, M. P. Prabhakaran, V. Thavasi, E. Marsano, and S. Ramakrishna, 'Simultaneous electrospin-electrosprayed biocomposite nanofibrous scaffolds for bone tissue regeneration', *Acta Biomater.*, vol. 6, no. 10, pp. 4100–4109, 2010.

[289] K. Sisson, C. Zhang, M. C. Farach-Carson, D. B. Chase, and J. F. Rabolt, 'Fibre diameters control osteoblastic cell migration and differentiation in electrospun gelatin', *J. Biomed. Mater. Res. A*, vol. 94, no. 4, pp. 1312–1320, 2010.

[290] D. Gupta, J. Venugopal, S. Mitra, V. R. Giri Dev, and S. Ramakrishna, 'Nanostructured biocomposite substrates by electrospinning and electrospraying for the mineralization of osteoblasts', *Biomaterials*, vol. 30, no. 11, pp. 2085–2094, 2009.

[291] H.-W. Kim, H.-S. Yu, and H.-H. Lee, 'Nanofibrous matrices of poly(lactic acid) and gelatin polymeric blends for the improvement of cellular responses', *J. Biomed. Mater. Res. A*, vol. 87, no. 1, pp. 25–32, 2008.

[292] B. Dhandayuthapani, U. M. Krishnan, and S. Sethuraman, 'Fabrication and characterization of chitosan-gelatin blend nanofibres for skin tissue engineering', *J. Biomed. Mater. Res. B Appl. Biomater.*, vol. 94, no. 1, pp. 264–272, 2010.

[293] H. M. Powell and S. T. Boyce, 'Fibre density of electrospun gelatin scaffolds regulates morphogenesis of dermal-epidermal skin substitutes', *J. Biomed. Mater. Res. A*, vol. 84, no. 4, pp. 1078–1086, 2008.

[294] G. Yang, H. Lin, B. B. Rothrauff, S. Yu, and R. S. Tuan, 'Multilayered polycaprolactone/gelatin fibre-hydrogel composite for tendon tissue engineering', *Acta Biomater.*, vol. 35, pp. 68–76, 2016.

[295] S. Wang, Y. Zhang, H. Wang, G. Yin, and Z. Dong, 'Fabrication and properties of the electrospun polylactide/silk fibroin-gelatin composite tubular scaffold', *Biomacromolecules*, vol. 10, no. 8, pp. 2240–2244, 2009.

[296] M. A. Accardi, S. D. McCullen, A. Callanan, S. Chung, P. M. Cann, M. M. Stevens, and D. Dini, 'Effects of fibre orientation on the frictional properties and damage of regenerative articular cartilage surfaces', *Tissue Eng. Part A*, vol. 19, no. 19–20, pp. 2300–2310, 2013.

[297] K. K. Balan, V. Sivanesan, N. Moorthy, D. Budhhan, S. Jeyaseelan, and S. Sundaramoorthy, 'Effect of thickness of mat and testing parameters on tensile strength variability of electrospun nanofibrous mat', *Mater. Today Proc.*, vol. 3, no. 6, pp. 1320–1329, 2016.

[298] K. Ghosal, A. Chandra, G. Praveen, S. Snigdha, S. Roy, C. Agatemor, S. Thomas and I. Provaznik, 'Electrospinning over Solvent Casting: Tuning of Mechanical Properties of Membranes', *Sci. Rep.*, vol. 8, no. 1, p. 5058, 2018.

[299] A. A. Salifu, C. Lekakou, and F. H. Labeed, 'Electrospun oriented gelatin-hydroxyapatite fibre scaffolds for bone tissue engineering', *J. Biomed. Mater. Res. A*, vol. 105, no. 7, pp. 1911–1926, 2017.

[300] H. Y. Ang, R. Avrahami, U. Sarig, T. Bronshtein, E. Zussman, F. Y. Boey, M. Machluf, S. S. Venkatraman, 'Characterization of a bioactive fibre scaffold with entrapped HUVECs in coaxial electrospun core-shell fibre', *Biomatter*, vol. 4, no. 1, 2014.

[301] J. Zhan and P. Lan, 'The Review on Electrospun Gelatin Fibre Scaffold', *J. Res. Updat. Polym. Sci.*, vol. 1, no. 2, pp. 59–71, 2013.

[302] F. Han, X. Jia, D. Dai, X. Yang, J. Zhao, Y. Zhao, Y. Fan, X. Yuan, 'Performance of a multilayered small-diameter vascular scaffold dual-loaded with VEGF and PDGF', *Biomaterials*, vol. 34, no. 30, pp. 7302–7313, 2013.

[303] J. L. Ferreira, S. Gomes, C. Henriques, J. P. Borges, and J. C. Silva, 'Electrospinning polycaprolactone dissolved in glacial acetic acid: Fibre production, nonwoven characterization, and *In Vitro* evaluation', *J. Appl. Polym. Sci.*, vol. 131, no. 22, 2014.

[304] X. Zhu, S. Ni, T. Xia, Q. Yao, H. Li, B. Wang, J. Wang, X. Li, W. Su, 'Anti-Neoplastic Cytotoxicity of SN-38-Loaded PCL/Gelatin Electrospun Composite Nanofibre Scaffolds against Human Glioblastoma Cells *In Vitro*', *J. Pharm. Sci.*, vol. 104, no. 12, pp. 4345–4354, 2015.

[305] J. L. Lowery, *Characterization and modification of porosity in electrospun polymeric materials for tissue engineering applications*, Massachusetts Institute of Technology, Dept. of Chemical Engineering, 2009.

[306] J. Cruz, S. Rana, R. Fangueiro, and R. Guedes, 'Designing artificial anterior cruciate ligaments based on novel fibrous structures', *Fibres Polym.*, vol. 15, no. 1, pp. 181–186, 2014.

[307] M. J. Park, R. R. Gonzales, A. Abdel-Wahab, S. Phuntsho, and H. K. Shon, 'Hydrophilic polyvinyl alcohol coating on hydrophobic electrospun nanofibre membrane for high performance thin film composite forward osmosis membrane', *Desalination*, vol. 426, pp. 50–59, 2018.

[308] P. Shao, Z. Yan, H. Chen, and J. Xiao, 'Electrospun poly(vinyl alcohol)/permutite fibrous film loaded with cinnamaldehyde for active food packaging', *J. Appl. Polym. Sci.*, vol. 135, no. 16, 2018.

[309] M. S. Enayati, T. Behzad, P. Sajkiewicz, M. Rafienia, R. Bagheri, L. Ghasemi-Mobarakeh, D. Kolbuk, Z. Pahlevanneshan, S. H. Bonakdar, 'Development of electrospun poly (vinyl alcohol)-based bionanocomposite scaffolds for bone tissue engineering', *J. Biomed. Mater. Res. - Part A*, vol. 106, no. 4, pp. 1111–1120, 2018.

[310] S. Chao, Y. Li, R. Zhao, L. Zhang, Y. Li, C. Wang, X. Li, 'Synthesis and characterization of tigecycline-loaded sericin/poly(vinyl alcohol) composite fibres via electrospinning as antibacterial wound dressings', *J. Drug Deliv. Sci. Technol.*, vol. 44, pp. 440–447, 2018.

[311] M. Zhu, D. Hua, H. Pan, F. Wang, B. Manshian, S. J. Soenen, R. Xiong, C. Huang, 'Green electrospun and crosslinked poly(vinyl alcohol)/poly(acrylic acid) composite membranes for antibacterial effective air filtration', *J. Colloid Interface Sci.*, vol. 511, pp. 411–423, 2018.

[312] M. Ferrández-Rives, Á. A. Beltrán-Osuna, J. A. Gómez-Tejedor, and J. L. G. Ribelles, 'Electrospun PVA/bentonite nanocomposites mats for drug delivery', *Materials*, vol. 10, no. 12, 2017.

[313] S. J. Najafi, A. A. Gharehaghaji, and S. M. Etrati, 'Fabrication and characterization of elastic hollow nanofibrous PU yarn', *Mater. Des.*, vol. 99, pp. 328–334, 2016.

[314] C. Cai, C. Chen, G. Chen, F.Wang, L. Guo, L. Yin, D. Feng and L. Yang, 'Type I collagen and polyvinyl alcohol blend fibre scaffold for anterior cruciate ligament reconstruction', *Biomed. Mater. Bristol*, vol. 8, no. 3, 2013.

[315] D. Moreau, A. Villain, D. N. Ku, and L. Corté, 'Poly(vinyl alcohol) hydrogel coatings with tunable surface exposure of hydroxyapatite', *Biomatter*, vol. 4, 2014.

[316] D. Moreau, A. Villain, M. Bachy, H. Proudhon, D. N. Ku, D. Hannouche, H. Petite, L. Corté, '*In vivo* evaluation of the bone integration of coated poly(vinyl-alcohol) hydrogel fibre implants', *J. Mater. Sci. Mater. Med.*, vol. 28, no. 8, 2017.

[317] L. Bosworth, P. Clegg, and S. Downes, 'Electrospun nanofibres of polycaprolactone, and their use for tendon regeneration', *Int. J. Nano Biomater.*, vol. 1, no. 3, pp. 263–279, 2008.

[318] Z.-W. Li, C. W. Li, Q. Wang, S. J. Shi, M. Hu, Q. Zhang, H. H. Cui, J. B. Sun, M. Zhou, G. L. Wu, J. Z. Dang, L. C. Lu, 'The cellular and molecular mechanisms underlying silver nanoparticle/chitosan oligosaccharide/poly(vinyl alcohol) nanofibre-mediated wound healing', *J. Biomed. Nanotechnol.*, vol. 13, no. 1, pp. 17–34, 2017.

[319] S. Sirima, M. Phiriyawirut, and K. Suttisintong, 'Comparison of the release of aloe vera extracts from poly(Vinyl Alcohol) electrospun fibres and hydrogel films for wound healing applications', *Key Eng. Mater.*, vol. 751 KEM, pp. 592–598, 2017.

[320] J. Wang, S. Hao, T. Luo, T. Zhou, X. Yang, and B. Wang, 'Keratose/poly (vinyl alcohol) blended nanofibres: Fabrication and biocompatibility assessment', *Mater. Sci. Eng. C*, vol. 72, pp. 212–219, 2017.

[321] Z. Zarekhalili, S. H. Bahrami, M. Ranjbar-Mohammadi, and P. B. Milan, 'Fabrication and characterization of PVA/Gum tragacanth/PCL hybrid nanofibrous scaffolds for skin substitutes', *Int. J. Biol. Macromol.*, vol. 94, pp. 679–690, 2017.

[322] Y. Zhou, K. Liang, C. Zhang, J. Li, H. Yang, X. Liu, X. Yin, D. Chen, W. Xu, P. Xiao, 'Photocrosslinked methacrylated chitosan-based nanofibrous scaffolds as potential skin substitute', *Cellulose*, vol. 24, no. 10, pp. 4253–4262, 2017.

[323] U. Anjaneyulu, B. Priyadarshini, A. N. Grace, and U. Vijayalakshmi, 'Fabrication and characterization of Ag doped hydroxyapatite-polyvinyl alcohol composite nanofibres and its *in vitro* biological evaluations for bone tissue engineering applications', *J. Sol-Gel Sci. Technol.*, vol. 81, no. 3, pp. 750–761, 2017.

[324] S. Chahal, F. S. J. Hussain, A. Kumar, M. S. B. A. Rasad, and M. M. Yusoff, 'Fabrication, characterization and *in vitro* biocompatibility of electrospun hydroxyethyl cellulose/poly (vinyl) alcohol nanofibrous composite biomaterial for bone tissue engineering', *Chem. Eng. Sci.*, vol. 144, pp. 17–29, 2016.

[325] S. Zupančič, S. Sinha-Ray, S. Sinha-Ray, J. Kristl, and A. L. Yarin, 'Controlled Release of Ciprofloxacin from Core-Shell Nanofibres with Monolithic or Blended Core', *Mol. Pharm.*, vol. 13, no. 4, pp. 1393–1404, 2016.

[326] R. D. Prabha, D. C. E. Kraft, L. Harkness, B. Melsen, H. Varma, P. D. Nair, J. Kjems, M. Kassem, 'Bioactive nano-fibrous scaffold for vascularized craniofacial bone regeneration', *J. Tissue Eng. Regen. Med.*, vol. 12, no. 3, pp. 1537–1548, 2018.

[327] V. M. Merkle, P. L. Tran, M. Hutchinson, K. R. Ammann, K. De Cook, X. Wu, M. J. Slepian, 'Core-shell PVA/gelatin electrospun nanofibres promote human umbilical vein endothelial cell and smooth muscle cell proliferation and migration', *Acta Biomater.*, vol. 27, pp. 77–87, 2015.

[328] Y. Liu, H. Zahedmanesh, C. Lally, P. A. Cahill, and G. B. McGuinness, 'Compliance properties of a composite electrospun fibre - Hydrogel blood vessel scaffold', *Mater. Lett.*, vol. 178, pp. 296–299, 2016.

[329] V. M. Merkle, D. Martin, M. Hutchinson, P.L. Tran, A. Behrens, S. Hossainy, J. Sheriff, D. Bluestein, X. Wu, and M. J. Slepian, 'Hemocompatibility of poly(vinyl alcohol)-gelatin core-shell electrospun nanofibres: A scaffold for

modulating platelet deposition and activation', *ACS Appl. Mater. Interfaces*, vol. 7, no. 15, pp. 8302–8312, 2015.

[330] Z. Tan, H. Wang, X. Gao, T. Liu, and Y. Tan, 'Composite vascular grafts with high cell infiltration by co-electrospinning', *Mater. Sci. Eng. C*, vol. 67, pp. 369–377, 2016.

[331] W. Zhang, L. Zhao, J. Ma, X. Wang, Y. Wang, F. Ran, Y. Wang, H. Ma, S. Yu, 'Electrospinning of fucoidan/chitosan/poly(vinyl alcohol) scaffolds for vascular tissue engineering', *Fibres Polym.*, vol. 18, no. 5, pp. 922–932, 2017.

[332] H. Bodugoz-Senturk, C. E. Macias, J. H. Kung, and O. K. Muratoglu, 'Poly(vinyl alcohol)-acrylamide hydrogels as load-bearing cartilage substitute', *Biomaterials*, vol. 30, no. 4, pp. 589–596, 2009.

[333] R. Ma, D. Xiong, F. Miao, J. Zhang, and Y. Peng, 'Novel PVP/PVA hydrogels for articular cartilage replacement', *Mater. Sci. Eng. C*, vol. 29, no. 6, pp. 1979–1983, 2009.

[334] Y. Pan and D. Xiong, 'Friction properties of nano-hydroxyapatite reinforced poly(vinyl alcohol) gel composites as an articular cartilage', *Wear*, vol. 266, no. 7–8, pp. 699–703, 2009.

[335] Y. Zheng, H. Lv, Y. Wang, H. Lu, L. Qing, and T. Xi, 'Performance of novel bioactive hybrid hydrogels *in vitro* and *in vivo* used for artificial cartilage', *Biomed. Mater.*, vol. 4, no. 1, 2009.

[336] C. M. Hassan and N. A. Peppas, 'Structure and Applications of Poly(vinyl alcohol) Hydrogels Produced by Conventional Crosslinking or by Freezing/Thawing Methods', in *Biopolymers · PVA Hydrogels, Anionic Polymerisation Nanocomposites*, Springer, Berlin, Heidelberg, pp. 37–65, 2000.

[337] X. Luo, Z. Guo, P. He, T. Chen, L. Li, S. Ding, H. Li, 'Study on structure, mechanical property and cell cytocompatibility of electrospun collagen nanofibres crosslinked by common agents', *Int. J. Biol. Macromol.*, vol. 113, pp. 476–486, 2018.

[338] E. Roldán, N. D. Reeves, G. Cooper, and K. Andrews, 'Suitability of optimised PVA electrospun scaffolds for ACL replacement', *ECM Meet Abstr*, vol. 4, p. 118, 2018.

[339] C. M. Hassan, P. Trakampan, and N. A. Peppas, 'Water Solubility Characteristics of Poly(vinyl alcohol) and Gels Prepared by Freezing/Thawing Processes', in *Water Soluble Polymers: Solutions Properties and Applications*, Z. Amjad, Ed. Boston, MA: Springer US, pp. 31–40, 2002.

[340] L. C. Ionescu and R. L. Mauck, 'Porosity and Cell Preseeding Influence Electrospun Scaffold Maturation and Meniscus Integration *In Vitro*', *Tissue Eng. Part A*, vol. 19, no. 3–4, pp. 538–547, 2013.

[341] J. M. Yang, J. H. Yang, S. C. Tsou, C. H. Ding, C. C. Hsu, K. C. Yang, C. C. Yang, K. S. Cheng, S. W. Chen, J. S. Wang, 'Cell proliferation on PVA/sodium alginate and PVA/poly(γ-glutamic acid) electrospun fibre', *Mater. Sci. Eng. C Mater. Biol. Appl.*, vol. 66, pp. 170–177, 2016.

[342] C.-Y. Huang, K.-H. Hu, and Z.-H. Wei, 'Comparison of cell behaviour on pva/pva-gelatin electrospun nanofibres with random and aligned configuration', *Sci. Rep.*, vol. 6, 2016.

[343] C. T. Laurencin and J. W. Freeman, 'Ligament tissue engineering: an evolutionary materials science approach', *Biomaterials*, vol. 26, no. 36, pp. 7530–7536, 2005.

[344] G. H. Altman, R. L. Horan, H. H. Lu, J. Moreau, I. Martin, J. C. Richmond, D. L. Kaplan, 'Silk matrix for tissue engineered anterior cruciate ligaments', *Biomaterials*, vol. 23, no. 20, pp. 4131–4141, 2002.

[345] J. W. Freeman, M. D. Woods, and C. T. Laurencin, 'Tissue engineering of the anterior cruciate ligament using a braid-twist scaffold design', *J. Biomech.*, vol. 40, no. 9, pp. 2029–2036, 2007.

[346] J. A. Weiss, J. C. Gardiner, and C. Bonifasi-Lista, 'Ligament material behaviour is nonlinear, viscoelastic and rate-independent under shear loading', *J. Biomech.*, vol. 35, no. 7, pp. 943–950, 2002.

[347] A. Sensini, C. Gualandi, L. Cristofolini, G. Tozzi, M. Dicarlo, G. Teti, M. Mattioli-Belmonte and M. L. Focarete, 'Biofabrication of bundles of poly(lactic acid)-collagen blends mimicking the fascicles of the human Achille tendon', *Biofabrication*, vol. 9, no. 1, 2017.

[348] Hudson PB, Clapp AC, and Kness D. Joseph's, *Introductory Textile Science.* 6. Harcourt Brace Jovanovich College Publishers; New York, 1993.

[349] Cooper JA., 'Design, Optimisation and *In Vivo* Evaluation of a Tissue-Engineered Anterior Cruciate Ligament Replacement', Drexel University Press; Philadelphia, 2002.

[350] J. Chen, G. H. Altman, V. Karageorgiou, R. Horan, A. Collette, V. Volloch, T. Colabro, D. L. Kaplan, 'Human bone marrow stromal cell and ligament fibroblast responses on RGD-modified silk fibres', *J. Biomed. Mater. Res. A*, vol. 67, no. 2, pp. 559–570, 2003.

[351] G. Vunjak-Novakovic, G. Altman, R. Horan, and D. L. Kaplan, 'Tissue engineering of ligaments', *Annu. Rev. Biomed. Eng.*, vol. 6, pp. 131–156, 2004.

[352] J. A. Cooper, H. H. Lu, F. K. Ko, J. W. Freeman, and C. T. Laurencin, 'Fibre-based tissue-engineered scaffold for ligament replacement: design considerations and *in vitro* evaluation', *Biomaterials*, vol. 26, no. 13, pp. 1523–1532, 2005.

[353] H. H. Lu, J. A. Cooper, S. Manuel, J. W. Freemand, M. A. Attawia, F. K. Ko, C. T. Laurencin, 'Anterior cruciate ligament regeneration using braided biodegradable scaffolds: *in vitro* optimisation studies', *Biomaterials*, vol. 26, no. 23, pp. 4805–4816, 2005.

[354] P.-A. Mouthuy, N. Zargar, O. Hakimi, E. Lostis, and A. Carr, 'Fabrication of continuous electrospun filaments with potential for use as medical fibres', *Biofabrication*, vol. 7, no. 2, 2015.

[355] B. B. Rothrauff, B. B. Lauro, G. Yang, R. E. Debski, V. Musahl, and R. S. Tuan, 'Braided and Stacked Electrospun Nanofibrous Scaffolds for Tendon and Ligament Tissue Engineering', *Tissue Eng. Part A*, vol. 23, no. 9–10, pp. 378–389, 2017.

[356] K. B. Shelburne, M. G. Pandy, and M. R. Torry, 'Comparison of shear forces and ligament loading in the healthy and ACL-deficient knee during gait', *J. Biomech.*, vol. 37, no. 3, pp. 313–319, 2004.

[357] K. E. Wilk, R. F. Escamilla, G. S. Fleisig, S. W. Barrentine, J. R. Andrews, and M. L. Boyd, 'A Comparison of Tibiofemoral Joint Forces and Electromyographic Activit During Open and Closed Kinetic Chain Exercises', *Am. J. Sports Med.*, vol. 24, no. 4, pp. 518–527, 1996.

[358] M. G. Pandy and K. B. Shelburne, 'Dependence of cruciate-ligament loading on muscle forces and external load', *J. Biomech.*, vol. 30, no. 10, pp. 1015–1024, 1997.

[359] R. Nisell, M. O. Ericson, G. Nemeth, and J. Ekholm, ‘Tibiofemoral joint forces during isokinetic knee extension’, *Am. J. Sports Med.*, vol. 17, no. 1, pp. 49–54, 1989.

[360] D. R. Bennett, J. T. Blackburn, M. C. Boling, M. McGrath, H. Walusz, and D. A. Padua, ‘The relationship between anterior tibial shear force during a jump landing task and quadriceps and hamstring strength’, *Clin. Biomech. Bristol Avon*, vol. 23, no. 9, pp. 1165–1171, 2008.

[361] K. E. Wilk and J. R. Andrews, ‘The effects of pad placement and angular velocity on tibial displacement during isokinetic exercise’, *J. Orthop. Sports Phys. Ther.*, vol. 17, no. 1, pp. 24–30, 1993.

[362] Q. Shao, T. D. MacLeod, K. Manal, and T. S. Buchanan, ‘Estimation of Ligament Loading and Anterior Tibial Translation in Healthy and ACL-Deficient Knees During Gait and the Influence of Increasing Tibial Slope Using EMG-Driven Approach’, *Ann. Biomed. Eng.*, vol. 39, no. 1, pp. 110–121, 2011.

[363] E. Roldán, N. D. Reeves, G. Cooper, and K. Andrews, ‘Assessment of 2D and 3D electrospun structures for use as tissue engineered ligaments: A mechanical and morphological perspective’, *ECM Meet Abstr*, vol. 4, p. 53, 2018.

[364] E. Roldán, N. D. Reeves, G. Cooper, and K. Andrews, ‘Mechanical and morphological evaluation of 2D and 3D electrospun structures for the manufacture of tissue engineered ligaments’, presented at the 29th European Conference on Biomaterials, Maastricht, Netherlands, 2018.

[365] X. Dai and Y. Cai, ‘Measurement of anterior cruciate ligament angles in single-bundle reconstruction using the anteromedial portal’, *Am. J. Orthop. Belle Mead NJ*, vol. 41, no. 6, pp. 268–272, 2012.

[366] Y. Cho, J. Cho, and D. Kim, 'Normal sagittal of the anterior cruciate ligament can be reproduced using accessory anteromedial portal technique: a magnetic resonance imaging study', *Arch. Orthop. Trauma Surg.*, vol. 132, no. 7, pp. 1011–1019, 2012.

[367] J. C. Reid, B. Yonke, and M. Tompkins, 'The angle of inclination of the native ACL in the coronal and sagittal planes', *Knee Surg. Sports Traumatol. Arthrosc. Off. J. ESSKA*, vol. 25, no. 4, pp. 1101–1105, 2017.

[368] 'SimTK: MB Knee: Multibody Models of the Human Knee: Project Home'. [Online]. Available: https://simtk.org/projects/mb_knee. [Accessed: 24 Mar. 2018].

[369] D. H. Kim, D. R. Wilson, A. T. Hecker, T. M. Jung, and C. H. Brown, 'Twisting and braiding reduces the tensile strength and stiffness of human hamstring tendon grafts used for anterior cruciate ligament reconstruction', *Am. J. Sports Med.*, vol. 31, no. 6, pp. 861–867, 2003.

[370] J. W. S. Hearle, P. Grosberg, and S. Backer, *Structural mechanics of fibres, yarns, and fabrics*. Wiley-Interscience, 1969.

[371] Y. Zhang, M. Song, Y. Diao, B. Li, L. Shi, and R. Ran, 'Preparation and properties of polyacrylamide/polyvinyl alcohol physical double network hydrogel', *RSC Adv.*, vol. 6, no. 113, pp. 112468–112476, 2016.

[372] S. Kawabata and M. Niwa, 'Fabric Performance in Clothing and Clothing Manufacture', *J. Text. Inst.*, vol. 80, no. 1, pp. 19–50, 1989.

[373] V. I. Walters, *Design and Analysis of a Collagenous Anterior Cruciate Ligament Replacement*, Thesis, Virginia Tech, 2011.

[374] A. P. Kishan, R. M. Nezarati, C. M. Radzicki, A. L. Renfro, J. L. Robinson, M. E. Whitelya and E. M. Cosgriff-Hernandez, 'In situ crosslinking of electrospun

gelatin for improved fibre morphology retention and tunable degradation', *J. Mater. Chem. B*, vol. 3, no. 40, pp. 7930–7938, 2015.

[375] S. Jiang, S. Liu, and W. Feng, 'PVA hydrogel properties for biomedical application', *J. Mech. Behav. Biomed. Mater.*, vol. 4, no. 7, pp. 1228–1233, 2011.

[376] G. Paradossi, F. Cavalieri, E. Chiessi, C. Spagnoli, and M. K. Cowman, 'Poly(vinyl alcohol) as versatile biomaterial for potential biomedical applications', *J. Mater. Sci. Mater. Med.*, vol. 14, no. 8, pp. 687–691, 2003.

[377] S. Nkhwa, K. F. Lauriaga, E. Kemal, and S. Deb, 'Poly(vinyl alcohol): Physical Approaches to Designing Biomaterials for Biomedical Applications', *Conference Papers in Science*, 2014. [Online]. Available: https://www.hindawi.com/journals/cpis/2014/403472/. [Accessed: 24 Mar. 2018].

[378] S. M. Pawde and K. Deshmukh, 'Characterization of polyvinyl alcohol/gelatin blend hydrogel films for biomedical applications', *J. Appl. Polym. Sci.*, vol. 109, no. 5, pp. 3431–3437, 2008.

[379] K. D. Andrews, J. A. Hunt, and R. A. Black, 'Effects of sterilisation method on surface topography and *in-vitro* cell behaviour of electrostatically spun scaffolds', *Biomaterials*, vol. 28, no. 6, pp. 1014–1026, 2007.

[380] P.-A. Mouthuy, N. Zargar Baboldashti, O. Hakimi, E. Lostis, and A. Carr, 'Fabrication of continuous electrospun filaments with potential for use as medical fibres', *Biofabrication*, vol. 7, 2015.

10. Appendix

Chemical characterization of gelatin samples was performed through use of a Fourier Transform Infrared Spectrometer. The aim of characterizing the gelatin scaffolds was to observe any significant changes to the chemical bonds of the gelatin after being dissolved in different concentrations of Acetic Acid (HAc) and Dimethyl sulfoxide (DMSO).

The results presented in Figures 10.1 and 10.2 show that the peaks for each concentration of solvent are coincident with the same wavenumber; therefore, the chemical structure of the polymer was not affected by the concentration of the solvent.

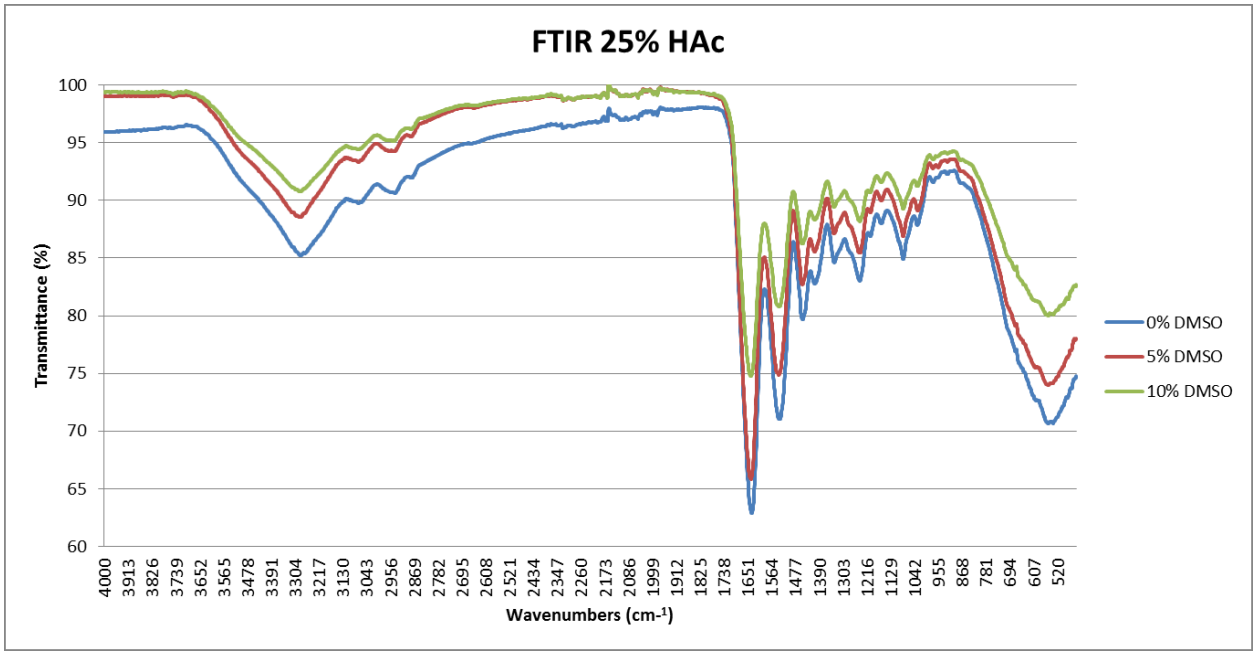

Figure 10.1 Fourier Transform Infrared Spectrosmetry for gelatin samples with 25% HAc and 0%, 5% and 10% DMSO.

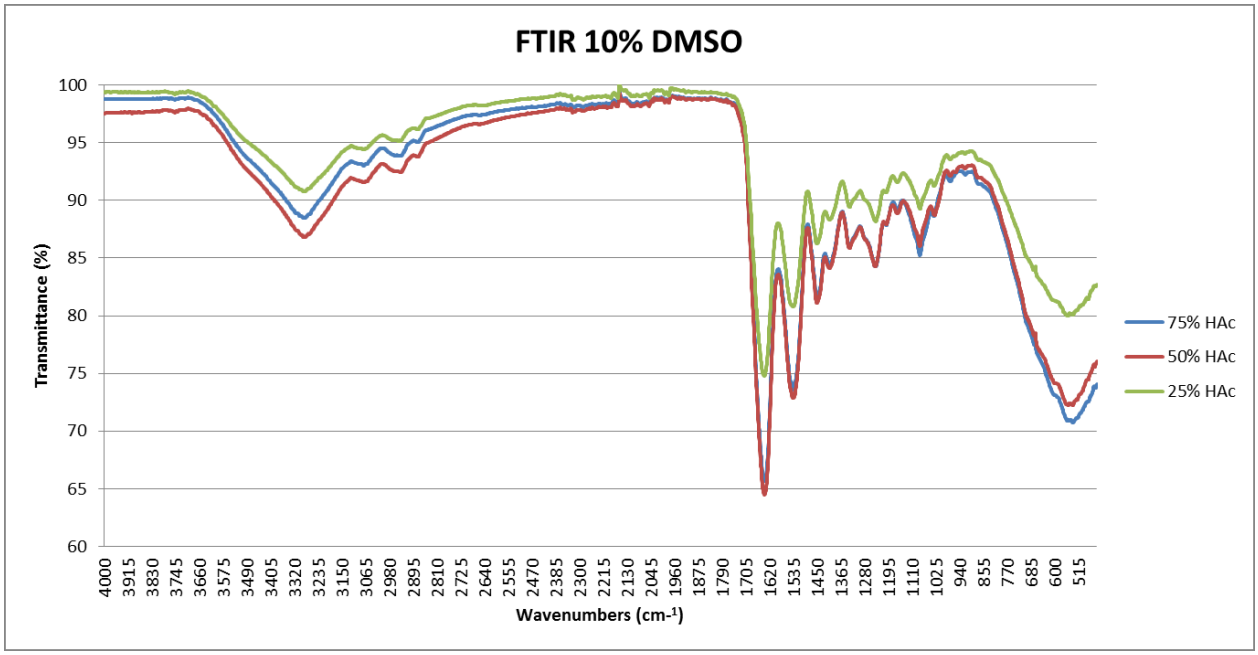

Figure 10.2 Fourier Transform Infrared Spectrosmetry for gelatin samples with 10% DMSO and 75%, 50% and 25% HAc.